

This file is part of the following work:

Cheng, Yanbo (2012) *Geological evolution of the world class Gejiu Ore District, SW China: information from magmatism, mineralization and microanalysis studies*. PhD Thesis, James Cook University.

Access to this file is available from:

<https://doi.org/10.25903/f2w4%2Dnv83>

Copyright © 2012 Yanbo Cheng

The author has certified to JCU that they have made a reasonable effort to gain permission and acknowledge the owners of any third party copyright material included in this document. If you believe that this is not the case, please email

researchonline@jcu.edu.au

ResearchOnline@JCU

This file is part of the following reference:

Cheng, Yanbo (2012) *Geological evolution of the world class Gejiu Ore District, SW China: information from magmatism, mineralization and microanalysis studies.* PhD thesis, James Cook University.

Access to this file is available from:

<http://eprints.jcu.edu.au/29014/>

The author has certified to JCU that they have made a reasonable effort to gain permission and acknowledge the owner of any third party copyright material included in this document. If you believe that this is not the case, please contact ResearchOnline@jcu.edu.au and quote <http://eprints.jcu.edu.au/29014/>

**Geological Evolution of the World Class
Gejiu Ore District, SW China: Information
from Magmatism, Mineralization and
Microanalysis Studies**

Thesis submitted by
Yanbo Cheng PhD (China University of Geosciences (Beijing))
in December 2012

for the degree of Doctor of Philosophy
in the School of Earth and Environmental Sciences
James Cook University

Statement of Contributions

Financial contributions towards this study have included:

- China Scholarship Council Scholarship Program
- National Natural Science Foundation of China (40930419)
- Special Research Funding for the Public Benefits Sponsored by MLR of China (200911007-12)
- Research Program of Yunnan Tin Group (2010-04A)
- Fundamental Research Funds for the Central Universities of China (2-9-2010-21)

Statement of Contribution by Others

| Chapter # | Details of publication(s) on which chapter is based | Nature and nature and extent of the intellectual input of each author |
|---|---|---|
| 3 | Contribution to Mineralogy and Petrology | I contributed to the writing and development of concepts |
| <p>I confirm the candidate's contribution to this paper and consent to the inclusion of the paper in this thesis.</p> <p>Name (Please print): Carl Spandler</p> <p>Signature: (</p> <p>Date: 14-12-12</p> | | |

Statement of Contribution by Others

| Chapter # | Details of publication(s) on which chapter is based | Nature and nature and extent of the intellectual input of each author |
|--|---|---|
| 5 | Ore Geology Reviews | I contributed to primary idea discussion and language polishing. |
| <p>I confirm the candidate's contribution to this paper and consent to the inclusion of the paper in this thesis.</p> <p>Name (Please print): Zhaoshan Chang</p> <p>Signature:</p> <p>Date: 09 / 12 / 2012</p> | | |

| Chapter # | Details of publication(s) on which chapter is based | Nature and extent of the intellectual input of each author |
|-----------|---|---|
| 3 | Contribution to Mineralogy and Petrology | I contributed to the development of concepts |
| 5 | Ore Geology Reviews | I contributed to part of primary idea discussion and writing. |

I confirm the candidate's contribution to this paper and consent to the inclusion of the paper in this thesis.

Name (Please print): Brian Rusk

Signature: 

Date: *December 10, 2012*

Statement of Contribution by Others

| Chapter # | Details of publication(s) on which chapter is based | Nature and nature and extent of the intellectual input of each author |
|---|---|---|
| 2 | Lithos | I contributed to part of the field investigation, samples collection, and primary idea discussion |
| 3 | Contribution to Mineralogy and Petrology | I contributed to part of the field investigation and primary idea discussion |
| 4 | Ore Geology Reviews | I contributed to the field investigation |
| 5 | Ore Geology Reviews | I contributed to part of the field investigation, and primary idea discussion |
| 6 | Mineralium Deposita | I contributed to part of the field investigation and samples collection |
| <p>I confirm the candidate's contribution to this paper and consent to the inclusion of the paper in this thesis.</p> <p>Name (Please print): Jingwen Mao</p> <p>Signature:</p> <p>Date: 10/12/2012</p> | | |

Statement of Contribution by Others

| Chapter # | Details of publication(s) on which chapter is based | Nature and nature and extent of the intellectual input of each author |
|---|---|---|
| 5 | Ore Geology Reviews | I contributed to part of the field investigation and samples collection |
| 6 | Mineralium Deposita | I contributed to part of the field investigation and samples collection |
| <p>I confirm the candidate's contribution to this paper and consent to the inclusion of the paper in this thesis.</p> <p>Name (Please print): Zongxi Yang</p> <p>Signature:</p> <p>Date: 10/12/12</p> | | |

Acknowledgements

I would like to thank my supervisors, Dr. Carl Spandler, Dr. Brian Rusk, Dr. Tony Kemp and Dr. Zhaoshan Chang for their enthusiasm, dedication and patience on my studies. I thank them for their assistance and willingness to discuss all aspects of my works, and their many suggestions that helped me clear my thoughts. I would also like to acknowledge the support of the China Scholarship Council, Economic Geology Research Unit (EGRU) and the School of Earth & Environmental Sciences at James Cook University. My particularly grateful to Dr. Richard Wormald, Dr. Yi Hu, Ms Glen Connolly, Ms Judy Botting, Ms Kellie Johns and Ms Liz Elisabeth from JCU, who gave me many assistance during my PhD studies.

I want to thank Prof. Jingwen Mao from Chinese Academy of Geological Sciences for his professional field introduction and thoughtful discussion. I also benefited from Prof. Franco Pirajno, Prof. Peter Laznicka, Prof. Fuyuan Wu and Prof. Xianhua Li for many talks about my studies. Several Yunnan Tin Group geologists are thanked for facilitating underground visits, accommodation and discussion. They are Xiang Tong, Junde Wu, Guopei Mo, Bin Li, Baofu Yang, Dinghao Zhong and Deming Kang.

To my PhD fellas, Ryan Tucker, Mark Munro, Joao Babo, Johannes Harmmerli, Rob Holm, Berit Lehmann, Clemon Fay and Vicki Darlington. I would like to extend my thanks for making me feel welcome in Townsville and for showing me a good time. I also want to thank some of my Chinese friends, they are Jun Lu, Zengqiang Qian, Xugan Wu, Maoying Wu, Xin Gu, Pengjie Zhu and Bo Gao, and of course Hongzheng Hu, all of whom helped me a lot and made life less lonely especially in the very beginning I came Townsville.

I would like to thank my family in China for all support and understanding. I would like thank my parents, father-in-law, mother-in-law, brother, sister-in-law, and of course my little niece and nephew, although you cannot completely understand my

works, you still pay all your enthusiasm and always being supportive.

Mostly importantly, I would like to thank my beautiful wife, Dr. Yue Wang, for her endless love, patience and support. Thanks for bearing all the pressure for a whole year when I was not at home, and for moving countries so I can finish my studies off. I could not have this done without you. You do not know how much you have helped me over the past years and I will always be indebted to you!

Abstract

This study targets the magmatic rocks and Sn polymetallic ores in the Gejiu district, Yunnan Province, with the aim of resolving problems related to geodynamic setting, ore-forming processes and genesis of the mineralization in the study area.

Systematic new SHRIMP/LA-ICP-MS U-Pb zircon dating results indicate that all the intrusive rocks in the Gejiu district are broadly coeval, ranging from 78 Ma to 85 Ma. Elemental and isotopic geochemistry of these rocks reveal that the granites in the Gejiu district experienced different degrees of fractionation, and they were mainly sourced from crustal materials with minor input from mantle-derived magma. The Jiasha gabbro derived from the partial melting of the lithospheric mantle with some contamination of crustal materials, and the mafic microgranular enclaves represent the results of magma mingling and mixing between the crustal- and mantle-derived magmas. Both alkaline rocks and mafic dykes were sourced from lithospheric mantle but experienced different evolutionary processes. Based on all of these concepts, I conclude that extensive interaction between mantle and crustal materials occurred in Gejiu district during Late Cretaceous.

Metal zonation away from granitic intrusions, both in horizontal and vertical directions, are clearly developed in the Gejiu Sn polymetallic ore district, commonly from W-Be-Bi±Mo±Sn zone closest to the granites, out to Cu-Sn zone and then to a Pb-Zn zone. New data indicate that the homogenization temperature and salinity of the ore-forming fluid display continuous variations in different mineralization stages, which is a typical characteristic of the granite-related hydrothermal deposits. Sulfur isotopes of various sulfides, and hydrogen and oxygen isotopic compositions of different quartz generations exhibit obvious differences, which further supports varying conditions for mineralisation. Moreover, application of different geochronological methods on different minerals, which include mica Ar-Ar, molybdenum Re-Os and LA-ICP-MS cassiterite U-Pb dating, reveal that all the ore

styles in the Gejiu district formed in a short time period, and mineralization and magmatism ages are contemporaneous. Above all, the large scale metallic accumulation and mineralization in Gejiu district are of hydrothermal origin.

Iron isotope variations in ores from Gaosong deposit show primary sulfide ores enriched in lightest isotopes, while $\delta^{57}\text{Fe}$ values of oxidized ores and gossan ores becoming heavier progressively. Moreover, the range of $\delta^{57}\text{Fe}$ values of primary ores and oxidized ores are larger than that of gossan samples. Combined with the mineral association, this Fe isotope features suggest that Fe isotope compositions are affected by mineralogy, and it is the primary mechanism of the large Fe isotopic variations in the primary ores. On the whole, the systematic variations of Fe isotope composition show that Fe isotope studies have potential to constrain metal sources, ore genesis and evolutionary of hydrothermal deposit.

Furthermore, CL textural results indicate distance between samples and granites may be one of the key factors controlling the cassiterite size and internal micro-texture variations. Fe, Ti and W are the most abundant elements in cassiterite, and variation of Zr/Hf ratios maybe caused by various tourmaline and fluorite contents. Cassiterite geochemical and textural variations may reflect the temperature, oxygen fugacity and redox station of ore forming fluids experienced significant changes during the tin mineralization process.

TABLE OF CONTENTS

| | |
|--|-----------|
| Title Page | 1 |
| Statement of Contributions | 2 |
| Statement of Contribution by others | 3 |
| Acknowledgements | 9 |
| Abstract | 11 |
| Table of Contents | 13 |
| List of Tables | 20 |
| List of Figures | 22 |
| Chapter 1 Introduction and Background | 28 |
| 1 Thesis introduction | 29 |
| 2 Study background..... | 32 |
| Chapter 2 Age and Geochemistry of Granites in Gejiu area, Yunnan province, SW China: Constraints on their petrogenesis and tectonic setting | 34 |
| 1. Introduction..... | 35 |
| 2. Regional geology and geological characteristics of the Gejiu granitic intrusions | 35 |
| 2.1. Geological setting | 35 |
| 2.2. Granite petrography and sampling | 37 |
| 3. Analytical methods..... | 37 |
| 3.1. SHRIMP and LA-ICP-MS U–Pb zircon dating | 37 |
| 3.2. Major and trace elements | 37 |
| 3.3. Sr and Nd isotopes | 37 |
| 3.4. Zircon Hf isotopes..... | 39 |
| 4 Analytical results..... | 39 |
| 4.1 U–Pb zircon geochronology | 39 |
| 4.1.1 Porphyritic granite from the Laochang area (Sample CYB0807031) | 41 |

| | |
|---|-----------|
| 4.1.2. Porphyritic granite from the Longchahe area (samples CYB0707033 and CYB0807055) | 41 |
| 4.1.3. Porphyritic granite from the Masong area (sample CYB0707013)..... | 41 |
| 4.1.4. Equigranular granite from the Baishachong area (sample CYB0807032)... | 41 |
| 4.1.5. Equigranular granite from the Shenxianshui area (samples CYB0707020 and CYB0807049) | 41 |
| 4.1.6. Equigranular granite from the Xinshan area (sample CYB0807022) | 42 |
| 4.1.7. Equigranular granite from the Laochang area (sample D008) | 44 |
| 4.2 Geochemical and isotopic results..... | 44 |
| 4.2.1 Major and trace element data | 44 |
| 4.2.2 Sr–Nd isotopes | 44 |
| 4.2.3 Hf isotopes in zircons..... | 45 |
| 5. Discussion | 46 |
| 5.1 Fractional crystallization process | 46 |
| 5.2 Petrogenesis..... | 46 |
| 5.3 Genetic model for Cretaceous intraplate magmatism and mineralization in the western Cathaysia block..... | 48 |
| 5.4 Petrogenetic type: S-type, A-type or highly fractionated I-type granites?..... | 49 |
| 6. Conclusions | 50 |
| Reference..... | 51 |
| Chapter 3 Granite, gabbro and mafic microgranular enclaves in the Gejiu Area, Yunnan Province, China: a case of two stage mixing of crust- and mantle-derived magmas | 54 |
| 1 Introduction..... | 56 |
| 2 Geological setting | 56 |
| 3 Field relations and petrography..... | 58 |
| 4 Analytical Methods..... | 58 |
| 4.1 Zircon LA-ICP-MS dating | 58 |
| 4.2 Bulk-rock major and trace element concentrations..... | 60 |
| 4.3 Bulk-rock Nd and Sr isotopes..... | 61 |
| 4.4 Zircon Hf isotopes..... | 61 |

| | |
|---|-----------|
| 5 Results | 62 |
| 5.1 Zircon dating | 62 |
| 5.2 Major and trace elements | 62 |
| 5.3 Zircon Hf isotope..... | 62 |
| 5.4 Sr and Nd isotopic data..... | 62 |
| 6 Discussion | 62 |
| 6.1 Timing of magmatism..... | 62 |
| 6.2 Petrogenesis of the Jiasha Gabbro | 64 |
| 6.3 Petrogenesis of the Longchahe Granite | 67 |
| 6.4 Petrogenesis of Mafic Microgranular Enclaves..... | 68 |
| 6.5 Integrated model of magmatic processes..... | 69 |
| 7 Conclusions | 69 |
| Reference..... | 70 |
| Chapter 4 The origin of the world class tin-polymetallic deposits in the Gejiu district, SW China: constraints from metal zonation characteristics and ^{40}Ar-^{39}Ar geochronology | 73 |
| 1 Introduction..... | 75 |
| 2 Regional Geologic Setting | 76 |
| 3 Characteristics of the Gejiu Granitic Batholith | 78 |
| 4 Ore Deposit Geology | 79 |
| 4.1 Malage Sn-Cu deposit | 80 |
| 4.2 Songshujiao Sn-Pb deposit..... | 81 |
| 4.3 Gaosong Sn-Pb-Zn deposit..... | 82 |
| 4.4 Laochang Sn-W-Cu polymetallic deposit..... | 83 |
| 4.5 Kafang Cu-Sn deposit..... | 85 |
| 5 Metal Zonation..... | 86 |
| 6 Ar-Ar dating Techniques and Results..... | 88 |
| 6.1 Analytical Techniques | 88 |
| 6.2 Results | 89 |
| 7 Discussions and Conclusions | 92 |

| | |
|--|------------|
| 7.1 Timing of mineralization | 92 |
| 7.2 Implications of metal zonations | 93 |
| 7.3 Genetic implications and exploration significances | 94 |
| Reference..... | 95 |
| Chapter 5 Geology and vein tin mineralization in the Dadoushan deposit, Gejiu district, SW China..... | 102 |
| 1 Introduction..... | 103 |
| 2 Regional geology and mineralization | 105 |
| 3 Geology of the Dadoushan deposit | 105 |
| 3.1 Vein varieties | 107 |
| 3.2 Supergene ore modification | 107 |
| 4 Analytical methods..... | 107 |
| 4.1 Muscovite Ar–Ar dating..... | 107 |
| 4.2 Sulfur isotopes | 110 |
| 4.3 Oxygen and hydrogen isotopes | 110 |
| 5 Analytical results..... | 110 |
| 5.1 ⁴⁰ Ar- ³⁹ Ar dating | 110 |
| 5.2 Sulfur isotopes | 111 |
| 5.3 Hydrogen and oxygen isotopes..... | 111 |
| 6 Discussion | 111 |
| 6.1 Timing of mineralization | 111 |
| 6.2 Possible sources and evolution of ore-forming fluids..... | 112 |
| 6.3 Implications for ore formation..... | 112 |
| 7 Conclusion..... | 113 |
| Reference..... | 114 |
| Chapter 6 Geology and genesis of Kafang Cu-Sn deposit, Gejiu district, SW China..... | 115 |
| 1 Introduction..... | 116 |
| 2 Geological setting | 116 |
| 3 Geology of Kafang deposit..... | 117 |

| | |
|---|-----|
| 4 Hydrothermal alteration and mineralization styles | 117 |
| 4.1 Skarn type Cu-Sn mineralization..... | 117 |
| 4.2 Stratiform Cu mineralization hosted by basalt | 117 |
| 4.3 Stratiform Cu-Sn mineralization hosted by carbonate | 117 |
| 5 Analytical methods and sample description | 119 |
| 5.1 Fluid inclusions | 119 |
| 5.2 Isotopes | 122 |
| 5.2.1 Lead isotopes | 122 |
| 5.2.2 Sulfur isotopes | 122 |
| 5.2.3 Oxygen and hydrogen isotopes | 123 |
| 5.3 Geochronology | 123 |
| 5.3.1 Re-Os dating..... | 123 |
| 5.3.2 LA-ICP-MS | 123 |
| 6 Results | 124 |
| 6.1 Magmatism and mineralization dating | 124 |
| 6.1.1 LA-ICP-MS zircon U-Pb dating..... | 124 |
| 6.1.2 Molybdenite Re-Os dating..... | 124 |
| 6.2 Isotopes | 125 |
| 6.2.1 Sulfur isotopes | 125 |
| 6.2.2 Hydrogen and oxygen isotope data..... | 125 |
| 6.2.3 Pb isotopic compositions of the ore deposits and the country rocks..... | 125 |
| 6.3 Fluid inclusion studies..... | 126 |
| 6.3.1 Petrography and types..... | 126 |
| 6.3.2 Microthermometry | 126 |
| 7 Discussion | 127 |
| 7.1 Timing of magma emplacement and Cu-Sn mineralization | 127 |
| 7.2 Source and fluid evolution..... | 128 |
| 7.2.1 Source of ore-forming materials..... | 128 |
| 7.2.2 Fluid evolution..... | 128 |
| 7.3 Mineralization process and ore genesis | 129 |

| | |
|---|------------|
| 8 Conclusions | 130 |
| Reference..... | 131 |
| Chapter 7 Iron isotope fractionation during supergene weathering process and its application to constrain ore genesis in Gaosong deposit, Gejiu District, SW China..... | 133 |
| 1 Introduction..... | 134 |
| 2 Geological background | 135 |
| 3 Sampling and Analytical methods..... | 139 |
| 3.1 Sampling..... | 139 |
| 3.2 Sample preparation | 141 |
| 3.3 Mass spectrometry | 141 |
| 4 Results | 142 |
| 4.1 Primary skarn-sulfide samples | 142 |
| 4.2 Oxidized samples | 143 |
| 4.3 Fe isotope compositions of gossan samples..... | 143 |
| 5 Discussions | 143 |
| 5.1 Fe isotope fractionation during supergene weathering process..... | 144 |
| 5.2 Link between Fe isotopic compositions and mineralogy..... | 147 |
| 5.3 Fe source tracing by Fe isotopes | 148 |
| 6 Summary and conclusion..... | 149 |
| Reference..... | 150 |
| Chapter 8 Correlated cathodoluminescent textures, trace element chemistry and geochronology of cassiterite (SnO₂): Provenance studies on Sn mineralization in a world class tin district..... | 154 |
| 1 Introduction..... | 155 |
| 2 Geological background | 157 |
| 3 Sampling strategy and analytical techniques | 159 |
| 3.1 Sampling strategy | 159 |
| 3.2 Analytical methods..... | 162 |
| 3.2.1 SEM-CL | 162 |

| | |
|--|------------|
| 3.2.2 LA-ICP-MS | 162 |
| 4 Results | 163 |
| 4.1 Micro-textures and crystal size variations..... | 163 |
| 4.2 Trace elements quantitative analysis by LA-ICP-MS..... | 165 |
| 4.2.1 Cassiterite trace elements in different mineralization environments | 165 |
| 4.2.2 Trace element distribution in single cassiterite crystal..... | 166 |
| 4.3 LA-ICP-MS U-Pb dating..... | 168 |
| 5 Discussion | 170 |
| 5.1 Relations between micro-textures and trace elements..... | 170 |
| 5.2 Trace elements variation and substitution in cassiterite | 171 |
| 5.3 Cassiterite U-Pb dating in Gejiu district and significance..... | 176 |
| 5.4 Insights into ore genesis and mineralization process in Gejiu tin district | 177 |
| 6 Conclusions | 179 |
| 7 Reference | 180 |
| Chapter 9 Summary and Conclusion..... | 189 |
| Appendix..... | end |



List of Tables



List of Tables

Chapter 2 Age and Geochemistry of Granites in Gejiu area, Yunnan province, SW China: Constraints on their petrogenesis and tectonic setting

Table 1 Information about the samples for zircon U–Pb dating and In-situ zircon Hf analysis. 39

Table 2 Summary of the ages of the mineralization and magmatism in the west Cathaysia block 48

Chapter 4 The origin of the world class tin-polymetallic deposits in the Gejiu district, SW China: constraints from metal zonation characteristics and ⁴⁰Ar-³⁹Ar geochronology

Table 1 ⁴⁰Ar-³⁹Ar Dating Results of Gejiu Tin-Copper Deposits..... 89

Chapter 5 Geology and vein tin mineralization in the Dadoushan deposit, Gejiu district, SW China

Table 1 Characteristics of cassiterite from Dadoushan open pit, Gejiu district, SW China.....110

Chapter 6 Geology and genesis of Kafang Cu-Sn deposit, Gejiu district, SW China

Table 1 Classification and characteristics of samples124

Table 2 Characteristics and parameters of primary fluid inclusion in Kafang Cu–Sn deposit.....124

Table 3 Lead isotope compositions of samples from the Kafang Cu–Sn deposit 125

Table 4 Zircon LA-ICP-MS dating results of the Xinshan granite.....125

Table 5 Molybdenite Re–Os dating results of Kafang ore field.....126

Table 6 Composition of sulfur isotope in the Kafang copper deposit128

Table 7 Hydrogen and oxygen isotopes composition of Kafang copper deposit..128

Table 8 Abundance of Cu in different rocks in Gejiu ore district ($\omega\text{B}/10^{-6}$)131

List of Figures

List of Figures

Chapter 2 Age and Geochemistry of Granites in Gejiu area, Yunnan province, SW China: Constraints on their petrogenesis and tectonic setting

| | |
|--|----|
| Figure 1 (a) Simplified geological map of eastern Eurasia, showing major tectonic units. (b) Distribution of tin deposits in the Cathaysia block. (c) Sketch map showing the geology and the distribution of tin–polymetallic deposits in the Gejiu ore district.. | 36 |
| Figure 2 Hand samples and microphotographs of granites from the Gejiu area. | 38 |
| Figure 3 Internal structure of zircon grains shown by the cathodoluminescence (CL) analysis. | 39 |
| Figure 4 Single grain U–Pb zircon ages of Gejiu granites. | 40 |
| Figure 5 QAP, ANK versus ACNK diagram and (K_2O+Na_2O) versus SiO_2 diagram for Gejiu granitic rocks. | 41 |
| Figure 6 Harker diagrams for the Gejiu granites | 42 |
| Figure 7 Chondrite-normalized REE patterns and primitive-normalized incompatible element spider-diagrams for the Gejiu granites..... | 43 |
| Figure 8 Zircon Lu–Hf isotopic compositions of the studied granites from the Gejiu pluton | 44 |
| Figure 9 Characteristics of Gejiu granites resulting from fractional crystallization . | 45 |
| Figure 10 Nd and Sr isotopic variation diagram | 46 |
| Figure 11 Nd and Hf model ages of the Gejiu granitic rocks | 47 |
| Figure 12 Hf isotope evolution diagram..... | 48 |
| Figure 13 Summary of the published and new geochronologic determinations for the western Cathaysia block..... | 49 |
| Fig. 14 $(Al_2O_3+CaO) / (FeO^*+Na_2O+K_2O)$ vs. $100(MgO+FeO^*+TiO_2)/SiO_2$, $(Na_2O+K_2O) / CaO$ vs. $(Zr+Nb+Ce+Y)$, Y vs. Rb, Y vs. SiO_2 diagrams and A-type granite discrimination for the Gejiu granitic rocks..... | 50 |
| Figure 15 Zr versus SiO_2 and DI versus T_{Zr} diagrams | 51 |

Chapter 3 Granite, gabbro and mafic microgranular enclaves in the Gejiu Area, Yunnan Province, China: a case of two stage mixing of crust- and

mantle-derived magmas

| | |
|--|----|
| Figure 1 Geological map of Gejiu district | 57 |
| Figure 2 Field photographs of the associated gabbro–MME–granite rocks | 59 |
| Figure 3 Cross-polarized light photomicrographs of granite, MME, and gabbro from Gejiu district..... | 60 |
| Figure 4 Zircon U–Pb age data for the Jiasha Gabbro, MME, and Longchahe Granite..... | 61 |
| Figure 5 SiO ₂ versus K ₂ O+Na ₂ O of the gabbro–MME–granite association in Gejiu area | 62 |
| Figure 6 A/NK versus A/CNK of the gabbro–MME–granite association in Gejiu area | 63 |
| Figure 7 Harker plots (SiO ₂ vs. major elements) of the gabbro–MME–granite association in Gejiu area | 64 |
| Figure 8 SiO ₂ versus trace elements of the gabbro–MME–granite association in Gejiu area..... | 65 |
| Figure 9 Primitive mantle-normalized trace elements and chondrite normalized REE variation diagrams of the gabbro–MME–granite association in Gejiu area.... | 66 |
| Figure 10 Histograms of zircon eHf(t) values of the gabbro–MME–granite association in Gejiu area | 66 |
| Figure 12 SiO ₂ versus (⁸⁷ Sr/ ⁸⁶ Sr) _i and SiO ₂ versus e _{Nd} diagrams of the gabbro–MME–granite association in Gejiu area..... | 66 |

Chapter 4 The origin of the world class tin-polymetallic deposits in the Gejiu district, SW China: constraints from metal zonation characteristics and ⁴⁰Ar-³⁹Ar geochronology

| | |
|--|----|
| Figure 1 simplified geological map of the Gejiu ore district..... | 77 |
| Figure 2 Cross sections of the five deposits in the Gejiu district that show the spatial relationship of granite, orebodies and host rocks | 80 |
| Figure 3 Horizontal and vertical metal zoning patterns in the Gejiu district..... | 86 |
| Figure 4 Photographs showing field characteristics, mineral associations, mica analyzed in this study and their relationships with other intergrowth minerals from the Gejiu ore district..... | 88 |
| Figure 5 ⁴⁰ Ar- ³⁹ Ar age spectra of muscovite and phlogopite separates from the Gejiu tin polymetallic district, SW China..... | 91 |

Figure 6 Spatial-temporal relationships between granites and orebodies in the Gejiu mining district.....93

Chapter 5 Geology and vein tin mineralization in the Dadoushan deposit, Gejiu district, SW China

Figure 1 a Simplified geological map of eastern Asia, showing major tectonic units. b Distribution of tin deposits in the Cathaysia block. c Sketch map showing the geology and the distribution of tin–polymetallic deposits in the Gejiu ore district. 104

Figure 2 Location and geology of Dadoushan open pit and crosscutting section. 106

Figure 3 Vein-type ore photographs showing their field characteristics 108

Figure 4 Various types of veins in the Dadoushan area, Gejiu district..... 109

Figure 5 Vertical zonation of the vein mineralization in the Dadoushan open pit, Gejiu district..... 109

Figure 6 ^{40}Ar – ^{39}Ar age spectrum of muscovite from the Dadoushan open pit, Gejiu district 111

Figure 7 $\delta^{34}\text{S}$ distribution of different ore-related units of the Dadoushan open pit, Gejiu district..... 112

Figure 8 δD (‰)– $\delta^{18}\text{O}_{\text{H}_2\text{O}}$ (‰) plot of quartz from different ore veins in the Dadoushan open pit, Gejiu district 113

Figure 9 Schematic cartoon illustrating the formation of the vein type ores and their mineralization process in the Dadoushan area, Gejiu district 113

Chapter 6 Geology and genesis of Kafang Cu-Sn deposit, Gejiu district, SW China

Figure 1 (a) Simplified geological map of eastern Asia, showing major tectonic units. (b) Distribution of tin deposits in the Cathaysia block. (c) Sketch map showing the geology and the distribution of tin-polymetallic deposits in the Gejiu ore district.. 118

Figure 2 Geology of Kafang ore field and geological section..... 119

Figure 3 Schematic profile of the contact of granite, skarn and carbonate, including photographs of main alteration and mineralization styles in the profile 120

Figure 4 Schematic profile of the contact of granite, carbonate and skarn, including photographs of the main alteration and mineralization styles in the profile 121

| | |
|---|-----|
| Figure 5 Photographs of the main alteration and mineralization styles in the stratiform Cu ore hosted by basalt | 122 |
| Figure 6 Schematic profile of the manto type deposit hosted by carbonate, including photographs of the main alteration and mineralization styles in the profile | 123 |
| Figure 7 U–Pb isochron of zircon from Xinshan granite | 126 |
| Figure 8 Re–Os isochron of molybdenites from skarn and basalt hosted stratiform Cu ores | 127 |
| Figure 9 Characteristics of fluid inclusions from Kafang copper deposit | 129 |
| Figure 10 Histogram of fluid inclusion homogenization temperatures of the Kafang copper deposit | 130 |
| Figure 11 Diagram of lead isotope composition of the Kafang copper deposit | 130 |
| Figure 12 $\delta^{34}\text{S}$ distribution of the different ore-related units of the Kafang copper deposit | 130 |
| Figure 13 $\delta\text{D}(\text{‰})-\delta^{18}\text{O}_{\text{H}_2\text{O}}(\text{‰})$ plot of Kafang copper deposit. | 131 |
| Chapter 7 Iron isotope fractionation during supergene weathering process and its application to constrain ore genesis in Gaosong deposit, Gejiu District, SW China | |
| Figure 1 Sketch geological map of the Gejiu district, Yunnan Province, SW China | 135 |
| Figure 2 Representative cross section of the Gaosong deposit in Gejiu district .. | 136 |
| Figure 3 Typical hand specimen from the Gaosong deposit..... | 137 |
| Figure 4 Typical microscope images from the Gaosong deposit showing different oxidization degrees of the sample in this study | 140 |
| Figure 5 $\delta^{57}\text{Fe}$ versus $\delta^{56}\text{Fe}$ plot showing that all the Fe-isotope data of the samples in this study plot on a single mass-fractionation line | 142 |
| Figure 6 Fe isotopes of three different types of samples from the Gaosong deposit | 144 |
| Figure 7 Fe isotopes of various oxidation degrees of the oxidized ores from Gaosong deposit..... | 145 |
| Chapter 8 Correlated cathodoluminescent textures, trace element chemistry | |

and geochronology of cassiterite (SnO₂): Provenance studies on Sn mineralization in a world class tin district

| | |
|--|-----|
| Figure 1 Ionic charge against ionic radius (Shannon, 1976) for elements investigated in this study..... | 156 |
| Figure 2 Geological map and of the Gejiu ore district and the cross section of the mining district | 158 |
| Figure 3 Representative cross section of the Gejiu ore district..... | 160 |
| Figure 4 Six types of representative mineralization environments of the Gejiu ore district | 160 |
| Figure 5 Microscope images showing the intergrowth of K-feldspar, quartz and cassiterite | 161 |
| Figure 6 Selected cathodoluminescence (CL) images of the six types of cassiterite samples..... | 164 |
| Figure 7 X-Y plots showing the variations of some trace elements hosted by cassiterite from Gejiu ore district | 166 |
| Figure 8 Trace elements distribution in single cassiterite crystal, examples from greisen and tin granite sample | 167 |
| Figure 9 LA-ICP-MS cassiterite U–Pb age data for the seven samples from Gejiu ore district..... | 168 |
| Figure 10 Systematic variations of Zr/Hf ratios of the samples in this study | 172 |
| Figure 11 Positive correlations between Sc and V exhibit in all the six types of samples..... | 173 |
| Figure 12 3+ and 5+ charge balance calculation diagrams of cassiterite from the Gejiu ore district | 175 |
| Chapter 9 Summary and Conclusion | |
| Figure 1 Simplified illustration showing the magma generation and formation processes in the Gejiu district, as well as major controlling factors of the mineralization in this area | 190 |

Chapter 1

Introduction and Background

1 Thesis introduction

It is intended that the entire contents of this thesis (with the exception of this Introduction and the Summary and Conclusions chapter) will be published in internationally-recognized Earth Science journals. At the time of submission, Chapters 2, 3, 4 and 5 have already been published following rigorous peer review as part of publication process, and the Chapter 6 has been accepted by Ore Geology Reviews very recently, but I have not received the volumed version yet, thus I still keep it in its original format. According to the “**Thesis formats allowed at James Cook University**”, a published paper or an accepted manuscript “... can form a single chapter (or several papers may form successive chapters) without any editing”. Therefore the Chapters 2 to 5 are presented in this thesis in their published journal formats. Structuring of this thesis in this manner has inevitably led to repetition of some descriptive text, such as the Geological Setting and Analytical Techniques sections, and duplication of references between the reference lists of each chapter. However, it should be noted that the analytical methods used vary from chapter to chapter, and their geological backgrounds presented in each chapter do vary in order to emphasize on different aspects of relevance to that specific chapter. Most of the analytical data obtained in this study has been attached as an Electronic Appendix in the CD in the end of this thesis.

In this thesis I discuss the geology, geodynamic evolution and mineral resource in the world class Gejiu Sn-Cu-Pb-Zn District. Following this introductory chapter, the thesis comprises nine chapters, that can be considered as a stand-alone research work, but all of the chapters are related to the central theme of this thesis; “*Geological Evolution of the World Class Gejiu Ore District, SW China: Information from Magmatism, Mineralization and Microanalysis Studies*”.

Following this introductory chapter, the thesis first focusses on the petrology and petrogenesis of the granites in the study area. **Chapter 2** present geochronological data on 9 samples from two phases of Gejiu granitic intrusions, yielding ages ranging from 77.4 ± 2.5 Ma to 85.0 ± 0.85 Ma. Whole rock major and trace element analysis and

Nd-Hf isotopic characteristics indicate that the Gejiu granite magmas were possibly derived from partial melting of Mesoproterozoic continental crust, with minor input of mantle-derived melts, followed by extensive fractional crystallization.

In **Chapter 3**, I described the petrology of the gabbro, mafic microgranular enclaves and related granite in the Gejiu area. Combined with geochronological, geochemical, whole-rock Sr–Nd and zircon Hf isotopic analyses, it is suggested that the Jiasha gabbro derived from a mantle source that had undergone previous enrichment, possibly by subduction components, while the related granite have formed via mixing between crustally-derived peraluminous leucogranite magma and mantle-derived magma of similar heritage to the Jiasha Gabbro. Mingling and mixing processes within the convectively dynamic upper crustal magma chamber resulting in hybrid (MME) magma. Furthermore, element inter-diffusion is interpreted to be the dominant mixing process.

For **Chapter 4**, I describe the detailed ore deposit geology, and document the well developed metal zonation both vertically and horizontally over the entire district, from W+Be+Bi ± Mo ± Sn ores inside granite intrusions, to Sn+Cu-dominated ores at intrusion margins and farther out to Pb+Zn deposits in the surrounding host carbonate. This chapter also presents 13 mica Ar-Ar ages, which range from 77.4±0.6 Ma to 95.3±0.7 Ma, indicate genetic relationship between the mineralization and the intrusions. These data all indicate that the tin-polymetallic ores in the Gejiu district are hydrothermal in origin and are genetically related to the nearby granitic intrusions.

In **Chapter 5**, vein-type Sn mineralization in the Dadoushan deposit is studied. Muscovite Ar-Ar dating yielded a plateau age of 82.7±0.7 Ma which defines the age of the vein-type mineralization. Measured sulfur isotope compositions indicate that the sulfur in veins is mainly derived from a magmatic source. The sulfur isotope values of the ores are consistent with those from the underlying granite, but are different from the carbonate wall rocks of the Gejiu Formation. The oxygen and hydrogen isotope compositions of the ore-forming fluids suggest an initially magmatic fluid which gradually evolved towards meteoric water during tin mineralization.

Three types of Cu-Sn mineralization are discussed in **Chapter 6**, i.e., skarn

Cu-Sn ores, stratiform Cu ores hosted by basalt and stratiform Cu-Sn ores hosted by carbonate. Sulfur and Pb isotopic components hint that the sources of different types of mineralization are distinctive, and indicate that the skarn ore mainly originated from granitic magma, whereas the basalt-hosted Cu ores mainly derived from basalt. Microthermometry data and H-O isotopes indicate that the ore-forming fluid mainly derived from magma in the early stage and a mixture of meteoric and magmatic water in late stage. Molybdenite Re-Os ages of the skarn type mineralization and the stratiform ores hosted by basalt are consistent with the age of the related granite intrusion. The evidence listed above reflects the fact that different ore styles in the Kafang deposit belong to the same mineralization system.

Fe isotope compositions of bulk samples from Gaosong ore deposit were presented in **Chapter 7**. In this study, the $\delta^{57}\text{Fe}$ values of primary sulfide ores are lower than the oxidized ores, while the iron isotope compositions of gossan samples, which represent highest oxidation degree, are heavier than the oxidized ore samples. These data indicate that iron isotopes experienced fractionation during supergene weathering processes. Furthermore, heavier iron isotopes are enriched in the more oxidized products. Fe isotope compositions are shown to be affected by mineralogy, which is considered as the primary mechanism of the large Fe isotopic variations in the primary ores. Enrichment of light iron isotopes in primary sulfides ores suggests iron isotopes fractionated during fluid exsolution from its parental magma and the Fe source of skarn ores is mainly the magmatic source.

One of most important aspects of my PhD studies is the microanalysis on cassiterite, which is presented in **Chapter 8**. Cassiterite of 6 different mineralization environments from the Gejiu tin district was investigated using a combination of microscopy techniques and LA-ICP-MS. A range of CL images, LA-ICP-MS U-Pb ages, and high precision trace element concentration data were analyzed. The combined geochemical and textural data may reflect temperature, oxygen fugacity and redox state of ore forming fluids experienced significant changes during mineralization process. Cassiterite U-Pb geochronology results obtained by LA-ICP-MS return ages between 79 Ma to 84 Ma, which is consistent with previous

U/Pb zircon geochronology from the region. The cassiterite CL image, LA-ICP-MS trace element and U-Pb dating results show it is highly possible that cassiterite can be used as a trace element indicator and geochronometer of mineralizing systems.

Chapter 9 concludes the entire thesis with an overview on all the findings and suggestions for further research directions.

2 Study background

The Gejiu, the largest tin ore-field in the world and been well known as the “tin capital of China”, located in the southeast of Yunnan Province, China with reserves of more than 300 Mt Sn ores, 300 Mt Cu ores and 400 Mt Pb+Zn ores.

Gejiu is located at the western end of the Cathaysia block, adjacent to the Yangtze Craton to the northwest and the Red River Fold Belt in the southwest. The main sedimentary sequences exposed in the ore field are carbonate rocks, clastic rocks and basalts of Permian-Triassic age. Carbonates of the mid-Triassic Gejiu and Falang Formations are the most important ore-hosting strata. Numerous faults dissect the Gejiu district. Most ore bodies are located east of the N-trending Gejiu fault, which divides the district into two parts. A group of E-trending faults with their subordinate fractures are the most important ore-controlling structures. The Mesozoic magmatic rock association in the Gejiu area comprises gabbro, diorite, alkali-feldspar granite, porphyritic biotite granite, equigranular biotite granite, syenite and lamprophyre. Ore-related magmas are Late Cretaceous granitoids.

Studies on this region extend back for over 100 years. During the past 30 years, scientists have focused their attention on the genesis of the Gejiu tin-copper deposits, but different ideas have been proposed on the genesis of these ores in different stages. The most representative ideas are summarized as following. Hypothesis I: granite-related hydrothermal origin. Hypothesis II: syngenetic stratiform oxidized Sn ore of Triassic age. Hypothesis III: Triassic syngenetic mineralization (VMS + SEDEX), with some oorebodies, such as the skarn ores and the greisen ores, formed by the emplacement of the Cretaceous granite.

This research work will focus on resolving the debate around the formation of the orebodies and their association with neighbouring granitic rocks of the region, and the related magmatism process and the corresponding geodynamic setting.

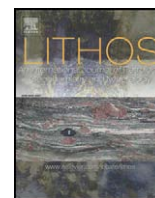
Chapter 2

Age and Geochemistry of Granites in Gejiu area: Constraints on their petrogenesis and tectonic setting



Contents lists available at ScienceDirect

Lithos

journal homepage: www.elsevier.com/locate/lithos

Age and geochemistry of granites in Gejiu area, Yunnan province, SW China: Constraints on their petrogenesis and tectonic setting

Cheng Yanbo ^a, Mao Jingwen ^{a,b,*}^a Faculty of Earth Science and Mineral Resources, China University of Geosciences, Beijing, 100083, PR China^b MLR Laboratory of Metallogeny and Mineral Assessment, Institute of Mineral Resources, Chinese Academy of Geological Sciences, Beijing, 100037, PR China

ARTICLE INFO

Article history:

Received 3 March 2010

Accepted 7 August 2010

Available online 20 August 2010

Keywords:

Gejiu granite

U–Pb zircon ages

Geochemistry

Sr–Nd–Hf isotopes

Gejiu

SE China

ABSTRACT

Gejiu is one of the largest polymetallic tin ore districts in the world. Located at the westernmost end of the South China tungsten–tin province (or Nanling tungsten–tin province), it is a granite-related (Gejiu granite) magmatic-hydrothermal system. Nine samples from two phases of Gejiu granitic intrusions have been analyzed by SHRIMP and/or LA-ICPMS zircon U–Pb techniques, yielding ages ranging from 77.4 ± 2.5 Ma to 85.0 ± 0.85 Ma. Whole rock analysis shows that both phases are high-K and alkali-rich granites and their ACNK values fall mainly into a small range of 1.0–1.1. Moreover, Harker diagrams indicate that granites experienced strong fractional crystallization during magmatic evolution. Most granites display relative enrichment in LREE and strong Eu depletion. The whole rock average $\epsilon_{\text{Nd}}(t)$ values of the Gejiu granites vary from -9.3 to -6.9 , whereas a range of $-8.12 < \epsilon_{\text{Hf}}(t) < 1.21$ is defined by magmatic zircons. Sr–Nd–Hf isotope data indicate that the granites have been mainly derived from crustal melts with minor input of mantle component. Two stage Nd and Hf model ages, together with isotopic characteristics, indicate that the Gejiu granite magmas were possibly derived from partial melting of Mesoproterozoic continental crust, with minor input of mantle-derived melts, followed by extensive fractional crystallization.

© 2010 Published by Elsevier B.V.

1. Introduction

Gejiu is the largest polymetallic tin ore field in the world (~300 Mt @ 1% Sn, and ~700 Mt of Cu, Pb, Zn, Sb, Ag, Mo, Au and Bi, Southwest Geological Exploration Corporation, 1984; Chen et al., 1992; Jiang et al., 1997; Mo, 2006). Gejiu is located in south-eastern Yunnan and western Guangxi Sn–W province, at the western end of the South China Sn–W province (Chen and Zhu, 1993; Mao et al., 2008a,b; Cheng et al., 2009). This ore field has previously been considered to be genetically associated with Late Cretaceous granitoid intrusions (Feng, 1982; Wang, 1983; Chen, 1983; 308 Geological Party, 1984; Wu et al., 1984; Peng, 1985; Li, 1985; Yu et al., 1988; Dai, 1996; Zhuang et al., 1996; Xu and Li, 1997; Mo, 2006; Wang et al., 2007; Mao et al., 2008a,b; Cheng et al., 2009). Although a number of research studies about granite ages and geochemistry had been carried out since the 1980 s, limitation of the analytical techniques and lack of systematic geochemical studies resulted in conflicting conclusions by different authors (Li, 1985; Mo, 2006; Wang et al., 2007).

In this paper we provide systematic geochemical data, LA-ICP-MS and SHRIMP zircon U–Pb, Sr–Nd, and in-situ zircon Hf isotopic data for

Gejiu granites in order to constrain the granite source, fractionation, petrogenesis and tectonic setting of the intrusions.

2. Regional geology and geological characteristics of the Gejiu granitic intrusions

2.1. Geological setting

The Gejiu granitic intrusions and related ore deposits are located in the junction area of the Eurasian, Pacific, and Indian plates, adjacent to the Yangtze Craton in the north and to the Three Rivers fold belt in the west (Fig. 1). The Gejiu ore field is in an area of long-lived depression filled by 3000 m of Middle Triassic carbonate rocks consisting of the Gejiu Formation and the Falang Formation that are the dominant strata in the ore field. The former comprises mainly carbonates that include dolomite, dolomitic limestone and minor littoral limestone. The latter is a gypsum-bearing algal carbonate deposited in a semi-enclosed bay and resembling a lagoon or sabkha facies. The NS-trending Gejiu Fault divides the ore field into two parts, eastern and western. Three NNE-trending faults, named Longchahe, Jiaodingshan and Yangjiatian in the western part, and the NW-trending Baishachong fault in the eastern part, are the main structures in the ore field. Six parallel NE to E–W trending district-scale faults, named Songshujiao, Beiyingshan, Mengzimiao, Laoxiongdong, Xianrendong and Bailong in the eastern part are the most important structures that

* Corresponding author. Faculty of Earth Science and Mineral Resources, China University of Geosciences, Beijing, 100083, PR China. Tel.: +86 10 68999037.

E-mail address: jingwenmao@263.net (M. Jingwen).

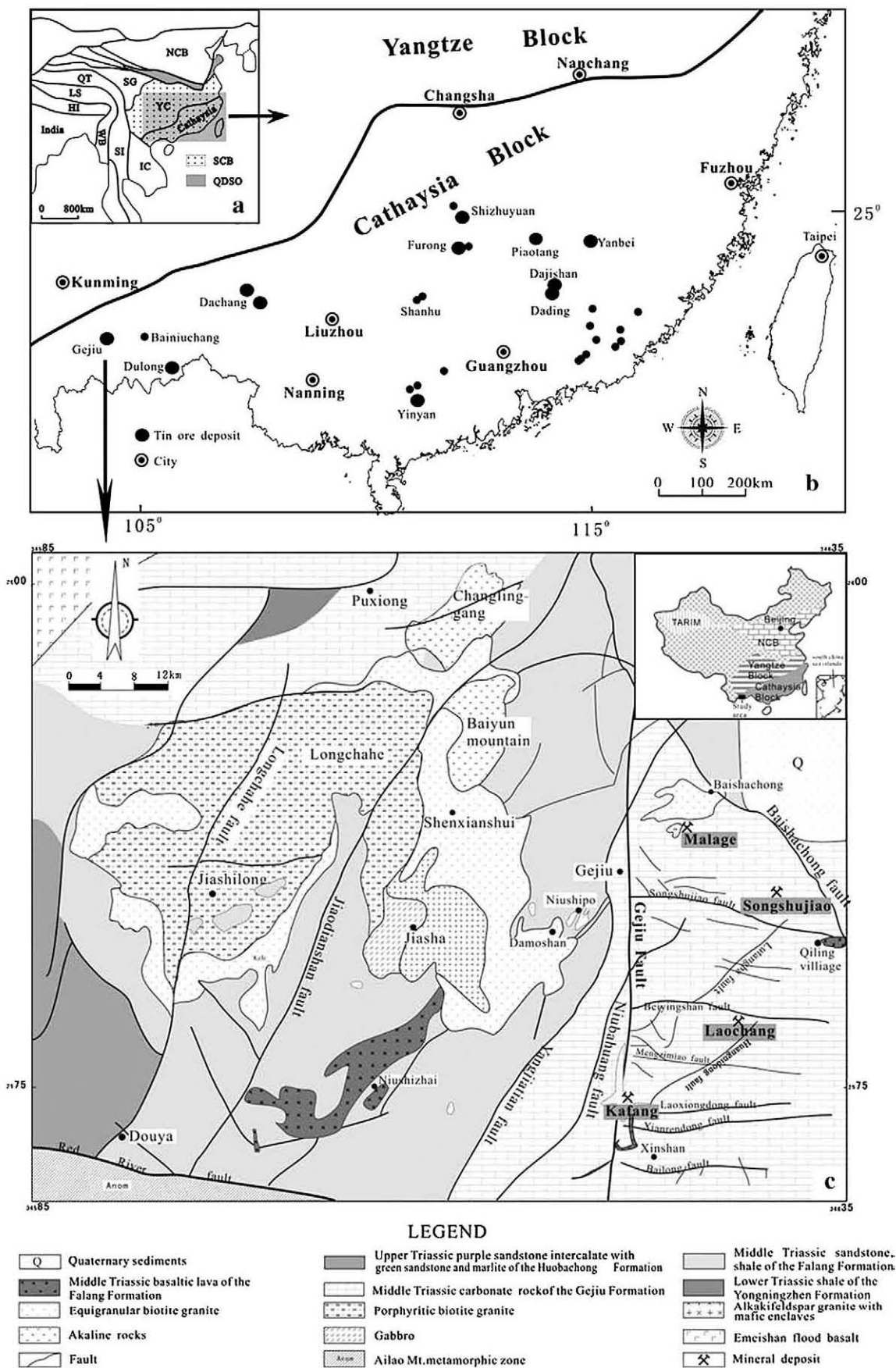


Fig. 1. (a) Simplified geological map of eastern Eurasia, showing major tectonic units (Wang et al., 2005). (b) Distribution of tin deposits in the Cathaysia block (Mao et al., 2004). (c) Sketch map showing the geology and the distribution of tin-polymetallic deposits in the Gejiu ore district (after 308 Geological Party, 1984). SCB = South China Block; NCB = North China Block; YC = Yangtze Craton; IC = Indochina Block; SI = Sibumasu Block; G = Songpan–Ganze Accretionary Complex; WB = West Burma; Hi = Himalayas; LS = Lhasa; QT = Qiangtang.

control the emplacement of granite intrusions and mineralization (Fig. 1). Granitic rocks in the Gejiu area include alkali-feldspar granite, porphyritic biotite granite and equigranular biotite granite. The granitoids are distributed throughout the area and the tin-polymetallic deposits are associated with the intrusions in space and time.

2.2. Granite petrography and sampling

Granitic rocks are the dominant, widely distributed magmatic rocks in the Gejiu area. Two distinct textural phases can be recognized: porphyritic and equigranular. The porphyritic granite variety includes mainly the Longchahe intrusion, the Malage-Songshujiao intrusion, and the Laochang intrusion exposed in underground workings. Porphyritic granite also forms a major portion of the Longchahe intrusion in the western part of the ore field. With an outcrop area of about 200 km², this is the largest granite body in the ore field. In the eastern part of the ore field porphyritic granites are sparsely distributed, outcropping only in a small area at Beipaotai, north of the Malage deposit. The country rock intruded by the Longchahe granite is part of the Falang Formation, whereas the remaining intrusions are emplaced into the Gejiu Formation (Fig. 1). The main rock-forming minerals in porphyritic granites include K-feldspar (33%), plagioclase (31%), quartz (26%) and biotite (8%). Accessory minerals are titanite, magnetite, ilmenite, allanite, zircon and monazite. Phenocrysts include K-feldspar, plagioclase and quartz. The K-feldspar has two varieties. The first forms grayish white to yellowish, euhedral to subhedral thick tabular megacrysts ranging in size between 3–5 cm, with some individuals more than 10 cm in length. The proportion of megacrysts is about 20%. The second variety of large feldspar megacrysts encloses 0.3–1 cm large grains of plagioclase, quartz and biotite. The feldspar crystals are tabular, with common Carlsbad twins and irregular perthitic textures. The groundmass is composed of plagioclase, K-feldspar, quartz and biotite the proportions of which vary in different rock bodies (Fig. 2).

The equigranular granite is mostly distributed in deep underground workings and only sporadically crops-out in the Gejiu ore field, mainly in the Shenxianshui area in its western part, and in the Baishachong, south Laochang, and Xinshan areas in its eastern part. A sharp contact between the porphyritic and the equigranular granites, lacking distinctive chilled margins, has been observed in the Laochang ore deposit. All these granites intrude the Gejiu Formation. The Shenxianshui and Baishachong granite intrusions are strongly weathered so that it is difficult to obtain fresh samples for geochemical and isotopic analysis. The main rock forming minerals of the equigranular granites are microcline (38%), plagioclase (27%), quartz (30%) and biotite (3%). The accessory minerals are zircon, apatite, titanite, magnetite, ilmenite, allanite, monazite, tourmaline and fluorite. Zircon is the main species among the accessory minerals. Compared with the porphyritic granite, the proportion of hydrothermal fluorite, tourmaline, topaz and muscovite in equigranular granites is much higher (Fig. 2).

Nine samples were selected for dating to constraint the ages and to determine the Lu–Hf isotopic composition of these granitic intrusions (Supplementary Table 1 and Table 2). An additional 59 samples were selected from different intrusions for major and trace element analysis (Supplementary Tables 2 and 3), and 25 samples were collected for Sr and Nd isotope analysis (Supplementary Table 3). Locations of samples for zircon U–Pb dating and for in-situ zircon Hf analyses are listed in Table 1 and shown in Fig. 1.

3. Analytical methods

3.1. SHRIMP and LA-ICP-MS U–Pb zircon dating

Zircons for analysis were separated from 5–15 kg bulk samples, using conventional heavy liquid and magnetic techniques. Represent-

tative zircon grains were handpicked under a binocular microscope, mounted in epoxy resin, polished, coated with gold, and mounted. The mounts were photographed in transmitted and reflected light, and cathodoluminescence (CL) was used to examine the internal structure of the analyzed zircons (Fig. 3).

The U–Pb isotopic analyses were performed using the SHRIMP-II (Sensitive High-Resolution Ion Microprobe) at the Chinese Academy of Geological Sciences, Beijing (Supplementary Table 1), following the procedure described in detail by Compston et al. (1992), Williams (1998) and Song et al. (2002). Single crystals were dated without air abrasion. The U–Pb isotope data were determined in sets of five scans throughout the masses, and every three or four unknown zircon grains in one sample were bracketed with values for the reference zircon TEM (417 Ma). The age uncertainties are cited as 1 σ , and the weighted mean ages are quoted at the 95% confidence level (2 σ).

Laser ablation techniques were used for additional age determinations (Supplementary Table 1). The U–Pb isotopic analyses were performed using the Elan 6100 DRC ICP-MS equipped with a 193 nm Excimer laser. Zircon 91500 was used as a standard and NIST 610 was used to optimise the instrument. A mean age of 1060 Ma was obtained for the 91500 zircon standard. The spot diameter was 30 μ m. Corrections for common lead were made using the method of Anderson (2002). The data were processed using the GLITTER and ISOPLOT (Ludwig, 2003) programs. Errors in individual LA-ICP-MS analyses are quoted at the 95% (1 σ) confidence level. Details of the analytical procedures are described by Yuan et al. (2003). All determinations were done at the State Key Laboratory for Mineral Deposit Research, Nanjing University.

3.2. Major and trace elements

Geochemical analyses were carried out at the Guangzhou Institute of Geochemistry, Chinese Academy of Sciences. Major element oxides were analyzed using a Rigaku RIX 2000 X-ray fluorescence spectrometer (XRF) on fused glass beads. Calibration lines used in quantification were produced by bivariate regression of data from 36 reference materials encompassing a wide range of silicate compositions (Li et al., 2005), and analytical uncertainties are mostly between 1% and 5%. Trace elements were analyzed using the Perkin-Elmer Sciex ELAN 6000 ICPMS, and the analytical procedures are similar to those described by Li (1997). About 50 mg of powdered sample was dissolved in high-pressure Teflon bombs using a HF + HNO₃ mixture. Rh was used as an internal standard to monitor signal drift during counting. The USGS rock standards GSP-1, G-2, W-2 and AGV-1 and the Chinese national rock standards GSR-1 and GSR-3 were chosen for calibrating element concentrations of the measured samples. Analytical uncertainties were generally less than 5% (Supplementary Table 2).

3.3. Sr and Nd isotopes

Sr and Nd isotopic analyses were performed using a Micromass Isoprobe multi-collector ICPMS at the Guangzhou Institute of Geochemistry, CAS, using analytical procedures described by Wei et al. (2002) and Li et al. (2004). Sr and REE were separated using cation columns, and Nd fractions were further separated by HDEHP-coated Kef columns. The mass fractionation corrections for ⁸⁷Sr/⁸⁶Sr and ¹⁴³Nd/¹⁴⁴Nd ratios were normalized to ⁸⁷Sr/⁸⁶Sr = 0.1194 and ¹⁴³Nd/¹⁴⁴Nd = 0.7219, respectively. The reported ⁸⁷Sr/⁸⁶Sr and ¹⁴³Nd/¹⁴⁴Nd ratios were adjusted, respectively, to the NBS SRM 987 standard ⁸⁷Sr/⁸⁶Sr = 0.71025 and the Shin Etsu JNdi-1 standard ¹⁴³Nd/¹⁴⁴Nd = 0.512115. The results, along with the calculated initial ⁸⁷Sr/⁸⁶Sr (*I*_{Sr}) and $\epsilon_{Nd}(t)$ values, are listed in Data Repository Supplementary Table 3.

Fig. 2. Hand samples and microphotographs of granites from the Gejiu area. LCH – Longchahe granite, BSC – Baishachong granite, LCB – Laochang porphyritic granite, MS – Malage and Songshujiao porphyritic granite, SXS – Shenxianshui equigranular granite, XS – Xinshan equigranular granite, LCL – Laochang equigranular granite.

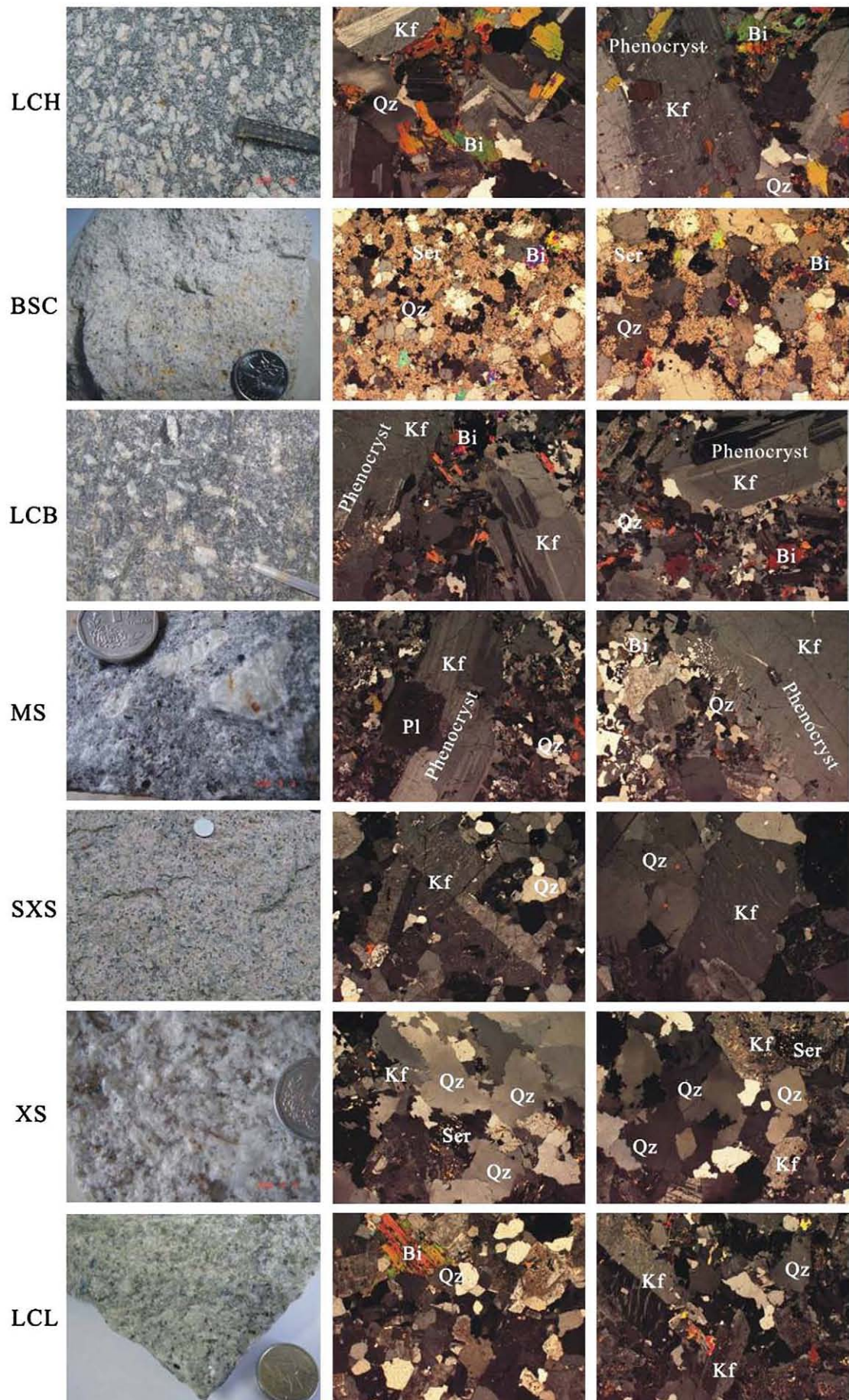


Table 1
Information about the samples for zircon U–Pb dating and In-situ zircon Hf analysis.

| Order | Sample number | Name of the pluton | Location | Lithology | Method |
|-------|---------------|--------------------|--|----------------------|----------|
| 1 | CYB0707033 | Longchahe(LCH) | 23°18'34"N,103°03'03"E | Porphyritic granite | LA-ICPMS |
| 2 | CYB0807055 | Longchahe(LCH) | 23°20'52"N,102°58'02"E | Porphyritic granite | SHRIMP |
| 3 | CYB0707013 | Masong(MS) | 2# tunnel of Songshujiao ore field | Porphyritic granite | SHRIMP |
| 4 | CYB0807031 | Laoka(LCB) | Zhuyeshan tunnel of Laochang ore field | Porphyritic granite | SHRIMP |
| 5 | CYB0707032 | Baishachong(BSC) | 23°24'12"N,103°22'44"E | Equigranular granite | SHRIMP |
| 6 | CYB0707032 | Baishachong(BSC) | 23°24'12"N,103°22'44"E | Equigranular granite | LA-ICPMS |
| 7 | CYB0707020 | Shenxianshui(SXS) | 23°21'35"N,103°01'28"E | Equigranular granite | LA-ICPMS |
| 8 | CYB0807049 | Shenxianshui(SXS) | 23°21'29"N,102°56'56"E | Equigranular granite | LA-ICPMS |
| 9 | CYB0807022 | Xinshan(XS) | Dakeng tunnel of Kafang ore field | Equigranular granite | LA-ICPMS |
| 10 | D008 | Laochang(LCL) | Zhuyeshan tunnel of Laochang ore field | Equigranular granite | LA-ICPMS |



Fig. 3. Internal structure of zircon grains shown by the cathodoluminescence (CL) analysis.

3.4. Zircon Hf isotopes

Zircon Hf isotope analysis was carried out in-situ using a NewWave UP213 laser-ablation microprobe, attached to a Neptune multi-collector ICP-MS at Institute of Mineral Resources, Chinese Academy of Geological Sciences, Beijing. Instrumental conditions and data acquisition were comprehensively described by Hou et al. (2007) and Wu et al. (2006). A stationary spot was used for the present analyses, with a beam diameter of 55 μm . He, mixed with Ar, was used as a carrier gas to transport the ablated compound from the laser-ablation cell to the ICP-MS torch via a mixing chamber. In order to correct the isobaric interferences of ^{176}Lu and ^{176}Yb on ^{176}Hf , $^{176}\text{Lu}/^{175}\text{Lu} = 0.02658$ and $^{176}\text{Yb}/^{173}\text{Yb} = 0.796218$ ratios were determined (Chu et al., 2002). For instrumental mass bias correction Yb isotope ratios were normalized to $^{172}\text{Yb}/^{173}\text{Yb}$ of 1.35274 (Chu et al., 2002) and Hf isotope ratios to $^{179}\text{Hf}/^{177}\text{Hf}$ of 0.7325 using an exponential law. The mass bias behavior of Lu was assumed to follow that of Yb; the mass bias correction protocol details are described by Wu et al. (2006) and Hou et al. (2007). Zircon GJ1 was used as the reference standard during our routine analyses, with a weighted mean $^{176}\text{Hf}/^{177}\text{Hf}$ ratio of 0.282008 ± 19 (2σ , $n = 10$). It is not distinguishable from a weighted mean $^{176}\text{Hf}/^{177}\text{Hf}$ ratio of 0.282013 ± 19 (2σ) from the in-situ analysis

by Elhoul et al. (2006). The results, along with the relative calculated values, are listed in the Data Repository (Supplementary Table 4).

4. Analytical results

4.1. U–Pb zircon geochronology

Four samples (CYB0807032, CYB0807031, CYB0807055 and CYB0707013) were selected for SHRIMP U–Pb zircon dating and 6 samples (CYB0807032, CYB0707033, CYB0707020, CYB0807049, CYB0807022 and D008) were analyzed by LA-ICP-MS. All samples are from five granite intrusions characterized in greater detail below. Most of the selected zircon grains are transparent and colorless under the microscope, although some appear brownish due to radiation damage from high U contents. Cathodoluminescence images show that representative zircons have commonly concentric oscillatory zoning with low to variable luminescence that indicates a magmatic origin (Fig. 3). No inherited zircons were detected. The age of each sample is given by the error-weighted mean of the common Pb-corrected $^{206}\text{Pb}/^{238}\text{U}$ ages of the selected grains at 95% confidence level (Supplementary Table 1). U–Pb data sets for all samples are given in Supplementary Table 1.

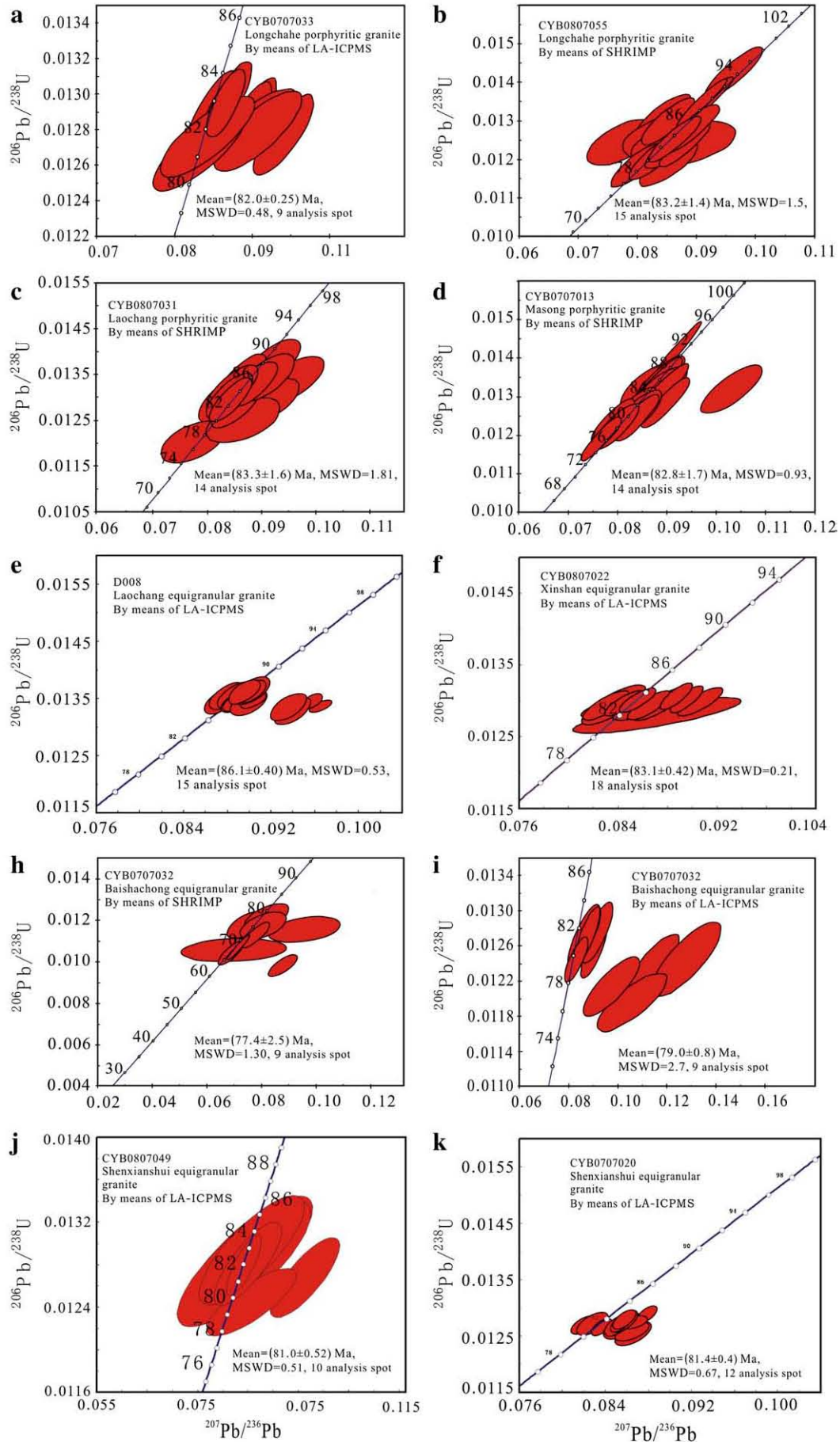


Fig. 4. Single grain U–Pb zircon ages of Gejiu granites.

4.1.1. Porphyritic granite from the Laochang area (sample CYB0807031)

Zircon grains in this sample are euhedral, 150–300 μm long, and have length to width ratios of about 2:1 to 4:1. Most are transparent and colorless, whereas a few high-uranium crystals are dark and opaque (Fig. 3). Euhedral concentric zoning is common in most crystals; no inherited zircon cores were observed.

Analyses of fourteen zircon grains from this sample were performed by SHRIMP (Data Repository Supplementary Table 1). Uranium and thorium concentrations are as follows: Th = 303–739 ppm and U = 644–3682 ppm, with Th/U ratios ranging from 0.18 to 0.49. The best estimate of the crystallization age of sample CYB0807031, based on the mean $^{206}\text{Pb}/^{238}\text{U}$ ratio, is 83.3 ± 1.6 Ma (95% confidence interval) (Fig. 4).

4.1.2. Porphyritic granite from the Longchahe area (samples CYB0707033 and CYB0807055)

Zircon grains in these samples were mostly clear and euhedral with concentric zoning, up to 150–400 μm long, with length to width ratios of about 2:1 to 4:1. Fifteen zircon analyses were performed by SHRIMP (Data Repository Supplementary Table 1). These analyses have variable medium to high concentrations of U (412–1398 ppm) and Th (1903–5449 ppm) (sample CYB0807055). They have indistinguishable $^{206}\text{Pb}/^{238}\text{U}$ ratios within analytical uncertainty, corresponding to a single age population with a weighted mean $^{206}\text{Pb}/^{238}\text{U}$ age of 83.2 ± 1.4 Ma (95% confidence interval) (Fig. 4).

LA-ICP-MS results from 9 grains in sample CYB0707033 yielded a weighted mean age of 82.0 ± 0.25 Ma (1σ) (MSWD = 0.48; Supplementary Table 1 and Fig. 4). This age is consistent with the above SHRIMP data and is interpreted as the best estimate of the crystallization age of the Laochang porphyritic granite.

4.1.3. Porphyritic granite from the Masong area (sample CYB0707013)

Zircon crystals in this sample are euhedral, up to 100–200 μm long, with length to width ratios of around 2:1 to 3:1. Most are clear and

colorless except for few dark brown and turbid crystals. Euhedral concentric zoning is common and no inherited zircon cores were observed.

Fourteen zircon analyses were obtained using SHRIMP (Data Repository Supplementary Table 1). They have variable abundances of Th (418–1118 ppm) and U (1719–13233 ppm). Th/U ratios vary between 0.09 and 0.35. All 14 analyses have indistinguishable $^{206}\text{Pb}/^{238}\text{U}$ ratios within analytical error, and a mean age of 82.8 ± 1.7 Ma (95% confidence interval) (Fig. 4). This is the best estimate of the crystallization age of sample CYB0707013.

4.1.4. Equigranular granite from the Baishachong area (sample CYB0807032)

Zircon grains in this sample are mostly euhedral, up to 100–300 μm long, with length to width ratios between 2:1 and 3:1 (Fig. 3). Most are transparent and colorless, although a few are dark brown and turbid due to high uranium content. Euhedral concentric zoning is common in most crystals, and no inherited zircon cores were observed.

Eleven grains were analysed by SHRIMP, and yield a weighted mean $^{206}\text{Pb}/^{238}\text{U}$ age of 77.4 ± 2.5 Ma (2σ) (MSWD = 1.3; Supplementary Table 1 and Fig. 4). The zircons have highly variable abundances of Th (2394–24484 ppm) and U (557–9391 ppm). Th/U ratios vary between 0.08 and 0.56, mostly clustering around 0.1–0.4.

LA-ICP-MS data on 13 grains from sample CYB0807032 yielded a weighted mean age of 79.1 ± 0.8 Ma (1σ) (MSWD = 2.7; Supplementary Table 1 and Fig. 4), which is the best estimate of the crystallization age of sample CYB0807032.

4.1.5. Equigranular granite from the Shenxianshui area (samples CYB0707020 and CYB0807049)

Zircon grains are mostly euhedral, ranging from 100 to 300 μm in length, with length to width ratios of about 2:1 to 3:1. The majority of

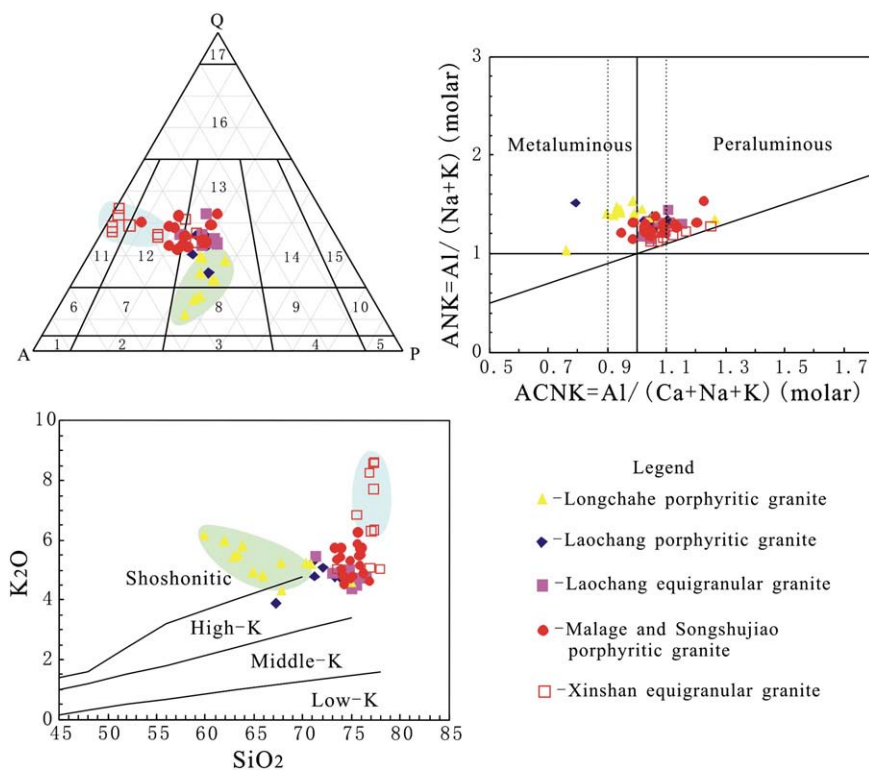


Fig. 5. QAP, ANK versus ACNK diagram and $(\text{K}_2\text{O} + \text{Na}_2\text{O})$ versus SiO_2 diagram for Gejiu granitic rocks (the compositional fields are from Middlemost, 1994; Streckeisen and Le Maitre, 1979; Rollinson, 1993; Maniar and Piccoli, 1989). 1-alkali-feldspar syenite; 2-syenite; 3-monzonite; 4-monzodiorite; 5-diorite; 6-alkali-feldspar quartz; 7-quartz syenite; 8-quartz monzonite; 9-quartz monzodiorite; 10-quartz diorite; 11-alkali-feldspar granite; 12-syenogranite; 13-monzogranite; 14-granodiorite; 15-tonalite; 16-quartz-rich granite; 17-quartzite.

the zircon grains are dark and opaque due to radioactive damage related to their high-uranium content.

Thirteen analyses of transparent zircon grains were performed by LA-ICP-MS (Data Repository Supplementary Table 1). They show variably high contents of Th (217–3695 ppm) and U (749–9798 ppm). Th/U ratios are between 0.11 and 1.05. $^{206}\text{Pb}/^{238}\text{U}$ ages determined in fourteen zircon grains are indistinguishable within analytical errors, with a mean $^{206}\text{Pb}/^{238}\text{U}$ age of 83.0 ± 0.35 Ma (Fig. 4). This is interpreted as the crystallization age of sample CYB0707020.

Another ten LA-ICP-MS determinations on zircon grains from sample CYB0807049 yielded a weighted mean age of 81.0 ± 0.53 Ma

(1σ) (MSWD = 0.51; Supplementary Table 1 and Fig. 4), consistent with the above age.

4.1.6. Equigranular granite from the Xinshan area (sample CYB0807022)

The analyzed zircons are mostly euhedral, ranging from 100 to 300 μm in length, and have length to width ratios of about 2:1 to 5:1. The majority of the zircon grains are dark and opaque due to radioactive damage related to high-uranium contents.

Eighteen zircon analyses were performed on transparent zircon grains using LA-ICP-MS (Data Repository Supplementary Table 1). They show high variable Th (100–3364 ppm) and U (194–16519 ppm)

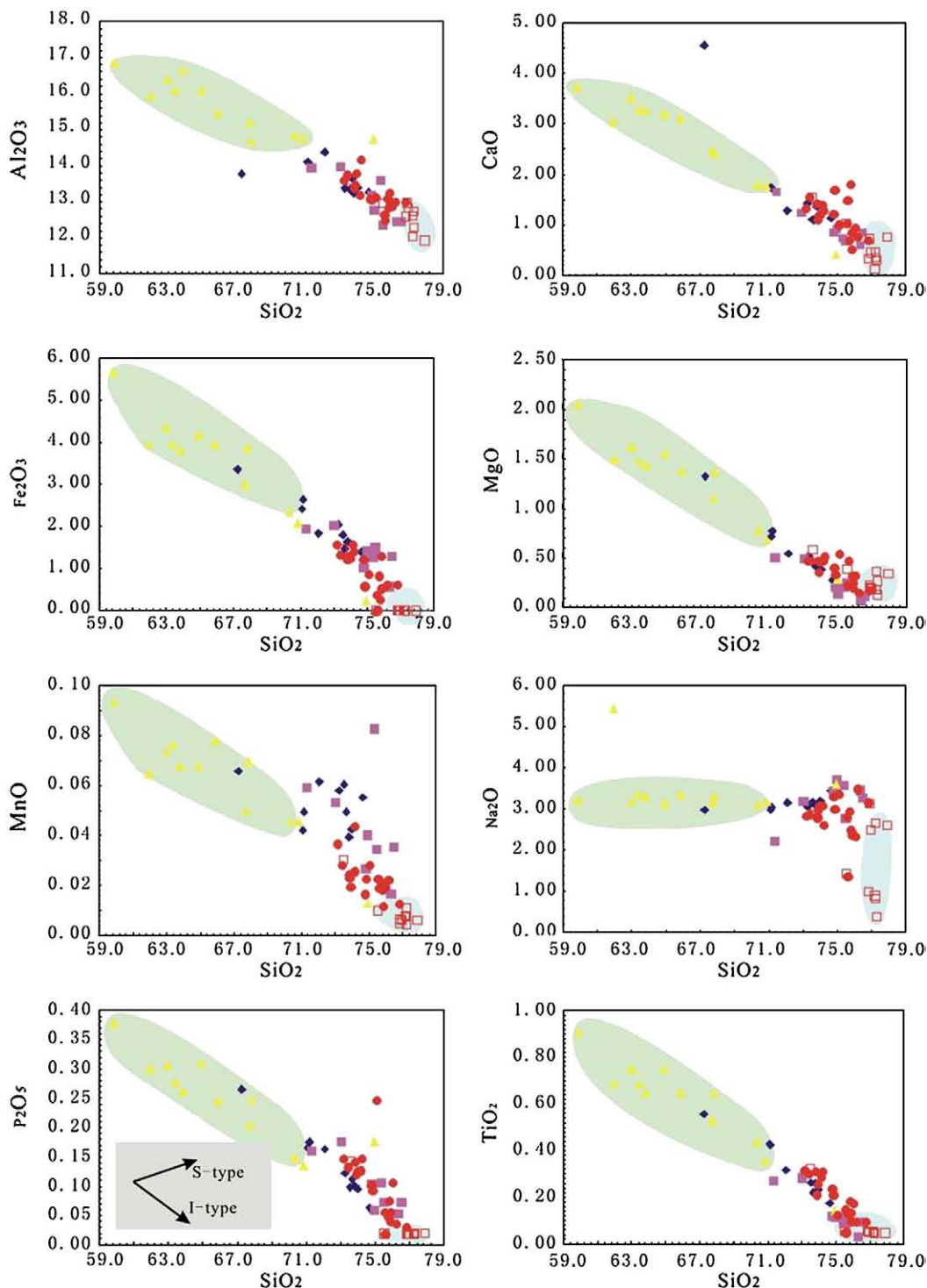


Fig. 6. Harker diagrams for the Gejiu granites.

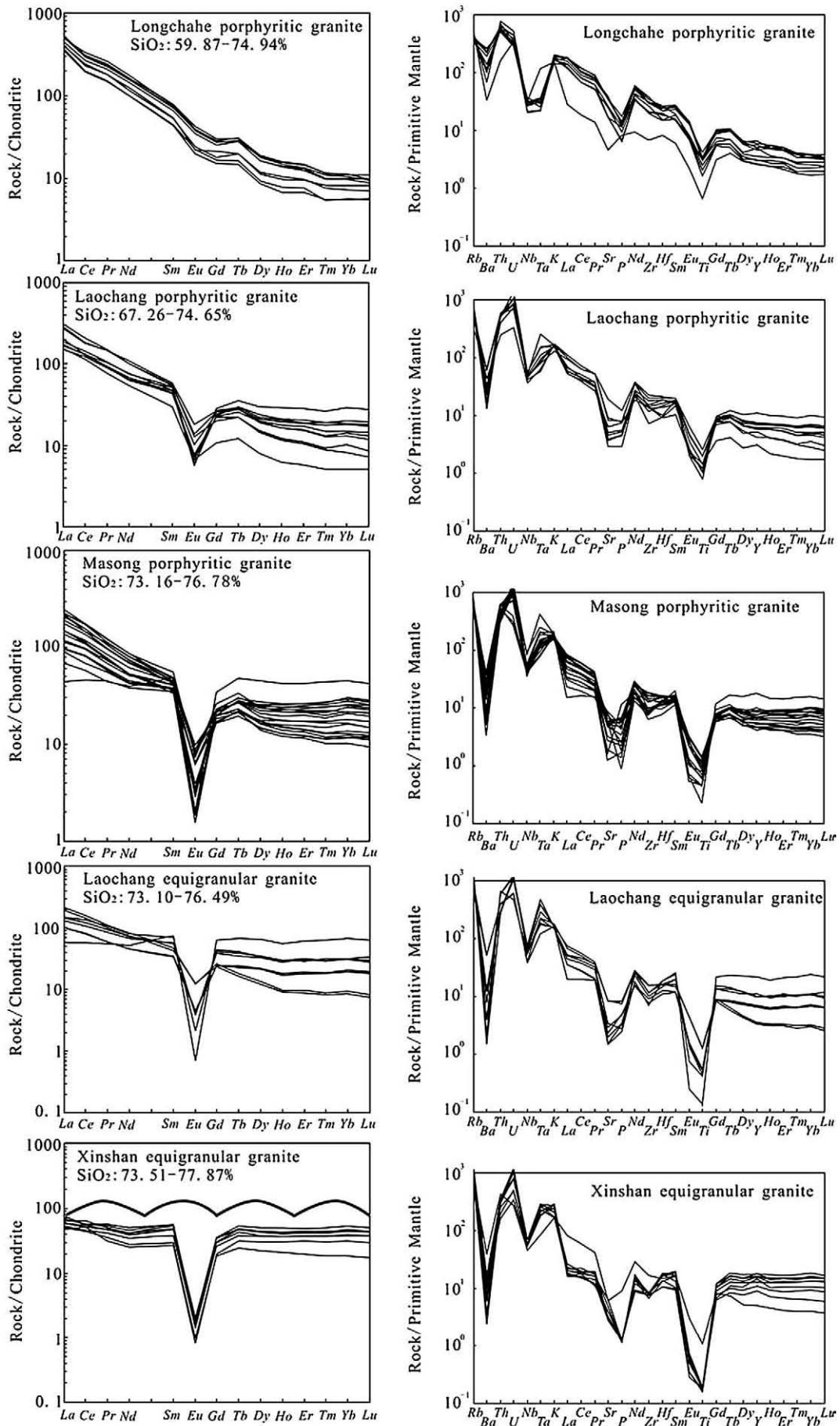


Fig. 7. Chondrite-normalized REE patterns and primitive-normalized incompatible element spider-diagrams for the Gejiu granites. Normalization values are from Sun and McDonough (1989).

contents. Th/U ratios are between 0.10 and 0.85. All samples have $^{206}\text{Pb}/^{238}\text{U}$ ages indistinguishable within analytical errors. The $^{206}\text{Pb}/^{238}\text{U}$ age is 83.1 ± 0.42 Ma, with $\text{MSWD} = 0.21$ (Fig. 4), which is interpreted as the crystallization age of sample CYB0807022.

4.1.7. Equigranular granite from the Laochang area (sample D008)

Zircon grains in this sample are euhedral, up to 100–200 μm in length, with length to width ratios of around 2:1 to 3:1. Most are clear and colorless apart from a few dark brown and turbid crystals. Euhedral concentric zoning is common. No inherited zircon cores were observed.

Twenty zircon grains analysed by LA-ICP-MS (Data Repository Supplementary Table 1) have variable abundances of Th (240–4685 ppm) and U (518–4885 ppm). Their Th/U ratios vary between 0.24 and 1.10. All analyses returned indistinguishable $^{206}\text{Pb}/^{238}\text{U}$ ratios within analytical error, resulting in a mean age of 85.0 ± 0.85 Ma (95% confidence interval) (Fig. 4). This is the best estimate of the crystallization age of sample D008.

4.2. Geochemical and isotopic results

4.2.1. Major and trace element data

A total of 59 granite samples were analyzed for major and trace element compositions. The loss on ignition (L.O.I.) for all samples was less than 1 wt.%. The Gejiu granites have a wide range of chemical compositions, with $\text{SiO}_2 = 59.87\text{--}77.87\%$, $\text{Al}_2\text{O}_3 = 11.94\text{--}16.85\%$, $\text{MgO} = 0.07\text{--}2.05\%$, $\text{Fe}_2\text{O}_3 = 0.01\text{--}5.65\%$, and $\text{CaO} = 0.14\text{--}4.45\%$ (Data Repository Supplementary Table 2). They are relatively high in total alkalis, with $\text{K}_2\text{O} = 3.89\text{--}8.64\%$ and $\text{Na}_2\text{O} = 0.39\text{--}5.43\%$, with the total $\text{K}_2\text{O} + \text{Na}_2\text{O}$ ranging from 6.87% to 11.42%. The granites are all rich in K_2O and thus fall into the field of high-K granite and shoshonite (Fig. 5). A/CNK values range from 0.76 to 1.27, from metaluminous to weakly peraluminous (Fig. 5), and normally demonstrate a positive correlation with SiO_2 . In the QAP diagram (Fig. 5), the Xinshan intrusion plots in the field of alkali-feldspar granite, and samples from the Masong and the Laochang intrusions plot in the syenogranite and monzogranite fields. The Longchahe intrusion plots into the quartz monzonite field. In the Harker diagram, Al_2O_3 , TiO_2 , Fe_2O_3 , MgO , MnO , CaO , P_2O_5 decrease with increasing SiO_2 , whereas Na_2O remains nearly constant (Fig. 6), suggesting fractional crystallization of ferromagnesian minerals, plagioclase, Ti-Fe oxides and apatite.

Chondrite-normalized REE patterns for the Gejiu granites show gradual change in REE abundances, LREE/HREE ratios, $(\text{La}/\text{Yb})_N$ and intensity of negative Eu anomalies that positively correlate with SiO_2 . In Fig. 7, as SiO_2 increases, LREE abundances decrease whereas the Eu depletion becomes stronger. The increase in the negative Eu anomaly is due to the fractionation of feldspar while the relative decrease in LREE is due to the fractionation of a minor LREE-rich phase. Wu et al. (2003) and Li et al. (2007) suggested that this might be a feature of the highly-fractionated I-type granites, and probably a result of fractionation of apatite, allanite, titanite and monazite.

In the primitive mantle-normalized variation diagrams (Fig. 7), both the porphyritic and equigranular granites show enrichment in Rb and U and marked depletion in Ba, Nb, P, and Ti. Rb and U, like REE, show positive and Ba, Nb, P and Ti negative correlations with SiO_2 (Fig. 7). From the Longchahe porphyritic granite, Laochang porphyritic granite, Masong porphyritic granite, Laochang equigranular granite, to Xinshan equigranular granite, the $(\text{Ce}/\text{Yb})_N$ ratios decrease with increasing $(\text{Yb})_N$ (Fig. 7), suggesting that fractional crystallization was a dominant process governing evolution of the Gejiu granitoids. Negative Ba, P, Eu and Ti anomalies (Fig. 7) indicate fractional crystallization of feldspar, apatite and ilmenite. It should be noted that Ta, Zr and Hf are not, or are only slightly, depleted implying limited or zero contribution of subduction-related material to the parent magma.

4.2.2. Sr–Nd isotopes

Rb, Sr, Sm and Nd contents, $^{143}\text{Nd}/^{144}\text{Nd}$ and $^{87}\text{Sr}/^{86}\text{Sr}$ ratios, and T_{DM} ages for granitoids in the Gejiu area are listed in Supplementary Table 3. The initial $^{87}\text{Sr}/^{86}\text{Sr}$ ($(^{87}\text{Sr}/^{86}\text{Sr})_i$) ratios and $\epsilon_{\text{Nd}}(t)$ values have been calculated using the U–Pb zircon ages determined in this study. Depleted mantle model ages (T_{DM}) are reported using the model of DePaolo (1981). The data are shown in a plot of $\epsilon_{\text{Nd}}(t)$ versus $(^{87}\text{Sr}/^{86}\text{Sr})_i$ (Fig. 10).

Twenty-five samples from the Gejiu intrusions exhibit a wide range of measured $^{87}\text{Rb}/^{86}\text{Sr}$ (0.96 to 71.86) and $^{87}\text{Sr}/^{86}\text{Sr}$ (0.71329 to 0.80601) ratios due to significant fractionation and variable chemical compositions, and their age-corrected $^{87}\text{Sr}/^{86}\text{Sr}$ ratios cluster within a broad interval between 0.7060 and 0.7202 (Supplementary Table 3 and Fig. 10).

The granites also display variable $^{147}\text{Sm}/^{144}\text{Nd}$ ratios ranging from 0.087 to 0.282 and the measured $^{143}\text{Nd}/^{144}\text{Nd}$ ratios vary between 0.512116 and 0.512245. Calculated initial $\epsilon_{\text{Nd}}(t)$ values range from -9.3 to -6.9 (Supplementary Table 3). The T_{DM} model ages are all between

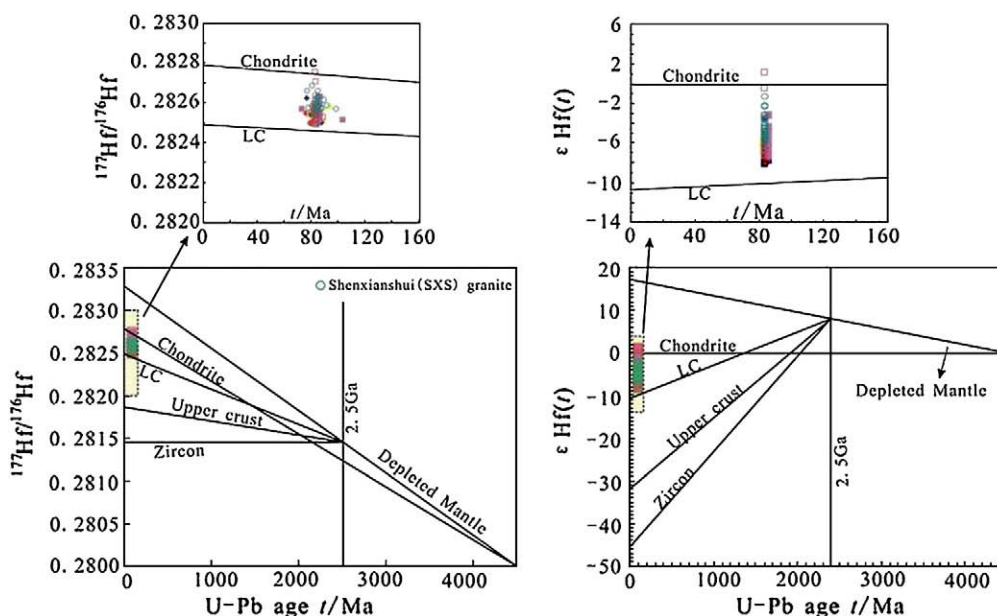


Fig. 8. Zircon Lu–Hf isotopic compositions of the studied granites from the Gejiu pluton.

1.4 and 1.6 Ga. The age-corrected initial $^{87}\text{Sr}/^{86}\text{Sr}$ (I_{Sr}) ratios show a wide variation while the $\epsilon\text{Nd}(t)$ values remain almost unchanged (Fig. 10).

4.2.3. Hf isotopes in zircons

A total of 105 sets of $^{176}\text{Hf}/^{177}\text{Hf}$ isotopic data on zircons from six samples are listed in Supplementary Table 4. The same results are also plotted as $\epsilon\text{Hf}(t)$ against their ages in Fig. 8. The $\epsilon\text{Hf}(t)$ values and T_{DM} (the Hf isotope crustal model ages based on a depleted-mantle source assuming that the protolith of the zircon-bearing magma had an average continental crustal $^{176}\text{Lu}/^{177}\text{Hf}$ ratio of 0.015) were calculated following Griffin et al. (2002), using the ^{176}Lu decay constant adopted in Blichert Toft and Albarede (1997).

Thirteen spot analyses were performed on sample CYB0707013 from the Masong granite, yielding $\epsilon\text{Hf}(t)$ values between -7.98 to -5.39 (average of -6.69) that corresponds to T_{DM} model ages between 1218 Ma and 1347 Ma. Two stage model ages show nearly normal distributions (Fig. 11), and the average T_{DM} is 1282 Ma. These Hf isotopic data indicate a major Late Mesoproterozoic crustal magma source.

Fifteen spot analytical results were obtained from sample CYB0807055 from the Longchahe porphyritic granite. Spot 3 gave the highest $\epsilon\text{Hf}(t)$ value of -4.54 and the lowest T_{DM} model age of 1182 Ma; spot 1 gave the lowest $\epsilon\text{Hf}(t)$ value of -7.33 and the highest T_{DM} model age of 1320 Ma. Results of these two analyses deviate significantly from the remaining thirteen spots with $\epsilon\text{Hf}(t)$

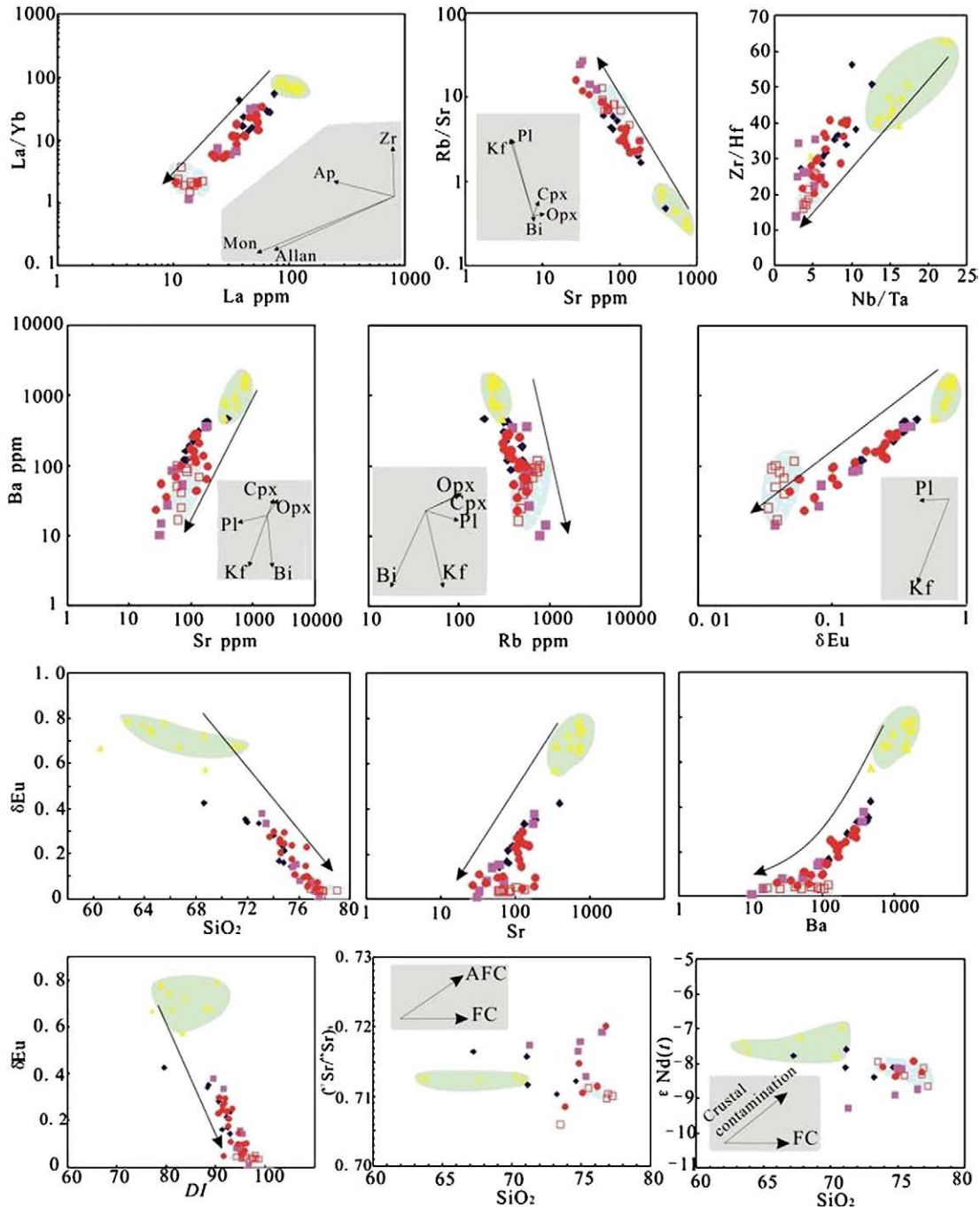


Fig. 9. Characteristics of Gejiu granites resulting from fractional crystallization. Mon – monazite; Allan – allanite; Ap – apatite; Zr – zircon; Kf – K-feldspar; Pl – plagioclase; Bi – biotite; CPX – clinopyroxene; OPX – orthopyroxene.

values between -5.19 to -6.73 (average -5.85), corresponding to T_{DM} model ages between 1211 Ma and 1285 Ma. In general, all analyses show a normal distribution of T_{DM} model ages, with an average of $T_{DM} = 1241$ Ma. This sample has Hf isotopic compositions similar to a sample from the Masong porphyritic granite, indicating a major Late Mesoproterozoic crustal magma source.

Twenty spots analyses were obtained for sample D008 from the Laochang equigranular granite. They show a limited range of $\epsilon_{Hf}(t)$ values between -3.09 and -7.77 with an average of -5.67 , corresponding to T_{DM} model ages of 1101 Ma to 1338 Ma with an average around 1232 Ma (Fig. 11). A concentric-bimodal distribution is shown for the $\epsilon_{Hf}(t)$ values and the two stage model ages. These results suggest a major Late Mesoproterozoic crustal source for the Laochang equigranular granite.

Fourteen spot analyses were performed on sample CYB0807055 from the Laochang porphyritic granite, giving $\epsilon_{Hf}(t)$ values of -3.58 to -7.65 with an average value of -6.29 . This corresponds to T_{DM} model ages of 1119 Ma to 1335 Ma. These analyses display a single-peak distribution of T_{DM} model ages (Fig. 11) with an average of 1262 Ma. Combined with the distribution of $\epsilon_{Hf}(t)$ values this indicates Late Mesoproterozoic crustal source.

Twenty spot analyses were performed on sample CYB0807022 from the Xinshan equigranular granite. The $\epsilon_{Hf}(t)$ values extend from 1.21 to -8.09 with an average of -5.33 ; corresponding T_{DM} model ages range from 878 Ma to 1354 Ma, averaging 1213 Ma (Fig. 11). Such Hf isotope characteristics are likely indicative of a major Late Mesoproterozoic crustal component, but mantle derived materials also played a role in magma formation.

Twenty three spot analytical results were obtained from sample CYB0807049, from the Shenxiangshui equigranular granite. The highest $\epsilon_{Hf}(t)$ value is -1.29 and the lowest T_{DM} model age is 1004 Ma; spot 23 gives the lowest $\epsilon_{Hf}(t)$ values of -8.12 and the highest T_{DM} model age of 1355 Ma. The remaining spots with $\epsilon_{Hf}(t)$ values of -2.17 to -6.51 , with an average of $\epsilon_{Hf}(t) = -4.52$, correspond to T_{DM} model ages of 1051 Ma to 1273 Ma.

In general, The T_{DM} model ages in this study are similar with an average of T_{DM} of 1173 Ma. This, together with Hf isotopic compositions, suggesting derivation of the Gejiu granitic magma from a major Late Mesoproterozoic crustal source mixed with subordinate mantle components.

5. Discussion

5.1. Fractional crystallization process

The majority of the quartz monzonites and granites in the Gejiu area are peraluminous and high in total alkalis ($K_2O + Na_2O$ 7.5%) due to strong fractionation. This also agrees with the criteria of Sylvester (1989) who proposed that the $(Al_2O_3 + CaO)/(FeO^* + Na_2O + K_2O)$ vs. $100 (MgO + FeO^* + TiO_2)/SiO_2$ relationship was a fairly effective discriminant between fractionated granites of calc-alkaline, alkaline, and strongly peraluminous petrochemistry. Again, in the $(Na_2O + K_2O)/CaO$ vs. $(Zr + Nb + Ce + Y)$ discriminant diagram (Whalen et al., 1987) most Gejiu data fall in the field of fractionated granites. We, therefore, conclude that all porphyritic and equigranular granites in Gejiu area are highly fractionated.

As mentioned before, the negative correlations between Al_2O_3 , CaO , P_2O_5 , MgO , Fe_2O_3 , MnO , TiO_2 and SiO_2 suggest that the granites are likely the result of fractional crystallization during magmatic evolution, which is also confirmed by the P and Ti depletions and negative Eu anomalies (Fig. 7). The decrease in P_2O_5 , MgO and Fe_2O_3 during magmatic evolution indicates separation of apatite and mafic minerals (such as biotite) during crystallization. Crystal fractionation is also confirmed by the Rb–Ba and Sr–Ba variations (Fig. 9), the negative correlation between SiO_2 and Sr, Eu, δEu , and the strong negative Ba, Sr, P, Ti anomalies (Fig. 9).

Pronounced depletion of Ba, Nb, P and Ti (Fig. 7) further demonstrate that fractional crystallization occurred during the formation of the granites. Separation of Ti-bearing phases such as ilmenite and titanite resulted in depletion of Nb (Ta)–Ti and P, respectively. Moreover, δEu ratios correlate positively with Sr and Ba but negatively with Rb (Fig. 9), suggesting that these elements are mainly controlled by separation of plagioclase and K-feldspar from fractionating melt.

In Ba vs. Sr and Ba/Sr vs. Sr plots (Fig. 9) the Sr concentration decreases sharply from about 805.0 to 26.6 ppm and the Ba concentration decreases from about 1830 to 10.3 ppm. This can be explained by K-feldspar separation as indicated by the general decrease in K_2O concentration with increasing SiO_2 in granites. The FC process seems to be clear during crystallization of hybrid felsic magma as indicated by $(^{143}Nd/^{144}Nd)_i$ vs. silica and $(^{87}Sr/^{86}Sr)_i$ vs. silica (Faure, 2001) (compare Fig. 9).

5.2. Petrogenesis

The Gejiu granitic rocks have moderately negative $\epsilon_{Nd}(t)$ values (-6.82 to -9.27) (Supplementary Table 3; Fig. 10). In this they are similar to the 90–95 Ma granites in the supergiant Dachang ore district in Guangxi interpreted as a product of melting of the upper continental crust (Fig. 1) (Chen and Zhu, 1993; Liang et al., 2008). Moreover, in combination with the chondrite-normalised REE diagrams (Fig. 7), the high concentrations of Th (13.5–66.1 ppm), Pb (17.5–119 ppm) and U (5.28–33.30 ppm), indicate that a crustal component was involved in generation of these granites. This conclusion is based on the

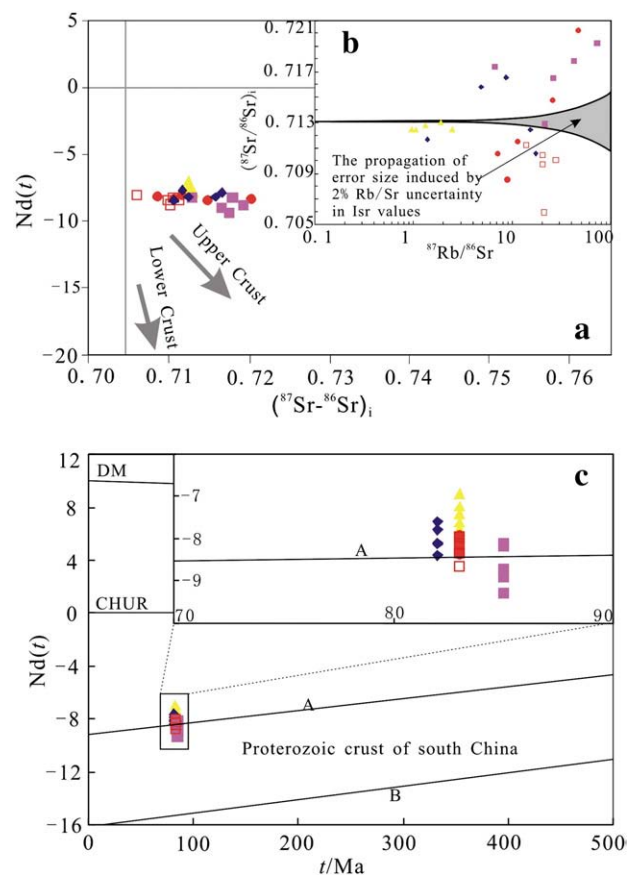


Fig. 10. (a) Nd and Sr isotopic variation diagram, (b) Initial $^{87}Sr/^{86}Sr$ (I_{Sr}) vs. $^{87}Rb/^{86}Sr$ plot for Gejiu granitoids. I_{Sr} values calculated from rocks with high to very high Rb/Sr ratios are too imprecise to have useful petrogenetic meanings. Grey area indicates the propagation of error size induced by 2% Rb/Sr uncertainty in I_{Sr} values, and (c) $\epsilon_{Nd}(t)$ versus t/Ma diagram for the Gejiu granites.

observations of Rudnick and Fountain (1995) that rocks derived from upper continental crustal sources should have high Th (>10 ppm), Pb (>20 ppm) and U (>2.0 ppm) contents.

Meanwhile, an uncommon phenomena found in the plot of $\epsilon_{Nd}(t)$ vs. $(^{87}\text{Sr}/^{86}\text{Sr})_i$ is that the $(^{87}\text{Sr}/^{86}\text{Sr})_i$ values change significantly while the $\epsilon_{Nd}(t)$ values remain relatively constant. Hence it is

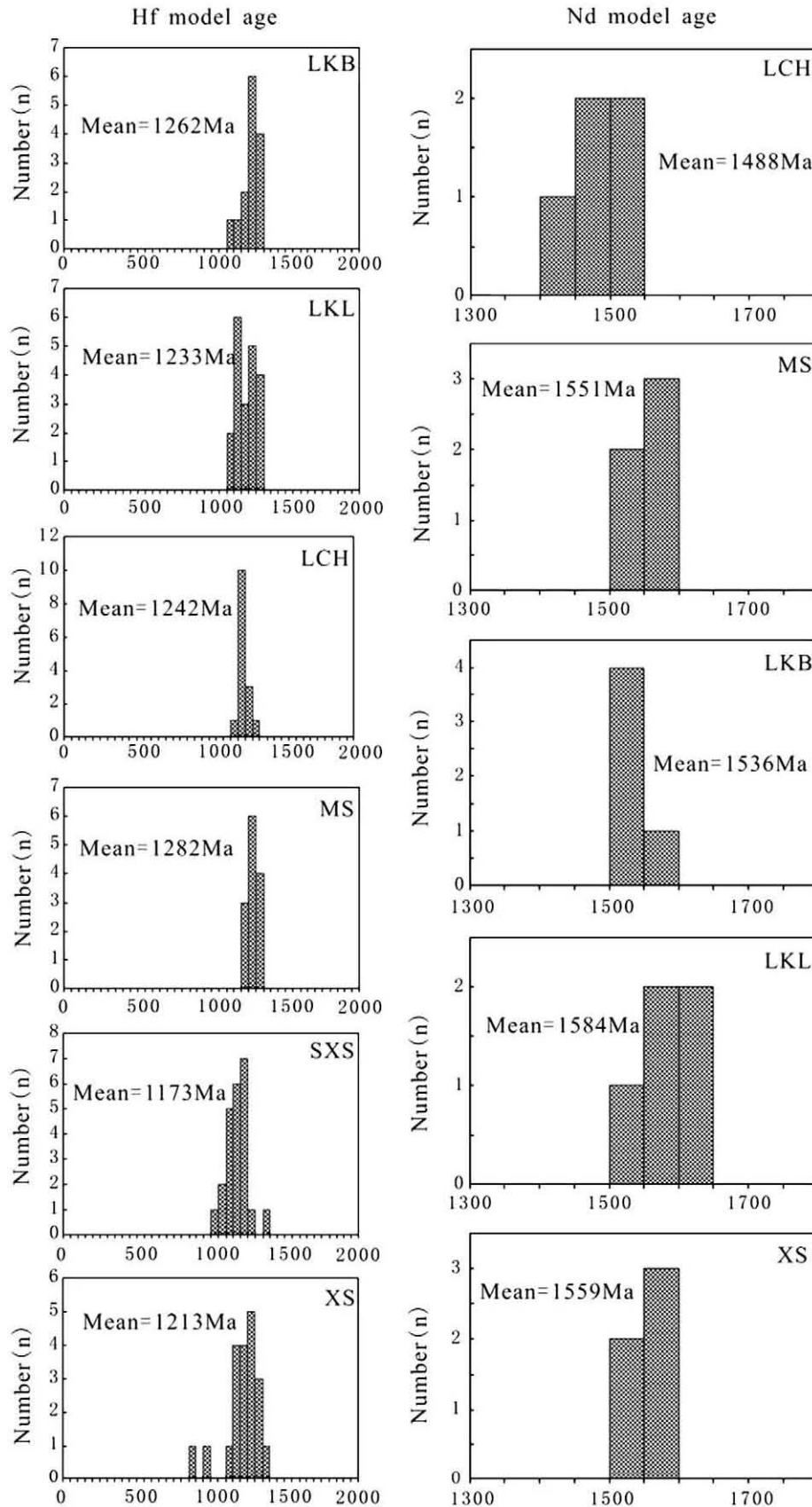


Fig. 11. Nd and Hf model ages of the Gejiu granitic rocks.

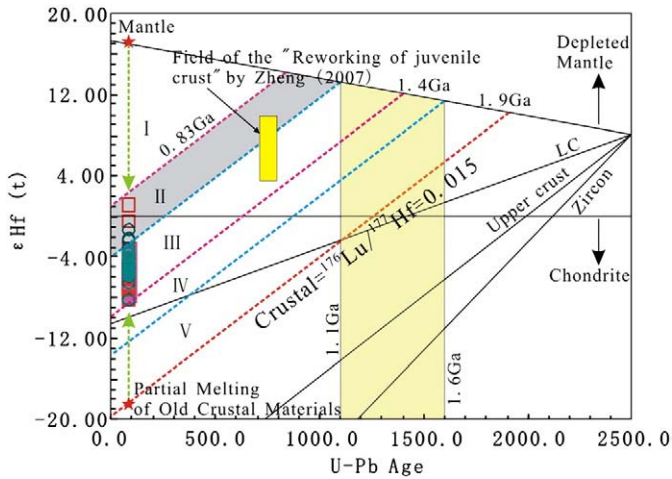


Fig. 12. Hf isotope evolution diagram. The Gejiu granitic magma may have been mixed with a newly introduced basaltic magma from the asthenosphere during the Mesozoic, accompanied by partial melting of old crustal materials. The DM line denotes the evolution of the depleted mantle with a present-day $^{176}\text{Hf}/^{177}\text{Hf}=0.28325$ and $^{176}\text{Lu}/^{177}\text{Hf}=0.0384$ (Griffin et al., 2000); the corresponding lines of crustal extraction are calculated by assuming a $^{176}\text{Lu}/^{177}\text{Hf}$ ratio of 0.015 for average continental crust (Jean et al., 2009).

important to know the uncertainty in the calculated initial Sr isotope ratios, especially in granitoids with high Rb/Sr ratios that are indicative of a high degree of differentiation. First, the highly variable initial Sr isotopes are not attributed to “granite weathering”, as the studied rocks are fairly fresh (very low LOI values). Moreover, most of the Gejiu granite samples plot outside the field of propagation error except for the Longchahe porphyritic granite (Fig. 10). This indicates that I_{Sr} values calculated from rocks with high to very high Rb/Sr ratios are too imprecise to have useful petrogenetic meaning (Jahn et al., 2000a,b; Wu et al., 2002). Hence, Nd isotopes are more suitable than Sr isotopes for constraining the petrogenesis of the Gejiu granites.

The Nd T_{DM} of 1488–1584 Ma, and zircon Hf T_{DM} of 1173–1282 Ma (Fig. 11) obtained in this study, combined with other geochemical features, suggest that the Gejiu granitoids may have been derived from the Mesoproterozoic basement. However, as not all $\epsilon\text{Nd}(t)$ values fall into the field for the Proterozoic basement of south China (Fig. 10), a hybrid origin for the Gejiu granitoids is assumed. Fur-

thermore, taking into account the Lu–Hf isotopes, The $\epsilon\text{Hf}(T)$ values of zircons from the Gejiu granite vary from -8.1 to $+1.2$, implying a minor input of mantle-derived materials during the magma generation (Fig. 12).

5.3. Genetic model for Cretaceous intraplate magmatism and mineralization in the western Cathaysia block

Late Cretaceous granitic rocks are widespread not only in the Gejiu area, but also in other regions in south-eastern Yunnan and western Guangxi Provinces. Our high-precision geochronological data, together with the recently reported SHRIMP zircon U–Pb ages and the reliable LA-ICP-MS zircon U–Pb, mica Ar–Ar, molybdenite Re–Os ages, are summarized in Table 2, with the aim to understand the Mesozoic magmatism and mineralization events (Liu et al., 1999, 2007; Wang et al., 2004; Cai et al., 2006; Lin et al., 2008; Li et al., 2008; Chen et al., 2009; Yang et al., 2008, 2009). These data demonstrate that the magmatism in the south-eastern Yunnan and western Guangxi was of a short duration (98–77 Ma with a peak at 80–95 Ma; Fig. 13). Mafic and ultramafic rocks, mafic microgranular enclaves, alkaline rocks and lamprophyres in the Gejiu area, even in the south-eastern Yunnan and western Guangxi, were all emplaced within a similar age range of 75–100 Ma (Cheng et al., 2009; Chen et al., 2009). Demonstration of close connection between granitic magmatism and magmatic-hydrothermal metallogenesis in the same time interval is an important aspect of our study. The 76–85 Ma Gejiu granitic magmatism and the associated tin-polymetallic mineralization probably closely correlate in time with corresponding events elsewhere in the south-eastern Yunnan and western Guangxi regions, such as in the Dachang, Dulong and Bainiuchang ore districts (Fig. 1).

The magmatic and mineralization episode that took place in the western part of the Cathaysia block, however, displays different characteristics when compared with granitoids distributed in convergent continental margins which are considered related to lithospheric plate subduction (Cheng et al., 2010a). It is generally accepted that heat from upwelling asthenosphere beneath the continental crust can cause extensive melting of both the subcontinental lithospheric mantle (SCLM) and the lower continental crust to produce a bimodal magmatic association (Campbell and Hill, 1988; Zhang et al., 2006). In the Gejiu area, besides the granitic rocks, other coeval igneous rocks such as gabbro, diorite, alkaline rocks and lamprophyre are also widely distributed (Cheng et al., 2010a). Other

Table 2
Summary of the ages of the mineralization and magmatism in the west Cathaysia block.

| Order | Location | Lithology/minerals | Method | Data | Reference |
|-------|-------------|---------------------------|-------------------------------------|-----------------|----------------------|
| 1 | Bainiuchang | Granite | LA-ICP-MS | 87.54 ± 0.65 Ma | Cheng et al. (2010b) |
| 2 | Bainiuchang | Granite | LA-ICP-MS | 87.83 ± 0.39 Ma | Cheng et al. (2010b) |
| 3 | Bainiuchang | Granite | LA-ICP-MS | 86.51 ± 0.52 Ma | Cheng et al. (2010b) |
| 4 | Dulong | Cassiterite | TIMS | 79.8 ± 3.2 Ma | Liu et al. (2007) |
| 5 | Dulong | Cassiterite | U–Pb | 82.0 ± 9.6 Ma | Liu et al. (2007) |
| 6 | Dulong | Granite | SHRIMP | 92.9 ± 1.9 Ma | Liu et al. (2007) |
| 7 | Dulong | Granite porphyry | SHRIMP | 86.9 ± 1.4 Ma | Liu et al. (2007) |
| 8 | Dachang | Quartz(plateau age) | ^{40}Ar – ^{39}Ar | 94.52 ± 0.33 Ma | Wang et al. (2004) |
| 9 | Dachang | Quartz(isochron age) | ^{40}Ar – ^{39}Ar | 95.37 ± 0.45 Ma | Wang et al. (2004) |
| 10 | Dachang | Quartz(back isochron age) | ^{40}Ar – ^{39}Ar | 94.89 ± 0.16 Ma | Wang et al. (2004) |
| 11 | Dachang | Sanidine | ^{40}Ar – ^{39}Ar | 91.4 ± 2.9 Ma | Wang et al. (2004) |
| 12 | Dachang | Quartz(plateau age) | ^{40}Ar – ^{39}Ar | 94.56 ± 0.45 Ma | Wang et al. (2004) |
| 13 | Dachang | Quartz(isochron age) | ^{40}Ar – ^{39}Ar | 93.50 ± 1.20 Ma | Wang et al. (2004) |
| 14 | Dachang | Quartz(back isochron age) | ^{40}Ar – ^{39}Ar | 93.29 ± 0.16 Ma | Wang et al. (2004) |
| 15 | Dachang | Granite | SHRIMP | 93 ± 1 Ma | Cai et al. (2006) |
| 16 | Dachang | Granite | SHRIMP | 91 ± 1 Ma | Cai et al. (2006) |
| 17 | Dachang | Quartz diorite | SHRIMP | 91 ± 1 Ma | Cai et al. (2006) |
| 18 | Dachang | Granite porphyry | SHRIMP | 91 ± 1 Ma | Cai et al. (2006) |
| 19 | Kunlunguan | Granite | LA-ICP-MS | 93 ± 1 Ma | Tan et al. (2008) |
| 20 | Kunlunguan | Molybdenite | Re–Os | 93.8 ± 4.6 Ma | Lin et al. (2008) |
| 21 | Kunlunguan | Molybdenite | Re–Os | 95.40 ± 0.0 Ma | Lin et al. (2008) |
| 22 | Baiceng | ultrabasic dyke | SHRIMP | 84 ± 1 Ma | Chen et al. (2009) |

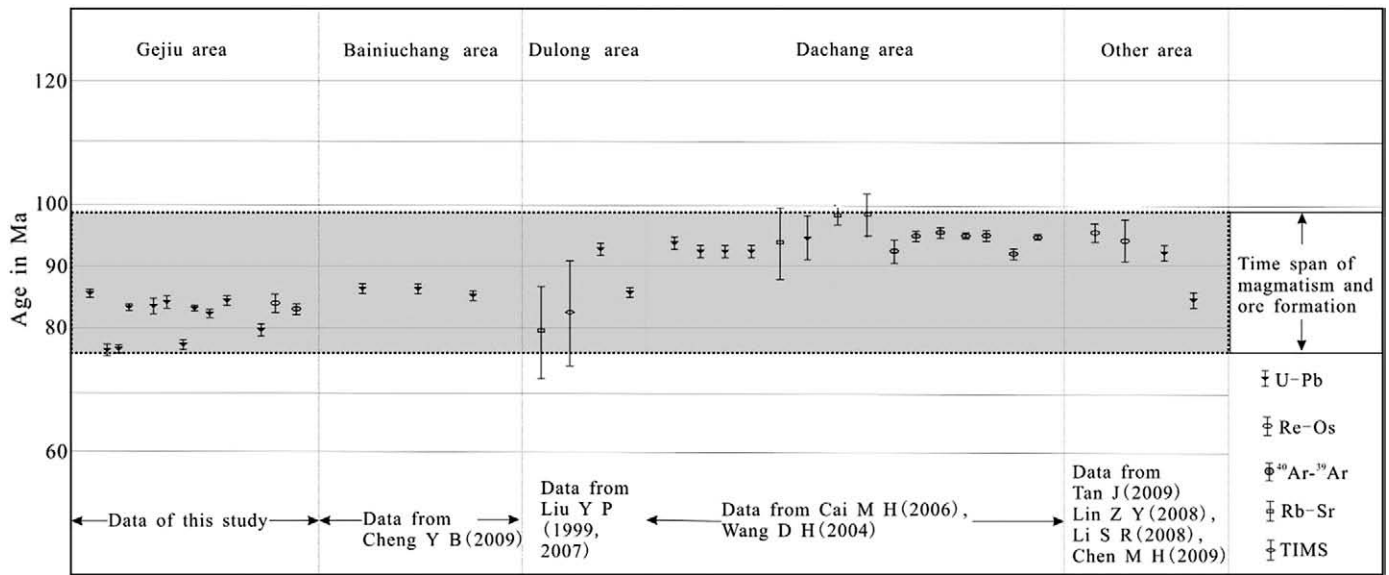


Fig. 13. Summary of the published and new geochronological determinations for the western Cathaysia block.

Late Cretaceous mafic, ultramafic and alkaline rocks are also widespread in the entire western Cathaysia block along extensional structures. The predominant granitoids and the synchronous mafic and ultramafic rocks thus constitute a bimodal magmatic association controlled by lithospheric extension and asthenosphere upwelling within the western Cathaysia block in Late Cretaceous (Yan et al., 2005; Chen and Zhu, 1993; Suo et al., 1999; Liang et al., 2008; Chen et al., 2008; Liu et al., 2010).

Trace elements and Sr–Nd–Hf isotopes demonstrate that the Gejiu granites were mainly derived from melting of continental crust in an intraplate environment. This interpretation is consistent with recent research (Xie et al., 2006; Li et al., 2007; Mao et al., 2010; Liu et al., 2010). Since all Late Cretaceous granitoids in western Cathaysia display a high degree of similarity with the Gejiu granite, they should have formed in a similar geodynamic environment. Suo et al. (1999), Yan et al. (2005) and Chen et al. (2008) suggested that during the Late Cretaceous, western Cathaysia underwent lithospheric extension with strong upwelling of the asthenospheric mantle that triggered mafic melt underplating and/or continental lithosphere delamination. In response to a significant increase in geothermal heat flux, a major igneous event took place throughout the south-eastern Yunnan and western Guangxi region, forming the widespread highly fractionated granites and related giant tin-polymetallic deposits.

5.4. Petrogenetic type: S-type, A-type or highly fractionated I-type granites?

When dealing with high-silica fractionated granites, most conventional petrogenetic schemes encounter difficulties because such rocks tend converge in terms of major elements and mineral compositions into haplogranite (King et al., 1997). This is possibly the main reason that the Gejiu granites were previously attributed to various types (e.g. S-, I-, A-type) by different authors (Li, 1985; Mo, 2006; Wang et al., 2007).

It is apparent that the A/CNK values are below 1.1 for most of the Gejiu peraluminous granites (Fig. 5), in contrast with the highly siliceous S-type granites that are usually strongly peraluminous with A/CNK values much higher than 1.1 (Chappell, 1999). Furthermore, these rocks show remarkable decreases in P_2O_5 with increasing SiO_2 content (Fig. 6). This feature is also an important criterion for distinguishing I-type granites from S-type granites, because apatite reaches saturation in metaluminous and mildly peraluminous mag-

mas ($A/CNK < 1.1$) but remains highly soluble in strongly peraluminous melts (Wolf and London, 1994). This has been applied in many studies (Chappell, 1999; Li et al., 2003; Wu et al., 2003). The Gejiu granite also exhibits an increase of Y concurrently with a Rb and SiO_2 increase that is similar to the evolutionary trend of I-type-affinity granite (Fig. 14) (Chappell, 1999; Li et al., 2007). But they cannot be simply grouped into I-type granite, as Gejiu granites also exhibit an A-type affinity. They have high $K_2O + Na_2O$, Zr, total FeO/MgO and Ga/Al ratios. In the discrimination diagrams of $K_2O + Na_2O$, Nb and Zr vs. Ga/Al (Fig. 14), they plot in the A-type granite field as defined by Whalen et al. (1987). Furthermore, in the $(K_2O + Na_2O)/CaO$ vs. $(Zr + Nb + Y + Ce)$ graph, all intrusions fall in the field of A-type granites as well (Fig. 14). However, the Gejiu granites exhibit continuously decreasing Zr values with increasing SiO_2 (Fig. 15) that suggests zirconium saturation occurred in the magma (Li et al., 2007; Zhong et al., 2009; Liu et al., 2009). The bulk rock Zr compositions the model of Watson and Harrison (1983) was used to calculate zirconium-saturation temperatures (T_{Zr}) for the Gejiu granites (Supplementary Table 2). The saturation temperatures (T_{Zr}) decrease in going from the Longchahe porphyritic granite to the Xinshan equigranular granite. In the case of gradual temperature decrease parallel with melt fractionation during the magmatic evolution, Wu et al. (2007) argued that A-type granite always cannot be generated along this trend.

Thus, the Gejiu granites share features of both A-type and highly fractionated I-type. Attempts to assign the Gejiu granites to one of the recognized petrochemical classes will run into problems (Chappell and White, 1974; Collins et al., 1982; King et al., 1997). The same problems are common with petrochemical assignments of Jurassic–Cretaceous granites from the entire Cathaysia block (Liang et al., 2008; Li et al., 2007; Zhao et al., 2005; Mao et al., 1998).

Geology department of Nanjing University (1981) and Xu et al. (1982) provided a sound basis for understanding the genetic-type of southern China granites by recognizing three local genetic varieties they named transformation type, syntexis type and mantle-derived type. This nomenclature, widespread in China especially for the syntexis type, emphasizes the contribution of mantle derived materials. It seems that this nomenclature is more sensitive to the Gejiu granites than other published alternatives. The idea of mantle contribution to intracrustally-melted magmas in southern China is gaining popularity (Gilder et al., 1996; Hong et al., 1998; Chen and Jahn, 1998; Liu et al., 2010). Although detailed

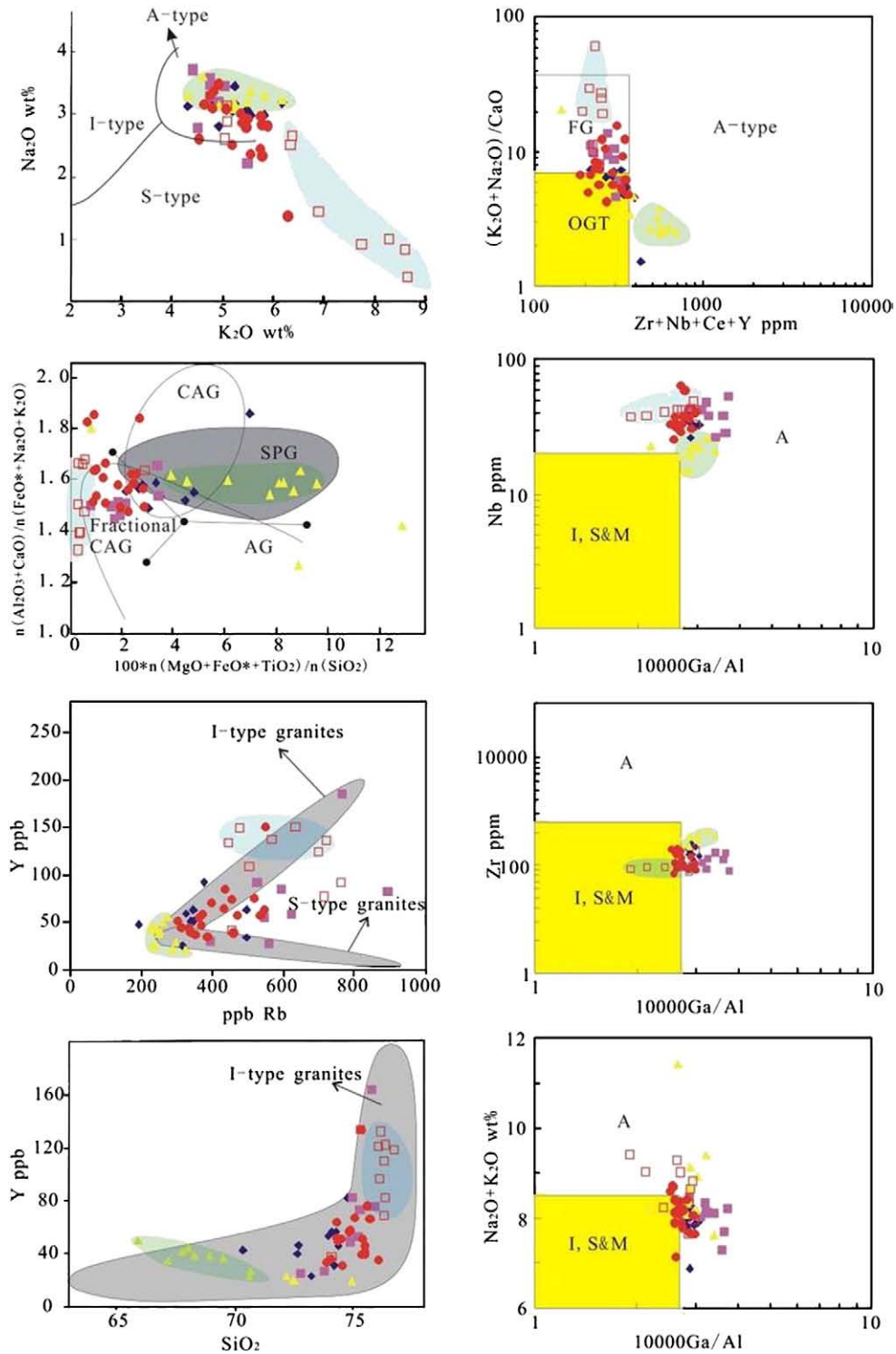


Fig. 14. $(Al_2O_3 + CaO) / (FeO^* + Na_2O + K_2O)$ vs. $100(MgO + FeO^* + TiO_2) / SiO_2$, $(Na_2O + K_2O) / CaO$ vs. $(Zr + Nb + Ce + Y)$, Y vs. Rb, Y vs. SiO_2 diagrams and A-type granite discrimination for the Gejiu granitic rocks (Chappell, 1999) FG-Fractionated M-, I- and S-type felsic granites; OGT non-fractionated M-, I- and S-type granites.

description of the co-evolution relationship between gabbros, mafic microgranular enclaves, granites and syenites in Gejiu area is beyond the scope of this paper, we feel strongly about the crust-mantle interaction and believe that the term “crust-mantle syntectonic type” of Xu et al. (1982) best characterizes Gejiu granites. This concept is similar with the “I-type” granite which could be generated by reworking of sedimentary materials by mantle-derived magmas.

6. Conclusions

By joint application of zircon U–Pb geochronology, geochemistry, and isotope investigation, the following conclusions have been reached:

- (1) SHRIMP and LA-ICP-MS U–Pb zircon dating indicate that the two textural types of granites in the Gejiu area formed at

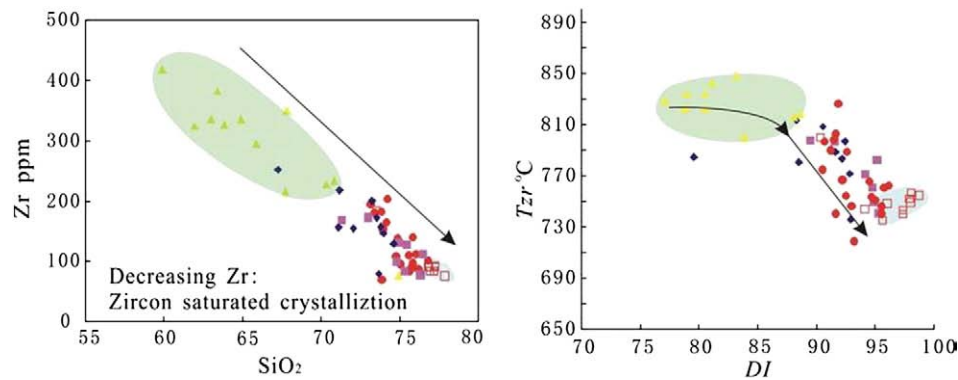


Fig. 15. Zr versus SiO_2 and DI versus T_{zr} diagrams.

around 80 Ma. The age of Longchahe porphyritic granite is between 82.0 ± 0.25 Ma to 83.2 ± 1.40 Ma, the Laochang porphyritic granite is 83.3 ± 1.60 Ma, the Masong porphyritic granite is 82.8 ± 1.70 Ma. The Laochang equigranite is 85.0 ± 0.85 Ma, the Xinshan equigranite is 83.1 ± 0.42 Ma, the Baishachong equigranite is 77.4 ± 2.50 Ma to 79.0 ± 0.80 Ma, and the Shexianshui equigranite is 81.0 ± 0.52 Ma to 83.0 ± 0.35 Ma.

- (2) Geochemical and Sr–Nd–Hf isotopic data suggest that the Gejiu granite magmas experienced a high degree of fractional crystallization after they have formed by partial melting of Mesoproterozoic crust with minor input from mantle-derived magmas. The Gejiu granites are one of the members of the extensive Late Cretaceous magmatic event in south-eastern Yunnan and western Guangxi region, close to the SW termination of the south China (Nanling) tin–tungsten province. Both the granites and the genetically-related tin–polymetallic mineralization reside in an intraplate extensional setting.
- (3) Granites in the Gejiu area are attributed to the “crust–mantle syntectonic type” of Xu et al. (1982) that display strong signs of mantle–crust interaction in an intraplate setting.

Supplementary materials related to this article can be found online at doi:10.1016/j.lithos.2010.08.013.

Acknowledgements

The authors are grateful for Prof. Nelson Eby, Prof. Xian-Hua Li and Prof. Franco Pirajno for their constructive reviews, which significantly improved the quality of this paper. We appreciate the assistance of Prof. Xu Xisheng, Liu Dunyi and Mr. Hou Kejun with zircon U–Pb dating, Ms. Hui Zhou with zircon CL imaging, Dr. Liang Xirong in major element analysis by XRF, Ms. Jing Hu for trace element analysis by ICP-MS, Mr. Jinlong Ma for Nd–Sr isotopes analysis by MC-ICP-MS, Mr. Hou Kejun for Hf isotope analysis by LA-MC-ICPMS. Prof. Peter Laznicka is thanked for polishing the language of this manuscript. This study was supported by the National Science Foundation of China (40930419), Special Research Funding for the Public Benefits Sponsored by MLR (200911007-12), Research Program of Yunnan Tin Group (2010-04A), and the Fundamental Research Funds for the Central Universities (2-9-2010-21).

References

- 308 Geological Party, 1984. Geology of tin deposit in Gejiu area. Metallurgical Industry Publishing House, Beijing, pp. 50–90.
- Anderson, T., 2002. Correction of common lead in U–Pb analysis that do not report ^{204}Pb . *Chemical Geology* 192, 59–79.
- Blichert Toft, J., Albarede, F., 1997. The Lu–Hf isotope geochemistry of chondrites and the evolution of the mantle–crust system. *Earth and Planetary Science Letters* 148, 243.
- Cai, M.H., He, L.Q., Liu, G.Q., 2006. SHRIMP zircon U–Pb dating of the intrusive rocks in the Dachang tin–polymetallic ore district, Guangxi and their geological significance. *Geological Review* 52, 409–414 (in Chinese with English abstract).
- Campbell, I.H., Hill, R.L., 1988. A two-stage model for the formation of the granite greenstone terrains of the Kalgoorlie–Norseman area, Western Australia. *Earth and Planetary Science Letters* 90, 11–25.
- Chappell, B.W., 1999. Aluminium saturation in I- and S-type granites and the characterization of fractionated haplogranites. *Lithos* 46, 535–551.
- Chappell, B.W., White, A.J.R., 1974. Two contrasting granite types. *Pacific Geology* 8, 173–174.
- Chen, J.C., 1983. Preliminary study on the comparison of S and I type granite in Yunnan province. *Geology of Yunnan* 2, 28–37 (in Chinese).
- Chen, J.F., Jahn, B.M., 1998. Crustal evolution of southeastern China: Nd and Sr isotopic evidence. *Tectonophysics* 284, 101–133.
- Chen, Y.C., Zhu, Y.S., 1993. Mineral deposits of China. Geological Publishing House, Beijing, pp. 209–211 (in Chinese).
- Chen, J., Hall, C., Stanley, C.J., 1992. Tin-bearing skarns of South China: geological setting and mineralogy. *Ore Geology Reviews* 7, 225–248.
- Chen, M.H., Cheng, Y.B., Zhang, W., Yang, Z.X., Lu, G., 2008. Primary Study on the Relationship between Yanshanian Magma Activity and Mineralization in Youjiang folded belt. In: Chen, Y.C., Xue, C.J., Zhang, C.Q. (Eds.), Main attacking deep, pushing forward western and scanning the world. 9th National Deposit Meeting. Geological Publishing House, Beijing, pp. 241–242 (in Chinese).
- Chen, M.H., Mao, J.W., Zhang, W., Yang, Z.X., Lu, G., Hou, K.J., Liu, J.H., 2009. Zircon U–Pb age and Hf isotopic composition of the Baiceng ultrabasic rock veins in Zhenfeng county, southwestern Guizhou Province, China. *Mineral Deposits* 28, 240–250 (in Chinese with English abstract).
- Cheng, Y.B., Mao, J.W., Xie, G.Q., 2009. Zircon U–Pb dating of the granites in Gejiu supergiant tin polymetallic ore-field and its significance. *Mineral Deposits* 28, 297–312.
- Cheng, Y.B., Tong, X., Wu, J.D., Mo, G.P., 2010a. Geochronology framework of the W–Sn mineralization granites in western south China and their geological significance. *Acta Petrologica Sinica* 26 (3), 809–818 (in Chinese with English abstract).
- Cheng, Y.B., Mao, J.W., Chen, X.L., Li, W., 2010b. LA-ICP-MS zircon dating of the Bozhushan granite in southeastern Yunnan province and their significance. *Journal of Jilin University (Earth Science)* 40, 869–878.
- Chu, N.C., Taylor, R.N., Chavagnac, V., Nesbitt, R.W., Boella, R.M., Milton, J.A., German, C.R., Bayon, G., Burton, K., 2002. Hf isotope ratio analysis using multi-collector inductively coupled plasma mass spectrometry: an evaluation of isobaric interference corrections. *Journal of Analytical Atomic Spectrometry* 17, 1567–1574.
- Collins, W.J., Beams, S.D., White, A.J.R., Chappell, B.W., 1982. Nature and origin of A-type granites with particular reference to southeastern Australia. *Contribution to Mineralogy And Petrology* 80, 189–200.
- Compton, W., Williams, I.S., Kirschvink, J.L., 1992. Zircon U–Pb ages for the early Cambrian timescale. *Journal of the Geological Society* 149, 171–184.
- Dai, F.S., 1996. Characteristics and evolution of rock series, lithogenesis, metallogenesis of crust-derived anatectic magma in Gejiu ore district. *Geology of Yunnan* 15, 330–344 (in Chinese with English abstract).
- DePaolo, D.J., 1981. A neodymium and strontium isotopic study of the Mesozoic calc-alkaline granitic batholiths of the Sierra Nevada and Peninsular Ranges, California. *Journal of Geophysical Research* 86, 10470–10488.
- Elhoul, S., Belousova, E., Griffin, W.L., 2006. Trace element and isotopic composition of GJ-red zircon standard by laser ablation. *Geochim Cosmochim Acta* A158 suppl.
- Faure, G., 2001. *Origin of Igneous Rocks*. Springer-Verlag, Berlin Heidelberg New York, pp. 1–117.
- Feng, X.R., 1982. The accessory mineral of the granites in Gejiu ore district, and its genesis and relationship with mineralization. *Yunnan Geology* 1, 129–133.
- Geology department of Nanjing University, 1981. Different Era granitoids in south China and their mineralization relation. Science Press, Beijing, pp. 1–395 (In Chinese).
- Gilder, S.A., Gill, J., Coe, R.S., 1996. Isotopic and paleomagnetic constraints on the Mesozoic tectonic evolution of south China. *Journal of Geophysical Research* 101 (B7), 13137–16154.
- Griffin, W.L., Pearson, N.J., Belousova, E., Jackson, S.E., van Achterbergh, E., O'Reilly, S.Y., Shee, S.R., 2000. The Hf isotope composition of cratonic mantle: LAM-MC-ICPMS analysis of zircon megacrysts in kimberlites. *Geochimica et Cosmochimica Acta* 4, 133–147.

- Griffin, W.L., Wang, X.W., Jackson, S.E., Pearson, N.J., O'Reilly, S.Y., Xu, X., Zhou, X., 2002. Zircon chemistry and magma mixing, SE China: in-situ analysis of Hf isotopes, Tonglu and Pingtan igneous complexes. *Lithos* 61, 237–269.
- Hong, D.W., Xie, X.L., Zhang, J.S., 1998. Isotope geochemistry of world-class gold deposits: characteristics, space-time distribution and origin. *Gold in 2000: In: Hagemann, S.G., Brown, P.E. (Eds.), Reviews in Economic Geology*, 13, pp. 501–551.
- Hou, K.J., Li, Y.H., Zou, T.R., Qu, X.M., Shi, Y.R., Xie, G.Q., 2007. Laser ablation-MC-ICP-MS technique for Hf isotope microanalysis of zircon and its geological applications. *Acta Petrologica Sinica* 23, 2595–2604 (In Chinese with English abstract).
- Jahn, B.M., Wu, F.Y., Chen, B., 2000a. Granitoids of the central Asian orogenic belt and continental growth in the Phanerozoic. *Transaction of the Royal Society of Edinburgh: Earth Sciences* 91, 181–193.
- Jahn, B.M., Wu, F.Y., Hong, D.W., 2000b. Important crustal growth in the Phanerozoic: isotopic evidence of granitoids from east-central Asia. *Proceedings of the Indian Academy of Sciences (Earth Planet. Sci.)* 109, 5–20.
- Jean, W., Min, S., Xing, G.F., Li, X.H., Zhao, G.C., Wong, K., Yuan, C., Xia, X.P., Li, L.M., Wu, F.Y., 2009. Geochemical and zircon U–Pb and Hf isotopic study of the Baijuehuajian metaluminous A-type granite: extension at 125–100 Ma and its tectonic significance for South China. *Lithos* 112, 289–305.
- Jiang, Z.W., Oliver, N.H.S., Barr, T.D., Power, W.L., Ord, A., 1997. Numerical modeling of fault-controlled fluid flow in the genesis of the deposits of the Malage ore district, Gejiu Mining District, China. *Economic Geology* 92, 228–247.
- King, P.L., White, A.J.R., Chappell, B.W., Allen, C.M., 1997. Characterization and origin of aluminous A-type granites from the Lachlan Fold Belt, Southeastern Australia. *Journal of Petrology* 38, 371–391.
- Li, J.H., 1985. Characteristic and original study on granites in Gejiu area. *Geology of Yunnan* 4, 327–352 (in Chinese with English abstract).
- Li, X.H., 1997. Geochemistry of the Longsheng Ophiolite from the southern margin of Yangtze Craton, SE China. *Geochemical Journal* 31, 323–337.
- Li, X.H., Li, Z.X., Ge, W., Zhou, H., Li, W., Liu, Y., Wingate, M.T.D., 2003. Neoproterozoic granitoids in South China: crustal melting above a mantle plume at ca. 825 Ma? *Precambrian Research* 122, 45–83.
- Li, X.H., Liu, D.Y., Sun, M., Li, W.X., Liang, X.R., Liu, Y., 2004. Precise Sm–Nd and U–Pb isotopic dating of the supergiant Shizhuoyuan polymetallic deposit and its host granite, Southeast China. *Geological Magazine* 141, 225–231.
- Li, X.H., Qi, C.S., Liu, Y., Liang, X.R., Tu, X.L., Xie, L.W., Yang, Y.H., 2005. Petrogenesis of the Neoproterozoic bimodal volcanic rocks along the western margin of the Yangtze Block: new constraints from Hf isotopes and Fe/Mn ratios. *Chinese Science Bulletin* 50, 2481–2486.
- Li, X.H., Li, Z.X., Li, W.X., Liu, Y., Yuan, C., Wei, G.J., Qi, C.S., 2007. U–Pb zircon, geochemical and Sr–Nd–Hf isotopic constraints on age and origin of Jurassic I- and A-type granites from central Guangdong, SE China: a major igneous event in response to foundering of a subducted flat-slab? *Lithos* 96, 186–204.
- Li, S.R., Wang, D.H., Liang, T., Qu, W.J., Ying, L.J., 2008. Metallogenic epochs of the Damingshan tungsten deposit in Guangxi and its prospecting potential. *Acta Geologica Sinica* 82, 873–879 (in Chinese with English abstract).
- Liang, T., Chen, Y.C., Wang, D.H., Cai, M.H., 2008. Geology and Geochemistry of the Dachang Tin Polymetallic Deposit, Guangxi province. *Geological Publishing House, Beijing*, pp. 1–229 (in Chinese).
- Lin, Z.Y., Wang, D.H., Li, S.R., 2008. Re–Os isotopic ages of molybdenite from the Wangshe copper–tungsten deposit in Guangxi Province and their implications. *Acta Geologica Sinica* 82, 1565–1571 (in Chinese with English abstract).
- Liu, Y.P., Li, C.Y., Zeng, Z.G., Wang, J.L., 1999. Monomineral Rb–Sr dating contour determination of Dulong tin and zinc deposit. *Journal of Kunming Metallurgy College* 15, 5–8.
- Liu, Y.P., Li, Z.X., Li, H.M., 2007. U–Pb geochronology of cassiterite and zircon from the Dulong Sn–Zn deposit: Evidence for Cretaceous large–scale granitic magmatism and mineralization events in southeastern Yunnan province, China. *Acta Petrologica Sinica* 23, 967–976 (in Chinese with English abstract).
- Liu, S., Hu, R.Z., Gao, S., Feng, C.X., Huang, Z.L., Lai, S.C., Yuan, H.L., Liu, X.M., Coulson, Ian M., Feng, G.Y., Wang, T., Qi, Y.Q., 2009. U–Pb zircon, geochemical and Sr–Nd–Hf isotopic constraints on the age and origin of Early Palaeozoic I-type granite from the Tengchong–Baoshan Block, Western Yunnan Province, SW China. *Journal of Asian Earth Sciences* 36, 168–182.
- Liu, S., Su, W.C., Hu, R.Z., Feng, C.X., Gao, S., Coulson, Ian M., Wang, T., Feng, G.Y., Tao, Y., Xia, Y., 2010. Geochronological and geochemical constraints on the petrogenesis of alkaline ultramafic dykes from southwest Guizhou Province, SW China. *Lithos* 253–264.
- Ludwig, K.R., 2003. *ISOPLOT 3.0: a geochronological toolkit for Microsoft Excel*, Berkeley Geochronology Center: Special Publication, 4.
- Maniar, P.D., Piccoli, P.M., 1989. Tectonic discrimination of granitoids. *Geological Society of America Bulletin* 101, 635–643.
- Mao, J.W., Li, H.Y., Song, X.X., 1998. Geology and geochemistry of the Shizhuoyuan W–Sn–Mo–B Polymetallic deposit, Hunan, China. *Geological Publishing House, Beijing*, pp. 1–182 (in Chinese).
- Mao, J.W., Xie, G.Q., Li, X.F., 2004. Mesozoic large-scale mineralization and multiple lithospheric extension in South China. *Earth Science Frontiers* 11, 45–55 (in Chinese with English abstract).
- Mao, J.W., Cheng, Y.B., Guo, C.L., 2008a. Gejiu tin polymetallic ore-field: deposit model and discussion. *Acta Geologica Sinica* 81, 1456–1468 (in Chinese with English abstract).
- Mao, J.W., Xie, G.Q., Guo, C.L., Yuan, S.D., Cheng, Y.B., Chen, Y.C., 2008b. Spatial-temporal distribution of Mesozoic ore deposits in South China and their metallogenic settings. *Geological Journal of China Universities* 14, 510–526.
- Mao, J.W., Xie, G.Q., Pirajno, F., Ye, H.S., Wang, Y.B., Li, Y.F., Xiang, J.F., Zhao, H.J., 2010. Late Jurassic–Early Cretaceous granitoid magmatism in Eastern Qinling, central-eastern China: SHRIMP zircon U–Pb ages and tectonic implications. *Australian Journal of Earth Sciences* 57, 51–78.
- Middlemost, E.A.K., 1994. Naming materials in the magma/igneous rock system. *Earth Science Reviews* 37, 215–224.
- Mo, G.P., 2006. Genetic type of granites in Gejiu super large tin polymetallic deposit. *Mineral Resources and Geology* 20, 413–417.
- Peng, C.D., 1985. A discussion on the condition, types and model of Gejiu tin deposit. *Yunnan Geology* 4, 17–32 (in Chinese with English abstract).
- Rollinson, H.R., 1993. *Using geochemical data: evaluation, presentation, interpretation*. Longman Scientific and Technical, New York, pp. 1–352.
- Rudnick, R.L., Fountain, D.M., 1995. Nature and composition of the continental crust: a lower crustal perspective. *Reviews of Geophysics* 33, 267–309.
- Song, B., Zhang, Y.H., Wan, Y.S., Jian, P., 2002. The SHRIMP sample manufacture, test and explanation of some phenomena for the zircon. *Geological Review* 48, 26–30 (in Chinese).
- Southwest Geological Exploration Corporation, 1984. *Geology of tin deposits in Gejiu*. Metallurgical Industry Publishing House, Beijing, p. 256 (in Chinese).
- Strecheisen, A., Le Maitre, R.W., 1979. A chemical approximation to the modal QAPF classification of the igneous rocks. *Neues Jahrbuch für Mineralogie Abhandlungen* 136, 169–206.
- Sun, S.S., McDonough, W.F., 1989. Chemical and Isotopic Systematics of Oceanic Basalts: Implications for Mantle Composition and Processes. *Magmatism in the Ocean Basins: In: Saunders, A.D., Norry, M.J. (Eds.), Geol. Soc. London Special Publ.*, vol. 42, pp. 313–345.
- Suo, S.T., Bi, X.H., Zhou, H.W., 1999. Very low grade metamorphism. *Geological Publishing House, Beijing*, pp. 1–68.
- Sylvester, P.J., 1989. Post-collisional alkaline granites. *Journal of Geology* 97, 261–280.
- Tan, J., Wei, J.H., Li, S.R., 2008. Geochemical characteristics and tectonic significance of Kunlun A-type granite, Guangxi. *Earth Science (Journal of China University of Geosciences)* 33 (6), 743–754.
- Wang, Z.F., 1983. Discussion on some problems in mineralization of Gejiu Tin deposit. *Acta Geologica Sinica* 57, 154–163.
- Wang, D.H., Chen, Y.C., Chen, W., Sang, H.Q., Li, H.Q., 2004. Dating the Dachang giant tin-polymetallic deposit in Nandan, Guangxi. *Acta Geologica Sinica* 78, 132–139 (in Chinese with English abstract).
- Wang, Q., Li, J.W., Jian, P., Zhao, Z.H., Xiong, X.L., Bao, Z.W., Xu, J.F., Li, C.F., Ma, J.L., 2005. Alkaline syenites in eastern Cathaysia (south China): link to Permian–Triassic transtension. *Earth and Planetary Science Letters* 230, 339–354.
- Wang, Y.L., Pei, R.F., Li, J.W., Wu, J.D., Li, L., Wang, H.L., 2007. Geochemical characteristics and tectonic setting of Laochang granite in Gejiu. *Acta Geologica Sinica* 81, 979–985 (in Chinese with English abstract).
- Watson, E.B., Harrison, T.M., 1983. Zircon saturation revisited: temperature and composition effects in a variety of crustal magma types. *Earth and Planetary Science Letters* 64, 295–304.
- Wei, G.J., Liang, X.R., Li, X.H., Liu, Y., 2002. Precise measurement of Sr isotopic compositions of liquid and solid base using (LA) MCICP-MS. *Geochemistry* 31, 295–305 (in Chinese with English abstract).
- Whalen, J.B., Currie, K.L., Chappell, B.W., 1987. A-type granites: geochemical characteristics, discrimination and petrogenesis. *Contribution to Mineralogy And Petrology* 95, 407–419.
- Williams, I.S., 1998. U–Th–Pb geochronology by ion microprobe. *Reviews in Economic Geology* 7, 1–35.
- Wolf, M.B., London, D., 1994. Apatite dissolution into peraluminous haplogranite melts: an experimental study of solubilities and mechanisms. *Geochimica et Cosmochimica Acta* 58, 4127–4145.
- Wu, Q.S., Xu, J.Z., Yang, Z., 1984. Study on Sr isotope character and prospecting criteria of Tin-bearing granite of Gejiu area. *Geochemica* 4, 293–302.
- Wu, F.Y., Sun, D.Y., Li, H.M., Jahn, B.M., Bor-ming, Wilde, S., 2002. A-type granites in northeastern China: age and geochemical constraints on their petrogenesis. *Chemical Geology* 187, 143–173.
- Wu, F.Y., Jahn, B.M., Wilder, S.A., Lo, C.H., Yui, T.F., Lin, Q., Ge, W.C., Sun, D.Y., 2003. Highly fractionated I-type granites in NE China (I): geochronology and petrogenesis. *Lithos* 66, 241–273.
- Wu, F.Y., Yang, Y.H., Xie, L.W., 2006. Hf isotopic compositions of the standard zircons and baddeleyites used in U–Pb geochronology. *Chemical Geology* 234, 105–126.
- Wu, F.Y., Li, X.H., Yang, J.H., Zheng, Y.F., 2007. Discussions on the petrogenesis of granites. *Acta Petrologica Sinica* 23 (6), 1217–1238.
- Xie, G.Q., Hu, R.Z., Mao, J.W., 2006. K–Ar dating, geochemical, and Sr–Nd–Pb isotopic systematics of late Mesozoic mafic dykes, southern Jiangxi province, Southeastern China: petrogenesis and tectonic implication. *International Geological Reviews* 8, 1023–1051.
- Xu, Y.R., Li, Y.X., 1997. A tin shoot-granitic type tin orebody—discovered in the Gejiu mining area. *Mineral Resources and Geology* 11 (2), 99–102 (in Chinese with English abstract).
- Xu, K.Q., Sun, N., Wang, D.Z., 1982. Petrogenesis of the Granitoids in South China and their Metallogenetic Relations. In: Xu, K.Q., Tu, G.C. (Eds.), *Geology of granites and their metallogenetic relations*. Science Press, Beijing, pp. 1–31 (in Chinese).
- Yan, D.P., Zhou, M.F., Wang, Y., Wang, C.L., Zhao, T.P., 2005. Structural styles and chronological evidences from Dulong–Song Chay tectonic dome: earlier spreading of south china sea basin due to late mesozoic to early cenozoic extension of south china block. *Earth Science-Journal of China University of Geosciences* 30 (4), 402–412.
- Yang, Z.X., Mao, J.W., Chen, M.H., 2008. Re–Os dating of molybdenite from the Kafang skarn copper (tin) deposit in the Gejiu tin polymetallic ore district and its geological significance. *Acta Petrologica Sinica* 24 (8), 1937–1944.
- Yang, Z.X., Mao, J.W., Chen, M.H., 2009. ⁴⁰Ar–³⁹Ar dating of muscovite from Laochang veinlet-like Sn deposit in Gejiu tin polymetallic ore district and its geological significance. *Mineral Deposits* 28 (3), 336–344.
- Yu, C.W., Tang, Y.J., Shi, P.F., Deng, B.L., 1988. The denamic system of endogenic ore formation in Gejiu tin–polymetallic ore region, Yunnan province. *China University of Geosciences Press, Wuhan*, pp. 42–251 (in Chinese).

- Yuan, H.L., Wu, F.Y., Gao, S., Liu, X.M., Xu, P., Sun, D.Y., 2003. Determination of U–Pb age and rare earth element concentrations of zircon from Cenozoic intrusions in northeastern China by laser ablation ICP-MS. *Chinese Science Bulletin* 48, 2411–2421.
- Zhang, Z.C., Mahoney, J.J., Mao, J.W., Wang, F.S., 2006. Geochemistry of picritic and associated flows of the western Emeishan flood basalt province, China. *Journal of Petrology* 47, 1997–2019.
- Zhao, K.D., Jiang, S.Y., Jiang, Y.H., Wang, R.C., 2005. Mineral chemistry of the Qitianling granitoid and the Furong tin ore deposit in Hunan Province, South China: implication for the genesis of granite and related tin mineralization. *European Journal of Mineralogy* 17 (4), 635–648. doi:10.1127/0935-1221/2005/0017-0635.
- Zhong, H., Zhu, W.G., Hu, R.Z., Xie, L.W., He, D.F., Liu, F., Chu, Z.Y., 2009. Zircon U–Pb age and Sr–Nd–Hf isotope geochemistry of the Panzhihua A-type syenitic intrusion in the Emeishan large igneous province, southwest China and implications for growth of juvenile crust. *Lithos* 110, 109–128.
- Zhuang, Y.Q., Wang, R.Z., Yang, S.P., 1996. Tin–Copper Polymetallic deposit. Earthquake Publishing House, Beijing, pp. 38–101 (in Chinese).

Chapter 3

Granite, gabbro and mafic microgranular enclaves in the Gejiu Area: a case of two stage mixing of crust- and mantle-derived magmas

Granite, gabbro and mafic microgranular enclaves in the Gejiu area, Yunnan Province, China: a case of two-stage mixing of crust- and mantle-derived magmas

Yanbo Cheng · Carl Spandler ·
Jingwen Mao · Brian G. Rusk

Received: 2 November 2011 / Accepted: 9 May 2012 / Published online: 24 May 2012
© Springer-Verlag 2012

Abstract Geochronological, geochemical, whole-rock Sr–Nd, and zircon Hf isotopic analyses were carried out on the Jiasha Gabbro, mafic microgranular enclaves (MME) and host Longchahe Granite samples from the Gejiu area in the southeast Yunnan province, SW China, with the aim of characterizing their petrogenesis. Compositional zoning is evident in the gabbro body as the cumulate textures and mineral proportions in the gabbro interior are distinct from the gabbro margin. The Longchahe Granite largely comprises metaluminous quartz monzonite with distinctive K-feldspar megacrysts, but also contains a minor component of peraluminous leucogranite. The MME have spheroidal to elongated/lenticular shapes with sharp, crenulated and occasionally diffuse contacts with the host granite, which we attribute to the undercooling and disaggregation of mafic magma globules within the cooler host felsic magma. Field observations, geochronology, geochemistry,

Sr–Nd and zircon Hf isotopic compositions point to a complex petrogenesis for this granite–MME–gabbro association. Zircon $^{206}\text{Pb}/^{238}\text{U}$ ages determined by LA-ICP-MS for a mafic enclave, its host granite and the gabbro body are 83.1 ± 0.9 Ma, 83.1 ± 0.4 Ma and 83.2 ± 0.4 Ma, respectively, indicating coeval crystallization of these igneous rock units. Crystal fractionation processes can explain much of the compositional diversity of the Jiasha Gabbro. The geochemical features of the gabbro, such as high $\text{Mg}^\#$ (up to 70) and Cr (up to 327 ppm), enrichment in LILEs (e.g., Rb, Ba, K_2O) and LREEs, and depletion in HFSE (e.g., Nb, Ta, Ti), together with initial $^{87}\text{Sr}/^{86}\text{Sr}$ ratios of 0.708–0.709 and negative $\epsilon\text{Nd}(t)$ values (-5.23 to -6.45), indicate they were derived from a mantle source that had undergone previous enrichment, possibly by subduction components. The Longchahe Granite has a large range of SiO_2 (59.87–74.94 wt%), is distinctly alkaline in composition, and has Sr–Nd–Hf isotopic compositions ($(^{87}\text{Sr}/^{86}\text{Sr})_i > 0.712$, $\epsilon\text{Nd}(t) = -6.93$ to -7.62 and $\epsilon\text{Hf}(t) = -5.8$ to -9.9) that are indicative of derivation from a crustal source. However, the most primitive rocks of Longchahe Granite are compositionally distinct from any feasible crustal melt. We interpret the spectrum of rock types of the Longchahe Granite to have formed via mixing between crustally derived peraluminous leucogranite magma and mantle-derived magma of similar heritage to the Jiasha Gabbro. We speculate that this mixing event occurred early in the magmatic history of these rocks at relatively high temperature and/or deep in the crust to allow efficient physical mixing of magmas. Saturation and accumulation of K-feldspar and zircon in the mixed magma is invoked to explain the megacrystic K-feldspar and elevated K_2O and Zr content of some of the granitic rocks. A later episode of magma mixing/mingling is preserved as the MME that have geochemical and isotopic compositions

Communicated by J. Hoefs.

Electronic supplementary material The online version of this article (doi:10.1007/s00410-012-0766-0) contains supplementary material, which is available to authorized users.

Y. Cheng (✉) · J. Mao
Faculty of Earth Science and Mineral Resources,
China University of Geosciences, Beijing 100083,
People's Republic of China
e-mail: chamboll@yahoo.cn

Y. Cheng · C. Spandler · B. G. Rusk
School of Earth and Environmental Sciences,
James Cook University, Townsville 4811, Australia

J. Mao
MLR Laboratory of Metallogeny and Mineral Assessment,
Institute of Mineral Resources, Chinese Academy of Geological
Sciences, Beijing 100037, People's Republic of China

that, for the most part, are intermediate between the granite and the gabbro. The MME are interpreted to be fractionated melts of mafic magma related to gabbro that were subsequently injected into the cooler, partly crystalline granitic magma. Mingling and mixing processes within the convectively dynamic upper crustal magma chamber resulting in a hybrid (MME) magma. During this second mixing episode, element interdiffusion, rather than bulk physical mixing, is interpreted to be the dominant mixing process.

Keywords Magma mixing · Magma mingling · Mafic microgranular enclaves · Gabbro · Gejiu

Content has been removed
due to copyright restrictions



Chapter 4

**The origin of the world class
tin-polymetallic deposits in the Gejiu
district: constraints from metal zoning
characteristics and ^{40}Ar - ^{39}Ar
geochronology**



The origin of the world class tin-polymetallic deposits in the Gejiu district, SW China: constraints from metal zoning characteristics and ^{40}Ar - ^{39}Ar geochronology

Yanbo Cheng ^{a, b, c*}, Jingwen Mao ^c, Zhaoshan Chang ^b, Franco Pirajno ^d

^a Faculty of Earth Science and Mineral Resources, China University of Geosciences, Beijing, 100083, China

^b School of Earth and Environmental Sciences, James Cook University, Townsville, 4811, Australia

^c MLR Key Laboratory of Metallogeny and Mineral Assessment, Institute of Mineral Resources, Chinese Academy of Geological Sciences, Beijing, 100037, China

^d School of Earth and Environment, University of Western Australia, 35 Stirling Highway, Crawley WA 6008, Australia

*Corresponding author: email, chamboll@yahoo.cn

Abstract

The Gejiu tin-polymetallic deposits in the Western Cathaysia Block of South China comprise the world's largest primary tin district, with a total resource of approximately 300 million metric tons at an average grade of 1 wt percent Sn. Tin polymetallic mineralization occurs in five deposits and have four ore types, i.e., greisen, skarn, stratabound cassiterite-sulfide (mostly oxidized) and vein type ore. In each deposit the orebodies typically occur in an extensive hydrothermal system centered on a shallow Late

Cretaceous granitoid cupola. Metal zoning is well developed both vertically and horizontally over the entire district, from W+Be+Bi ± Mo ± Sn ores inside granite intrusions, to Sn+Cu-dominated ores at intrusion margins and farther out to Pb+Zn deposits in the surrounding host carbonate. This zoning pattern is similar to that of other hydrothermal deposits in other parts of the world, indicating a close genetic relationship between magmatism and mineralization. In this paper, we dated thirteen mica samples from all types of mineralization and from the five deposits in the Gejiu district. The ages range from 77.4 ± 0.6 Ma to 95.3 ± 0.7 Ma and are similar to the existing zircon U-Pb age of the granitic intrusions (77.4 ± 2.5 - 85.8 ± 0.6), indicating a genetic relationship between the mineralization and the intrusions. Geological characteristics, metal zoning patterns and new geochronological data all indicate that the tin-polymetallic ores in the Gejiu district are hydrothermal in origin and are genetically related to the nearby granitic intrusions. It is unlikely that the deposits are syngenetic, as has been proposed in recent years.

Key words: deposit geology; metal zoning; ^{40}Ar - ^{39}Ar dating; ore genesis; Gejiu

Introduction

The Gejiu tin-polymetallic ore district is located approximately several to tens of kilometers southeast of Gejiu city, Yunnan Province, SW China. It is one of the largest and oldest mining districts in the world. It has been mined since the Han dynasty (202 B.C. to 220 A.D.), intermittently for more than 2,000 years. The Gejiu district comprises five Sn-Cu-Pb-Zn polymetallic deposits, namely Malage, Songshujiao, Gaosong, Laochang and Kafang, containing approximately 300 Mt of Sn ores at an average grade of 1% Sn, another 300 Mt of Cu ores averaging 2% Cu, and 400 Mt of Pb-Zn ores with an average grade of 7% Pb+Zn (Zhuang et al., 1997). It is the largest tin district in the world. Exploration in this district is still finding more ores to this day.

Tin polymetallic ores in the Gejiu district, characterized by extensive skarn alteration, multiple mineralization styles and well defined metal zoning around granitic cupolas, have long been considered genetically related to Cretaceous granites (e.g., [308 Geological](#)

Party, 1984; Peng, 1985; Zhao and Li, 1987; Luo, 1995; Zhuang et al., 1996; Mao et al., 2008). Theories based on this understanding have contributed a great deal to exploration efforts (e.g., 308 Geological Party, 1984; Peng, 1985; Zhuang et al., 1996; Jiang et al., 1997). However, as many orebodies are approximately stratabound, some authors have challenged this view, arguing that the ores may be syngenetic (Zhou, 1988; Jin, 1991; Peng, 1992). Metacolloidal textures and resembling oolite aggregates have been found in some of the orebodies, leading to speculation as to a submarine exhalation hypothesis (Zhou et al., 1997, 1999; Zhang et al., 2004). Based on K-Ar, Ar-Ar and Pb-Pb dating on different minerals (see below for details), it has been argued that Sn polymetallic mineralization may be of VHMS style and/or SEDEX deposits (Qin et al., 2006; Qin and Li, 2008; Li et al., 2006, 2009; Qian et al., 2011a, 2011b).

Dating is one of the most powerful tools that place constraints on the genesis of ore. However, the above mentioned mineralisation ages have a wide range and are somewhat inconsistent. Qin et al. (2006) obtained several mica ^{40}Ar - ^{39}Ar ages ranging from 83.23 ± 2.07 to 205.11 ± 4.38 Ma, while another group of ~ 200 to ~ 240 Ma ages were obtained through the use of Pb-Pb methods on sulfides. Qin et al. (2006) and Li et al. (2009) reported K-Ar ages of 43.49 ± 0.87 Ma to 186.01 ± 3.72 Ma for cassiterite. These data were viewed as important evidence for the syngenetic model (Qin et al., 2006, 2008; Li 2009), as the ores had been considered to be Triassic in ages.

In this study, we document the geological characteristics of the Gejiu district, demonstrating the clear metal zoning, both vertically and horizontally, around granitic intrusions in all deposits in the Gejiu district. Moreover, due to lack of precise and systematic dating of the mineralization, we have also completed Ar-Ar dating of 13 representative muscovite and phlogopite samples from all ore types to constrain the age of mineralization. Comparing these dating results with U-Pb zircon ages of the granitic intrusions in the Gejiu district provides further constraints on the ore genesis.

Regional Geologic Setting

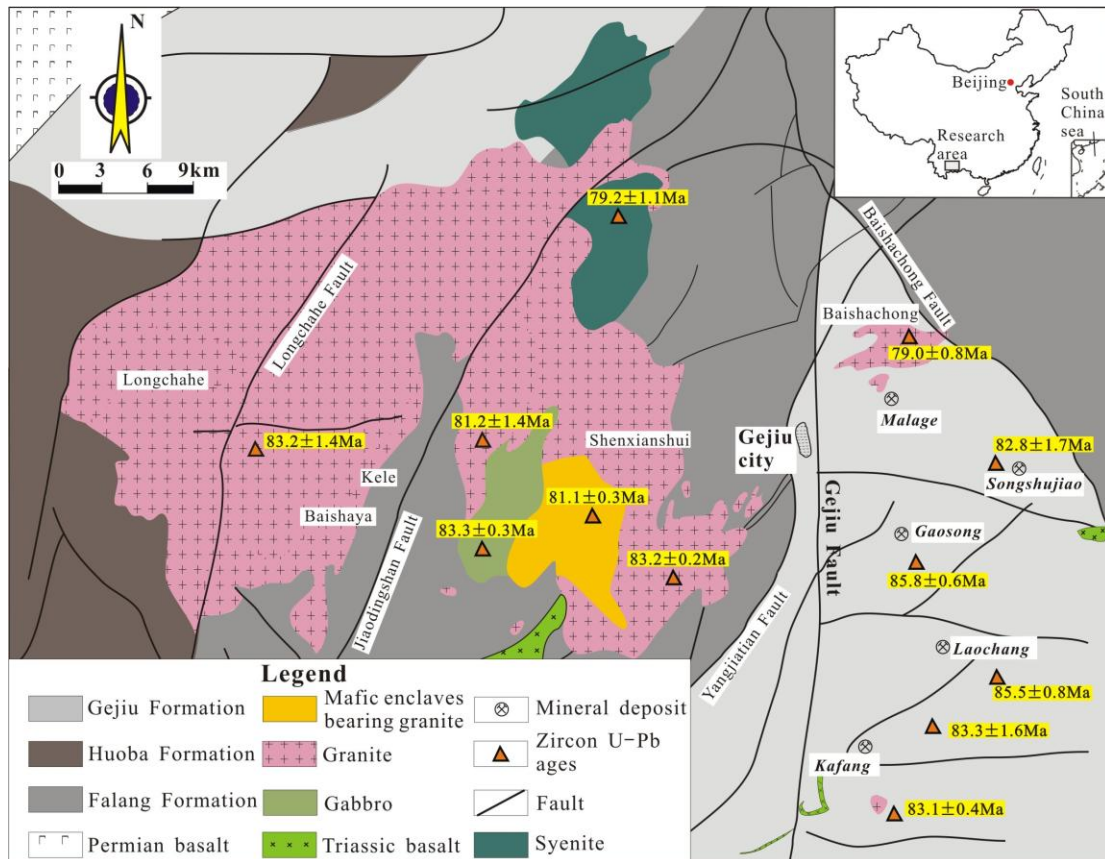


Figure 1 A simplified geological map of the Gejiu ore district (modified from Mao et al., 2008). The triangles and data represent the sample locations and U-Pb zircon ages of intrusions from Cheng and Mao (2010). Some samples in the eastern sector were from underground mine workings.

The world class Gejiu tin polymetallic ore district is located on the western margin of the South China Block, adjacent to the Yangtze Craton in the north and the Sanjiang Fold Belt in the west (Fig. 1). It is bounded by the Mile–Shizong Fault to the north, the regional strike–slip Ailaoshan–Honghe Fault to the west, and the North Vietnam Block to the south. The Gejiu District is ~1600 km² in area and was a tectonic sag or depression for much of its geological history (308 Geological Party, 1984). Cambrian to Quaternary rock successions are well-preserved (mostly not exposed and not shown in Fig. 1), and the late Triassic to Cretaceous strata are preferentially exposed near and at the surface due to uplift associated with Yanshanian (Mesozoic) tectonic movements (308 Geological Party, 1984). Most of the outcrops in the Gejiu area consist of Middle Triassic Gejiu Formation carbonate (>3000 m thick), and Middle Triassic Falang Formation fine-grained clastic sediment and carbonate with interlayering mafic lavas (1800 to 2800 m thick; Qin and Li,

2008). Numerous faults are present in the Gejiu region, including the NNE-trending Longchahe, Jiaodingshan and Yangjiatian faults, the NE-trending Baishachong fault and the NS-trending Gejiu fault. The Gejiu fault, which is the dominant structure in the Gejiu District, divides the Gejiu area into its eastern and western sectors (Fig. 1), with the major deposits in the eastern sector. The Gejiu batholith is a prominent igneous body in this area, composed of Mesozoic gabbro, mafic microgranular enclaves (MMEs; Cheng et al., 2012), porphyritic biotite granite, equigranular biotite granite, syenites and mafic dykes. Mafic-intermediate rocks and alkaline rocks occur mostly in the western sector, while granitoids are distributed throughout the region. Granites in the vicinity of orebodies have intense greisen alteration, albite alteration and K-feldspar alteration, with or without skarns in carbonate wallrocks.

Characteristics of the Gejiu Granitic Batholith

The Gejiu granitic batholith has an outcrop area of ~300 km² and is one of the largest intrusions in the western Cathaysia Block (Fig. 1), intruding the Mid-Triassic sedimentary rocks. Based on texture and mineralogy, the Gejiu granitic batholith comprises six phases (308 Geological Party, 1984; Li, 1985; Lu, 1987; Dai, 1996; Zhuang et al., 1996; Cheng and Mao, 2010), which are summarized below.

Phase 1 is represented by porphyritic biotite granite with large euhedral K-feldspar phenocrysts that mostly measure 3 – 5 cm in length, but that may reach up to 10 cm. Phase 1 is represented by the Longchahe stock in the western sector. The rock-forming minerals include plagioclase (~40%), quartz (15% – 20% vol%), K-feldspar (10% – 25% vol%) and biotite (10% – 20% vol%). Accessory minerals are magnetite, titanite, apatite, zircon and allanite. Phase 2 is fine-grained porphyritic biotite granite, typically distributed around the Baishaya area, which is close to the Longchahe stock. The size and shape of phenocrysts vary in this phase. The major minerals are K-feldspar (~40% vol%), plagioclase (~25% vol%), quartz (~25% vol%) and biotite (5% – 10% vol%). The accessory minerals are the same as those from Phase 1. Phase 3 is porphyritic biotite granite with medium-grained euhedral to subhedral K-feldspar phenocrysts, which is best

represented in the Malage, Songshujiao and Laochang ore deposits. Phenocryst size is generally between 1 – 3 cm, with larger phenocrysts reaching 6 cm. Minerals include plagioclase (~25% vol%), K-feldspar (10% – 20% vol%), quartz (~30% vol%) and biotite (~10% vol%), with magnetite, zircon, apatite, titanite, fluorite, allanite and tourmaline as accessory minerals. Phase 4 is a coarse to medium-grained equigranular biotite granite, mostly distributed in the Laochang ore deposit and in the Shenxianshui, Baishachong and Kele areas. The major minerals include quartz (> 30% vol%), K-feldspar (~40% vol%), plagioclase (~20% vol%) and biotite (~5% vol%). Accessory minerals include zircon, magnetite, monazite, apatite and minor titanite. Phase 5 is medium to fine-grained leucogranite in the Xinshan area of the Kafang deposit. Rocks of this phase are fine-grained equigranular and light in color, containing little or no biotite, and with a high content of quartz (~40% vol%), K-feldspar (~35% vol%) and plagioclase (~30% vol%). Accessory minerals include zircon, apatite and monazite. Phase 6 refers to the fine-grained equigranular granitic dyke swarm and small stocks around granite margins, especially around the Baishachong and Shenxianshui stocks. The major minerals are quartz (~60% to ~70% vol%) and K-feldspar (~25% vol%), with minor occurrences of plagioclase, muscovite, zircon.

Recent studies have revealed that the Gejiu granite batholith formed between ~85 Ma and 77 Ma, is transitional from metaluminous to weakly peraluminous and is high-K and alkali-rich (Cheng and Mao, 2010). Geochemical and Sr–Nd–Hf isotopic data suggest that the Gejiu granitic magma experienced high degrees of fractional crystallization following its formation due to the partial melting of the Mesoproterozoic crust with minor input from mantle-derived magmas (Cheng and Mao, 2010). The geochemical data indicate that degrees of fractional crystallization are distinctive from each other and that the later phases tend to be more evolved. Mineralization is spatially related to highly evolved granitic phases.

Ore Deposit Geology

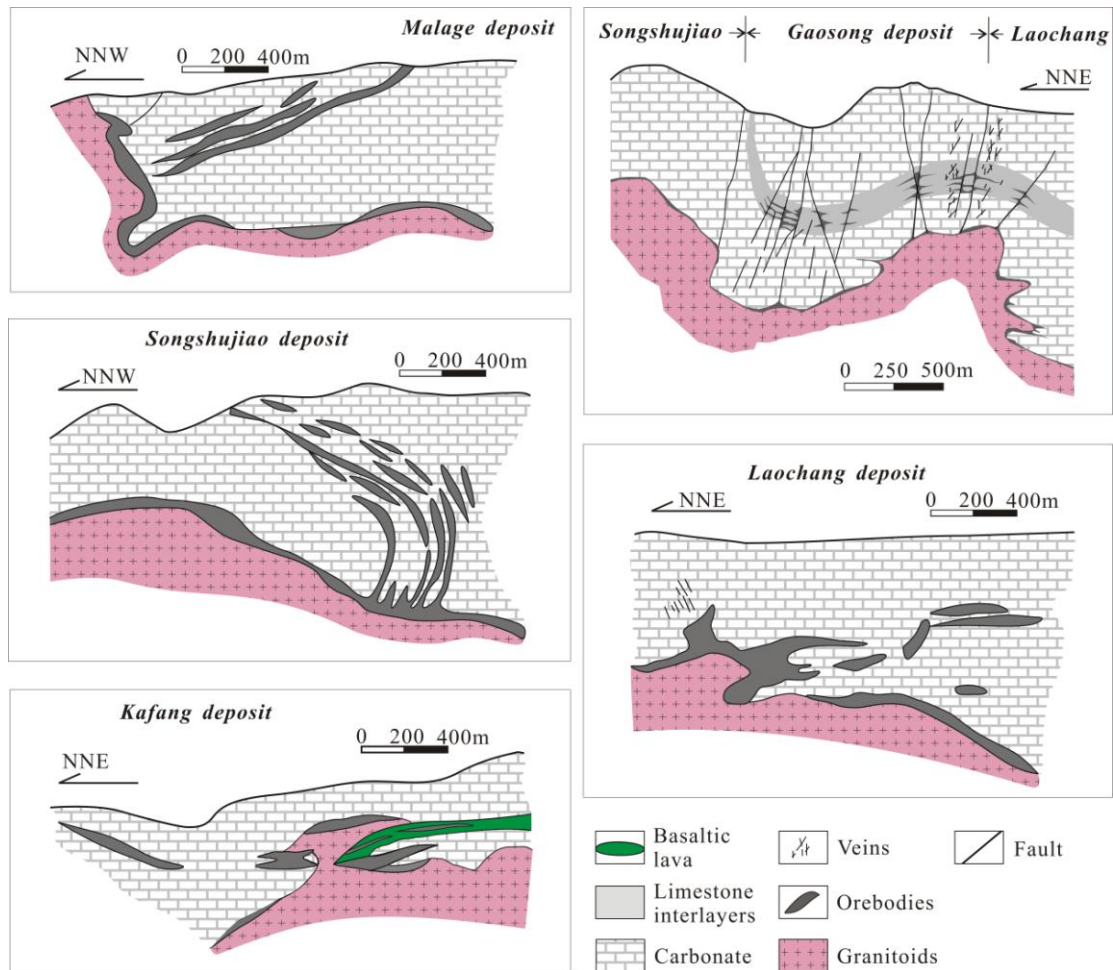


Figure 2 Cross sections of the five deposits in the Gejiu district that show the spatial relationship of granite, orebodies and host rocks (modified from Mao et al., 2008).

Malage Sn-Cu deposit

The Malage deposit is located in the northernmost part of the Gejiu district and occurs over approximately 40 km². The deposit is mostly underlain by the Mid-Triassic Gejiu Formation, which reaches a thickness of more than 1000 m and consists of limestone, dolomitic limestone, and dolomite. The NW-trending Masong anticline and its associated faults are the major ore-controlling structures of the Malage ore (Sun et al., 1987). The faults in the Malage deposit are considered crucial for the ore-forming fluid migration and ore genesis as they affected the interaction between fault deformation and fluid flow (Jiang et al., 1997). The Late Cretaceous granites, the Baishachong equigranular granite in the north and the Beipaotai porphyritic granite in the south, are the main igneous rocks

in this area. Although they have different petrological and geochemical compositions, they are believed to be derived from the same magma chamber, with different degrees of fractionation (Lu, 1987; Cheng and Mao, 2010).

The Malage deposit is Sn-Cu-dominant, with varying amounts of Pb, Zn, W, Mo and Be mineralization. Two types of ore styles have been recognized in this deposit (Fig. 2). The first is skarn, located in the contact areas between porphyritic granite and carbonate wallrocks. Tin and Cu grades range from 0.02% to 0.05% and 0.3% to 1.56%, respectively (308 Geological Party, 1984). Ore minerals include pyrrhotite, chalcopyrite, pyrite, beryl, bismuth, molybdenite, scheelite, sphalerite, galena, cassiterite and arsenopyrite. These ore minerals commonly occur as disseminations and/or as veins in skarn. The orebodies are generally lenticular, centered on Beipaotai porphyritic granite and are characterized by a clear metal zoning (308 Geological Party, 1984). The second type of ore style found in the Malage deposit is stratabound ore (weathered), examples of this ore style are present in some layers of various sedimentary rocks and are commonly distal to granite, with an average tin grade of 2.39% by weight (308 Geological Party, 1984). Tin is the major metallic element in this stratabound ore and is generally associated with varying amounts of Cu, Pb, Zn, In and Bi, with a few gangue minerals of quartz, muscovite and chlorite. The shape of these orebodies is quite complicated, including stratabound, vein and tabular. Alteration in the Malage deposit is extensive, with skarn being the major alteration type, comprising garnet, pyroxene, tremolite, actinolite, wollastonite, epidote and phlogopite. However, other alteration types also occur, including alkali metasomatism (potassic and sodic), greisen (quartz-muscovite), sericite and chlorite alteration of the intrusive rocks.

Songshujiao Sn-Pb deposit

The Songshujiao Sn-Pb deposit is located to the southeast of the Malage deposit and to the northeast of the Gaosong deposit (Fig. 1). The Mid-Triassic Gejiu Formation in this deposit consists of dolomite, interbedded dolomitic limestone and limestone. The NNE-trending Wuzishan anticline and the NW-trending Baishachong fault, together with various folds and fractures, are the main structural components in the area of the

Songshujiao deposit. Centered on granitic “humps” of the batholith are well developed fault slip zones between layers of different rock types (Fig. 2) that provide critical conduits for granitic magma-derived hydrothermal fluids and space for the precipitation of ore minerals. Three groups of faults occur in the Songshujiao deposit that trend NW, NE and E-W. The fault zones are usually approximately 3 m wide and are infilled with small amounts of oxidized ores. The igneous rock in the Songshujiao deposit is porphyritic biotite granite. Skarn has commonly developed around the contact areas between granite and carbonate wallrocks.

Two types of mineralization are recognizable in the Songshujiao deposit. Skarn Sn-Cu ores have developed mainly along the contact areas between porphyritic granite and Gejiu Formation carbonates. This type of ore occurs as lenses, strata-bound bodies or as veins, and it is generally distributed around granitic cupolas. Thus, the size of the orebodies generally varies from ~5 to ~50 m thick (locally up to ~100 m thick), and from 100 m to 500 m long. The skarn minerals include pyroxene, scapolite and garnet. The ore minerals are pyrrhotite, chalcopyrite, arsenopyrite, marmatite, pyrite, magnetite, cassiterite, scheelite, and molybdenite. The deposit contains Sn, Cu, Zn and W with minor amounts of In, Bi and Ag. Skarn type ore constitutes approximately 66% of the Sn and ~80% of the Cu resources in the Songshujiao deposit (308 Geological Party, 1984).

Stratabound Sn-Pb ore, the second type of ore, is mainly hosted in interbedded limestone and dolomite and is distal from the granite (Fig. 2). Lead ore of this type accounts for approximately 60% - 70% of the total Pb resources in the Songshujiao deposit (308 Geological Party, 1984). The occurrence of such ores is relatively complex and commonly controlled by fault, fold and/or fault slip structures. The strike length of the stratabound orebodies is 20-50 m, with a few reaching more than 100 m; their thickness is commonly >20 m. Most of these ores are weathered, containing limonite (~70%), calcite (~15%), and quartz (~ 5%), with minor concentrations of fluorite, cassiterite, pyrite, arsenopyrite, cerussite and malachite.

Gaosong Sn-Pb-Zn deposit

The Gejiu Formation in Gaosong consists of the following three units: 1) the Bainidong Unit, consisting primarily of light gray to gray limestone, with minor banded and lenticular calcareous dolomite; 2) the Malage Unit, consisting primarily of dark gray to gray limey dolomite, with minor dolomitic limestone; 3) the Kafang Unit, which is mainly composed of gray to light gray limestone and limey dolomite interlayers. The Kafang Unit is the main host of the Gaosong mineralisation. The 8-km long NE-trending Lutangba fault and its associated subsidiary faults are the major structures controlling ore. They cut the Kafang Unit, acting as major conduits for ore-forming fluids. Greisen (quartz-muscovite) alteration, muscovite, sericite and skarn minerals have developed intensively on the margins of the granitic cupola and in the contact zone between granite and carbonate.

Two types of ore occur in Gaosong. Type 1 skarn-sulfide ore occurs along the contact zones between granite and limestone and/or dolomite, with disseminated, veinlet and massive ores hosted by skarn. The primary skarn minerals are pyroxene, garnet and scapolite. The sulfides are associated with retrograde skarn minerals (actinolite, tremolite and chlorite). The major ore minerals include arsenopyrite, pyrrhotite, chalcopyrite and marmatite, with lesser amounts of cassiterite, pyrite, scheelite, native bismuth, molybdenite and magnetite. The average Sn grade is ~0.5-1%, with the highest grade up to 3% (308 Geological Party, 1984).

Type 2 ores are weathered and have complex orebody shapes, including stratabound, irregular banded, lenticular and veinlet. The orebodies occur in different layers that are controlled by fault slip zones and fractures (Fig. 2) and typically consist of several ore layers at different levels, generally 3-5 layers, locally up to 8-9 layers. Type 2 orebodies can be tens to hundreds of meters long and 100 - 200 m wide. The weathered ores consist of limonite, hematite, goethite and clay minerals, with minor amounts of cassiterite, marmatite, anglesite, pyrolusite and malachite. Gangue minerals include primarily scorodite, siderite, calcite, quartz, phlogopite, fluorite, tourmaline, chlorite, garnet, tremolite, pyroxene, with minor amounts of plagioclase, jarosite and kaolinite. The average Sn grade is ~2%.

Laochang Sn-W-Cu polymetallic deposit

The Laochang Sn-W-Cu polymetallic deposit is situated between the Gaosong deposit in the north and the Kafang deposit in the south. It is the most important deposit in the Gejiu district, containing ~50% of the tin resources of the whole district (308 Geological Party, 1984). The Laochang deposit is bounded by the Beiyinshan fault in the north and the Laoxiongdong fault in the south. In Laochang, six EW-trending faults provided conduits for the ore forming fluids and the space for the precipitation of ore minerals. Six NE- and/or NW-trending faults cut the Laochang deposit. The stratigraphy is similar to the deposits described above (Fig. 1), and the interlayer zones are the same ore-hosting locations. Equigranular and porphyritic granites are the major igneous rocks in this area, which intruded into the Mid-Triassic Gejiu Formation. The major mineralization styles in the Laochang deposit are skarn ores, stratabound ores and carbonate hosted veins (Fig. 2).

Skarn ores include skarn W ores, skarn-sulfide Sn ores and Cu ores, associated with minor amounts of Bi, In and Ga mineralization. Tin in skarns accounts for ~60% of all the Sn resources in Laochang. The distribution of orebodies is influenced by the geometry of the granite contact areas, with most ores occurring around granitic “humps”. Major metallic minerals are pyrrhotite, arsenopyrite, chalcopyrite, pyrite, marmatite, cassiterite and scheelite. Major gangue minerals are pyroxene, garnet, plagioclase, fluorite, phlogopite, quartz and chlorite. Small amounts of ores are weathered to an assemblage of limonite, goethite, malachite and plumbojarosite, and these are associated with sericite, phlogopite, muscovite, quartz and calcite.

Stratabound ores occur in the interlayer zones of limestone and dolomite, and these types of ores contain approximately 25% of the total Sn resources in Laochang (308 Geological Party, 1984). The ores have been strongly weathered, currently composed of cassiterite, hematite, limonite, goethite, malachite, scorodite, conicalcite, anglesite, cerusite, plumbojarosite and wadite, with minor amounts of arsenopyrite, pyrite, chalcopyrite, sphalerite, galena and marmatite.

Vein-type mineralization comprising tourmaline-quartz veins, tourmaline-K feldspar-skarn veins, tourmaline-skarn-cassiterite veins, and tourmaline-phlogopite veins in Gejiu Formation carbonate. The scale of mineralization and vein distribution is

influenced by host rock type, stratigraphy, structure, and association with nearby granite (Cheng et al., 2012). The host rocks are folded and faulted limestone and dolomite of the Mid-Triassic Gejiu Formation. The ore zone has an approximately rhombic shape, bordered by the Huangnidong fault in the east, the Aotoushan fault in the west, the Meiyuchong fault in the north and the Longshupo fault in the south. Granite bodies occur 200-1000 m beneath the surface and are aligned along a NE trend beneath the ore veins. The dimensions of the veins vary in length from several centimeters to more than 200 meters and in width from several millimeters to approximately 1 meter. Tin is the major metal produced from these ore veins and the average grades of Sn, Be and WO_3 of the vein-type orebodies are 0.42%, 0.13%, and 0.11%, respectively (308 Geological Party, 1984).

Kafang Cu-Sn deposit

The Kafang Cu-Sn deposit is located in the southernmost part of the Gejiu district (Fig. 1), to the east of the Gejiu fault and between the parallel EW-striking Laoxiongdong and Xianrendong Faults. Basaltic lava flows with a thickness of 60-100 m are intercalated with the Gejiu Formation carbonate beds (Fig. 2). The Xinshan granitic pluton is fine-grained equigranular biotite granite intruded into the Gejiu Formation carbonates and the interbedded lava. Three types of ores are recognizable in Kafang (Fig. 2).

Type 1 skarn Cu-Sn-Mo-W-Au-Bi polymetallic ores occur in the contact areas between Xinshan granite and carbonate wallrocks (Fig. 2). Ore minerals include magnetite, chalcopyrite, pyrrhotite and cassiterite, and minor minerals include pyrite, scheelite, native bismuth, native gold, sphalerite, galena, molybdenite, wolframite and arsenopyrite. Skarn minerals include garnet, pyroxene, epidote, actinolite, tremolite, sericite, chlorite, calcite and quartz.

Type 2 stratabound Cu-dominant ores are hosted in the basaltic lavas. The orebodies are ~200-400 m long and up to 10 m wide. The gangue minerals include actinolite, phlogopite and tremolite, with minor amounts of pyroxene, calcite and fluorite. The ore

minerals are primarily chalcopyrite, pyrite, arsenopyrite, molybdenite and pyrrhotite. The orebodies are roughly sheet-like or tabular.

Type 3 stratabound Cu-Sn-Pb-Zn polymetallic ores are hosted in limestone and/or dolomitic limestone layers up to 2000 m from the granitic pluton. The metallic minerals include pyrrhotite, cassiterite and pyrite, and the gangue minerals are variable amounts of quartz, tourmaline, tremolite and fluorite. The contact areas between orebodies and host rocks are sharp. Localized ore veins, emanating from the main orebodies, cut the host rock. Alteration around these orebodies is minor, but some banded skarns (garnet, pyroxene, wollastonite and calcite) occur parallel to the bedding of the host rocks and parallel to the orebodies; these are better developed closer to the orebodies.

Metal Zoning

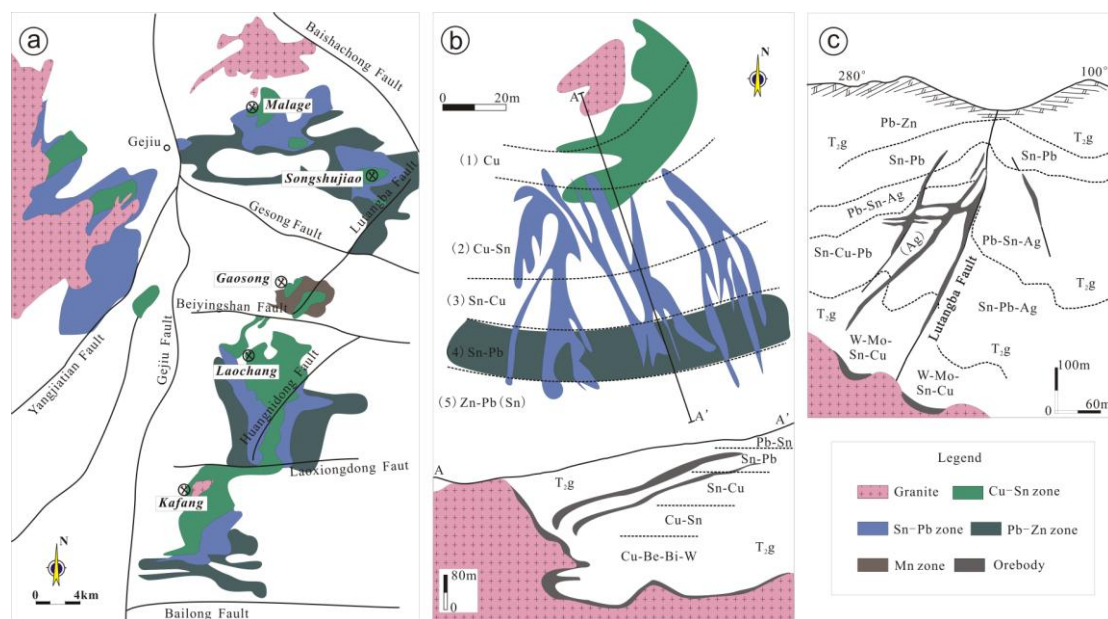


Figure 3 Horizontal and vertical metal zoning patterns in the Gejiu district (modified from 308 Geological Party, 1984). a-Horizontal zoning of metallic elements in the whole eastern mining district. The zoning pattern is similar in individual deposits, which center on granitic cupolas in each deposit. b-Plan map showing horizontal metal zoning in the Malage deposits (above) and the cross section along A-A' showing vertical zoning (below). c-Vertical metal zoning pattern in the Gaosong deposit.

The mineral deposits in the Geiju district are zoned outward from W+Be+Bi ± Mo ± Sn deposits in the granite cuppolas, to Sn+Cu-dominated deposits at the granite contact zones, and Pb+Zn deposits in the surrounding host rocks (Fig. 3). This metal zoning is developed both vertically and horizontally (Fig. 3).

(1) Inner W-Be-Bi± Mo ± Sn zone

This zone mostly occurs in the interior of granite (endogranitic) or its margins. The size of the W, Be, Bi, and Mo orebodies are usually limited. Examples of this style of mineralization include the Malage and Laochang Be deposits, the Xinshan W deposit and the Xinshan Bi deposit. Tungsten is generally more abundant and more widespread than Be and Bi (308 Geological Party, 1984). Be-Bi mineralization is most common around equigranular (non-porphyrific) granite, whereas W (scheelite) is developed in both equigranular and porphyritic granites (Fig. 4). Gangue minerals include large quartz/feldspar crystals, garnet and pyroxene.

(2) Middle Cu-Sn zone

Copper and Sn are the most abundant metals in this zone, which hosts almost 90% of the Cu-Sn resources in the Geiju area. The tin and Cu orebodies generally occur together, although the Cu ores are generally located closer to the granites than the Sn ores (Fig. 3). The ore minerals are mainly cassiterite and chalcopyrite, occurring locally primarily with pyrrhotite, pyrite, arsenopyrite, molybdenite and with minor amounts of sphalerite and galena. Prograde and retrograde skarn minerals are represented by garnet, pyroxene, wollastonite, tremolite, epidote, chlorite and phlogopite in this zone (Fig. 4).

(3) Distal Pb-Zn zone

Outwards from the Cu-Sn zone is a zone with dominant Pb and Zn sulfides (Fig. 3) that is closer to the surface and distal to granite. Examples include the Malage Pb-Zn deposit, the Songshujiao Pb deposit and the Laochang Pb deposit. Field evidence indicates that there were at least two episodes of Pb mineralization (308 Geological Party, 1984), with the above-mentioned deposits belonging to the early stages. A later Pb±Zn mineralization stage exists as veins in both wall rocks and granites with no Sn mineralization (Fig. 4) (308 Geological Party, 1984).

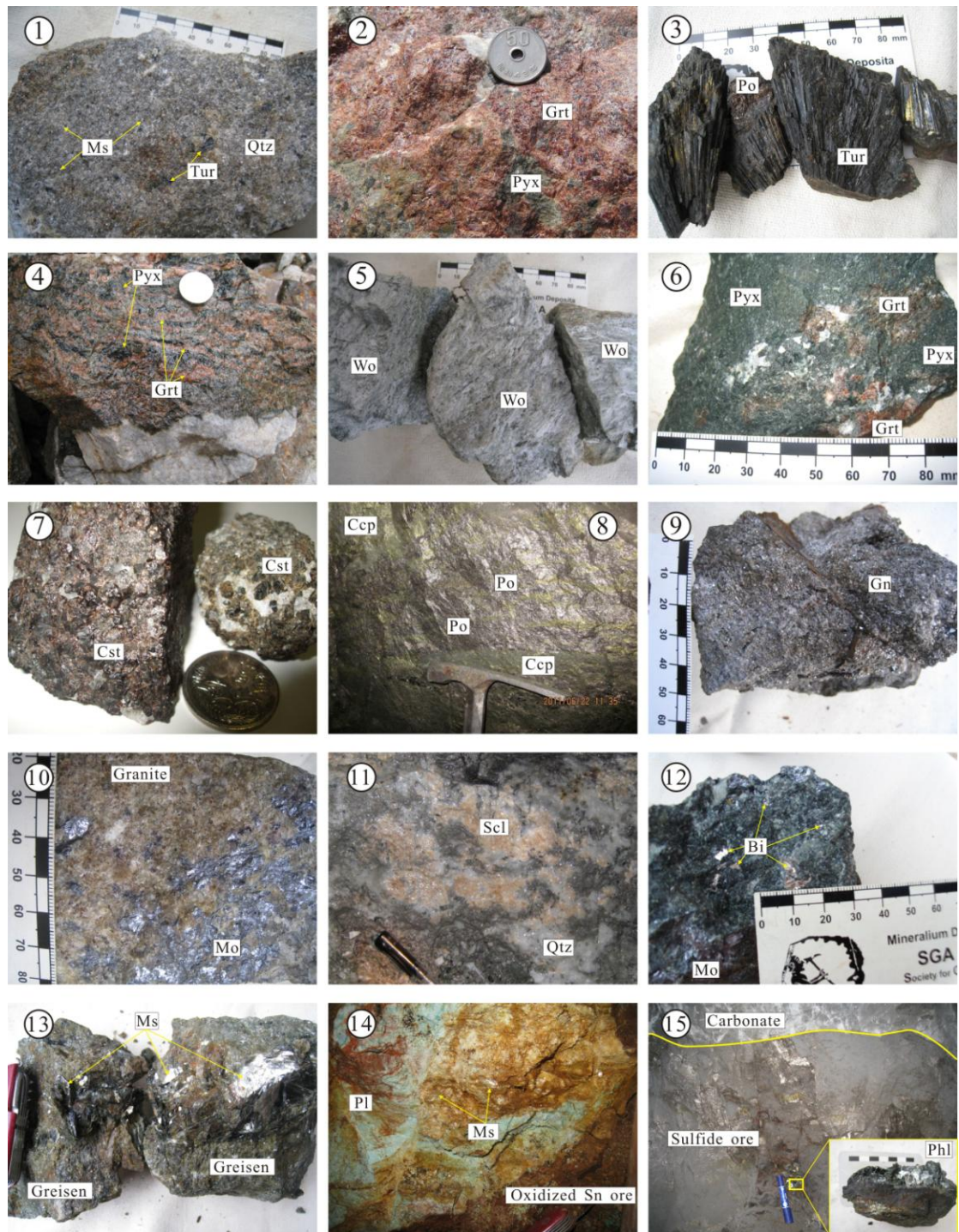


Figure 4 Photographs showing field characteristics, mineral associations, mica analyzed in this study and their relationships with other intergrowth minerals from the Gejiu ore district. 1-greisen; 2-garnet-pyroxene skarn; 3-tourmaline; 4-banded skarn; 5-wollastonite; 6-pyroxene-garnet skarn; 7-cassiterite ore; 8-sulfide ore; 9-bismuth-molybdenite ore; 10-molybdenite ore; 11-scheelite ore; 12-bismuth and molybdenite ore; 13-muscovite in greisens ore; 14-muscovite and plagioclase in strataband oxidized ore; 15-strataband sulfide ore host by Gejiu Formation carbonate.

Ar-Ar dating Techniques and Results

Analytical Techniques

For our study, thirteen samples containing 0.18 to 0.28 mm mica grains were wrapped in aluminum foil, loaded into an aluminum tube, then sealed into a quartz bottle and irradiated for 24 hours in the Swimming Pool Nuclear Reactor at the Chinese Institute of Atomic Energy in Beijing by fast neutrons with a flux of $2.2464 \times 10^{18} \text{ n cm}^{-2}$. The monitor used in this analysis was an internal standard of Fangshan biotite (ZBH-25) with an age of $132.7 \pm 1.2 \text{ Ma}$ and a potassium content of $7.579 \pm 0.030 \text{ wt. \%}$ (Wang, 1983). The measured isotopic ratios were corrected for mass discrimination, atmospheric argon components, blanks and irradiation-induced mass interference. The correction factors of interfering isotopes produced during irradiation were determined by an analysis of irradiated pure K_2SO_4 and CaF_2 . Their values corresponded to the following: $(^{36}\text{Ar}/^{37}\text{Ar})_{\text{ca}} = 0.000271$; $(^{40}\text{Ar}/^{39}\text{Ar})_{\text{k}} = 0.00703$; $(^{39}\text{Ar}/^{37}\text{Ar})_{\text{ca}} = 0.000652$. The $^{40}\text{Ar}/^{39}\text{Ar}$ step-heating analysis was performed at the ME Key Laboratory of Orogenic Belt of Crustal Evolution in Peking University and the detailed experimental process has been previously reported (Gong et al., 2008). The $^{40}\text{Ar}/^{36}\text{Ar}$ vs $^{39}\text{Ar}/^{36}\text{Ar}$ isochron diagram was defined by using the ISOPLOT version 3.0 program of Ludwig (2003).

Results

Table 1 ^{40}Ar - ^{39}Ar Dating Results of Gejiu Tin-Copper Deposits

| Sample no. | Sample representative | Sample locations | Minerals | Age | Error |
|------------|----------------------------|---------------------|------------|------|-------|
| 8255 | Oxidized ore | Malage deposit | Muscovite | 89.6 | 0.65 |
| 8253 | Skarn ore | Malage deposit | Muscovite | 95.3 | 0.66 |
| SSJ-01 | Greisen ore | Songshujiao deposit | Muscovite | 85.2 | 0.65 |
| 7060 | Skarn ore | Songshujiao deposit | Phlogopite | 92.6 | 0.63 |
| GS-01 | Skarn ore | Gaosong deposit | Muscovite | 84.3 | 0.59 |
| 7091 | Oxidized ore | Gaosong deposit | Muscovite | 85.4 | 0.66 |
| 8145 | Greisen ore | Laochang deposit | Muscovite | 85.5 | 0.57 |
| 8187 | Greisen ore | Laochang deposit | Muscovite | 87.4 | 0.58 |
| 8180 | Oxidized ore | Laochang deposit | Muscovite | 77.4 | 0.57 |
| 8120 | Vein ore | Laochang deposit | Muscovite | 87.7 | 0.63 |
| ZKF08-49 | Greisen ore | Kafang deposit | Muscovite | 79.7 | 0.57 |
| ZKF08-29 | Basalt host stratiform ore | Kafang deposit | Phlogopite | 79.8 | 0.47 |
| ZKF08-62 | Mineralized basalt | Kafang deposit | Phlogopite | 85.6 | 0.63 |

The $^{40}\text{Ar}/^{39}\text{Ar}$ analytical results are summarized in [Table 1](#) and the details are listed in [Appendix 1](#) and [Appendix 2](#), which are available as a digital supplement to this paper. In this study, apparent ages obtained from $^{40}\text{Ar}/^{39}\text{Ar}$ analyses at low temperatures are not considered to have geological significance because of the low percentage of $^{39}\text{Ar}_k$ released ([Guo et al., 2011](#)), which was likely caused by the initial loss of small quantities of Ar from the edges of mineral grains ([Hanson et al., 1975](#)). Plateau ages of this study were determined from six or more contiguous steps that comprise >75% of the total ^{39}Ar released. The uncertainties of the ages are reported at a 95% confidence level (2σ).

Two muscovite samples were collected from the Malage deposit for Ar-Ar analysis to constrain the age of the weathered ore (sample 8255) and the retrograde-skarn ore (sample 8253). $^{40}\text{Ar}/^{39}\text{Ar}$ stepwise heating analyses of muscovite over the higher temperature intervals yielded uniform and remarkably flat $^{40}\text{Ar}/^{39}\text{Ar}$ age spectra with plateau ages for 90.3% of the total ^{39}Ar released, indicating the absence of excess argon or any diffusive argon loss. Six plateau ages were obtained from sample 8255 at temperatures between 1000 and 1400 °C. These 6 pieces of data are consistent with the release of 90.2% of the total ^{39}Ar . The 95.4 ± 0.7 Ma and 89.7 ± 0.7 Ma ages for samples 8253 and 8255, respectively, are believed to be reliable estimates of the crystallization age of muscovite from the oxidized ore and skarn ore in the Malage deposit.

One muscovite sample (sample SSJ-01) from greisen ore and one phlogopite sample (sample 7060) from skarn ore in Songshujiao deposit were collected. Ten plateau ages were obtained from sample SSJ-01 at temperatures between 900 and 1400 °C, and these constitute a flat age plateau comprising 98.8% $^{39}\text{Ar}_k$ released. Eight plateau ages were obtained from sample 7060 at temperatures between 1000 and 1400 °C with 91.7% $^{39}\text{Ar}_k$ released. The plateau ages of 85.5 ± 0.7 Ma and 92.3 ± 0.6 Ma are believed to be the best estimates of the age of the greisen ore and the skarn ore in the Songshujiao deposit, respectively.

Two muscovite samples from Gaosong deposit were collected to represent the retrograde skarn ore (sample GS-01) and weathered ore (sample 7091). Eight plateau ages were obtained from sample 7091 at temperatures between 1000 and 1350 °C, with 96.2% $^{39}\text{Ar}_k$ released, yielding a well-defined plateau age of 85.6 ± 0.7 Ma. Twelve step-heating experiments at temperatures ranging from 850°C to 1400°C were performed for sample GS-01; of these, seven steps during 950°C to 1250°C constituted a flat age plateau encompassing 94% $^{39}\text{Ar}_k$ released and yielded a well-defined plateau age of 84.3 ± 0.6 Ma.

Four muscovite samples, including samples 8145 and 8187 from greisen ores in different locations, sample 8180 from oxidized ore, and sample 8120 from vein ore, were collected from the Laochang deposit to represent four different mineralization types. Greisen samples yielded well-defined plateau ages of 85.6 ± 0.6 Ma and 87.4 ± 0.6 Ma.

Sample 8145 was analyzed at a temperature between 950°C to 1250°C with 79.3% $^{39}\text{Ar}_k$ released, and sample 8187 was analyzed at a temperature between 950°C to 1400°C with 89.2% $^{39}\text{Ar}_k$ released. Seven plateau ages were obtained from the oxidized ore sample (sample 8180) at temperatures between 1000 and 1300 °C with 84.4% $^{39}\text{Ar}_k$ released to yield a plateau age of 77.4 ± 0.6 Ma. The plateau age of the vein ore (sample 8120) yielded 87.5 ± 0.6 Ma, based on 76.4% $^{39}\text{Ar}_k$ released between 950°C to 1400°C. As shown in [Appendix 2](#), the isochron ages and inverse isochron ages of these samples are indistinguishable from their plateau ages, and we therefore believe that these $^{40}\text{Ar}/^{39}\text{Ar}$ dates are reliable.

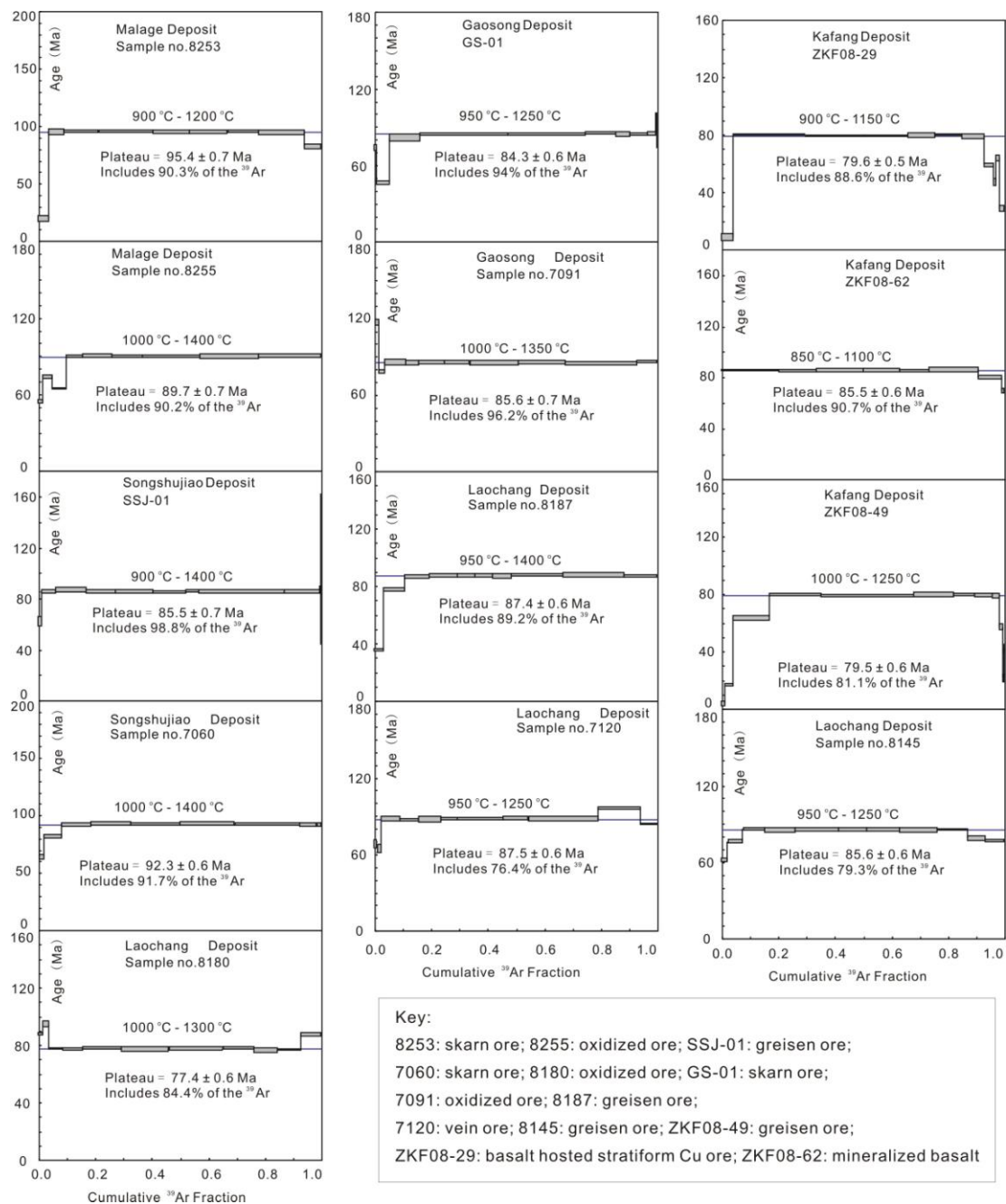


Figure 5 $^{40}\text{Ar}/^{39}\text{Ar}$ age spectra of muscovite and phlogopite separates from the Gejiu tin polymetallic district, SW China. Data uncertainty is given as 2σ .

One muscovite sample and two phlogopite samples were collected from the Kafang deposit to constrain the age of greisen ore (sample ZKF08-49), basalt host stratabound ore (sample ZKF08-29) and altered basalt (sample ZKF08-62). The plateau ages of these samples are 79.5 ± 0.6 Ma, 79.6 ± 0.5 Ma and 85.5 ± 0.6 Ma, respectively. Temperatures were relatively high (>850 °C) and the $^{39}\text{Ar}_k$ released at more than 80%. These three plateau ages agree with their isochron and inverse isochron ages, indicating that they are reliable and of high quality.

Discussion and Conclusions

Timing of mineralization

The 13 representative muscovite/phlogopite samples from different mineralization environments in this study show excellent agreement between the plateau age, the isochron age and the inverse isochron age, within the applicable analytical uncertainty, indicating the absence of excess argon or any diffusive argon loss ([Appendix 1](#) and [2](#)). Therefore, the 13 well-defined plateau ages, from 77.4 ± 0.6 Ma and 95.3 ± 0.7 Ma, that we report are accurate and believed to be a reliable estimate for the crystallization time of these micas ([Fig. 5](#)).

As shown in published works ([308 Geological party, 1984](#); [Li, 1984](#); [Lu, 1987](#); [Dai, 1996](#); [Zhuang et al., 1997](#); [Mo, 2006](#); [Cheng and Mao, 2010](#); [Li et al., 2011](#); [Cheng et al., 2011](#)), diverse textures, mineral associations, major and trace elements and isotopic compositions of granites in the Gejiu district indicate multi-stage crystal fractionation. However, unlike the intrusive rocks in the western sector that are commonly exposed and whose petrochemical features are available for study, exposures of granites in the eastern part of the Gejiu mining district are limited ([Fig. 1](#)). The majority of the mineralization associated with the granitic cupolas is well below the surface and can be observed only in drill cores or in mining adits, thereby precluding a direct understanding of the granite-phase variations. Existing high precision zircon U-Pb LA-ICP-MS/SHRIMP dating

results reveal that the crystallization age of the granites is Late Cretaceous (~78 Ma to ~85 Ma, Cheng and Mao, 2010; Cheng et al., 2012), which is approximately consistent with the mineralization-alteration Ar-Ar age of the mica samples (~78 Ma to ~95 Ma) presented in this study (Fig. 6).

Although our mineralization ages are not completely consistent with magmatism dating results, this is not unusual. For example, long-lived hydrothermal systems can last for several to tens of million years, such as in La Escondida, Chile (Padilla-Garza et al., 2004), Chuquicamata, Chile (Ballard et al., 2001), El Teniente (Maksaev et al., 2004), Río Blanco, Argentina (Deckart et al., 2005), Bajo de la Alumbrera, Argentina (Harris et al., 2008), Fresnillo, Mexico (Velador et al., 2010), and Laramide, Mexico (Barra et al., 2005). In this case, as the Gejiu granitic batholith is made up of multiple phases, each with a corresponding long-lived magma chamber related to mineralization is possible. Therefore, it would be reasonable to assume that these different phases were accompanied by multiple alteration-mineralization events. Moreover, the Mesozoic magmatism and mineralization events in the western Cathaysia Block occurred from approximately 100 Ma to 80 Ma (Mao et al., 2008; Cheng et al., 2010), which supports the contention that the mineralization ages of the Sn-Cu ores in the Gejiu district lie in the range of ~77 Ma to ~95 Ma, as measured by this work.

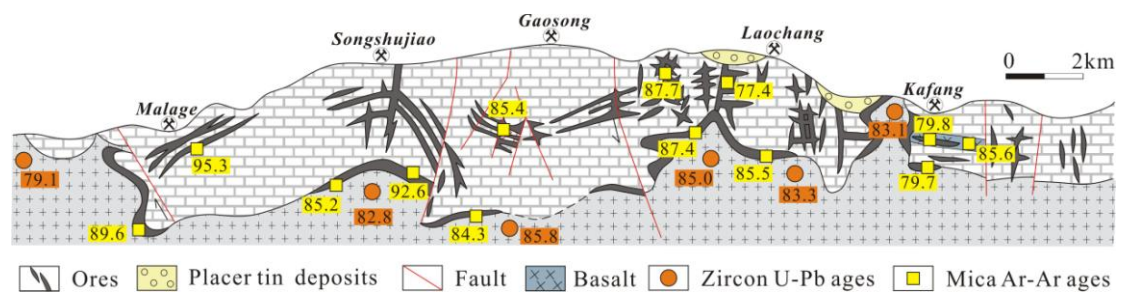


Figure 6 Spatial-temporal relationships between granites and orebodies in the Gejiu mining district (modified from Cheng et al., 2008).

Implications of metal zonation

Metal/mineral/alteration zoning of granite-related ore systems has been recognized since the 1920s (Wong, 1920; Emmons, 1924; Park, 1955) and has been identified by many scientists all over the world. This is exemplified by Sn-W deposits from around the

world, including in the Bolivian tin deposits (Ahlfeld, 1941; Lehmann, 1990), the Cornwall Sn polymetallic district (Bromley and Holl, 1986), the Erzgebirge Sn deposits (Stemprok, 2003), and in the Dachang Sn district (Chen and Li, 1993). Metal zoning also found with other ores, such as Au-polymetallic deposits (Meinert et al., 1997; So et al., 1998; James and Baker, 2001; Markowski et al., 2006) and Pb-Zn-Ag deposits (Newberry et al., 1991; Plumlee et al., 1994; Baumgartner et al., 2008). For the origin of these metal zonings and their implications, Ashley and Plimer (1989) re-examined the controversial Zn/Sn skarn deposits in eastern Australia and proved that the mineralization of these deposits is closely associated with granites, emphasizing that there was no possibility that the ores were of syngenetic origin. Newberry et al. (1991) further strengthened the theory that the genesis of the Pb-Zn-Ag zoning of the Darwin deposit in California should be attributed to the variations of temperature, pH and oxidation state of the granitic magma-derived ore-forming fluids. Temperature changes of hydrothermal fluids are very important for the precipitation of ore minerals and therefore metal zoning, as revealed by several studies (Pirajno, 2009; Wu and Jin, 1993). Audetat (2000) suggested that the metal zoning of Sn-W deposits around the Mole Granite reflected both compositional variations of the source fluid and sequential metal precipitation. For the Ertzgebirge Sn-bearing granite batholith, Stemprok (2003) proposed that the tectonics along the granite contact areas and several deep-seated fault zones were also important for the mobilization of the hydrothermal fluids and distribution of the ore zoning around the granite pluton. Thus, we can conclude that the above-mentioned metal/alteration zonation are genetically related to intrusions (mostly granitic) and are influenced by the nature of the hydrothermal fluids and surrounding geological characteristics.

Figure 3 shows that metal zoning occurs both vertically and laterally away from the various granitic bodies in the Gejiu Sn-polymetallic district. The general sequence of zoning is upward and outward from W-Be-Bi±Mo±Sn to Cu-Sn to Pb-Zn at the periphery. Mineralization types change consistently upward, from disseminated in granite outward to skarn along the contact area with carbonate beds, to oxidized ores and eventually to veins in limestone units distal to granites. This pattern is similar to those established for the Cornwall W-Bi-Sn-Cu-Pb-Zn-Ag ore district in SW England (Bromley and Holl, 1986).

The zonings suggest a close genetic relationship between magmatism and mineralization. The metal zonings are believed to have been caused by the progressive cooling of magma-derived hydrothermal fluids, perhaps combined with fluid-rock interaction or fluid-fluid mixing, as they move upward and outward away from the magmatic source.

Genetic implications and exploration significance

Controversies are long-standing about the genesis of the Gejiu Sn-Cu polymetallic district, with arguments focusing on whether the deposit are of the SEDEX type or granitic intrusion-related (308 Geological Party, 1984; Yu et al., 1988; Zhuang et al., 1996; Zhou et al., 1997, 1999; Zhang et al., 2003; Qin et al., 2006; Zhang et al., 2005; Mao et al., 2008; Qian et al., 2011a, 2011b; and the references therein). The genetic link between magmatism and mineralization is demonstrated by the distinctive spatial association and zoning around granitic cupolas and their greisen-style alteration with Sn-W mineralization that leads outward to a sequence of exoskarns with metal associations from proximal to distal. Importantly, the granite-mineral system genetic coupling is supported by systematic geochronologic constraints from the Ar-Ar ages in this study. The age data show a mineralization age of 77 Ma to 95 Ma, much younger than the age of the host Mid-Triassic Gejiu Formation sedimentary carbonate rocks and correlating closely with the timing of the granite intrusions (Cheng and Mao, 2010; Figure 6). We conclude that the Sn-Cu polymetallic ores of the Gejiu ore district are of hydrothermal origin and granite-related.

Acknowledgments

Two anonymous reviewers are thanked for their professional review of the paper. We appreciate the assistance of Jiyao Tu, Rongshuang Sun and Jianqing Ji with ^{40}Ar - ^{39}Ar dating analysis in Peking University, China. We also want to express our thanks to Guopei Mo, Xiang Tong, Junde Wu and other local geologists from the Yunnan Tin Group for their assistance during our field work. Xiaolong Li and Juan Zhang from China University of Geosciences (Beijing) are thanked for their help on field works. This study was supported

by the National Natural Science Foundation of China (40930419), Special Research Funding for the Public Benefits Sponsored by MLR (200911007-12), Research Program of Yunnan Tin Group (2010-04A), and the Fundamental Research Funds for the Central Universities (2-9-2010-21).

Reference

- 308 Geological Party, 1984, Geology of tin deposit in Gejiu area: Metallurgical Industry Publishing House, Beijing, pp. 50–90 (in Chinese with English abstract).
- Ahlfeld, F., 1941, Zoning in the Bolivia tin belt: *Economic Geology*, v. 36, p. 569–588.
- Ashley, P.M., and Plimer, I.R., 1989, “Stratabound skarns”: A re-evaluation of three eastern Australian deposits: *Mineralium Deposita*, v. 24, p. 289–298.
- Audétat, A., Günther, D., and Heinrich, C.A., 2000, Causes for large-scale metal zonation around mineralized plutons: fluid inclusion LA-ICP-MS evidence from the Mole granite, Australia: *Economic Geology*: v. 95, p.1563–1581.
- Ballard, J.R., Palin, J.M., Williams, I.S., Campbell, I.H., 2001, Two ages of porphyry intrusion resolved for the super-giant Chuquicamata copper deposit of northern Chile by ELA-ICP-MS and SHRIMP: *Geology*, v. 29, p. 383–386.
- Barnes, H.L., 1962, Mechanisms of mineral zoning: *Economic Geology*, v. 57, p. 30–37.
- Barra, F., Ruiz, J., Valencia, J.A., Ochoa-Landin, L., Chesley J.T., Zurcher, L., 2005, amide porphyry Cu-Mo mineralization in Northern Mexico: age constraints from Re-Os geochronology in molybdenite: *Economic Geology*, v. 100, p. 1605–1616.
- Baumgartner, R., Fontbote, L., Vennemann, T., 2008, Mineral zoning and geochemistry of epithermal polymetallic Zn-Pb-Ag-Cu-Bi mineralization at Cerro de Pasco, Peru: *Economic Geology*, v. 103, p. 493–537.
- Bromley, A. V., and Holl, C. J., 1986, Tin mineralization in Southwest England, in Wills, B. A., and Barley, R. W., eds., *Mineral processing at a crossroads*: Dordrecht, Martinus Nijhoff, p. 195–262.
- Bromley, A.V., and Holl, C., 1986, Tin mineralization in southwest England. In: *Mineral Processing at a Crossroads*, Eds: B. A. Wills and R. W. Barley. Martins Nijoff, Dordrecht. 195–262.
- Chen, Y.C., and Li, G.C., 1993, Tin deposit in Dachang. Geological Publishing Hourse, 1–361 (in Chinese with English abstract).
- Cheng, Y.B., Mao, J.W., Xie, G.Q., Chen, M.H., Zhao, C.S., Yang, Z.X., Zhao, H.J., Li, X.Q., 2008, Prelimarny study of the petrogenesis of Laochang-Kafang granite in the Gejiu area, Yunnan province: Constraints from geochemistry and zircon U-Pb dating: *Acta Geologica Sinica*, v. 81, p. 1478–1493 (in Chinese with English abstract).

- Cheng, Y.B., and Mao, J.W., 2010, Age and geochemistry of granites in Gejiu area, Yunnan province, SW China: constraints on their petrogenesis and corresponding tectonic setting: *Lithos*, v. 120, p. 258–276.
- Cheng, Y.B., and Mao, J.W., 2012, Petrogenesis and geodynamic setting of the Gejiu igneous complex from the western Cathaysia block, South China: *Lithos*, in revision.
- Cheng, Y.B., Mao, J.W., Rusk, B., Spandler, C., 2012, Mafic Microgranular Enclaves in Gejiu Area, Yunnan Province, China: a case of interaction of crust- and mantle-derived magmas: *Contribution to Mineralogy and Petrology*, doi: 10.1007/s00410-012-0766-0.
- Dai, F.S., 1996, Characteristics and evolution of rock series, lithogenesis, metallogenesis of crust-derived anatectin magma in Gejiu ore field: *Geology of Yunnan*, v. 15, p. 330 – 344 (in Chinese with English abstract).
- Deckart, K., Clark, A.H., Aguilar, C., Vargas, R., Bertens, A., Mortensen, J.K., Fanning, M., 2005, Magmatic and hydrothermal chronology of the giant Rio Blanco porphyry copper deposit, central Chile: implications of an integrated U-Pb and $^{40}\text{Ar}/^{39}\text{Ar}$ database: *Economic Geology*, v. 100, p. 905–934.
- Emmons, W. I., 1924, Relations of metalliferous lode systems to igneous intrusions: *A. I. M. E. Trans.* v. 70, p. 29–70.
- Gong, J.F., Ji, J.Q., Chen, J.J., Sang, H.Q., Li, B.L., Liu, Y.D., Han, B.F., 2008, The $^{40}\text{Ar}/^{39}\text{Ar}$ geochronology studies of rocks in eastern Himalaya syntaxis: *Acta Petrologica Sinica*, v. 24, p. 2255–2272 (in Chinese with English abstract).
- Guo, C.L., Mao, J.W., Bierli, F., Chen, Z.H., Chen, Y.C., Li, C.B., Zeng, Z.L., 2011, SHRIMP U–Pb (zircon), Ar–Ar (muscovite) and Re–Os (molybdenite) isotopic dating of the Taoxikeng tungsten deposit, South China Block: *Ore Geology Reviews*, doi: 10.1016/j.oregeorev.2010.11. 005
- Hanson, G.N., Simmons, K.R., Bence, A.E., 1975, $^{40}\text{Ar}/^{39}\text{Ar}$ spectrum ages for biotite, hornblende and muscovite in a contact metamorphic zone: *Geochimica et Cosmochimica Acta* v. 39, p. 1269–1278.
- Harris, A., Dunlap, W., Reiners, P., Allen, C., Cooke, D., White, N., Campbell, I., Golding, S., 2008. Multimillion year thermal history of a porphyry copper deposit: Application of U-Pb, $^{40}\text{Ar}/^{39}\text{Ar}$ and (U-Th)/He chronometers, Bajo de la Alumbrera copper-gold deposit, Argentina: *Mineralium Deposita*, v. 43, p. 295–314.
- Hedenquist, J.W., and Lowenstern, J.B., 1994, The role of magmas in the formation of hydrothermal ore deposits: *Nature*, v. 370, p. 519–527.
- Heinrich, C.A., 1990, The chemistry of hydrothermal tin-tungsten ore deposition: *Economic Geology*, v. 85, p. 457–481.
- Heinrich, C.A., 1995, Geochemical evolution and hydrothermal mineral deposition in Sn (-W-base metal) and other granite related ore systems, some conclusions from

- Australian examples, in Thompson, J.F.H, ed., *Magma, fluids and ore deposits: Mineral Association of Canada Short Course Series*, v. 23, p. 203–220.
- James, J.R., and Baker, T., 2001, Intrusion-related gold system: the present level of understanding: *Mineralium Deposita*, v. 36, p. 477–489.
- Jiang, Z.W., Nicholas, H.S.O., Teren, D.B., 1997, Numerical modeling of fault-controlled fluid flow in the genesis of tin deposits of the Malage ore field Gejiu mining district: *Economic Geology*, v. 92, p. 228–247.
- Jin, Z.D., 1991, Disavowal on the hydrothermal origin of the Gejiu tin deposits: *Geology and Exploration*, v. 27, p. 19–20 (in Chinese with English abstract).
- Lehmann, B., 1990, *Metallogeny of tin*: Berlin, Springer, 211 p.
- Lehmann, B., 1992, Tin granites, geochemical heritage, magmatic differentiation: *International Journal of Earth Sciences*, v. 76, p. 177–185.
- Li, J.H., 1985, Characteristic and original study on granites in Gejiu area: *Geology of Yunnan*, v. 4, p. 327 – 352 (in Chinese with English abstract).
- Li, X.L., Mao, J. W., Cheng, Y. B., 2011, Petrology, Geochemistry and Petrogenesis of the Baishachong and Beipaotai Granitic Stocks in Gejiu, Yunnan Province, Southwest China: *Geological Review*, v. 57, p. 837–850 (in Chinese with English abstract).
- Li, Y.S., Qin, D. X., Dang, Y.T., Xue, C.D., 2006, Lead and sulfur isotope in Gejiu tin deposit in Yunnan province: *Geology and Prospecting*, v. 4, p. 49–53 (in Chinese with English abstract).
- Li, Y.S., Qin, D.X., Cheng, X.Y., Guo, N.N., Luo, X., Xie, Y., Zou, T., 2009, Evidences of exhalative hydrothermal sedimentary mineralization of Indo-Chinese epoch of Gejiu tin-polymetallic deposits: *Nonferrous Metal*, v. 61, p. 120–125 (in Chinese with English abstract).
- Lu, J., 1987, Geochemical evolution characteristics of trace elements and REE in Gejiu granites: *Geochimica*, v. 3, p. 249–259 (in Chinese with English abstract).
- Ludwig, K.R., 2003, *User's manual for Isoplot 3.00: a geochronological toolkit for Microsoft Excel*, 4. Berkeley Geochronology Center Special Publication.
- Luo, J.L., 1995, The model of Tin, W, Zn, Pb, Ag deposit in southeast Yunnan Province: *Yunnan Geology*, v. 14, p. 319–332 (in Chinese with English abstract).
- Maksaev, V., Munizaga, F., McWilliams, M., Fanning, M., Marthur, R., Ruiz, J., Zentilli, M., 2004, New chronology for El Teniente, Chilean Andes, from U-Pb, $^{40}\text{Ar}/^{39}\text{Ar}$, Re-Os, and fission track dating: implications for the evolution of a supergiant porphyry Cu-Mo deposit: *Society of Economic Geologists Special Publication*, v. 11, p. 15–54.
- Mao, J.W, Cheng, Y.B., Guo, C.L., Yang, Z.X., Zhao, H.J., 2008, Gejiu tin polymetallic ore-field: deposit model and discussion: *Acta Geologica Sinica*, v. 81, p. 1456–1468 (in Chinese with English abstract).

- Markowski, A., Vallance, J., Chiaradia, M., Fontbote, L., 2006, Mineral zoning and gold occurrence in the Fortuna skarn mine, Nambija district, Ecuador: *Mineralium Deposita*, v. 41, p. 301–321.
- Meinert, L.D., Hefton, K.K., Mayes, D., Tasian, I., 1997, Geology aonation and fluid Evolution of the Big Gossan Cu-Au skarn deposit, Ertzberg district, Irian Jaya: *Economic Geology*, v. 92, p. 509–534.
- Mo, G.P., 2006, Genetic type of granites in Gejiu super large tin polymetallic deposit: *Mineral Resources and Geology*, v. 20, p. 413 – 417 (in Chinese with English abstract).
- Newberry, R.J., Einaudi, M.T., Eastman, H.S., 1991, Zoning and genesis of the Darwin Pb-Zn-Ag skarn deposit, California: a reinterpretation based on new data: *Economic Geology*, v. 86, p. 960–982.
- Padilla-Garza, R.A., Titley, S.R., Eastoe, C.J., 2004, Hypogene evolution of the Escondida porphyry copper deposit, Chile: *Society of Economic Geologists Special Publication*, v. 11, p. 141–165.
- Park, C.F.J., 1955, The zonal theory of ore deposits: *Econ. Geol.*, Fiftieth Anniversary, p. 226–248.
- Peng, C.D., 1985, Discussions on the type and model of the tin ore formation in the Gejiu district: *Yunnan Geology*, v. 4, p. 154–163 (in Chinese).
- Peng, Z.X., 1992, Discussions on the Gejiu tin deposit model: *Yunnan Geology*, v. 11, p. 362–368 (in Chinese).
- Pirajno, F., 1992, *Hydrothermal mineral deposits: Principles and fundamental concepts for the exploration geologist*. Berlin, Springer, p 709.
- Plumlee, G., and Whitehouse-Veaux, P.H., 1994, Mineralogy, paragenesis, and mineral Zoning of the Bulldog Mountain vein system, Creede District, Colorado: *Economic Geology*, v. 98, p. 1883–1905.
- Qian, Z.K., Luo, T.Y., Huang, Z.L., Tong, X., Yang, B.F., Yang, W.B., Lu, R.Y., 2011b, Geology, geochemistry and genesis of Xinshan stratabound diopside rocks in Gejiu, Yunnan: *Acta Mineralogica Sinica*, v. 31, p. 338–352 (in Chinese with English abstract).
- Qian, Z.K., Wu, J.D., Kang, D.M., Lu, R.Y., Yang, B.F., Hu, Y., Luo, T.Y., Huang, Z.L., 2011a, Geological characteristics of cassiterite-hematite-calcite vein-type orebody and its geological significance: *Acta Mineralogica Sinica*, v. 31, p. 328–337 (in Chinese with English abstract).
- Qin, D.X., and Li, Y.S., 2008, *Studies on the geology of the Gejiu Sn-Cu deposit*: Science Press, Beijing, pp 1–180 (in Chinese with English abstract).

- Qin, D.X., Li, Y.S., Tan, S.C., 2006, Metallogenic ages of Gejiu tin deposit in Yunnan Province: *Chinese Journal of Geology*, v. 41, p. 122–132 (in Chinese with English abstract).
- So, C.S., Zhang, D.Q., Yun, S.T., Li, D.X., Alteration-mineralization zoning and fluid inclusions of the high sulfidation Epithermal Cu-Au mineralization at Zijinshan, Fujian Province, China: *Economic Geology*, v. 93, p. 961–980.
- Stemprok, M., 2003, The origin and mineralization of the tin-bearing granites of the Krusne hory Province: A 3-D approach with new data on ore deposit zoning around a granite batholith: *Global Tectonics and Metallogeny*, v. 8, p. 1–4.
- Sun, J.C., Jiang, Z.W., Lei, Y.S., 1987, Structure-geochemistry of Malage deposit in Gejiu district: *Geochimica*, v. 4, p. 303–311 (in Chinese with English abstract).
- Velador, J.M., Heizler, M.T., Campbell, A.R., 2010, Timing of magmatic activity and mineralization and evidence of a long-lived hydrothermal system in the Fresnillo silver district, Mexico: constraints from $^{40}\text{Ar}/^{39}\text{Ar}$ geochronology: *Economic Geology*, v. 105, p. 1335–1349
- Wang, S.S., 1983, Dating of the Chinese K–Ar standard sample (Fangshan biotite, ZBH-25) by using the $^{40}\text{Ar}/^{39}\text{Ar}$ method: *Scientia Geologica Sinica*, v. 4, p. 315–321 (in Chinese with English abstract).
- Wong, W.H., 1920, Les provinces metallogeniques de China: *China Geol. Surv. Bull.* v. 2, p. 37
- Wu, Z.H., and Jin, Y.F., 1993, Some problems concerning element zoning and its application to geological prospecting: *Geophysical & Geochemical Exploration*, v. 17 p. 7–13 (in Chinese).
- Yu, C.W., Tang, Y.J., Shi, P.F., Deng, B.L., 1988, The denamic system of endogenic ore formation in Gejiu tin-polymetallic ore district, Yunnan province. Wuhan, China University of Geosciences Press, 42–251 (in Chinese).
- Zhang, H., Gao, Z.M., Ma, D.Y., Tao, Y., 2003, The genesis of the Gejiu tin deposit—a review: *Geology-geochemistry*, v. 31, p. 70–75 (in Chinese with English abstract).
- Zhang, H., Gao, Z.M., Ma, D.Y., 2005, Lead and sulfur isotopic tracing for source of ore-forming material in the Gejiu tin polymetallic deposit: *Geology and Prospecting*, v. 4, p. 17–20 (in Chinese with English abstract).
- Zhao, Y.M., and Li, D.X., 1987, Metasomatism in granite contact in Gejiu tin deposits, Yunnan Province: *Journal of Chinese Academy of Geosciences*, v. 16, p. 237–252 (in Chinese).
- Zhou, H.Y., 1988, Metallogenic condition and geological character of the Gejiu-Dachang sedex-granite related cassiterite sulphide ore deposit: Unpublished PhD thesis, Nanjing, China, Nanjing University. 66p (in Chinese).

- Zhou, J.P., Xu, K.Q., Hua, R.M., 1999, New ideas about the genesis of Gejiu tin mineralization based the discovery of sedimental texture: Progress in Natural Sciences, v. 9, p. 419–422 (in Chinese).
- Zhou, J.P., Xu, K.Q., Hua, R.M., Zhao, Y.Y., 1997, Discussions on the deposit model of the tin mineralization in SE Yunnan province: Yunnan Geology, v. 16, p. 309–349 (in Chinese).
- Zhuang, Y.Q., Wang, R.Z., Yang, S.P., 1996, Tin-copper polymetallic deposits: Earthquake publishing house, Beijing, pp 38–101 (in Chinese)



Chapter 5

Geology and vein tin mineralization in the Dadoushan deposit, Gejiu district



Geology and vein tin mineralization in the Dadoushan deposit, Gejiu district, SW China

Yanbo Cheng · Jingwen Mao · Zongxi Yang

Received: 20 October 2011 / Accepted: 29 February 2012 / Published online: 16 March 2012
© Springer-Verlag 2012

Abstract Vein-type tin mineralization in the Dadoushan deposit, Laochang ore field, Gejiu district, SW China, is predominantly hosted in Triassic carbonate rocks (Gejiu Formation) over cupolas of the unexposed Laochang equigranular granite intrusion. The most common vein mineral is tourmaline, accompanied by skarn minerals (garnet, diopside, epidote, phlogopite) and beryl. The main ore mineral is cassiterite, accompanied by minor chalcopyrite, pyrrhotite, and pyrite, as well as scheelite. The tin ore grade varies with depth, with the highest grades (~1.2 % Sn) prevalent in the lower part of the vein zone. Muscovite ^{40}Ar – ^{39}Ar dating yielded a plateau age of 82.7 ± 0.7 Ma which defines the age

of the vein-type mineralization. Measured sulfur isotope compositions ($\delta^{34}\text{S} = -4.1$ to 3.9 ‰) of the sulfides (arsenopyrite, chalcopyrite, pyrite, and pyrrhotite) indicate that the sulfur in veins is mainly derived from a magmatic source. The sulfur isotope values of the ores are consistent with those from the underlying granite (Laochang equigranular granite, -3.7 to 0.1 ‰) but are different from the carbonate wall rocks of the Gejiu Formation (7.1 to 11.1 ‰). The calculated and measured oxygen and hydrogen isotope compositions of the ore-forming fluids ($\delta^{18}\text{O}_{\text{H}_2\text{O}} = -2.4$ to 5.5 ‰, $\delta\text{D} = -86$ to -77 ‰) suggest an initially magmatic fluid which gradually evolved towards meteoric water during tin mineralization.

Editorial handling: B. Lehmann

Electronic supplementary material The online version of this article (doi:10.1007/s00126-012-0409-4) contains supplementary material, which is available to authorized users.

Y. Cheng · J. Mao · Z. Yang
Faculty of Earth Science and Mineral Resources,
China University of Geosciences,
Beijing 100083, China
e-mail: jingwenmao@263.net
e-mail: yang.zongxi@gmail.com

Y. Cheng (✉)
School of Earth and Environmental Sciences,
James Cook University,
Townsville 4811, Australia
e-mail: chamboll@yahoo.cn

J. Mao
MLR Laboratory of Metallogeny and Mineral Assessment,
Institute of Mineral Resources,
Chinese Academy of Geological Sciences,
Beijing 100037, China

Z. Yang
Development and Research Center, China Geological Survey,
Beijing 100037, China

Keywords Tin deposits · Dadoushan · Gejiu · China

Content has been removed
due to copyright restrictions



Chapter 6

**Geology and genesis of Kafang Cu-Sn
deposit, Gejiu district**





Geology and genesis of Kafang Cu–Sn deposit, Gejiu district, SW China

Yanbo Cheng ^{a,b}, Jingwen Mao ^{a,c,*}, Brian Rusk ^b, Zongxi Yang ^d

^a Faculty of Earth Science and Mineral Resources, China University of Geosciences, Beijing, 100083, China

^b School of Earth and Environmental Sciences, James Cook University, Townsville, Queensland, 4810, Australia

^c MLR Laboratory of Metallogeny and Mineral Assessment, Institute of Mineral Resources, Chinese Academy of Geological Sciences, Beijing, 100037, China

^d Development and Research Center, China Geological Survey, Beijing, 100037, China

ARTICLE INFO

Article history:

Received 28 April 2010

Received in revised form 13 March 2012

Accepted 15 March 2012

Available online 23 March 2012

Keywords:

Skarn type
Basalt-hosted
Carbonate-hosted
Stratiform
Cu–Sn deposit
Ore genesis
Kafang
Gejiu

ABSTRACT

Kafang is one of the main ore deposits in the world-class Gejiu polymetallic tin district, SW China. There are three main mineralization types in the Kafang deposit, i.e., skarn Cu–Sn ores, stratiform Cu ores hosted by basalt and stratiform Cu–Sn ores hosted by carbonate. The skarn mainly consists of garnet and pyroxene, and retrograde altered rocks. These retrograde altered rocks are superimposed on the skarn and are composed of actinolite, chlorite, epidote and phlogopite. Major ore minerals are chalcopyrite, pyrrhotite, cassiterite, pyrite and scheelite. Sulfur and Pb isotopic components hint that the sources of different types of mineralization are distinctive, and indicate that the skarn ore mainly originated from granitic magma, whereas the basalt-hosted Cu ores mainly derived from basalt. Microthermometry results of fluid inclusions display a gradual change during the ore-forming process. The homogenization temperature of different types of inclusions continuously decreases from early to late mineralization stages. The salinities and freezing temperatures exhibit similar evolutionary tendencies with the $T_{\text{homogenization}}$, while the densities of the different types keep constant, the majority being less than 1. Oxygen and hydrogen isotopic values ($\delta^{18}\text{O}$ and δD) of the hydrothermal fluids fall within ranges of 3.1 to 7.7‰ with an average of 6.15‰, calculated at the corresponding homogenization temperature, and -73 and -98 ‰ with an average of -86.5 ‰, respectively. Microthermometry data and H–O isotopes indicate that the ore-forming fluid of the Kafang deposit is mainly derived from magma in the early stage and a mixture of meteoric and magmatic water in late stage. Molybdenite Re–Os age of the skarn type mineralization is 83.4 ± 2.1 Ma, and the stratiform ores hosted by basalt is 84.2 ± 7.3 Ma, which are consistent with the LA-ICP-MS zircon age of the Xinshan granite intrusion (83.1 ± 0.4 Ma). The evidence listed above reflects the fact that different ore styles in the Kafang deposit belong to the same mineralization system.

© 2012 Elsevier B.V. All rights reserved.

1. Introduction

The genesis of co-existing skarn and stratiform orebodies in the Gejiu ore district, the largest polymetallic tin area in the world, has been the subject of debate for decades. Theories to account for the origin of the orebodies include syngenetic (Li et al., 2009; Qian et al., 2009; Qin et al., 2006; Zhang et al., 2005; Zhou et al., 1998) and granite-related hydrothermal origin (308 Geological Party, 1984; Cheng and Mao, 2012; Cheng et al., 2008, 2009; Mao et al., 2008a; Peng, 1985; Xu et al., 2009; Yang et al., 2008, 2009, 2010; Yu et al., 1988; Zhuang et al., 1996). Most researchers accept that the skarn-type ores in the district are related to Cretaceous granites; however, in recent years, the origin of the stratiform ores has been interpreted as syngenetic based on their morphology and some K–Ar/Ar–Ar dating results (Li et al., 2009; Qin et al., 2006; Zhang et al., 2007). The Kafang Cu–Sn orefield, a

complex area containing two different types of stratiform ores, is located in the south Gejiu tin ore district. Mining began there during the Han Dynasty (2000 years ago) but large-scale exploration was not carried out until the 1970s, the Kafang deposit has defined reserves of about 40 Mt Cu at 1% and >10 Mt Sn at 0.7%. The Kafang deposit, which has significant mineralization hosted by Triassic volcanics and sediments, has a higher Cu/Sn ratio than most other deposits in the Gejiu district, which are predominantly hosted in granites and skarns. (Figs. 1 and 2). This is reflected at Kafang by higher Cu/Sn ratios in the stratiform ore bodies than in the skarn ore bodies. In this study we present new field observations, LA-ICP-MS zircon U–Pb dating, molybdenite Re–Os dating, S–Pb–H–O isotopes, and fluid inclusion microthermometry data, to constrain the origin of the Kafang Cu–Sn deposit and its relation to mineralization throughout the Gejiu ore deposits.

2. Geological setting

The Gejiu mining district is located in southeastern Yunnan province, approximately 300 km SE of Kunming, the capital of Yunnan

* Corresponding author at: Faculty of Earth Science and Mineral Resources, China University of Geosciences, Beijing, 100083, China.
E-mail address: chamboll@yahoo.cn (J. Mao).

(Fig. 1). Tectonically, the Gejiu ore district is located at the westernmost end of the Cathysian block (South China fold belt, adjacent to the Yangtze craton in the north and to the Sanjiang fold belt in the west (Fig. 1a, b). Strata in the Gejiu area are made up of a 3 km-thick sequence of Permian and Triassic clastic rocks with inter-layered basic lavas in the Middle Triassic sequence. The strata consist of 170 to 390 m of sandstone and shale of the Lower Triassic Feixian-guan Formation; ~400 to 460 m of sandstone and mudstones of the Lower Triassic Yongningzhen Formation; ~400 to 1400 m of the Mid-Triassic Gejiu Formation of carbonate with intercalations of mafic lavas; ~1800 to 2800 m of fine-grained sandstones and limestones, with interlayers of mafic lavas of the Mid-Triassic Falang Formation; and ~500 to 1200 m of the Upper Triassic Niaoge Formation (fine-grained clastic rock). No Jurassic or Cretaceous units exist in the region. The carbonate rocks of the Gejiu and Falang Formations, including the interlayered Triassic basic lavas in the Gejiu Formation, are the most important ore-hosting strata.

Numerous faults exist in the Gejiu area, including the NNE-trending Longchahe fault, Jiaodingshan fault, Yangjiantian fault, NE-trending Baishachong fault, and the N–S-trending Gejiu fault. The latter divides the Gejiu district into two parts (Fig. 1c). The ore deposits are mainly located in the eastern part. Structures in the eastern part include NS-, NNE- and EW-trending anticlines and faults. The NNE-trending Wuzhishan anticline is one of main structures controlling the location of the orebodies in the eastern Gejiu district (308 Geological Party, 1984). The EW-trending Longshujiao, Beiyingshan, Longxiangdong, Xianrendong and Bailong faults separate the Gejiu district into five distinct ore deposit areas, i.e., Malage, Songshujiao, Gaosong, Laochang and Kafang from north to south (Fig. 1c).

In addition to the Triassic lavas, the Mesozoic igneous rocks in the Gejiu district include gabbro, mafic microgranular enclave (MME)-bearing granites, porphyritic biotite granite, equigranular biotite granite, alkaline rocks and mafic dikes (Fig. 1c). Cheng and Mao (2010) reported SHRIMP and LA-ICP-MS zircon age data of 80–85 Ma for the following granitic rocks: Longchahe porphyritic granite (83.2 Ma), Songshujiao porphyritic granite (82.8 Ma), Laochang porphyritic granite (83.3 Ma), Shenxianshui equigranular granite (83.0 Ma), Baishachong equigranular granite (79.0 Ma), Laochang equigranular granite (85.5 Ma). These are consistent with the ^{40}Ar – ^{39}Ar age of 82.74 ± 0.68 Ma on phlogopite from the Laochang vein type orebody (Yang et al., 2009). These results demonstrate the magmatism and at least some mineralization were coeval in the Late Cretaceous.

3. Geology of Kafang Cu–Sn deposit

The Kafang Cu–Sn deposit is located in the southernmost part of the Gejiu ore district (Fig. 1), to the east of Gejiu fault and between the parallel EW-striking Laoxiangdong and Xianrendong Faults (Fig. 2A). Several EW trending faults occur in this area. The host rocks and wall rocks in the Kafang deposit are the Triassic Gejiu Formation of limestone, argillaceous limestone, dolomitic limestone and dolomite. The limestones and dolomite range from ~50 to >800 m in thickness. A Triassic basalt layer (60 to 100 m-thick) is intercalated in the Gejiu Formation (Fig. 2A).

The basalt includes olivine basalt and amygdaloidal basalt. Geological and geochemical data indicate that both basalts are silica-unsaturated, alkaline-rich, high-titanium, high-magnesium and low-aluminum, exhibiting the typical characteristics of continental alkali olivine basalt (Li et al., 2008). The Xinshan granitic pluton intruded into the Gejiu Formation carbonate and the intercalated basalt about 2 km NE of Kafang town. The Xinshan granite is a phase of the fine-grained equigranular biotite granite. It contains plagioclase feldspar, quartz and biotite, with accessory magnetite, apatite, and zircon. Similar to other granitic plutons in the Gejiu district, the Xinshan granite is an alkaline feldspar granite characterized by high silica and alkali content. Trace elements and REE patterns show that this is

highly fractionated granite that was likely generated in an intraplate setting (Cheng and Mao, 2010).

The Kafang orefield strikes >2 km N–S and 4–6 km E–W (Fig. 2A, B). Different from other four orefields, which are characterized by dominant Sn mineralization and lesser Cu ore, the Kafang orefield contains more Cu than Sn. Spatially, all the orebodies in Kafang occur around the Xinshan granite, but are hosted by different rocks (Fig. 2). In general, orebodies at Kafang occur at the contact of granite and carbonate, and are hosted by basalt, dolomitic limestone, and limestone, and the distance between ores and granite are generally <2 km (Fig. 2B). The ores at the contact are associated with extensive skarn-type alteration, and alteration is commonly weaker in the sediments and volcanic rocks more distal from the granite.

4. Hydrothermal alteration and mineralization styles

In the Kafang deposit, there are three mineralization styles: (1) skarn type Cu–Sn ores located at the contact of granite and carbonate; (2) stratiform Cu ores hosted by basalt; and (3) stratiform Cu–Sn ores hosted by carbonate (Fig. 2B). Copper orebodies are widely distributed in all the three mineralization types, whereas Sn mineralization only developed in the skarn type and stratiform orebodies hosted by carbonate.

4.1. Skarn type Cu–Sn mineralization

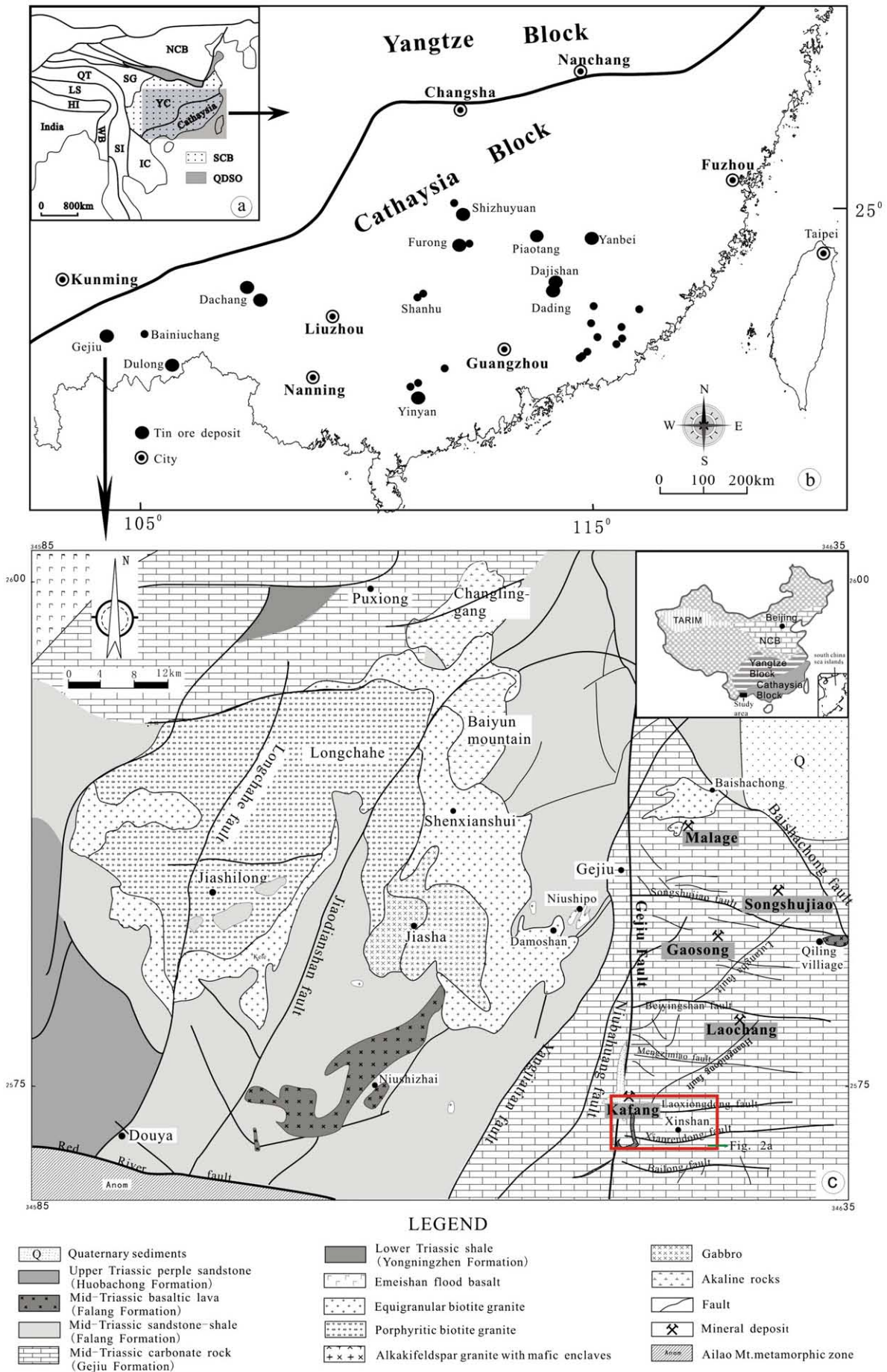
Skarn mineralization mainly developed at the contact zone between the Xinshan granite and carbonate sediments (Figs. 2–4). Ore minerals include chalcopyrite, pyrrhotite and cassiterite, and minor pyrite, native bismuth, native gold, sphalerite, galena, molybdenite and wolframite. Skarn minerals include grossularite, andradite, diopside, hedenbergite, actinolite, tremolite, sericite, magnetite, calcite and quartz. A characteristic feature of this type of alteration is the skarn mineral assemblage commonly occurs as bands intercalated in the host carbonate rocks (Figs. 2–4). Large calcareous skarn zones, ranging from several to tens of meters in thickness, occur at the contact of the Xinshan granite pluton (Fig. 3). In light of the mineral assemblages, the skarn can be sub-divided into garnet skarn, diopside–hedenbergite skarn, and diopside–garnet–magnetite skarn. The ore minerals corresponding to these skarn include scheelite, bismuthinite, chalcopyrite, pyrite and arsenopyrite. Retrograde skarn minerals including epidote, amphibole, chlorite, calcite and magnetite, typically overprint primary skarn minerals. Ore minerals associated with retrograde alteration are mainly sulfides, including arsenopyrite, pyrrhotite, and pyrite, with minor cassiterite and native bismuth. Two uncommon phenomena observed are a wiggly texture, mainly composed of garnet and diopside, and breccias containing fragments of white carbonate encapsulated by diopside \pm chlorite \pm epidote (Fig. 4).

4.2. Stratiform Cu mineralization hosted by basalt

The stratiform copper orebodies hosted by basalt contain actinolite, phlogopite and tremolite, with minor diopside and fluorite (Fig. 5), accompanying pyrrhotite and chalcopyrite mineralization. Generally, the basalt-hosted orebodies are about 200 to 400 m in length and the thickness ranges between 0.1 and 10 m. The ore minerals are commonly chalcopyrite, pyrite, arsenopyrite, molybdenite and pyrrhotite, and gangue minerals include calcite, actinolite, phlogopite, tremolite, and chlorite (Fig. 5). These massive ores generally are sheet- or tabular-like in morphology. The Cu content is generally higher in the central part of the host basalt and is always below economic grade towards the margins (Fig. 5). Calcite and/or fluorite veins are occasionally observed in these ores (Fig. 5).

4.3. Stratiform Cu–Sn mineralization hosted by carbonate

Stratiform orebodies also exist within limestones and dolomitic limestones distal to the granite pluton from 0 to 500 m (Fig. 2B),



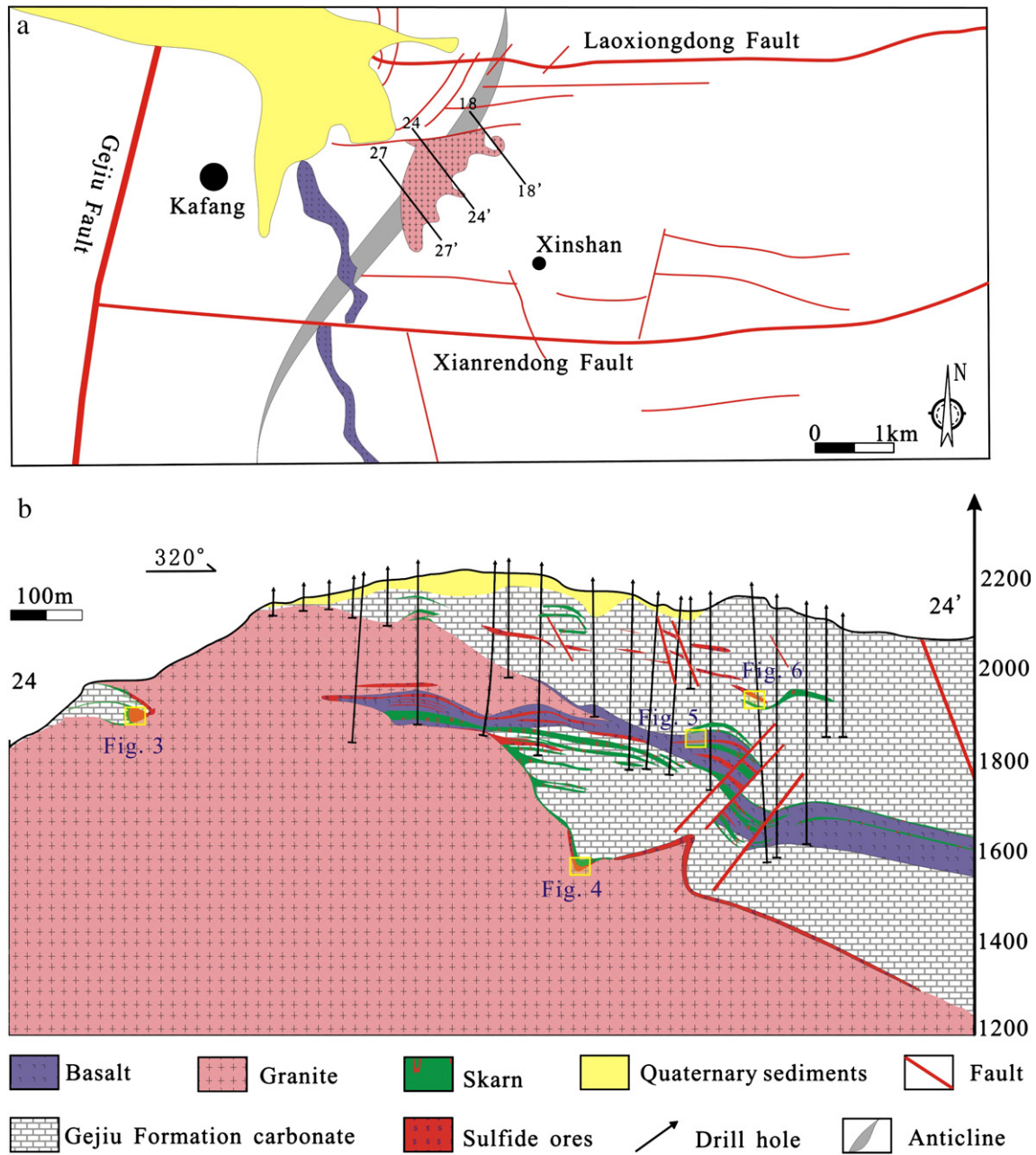


Fig. 2. a. Geology of Kafang ore field. b. Geological section of 24–24'. The location of investigation areas are marked on the cross-section. Panel a is modified after 308 Geological party (1984).

and ore metals include both Cu and Sn. The contacts of Cu–Sn stratiform orebodies and the wall rocks are clear. In some locations, veins from the ore bodies cut the host rocks, indicating mineralization is not coeval with carbonate formation (Fig. 6). Ore minerals include pyrrhotite, cassiterite, pyrite, and other sulfides, and variable amounts of quartz, tourmaline, tremolite, fluorite, and other gangue minerals. Unlike the basalt-hosted ore, the carbonate-hosted ore commonly contains coarse grained cassiterite. Little alteration exists around these orebodies, but some banded skarns, interbedded with the host strata extend along the same trend as the orebodies, and are developed close to these orebodies (Fig. 6). Minerals mainly

include garnet, diopside, and wollastonite. Carbonate minerals, such as calcite, dolomite and siderite, accompanied with weak cassiterite mineralization, and calcite ± fluorite veins cross-cut the orebodies.

5. Analytical methods and sample description

5.1. Fluid inclusions

We chose 12 quartz and calcite samples from the granite interior (CYB1008224, CYB0912032, CYB0912033), granite margin (CYB0912050, ZKF08-23), the contact between granite and carbonate

Fig. 1. (a) Simplified geological map of eastern Asia, showing major tectonic units (Wang et al., 2005). (b) Distribution of tin deposits in the Cathaysia block (Mao et al., 2004). (c) Sketch map showing the geology and the distribution of tin-polymetallic deposits in the Gejiu ore district. SCB = South China Block; NCB = North China Block; YC = Yangtze Craton; IC = Indochina Block; SI = Sibumasu Block; G = Songpan-Ganze Accretionary Complex; WB = West Burma; Hi = Himalayas; LS = Lhasa; QT = Qiangtang. Sketch map in Panel (c) is after 308 Geological Party (1984).

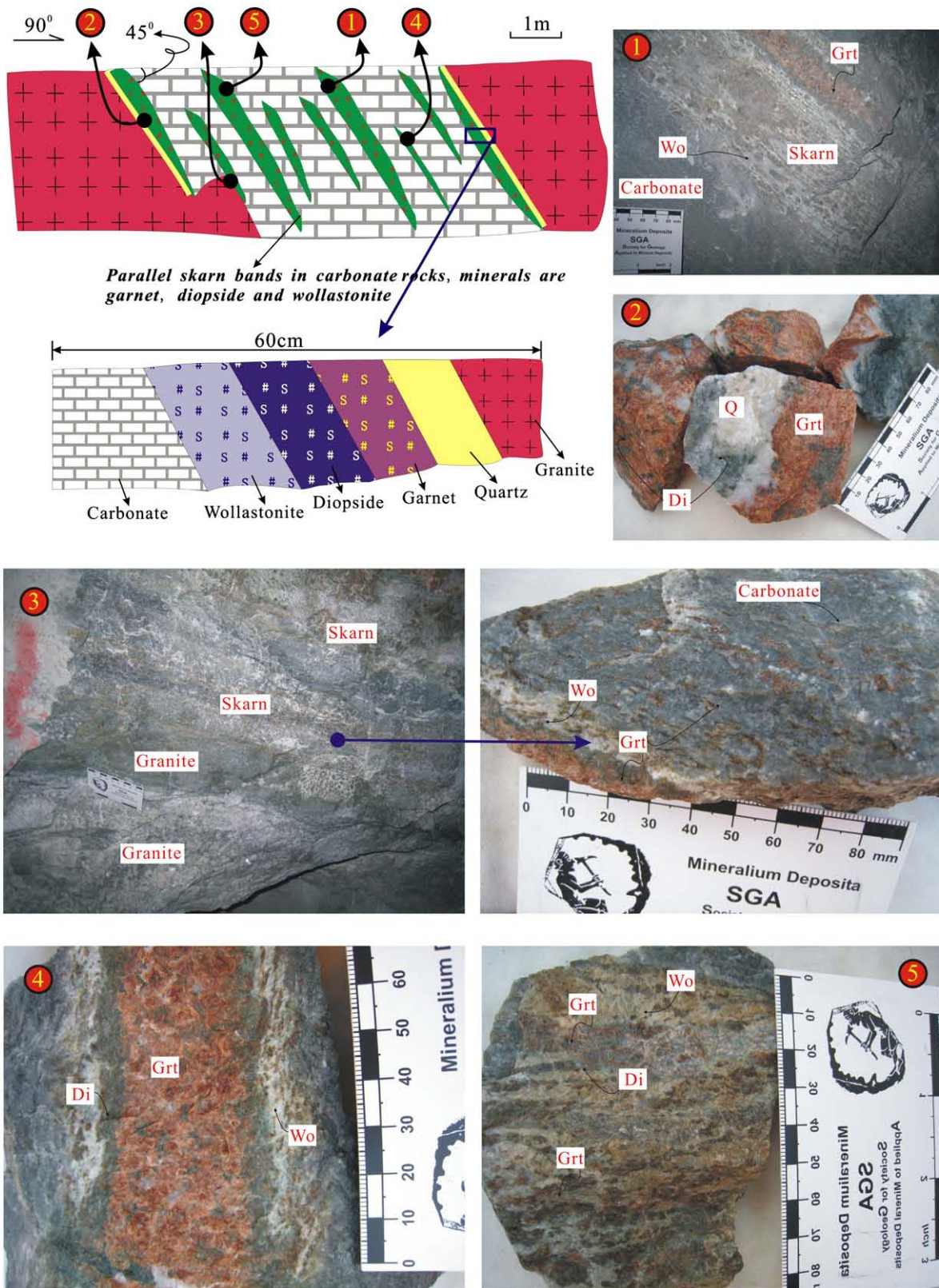
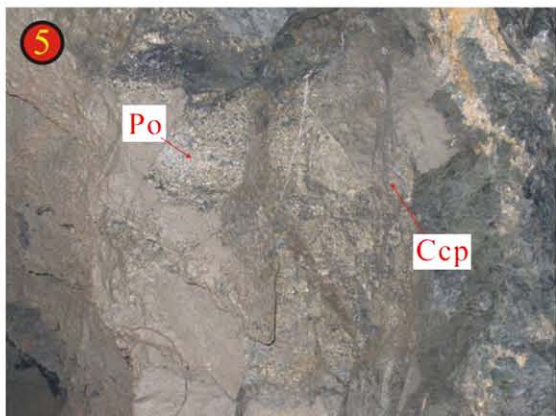
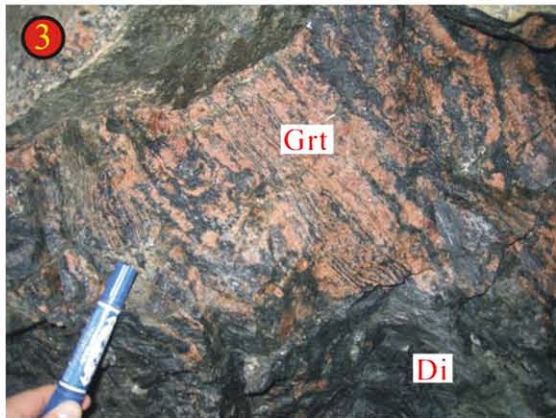
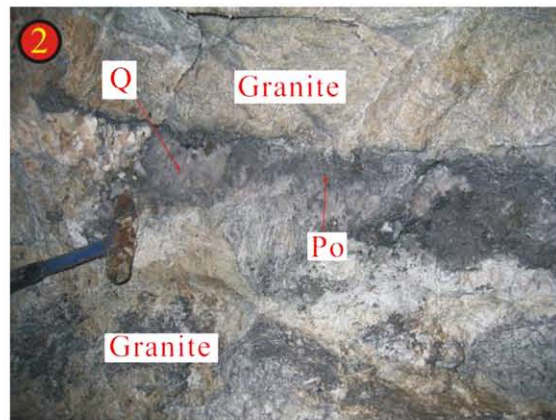
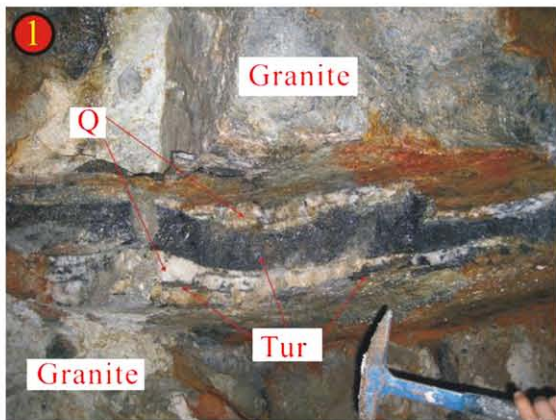
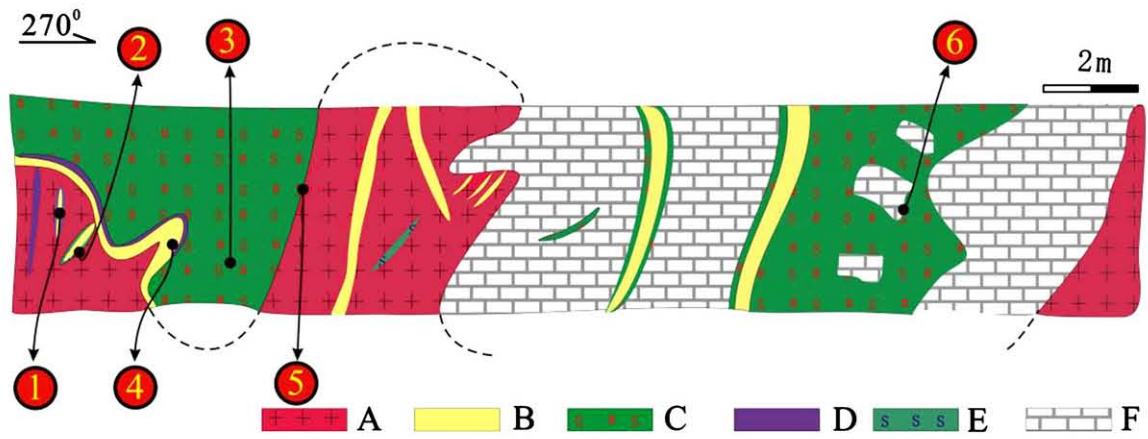


Fig. 3. Schematic profile of the contact of granite, skarn and carbonate, including photographs of main alteration and mineralization styles in the profile. The location of this investigation area is marked on the cross-section. Parallel-like skarn bands in carbonate rocks, minerals are garnet, diopside and wollastonite. 1—Banded skarn in carbonate. 2—Quartz and garnet skarn in the margin of granite. 3—Banded skarn in carbonate in the contact of granite and carbonate. 4—Banded skarn in carbonate. 5—Banded skarn in carbonate.

Fig. 4. Schematic profile of the contact of granite, carbonate and skarn, including photographs of the main alteration and mineralization styles in the profile. The location of this investigation area is marked on the cross-section. 1—Tourmaline and quartz vein in the granite. 2—Quartz vein and associate mineralization in granite. 3—Banded garnet ± diopside exoskarn. 4—Contact of garnet and diopside skarn and massive quartz in the margin of granite. 5—Mineralization in the skarn zone. 6—Massive carbonate enveloped by chlorite ± diopside skarn.



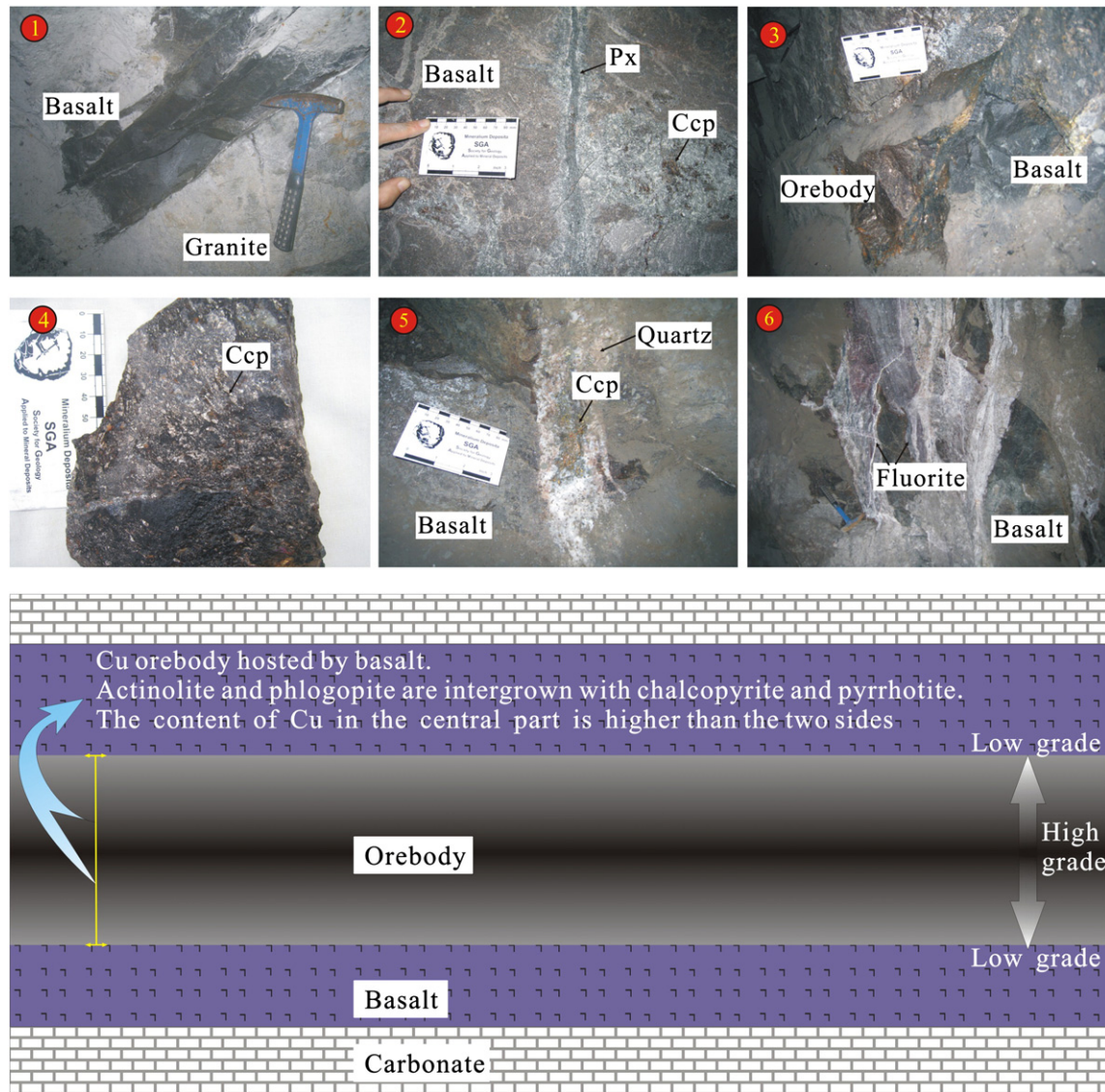


Fig. 5. Photographs of the main alteration and mineralization styles in the stratiform Cu ore hosted by basalt. 1—Contact of granite and basalt. 2—Skarn vein associate with mineralization in basalt. 3 and 4—Pyrrhotite mineralization in basalt. 5—Quartz vein and associate mineralization in basalt. 6—Fluorite vein in basalt.

(CYB0912006, CYB0912005, ZKF08-55), basalt interlayers (ZKF08-90, ZKF08-92, ZKF08-109), and the carbonate interlayer (CYB1007029) to study the characteristics and evolution of the ore-forming fluid in different mineralization units (Tables 1 and 2).

Microthermometric measurements were carried out at Resources Exploration laboratory, China University of Geosciences, Beijing. Fluid inclusion microthermometry data were obtained on a Linkam MDS 600 heating-freezing stage, coupled to a Zeiss microscope. The stage enables measurements within the range of -196 and 600 °C. For freezing runs, the precision is about ± 0.3 °C for melting CO_2 and ± 0.2 °C for ice melting; for heating runs, the precision is about ± 1 °C for critical point of H_2O .

5.2. Isotopes

5.2.1. Lead isotopes

Although published data have been presented, we collected several new samples from Kafang to complement these. The new samples were from Qianjin adit (QJK-16CP, QJK-19PR and QJK-29CP) and Donggualin adit (DGL-16PR, DGL-15CP, DGL-7PR and DGL-2CP) to represent to

mineralization in basalt interlayers and contact (Table 3). The mineral Qianjin adit samples mainly include chalcopyrite, pyrrhotite, actinolite and chlorite, while the Donggualin adit samples contain chalcopyrite, pyrrhotite, garnet, diopside and epidote.

Fresh chalcopyrite and pyrrhotite with $>99\%$ purity were hand-picked and cleaned ultrasonically in purified Milli-Q H_2O (18.2 M Ω). The purified samples were measured for Pb isotopes on a Nu Instruments multiple collector plasma source mass spectrometer at the Laboratory of Isotope Geology, MLR, Institute of Geology, Chinese Academy of Geological Sciences. The mass discrimination of instrument has been corrected by using the “TI-doping” method (He et al., 2005). The amount of TI is about 1/2 of Pb content. Pb isotope ratios of samples are reported relative to the measured ratio for NBS981 standard material.

5.2.2. Sulfur isotopes

We collected 27 samples from granite (CYB1008143, CYB1008193, CYB1008196, CYB1008210, CYB1008248), basalt (ZKF08-11, ZKF08-12, ZKF08-14, ZKF08-26, CYB1008194), carbonate (TSY-1, TSY-2, TSY-3), skarn ores (JZL-2CP, JZL-3PR, JZL-4PR, DGL-6PR, DGL-7PR, DGL-15CP, DGL-15PR, DGL-16CP) and basalt hosted ores (QJK-16CP,

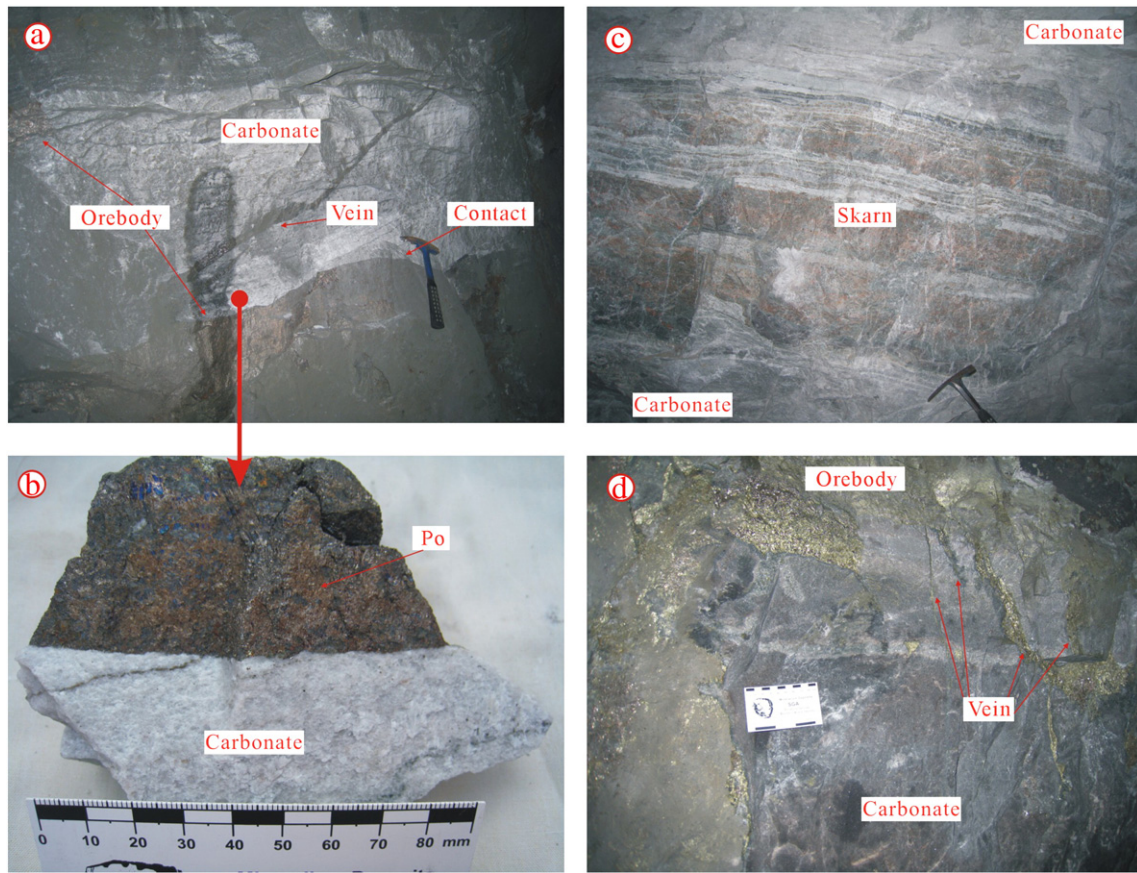


Fig. 6. Schematic profile of the manto type deposit hosted by carbonate, including photographs of the main alteration and mineralization styles in the profile. A and B—Stratiform orebody hosted by carbonate and the hand specimen. C—Banded skarn in carbonate. D—Sulfide veins cut the carbonate.

QJK-16PR, QJK-10CP, QJK-43CP, QJK-29CP, QJK-3CP) to study the S isotopic evolution in different parts of the Kafang orefield.

Sulfur isotope measurements were performed on pyrite and pyrrhotite. SO_2 was prepared from pyrite using the method of Robinson and Kusakabe (1975), and was analyzed with a MAT 251 EM mass spectrometer at the Stable Isotope Laboratory of Institute of Mineral Resources, Chinese Academy of Geological Sciences. Sulfur isotope ratios are reported as $\delta^{34}\text{S}$ relative to the Cañon Diablo Troilite (CDT); the analytical reproducibility is $\pm 0.2\%$ (Mao et al., 2008b).

5.2.3. Oxygen and hydrogen isotopes

Samples for H–O isotopes study were collected from the granite margin (ZYK-4), skarn Cu–Sn ores (JZL-5), and basalt interlayer-hosted Cu ores (ZYK-1), and carbonate-hosted ores (DGL-1) to represent the different mineralization environments of the Kafang deposit.

Oxygen was liberated from quartz by reaction with BrF_5 (Clayton and Mayeda, 1963) and converted to CO_2 on a platinum-coated carbon rod. The $\delta^{18}\text{O}$ analyses were made on a Finnigan Mat 253 mass spectrometer at the Stable Isotope Laboratory of Institute of Mineral Resources, Chinese Academy of Geological Sciences. Reproducibility for isotopically homogeneous pure quartz is about $\pm 0.2\%$ (1σ) (Mao et al., 2008b).

Hydrogen isotope ratios on bulk fluid inclusions in quartz were measured by mechanical crushing of about 5 g of quartz grains, 1 to 5 mm in size, according to the method described by Simon (2001). Samples were first degassed of labile volatiles and low temperature fluid inclusions by heating under vacuum to 120°C for 3 h. The released water was trapped, reduced to H_2 by zinc, and then analyzed with a Finnigan Mat Delta 251 S mass spectrometer at the Stable Isotope Laboratory of Institute of Mineral Resources, Chinese Academy of

Geological Sciences. Analyses of standard water samples suggest a precision for δD of $\pm 2\%$ (1σ) (Mao et al., 2008b).

5.3. Geochronology

5.3.1. Re–Os dating

Five molybdenite samples (C009-8, C009-12, C010-1, C010-2, C010-3) were collected from a Mo-bearing skarn, and another five molybdenite samples (CYB1008231, CYB1008225, CYB1008228, CYB1008230, CYB1008232) were collected from basalt interlayers associated with the Cu mineralization for Re–Os dating, to constraint the ages of these two styles of mineralization. Gravitational and magnetic separation were applied and molybdenite grains were hand-picked under a binocular microscope (purity >99%). The analyzed molybdenite is fine-grained (<0.1 mm), and thus likely avoided the decoupling of Re and Os within large molybdenite grains (Selby and Creaser, 2004; Stein et al., 2003). Re–Os isotope analyses were performed in the Re–Os Laboratory, National Research Center of Geoanalysis of Chinese Academy of Geological Sciences in Beijing using a Thermo Electron TJA X-series ICP-MS. The analytical procedures followed those of Shirey and Walker (1995), Mao et al. (1999) and Du et al. (2004). The model ages were calculated on following the equation: $t = [\ln(1 + ^{187}\text{Os}/^{187}\text{Re})]/\lambda$, where λ is the decay constant of ^{187}Re , $1.666 \times 10^{-11}/\text{yr}^{-1}$ (Smoliar et al., 1996).

5.3.2. LA-ICP-MS

Zircons for analysis were separated from 10 kg bulk samples of Xinshan granite, using conventional heavy liquid and magnetic techniques. Representative zircon grains were hand-picked under a binocular microscope, mounted in epoxy resin, polished, and coated with gold, which was used for CL imaging and removed before laser ablation.

Table 1
Classification and characteristics of samples.

| Location | Granite interior | | Granite margin | | | Skarn ores | | | Stratiform Cu ores | | |
|-----------------------------|------------------------|---------------------|---------------------|--------------------|--------------------|--------------------|--------------------|--------------------|---------------------|---------------------|---------------------|
| | Donggualin + 1800 m | Qianjin + 1870 m | Qianjin + 1800 m | Dakeng + 1800 m | Qianjin + 1820 m | Qianjin + 1820 m | Qianjin + 1820 m |
| Sample no. | CYB0910050 | CYB1008224 | ZKF08-23 | CYB0912032 | CYB0912033 | CYB0912015 | CYB0912006 | ZKF08-55 | ZKF08-90 | ZKF08-92 | ZKF08-109 |
| Distance from basalt (m) | 50 | 5 | 25 | 40 | 40 | 60 | 25 | 150 | – | – | – |
| Distance from granite (m) | – | – | – | – | – | 5 | 10 | 15 | 230 | 230 | 230 |
| Distance from carbonate (m) | 50 | 50 | 20 | 10 | 8 | 12 | 10 | 5 | 40 to 20 | 40 to 20 | 40 to 20 |
| Cu grade | 0.1% | 0.1% | 0.1% | 0.3% | 0.2% | 0.5% | 10% | 1.5% | 5% | 18% | 2% |

Laser ablation techniques were used for additional age determinations. The U–Pb isotopic analyses were performed using an Elan 6100 DRC ICP-MS instrument coupled with a 193 nm Excimer laser. Zircon 91500 was used as a standard and NIST 610 was used to optimize the machine. A mean age of 1060 Ma was obtained for the 91500 zircon standard. The spot diameter was 30 μm . Corrections for common lead were made using the method of Anderson (2002). The data were processed using the GLITTER and ISOPLOT (Ludwig, 2003) programs. Errors in individual LA-ICP-MS analyses are quoted at the 95% (1 σ) confidence level. Details of analytical procedures are described by Hou et al. (2009).

6. Results

6.1. Magmatism and mineralization dating

6.1.1. LA-ICP-MS zircon U–Pb dating

The zircon U–Pb analytical results are presented in Table 4. Most zircon grains have uniform U concentrations ranging from 142 to

12,102 ppm and variable Th concentrations from 98 to 3287 ppm, with Th/U ratios ranging between 0.14 and 1.14. In the analyses, 18 spots in 18 different zircons from 10 kg samples yielded $^{206}\text{Pb}/^{238}\text{U}$ ages of 81.9–83.8 Ma with a weighted mean age of 83.1 ± 0.4 Ma, and MSWD = 0.21 (Fig. 7), which is interpreted as the crystallization age of the Xinshan granite.

6.1.2. Re–Os molybdenite Re–Os dating

Results of molybdenite Re–Os dating are listed in Table 5. For the samples associated with skarn Cu–Sn mineralization, the concentrations of ^{187}Re and ^{187}Os range from 23.60 to 39.10 ppm and 20.69 to 34.14 ppb, respectively. Five samples give a Re–Os model age of 82.95–83.54 Ma and a weighted mean age of 83.30 ± 0.54 Ma. The data, processed using ISOPLOT/Ex (Ludwig, 2004), yielded an isochron age of 83.4 ± 2.1 Ma, with MSWD = 0.37 (Fig. 8a).

For samples associated with stratiform Cu mineralization in basalt interlayers, the concentrations of ^{187}Re and ^{187}Os range from 7.72 to 13.16 ppm and 6.81 to 11.56 ppb, respectively. Five samples give a Re–Os model age of 83.82–85.74 Ma and a weighted mean age of

Table 2
Characteristics and parameters of primary fluid inclusion in Kafang Cu–Sn deposit.

| Sample no. | Mineral | Location | Representation | Type | Inclusion number | Homogenization T (°C) | | Freezing point T (°C) | w(NaCl)/ | | Density(g/cm ³) | |
|------------|---------|-----------------------|----------------------|------|------------------|-----------------------|---------|-----------------------|-------------|---------|-----------------------------|---------|
| | | | | | | Range | Average | | Range | Average | Range | Average |
| CYB1008224 | Quartz | 1870 m in Qianjinkeng | Granite interior | A | 5 | 279.3–355.5 | 331.0 | –17.1––20.3 | 20.30–22.58 | 21.75 | 0.882–0.898 | 0.890 |
| | | | | B | 9 | 186.4–277.9 | 234.2 | –6.95––13.8 | 9.86–17.61 | 12.99 | 0.845–0.955 | 0.927 |
| | | | | C | 5 | 141.9–227.8 | 191.7 | –1.5––4.9 | 2.57–7.73 | 4.62 | 0.921–0.980 | 0.944 |
| CYB0912032 | Quartz | 1800 m in Dakeng | Granite margin | A | 2 | 287.4–376.7 | 323.5 | | | | | |
| | | | | B | 4 | 201.6–293.9 | 259.9 | | | | | |
| | | | | C | 7 | 151.1–159.2 | 155.2 | –3.6––4.7 | 5.86–7.45 | 6.60 | 0.952–0.970 | 0.961 |
| CYB0912033 | Quartz | | Granite margin | A | 9 | 293.2–341.7 | 319.3 | –18.5 | 21.33 | 21.33 | 0.903 | 0.903 |
| | | | | B | 6 | 170.4–286.7 | 242.4 | –6.7––13.3 | 10.11–17.17 | 13.64 | 0.909–0.917 | 0.913 |
| | | | | C | 10 | 173.1–177.6 | 175.4 | –2.0––1.1 | 1.91–3.39 | 2.65 | 0.908–0.922 | 0.915 |
| CYB0912050 | Quartz | 1800 m in Donggualin | Granite margin | A | 9 | 302.5–338.8 | 318.9 | –20.7 | 22.85 | 22.85 | 0.934 | 0.934 |
| | | | | B | 5 | 255.7–294.0 | 278.7 | –15.0––14.6 | 18.30–18.63 | 18.47 | 0.912–0.956 | 0.934 |
| | | | | C | 2 | 109.7–201.8 | 169.6 | –1.6––3.4 | 2.74–5.56 | 3.80 | 0.860–0.911 | 0.900 |
| ZKF08-23 | Quartz | 1800 m in Qianjinkeng | Granite margin | A | 7 | 329.1–339.6 | 326.8 | –18.5 | 21.33 | 21.33 | 0.911 | 0.911 |
| | | | | B | 6 | 195.–245.2 | 215.3 | –10.7 | 14.67 | 14.67 | 0.931 | 0.931 |
| | | | | C | 2 | 131.5–183.5 | 155.4 | –5.0––4.3 | 6.88–7.86 | 7.60 | 0.942–0.976 | 0.960 |
| CYB0912006 | Quartz | 1800 m in Dakeng | Contact | A | 12 | 302.9–362.3 | 335.2 | –17.0––13.7 | 17.52–20.22 | 18.58 | 0.870–0.886 | 0.878 |
| | | | | B | 9 | 171.2–342.3 | 241.7 | –15.1––6.4 | 9.73–18.72 | 13.48 | 0.905–1.036 | 0.957 |
| | | | | C | 6 | 105.2–178.3 | 139.7 | | | | | |
| CYB0912015 | Quartz | | Granite margin | A | 3 | 154.5–208.4 | 188.5 | | | | | |
| | | | | B | 10 | 311.7–350.4 | 327.5 | –17.1––11.4 | 15.37–20.3 | 18.37 | 0.860–0.895 | 0.883 |
| ZKF08-55 | Calcite | | Basalt interlayer | A | 8 | 286.2–452.0 | 344.1 | –15.8 | 19.29 | 19.29 | 0.823–0.941 | 0.888 |
| | | | | B | 12 | 170.4–299.7 | 247.9 | –8.3––6.6 | 9.98–12.05 | 11.02 | 0.839–0.867 | 0.853 |
| ZKF08-90 | Quartz | 1820 m in Qianjinkeng | Basalt interlayer | A | 11 | 288.3–432.7 | 347.5 | –20.5––14.9 | 18.55–22.71 | 20.63 | 0.789–0.919 | 0.854 |
| | | | | B | 11 | 161.6–288.5 | 219.4 | –8.6––6.0 | 9.21–12.39 | 10.44 | 0.858–0.976 | 0.914 |
| | | | | C | 2 | 186.1–202.4 | 194.3 | | | | | |
| ZKF08-109 | Quartz | | Granite margin | A | 15 | 323.8–443.8 | 394.3 | –20.3 | 22.58 | 22.58 | 0.773 | 0.773 |
| | | | | B | 3 | 205.5–254.5 | 237.8 | –15.5––6.1 | 9.34–19.05 | 14.20 | 0.871–1.009 | 0.940 |
| | | | | C | 15 | 109.7–207.4 | 147.1 | –12.9––3.8 | 6.16–16.80 | 12.53 | 0.937–1.055 | 1.007 |
| CYB1007029 | Quartz | 1690 m in Gaosong | Carbonate interlayer | A | 17 | 292.7–435.5 | 328.7 | –16.1––18.0 | 19.53–20.97 | 20.25 | 0.862–0.923 | 0.892 |
| | | | | B | 13 | 177.1–284.5 | 248.4 | –7.3 | 10.86 | 10.86 | 0.847 | 0.847 |

A: vapor volume is 15% to 40%; B: vapor volume is 5% to 15%; C: vapor volume is less than 5%.

Table 3
Lead isotope compositions of samples from the Kafang Cu–Sn deposit.

| Sample | Minerals | ²⁰⁸ Pb/ ²⁰⁴ Pb | ²⁰⁷ Pb/ ²⁰⁴ Pb | ²⁰⁶ Pb/ ²⁰⁴ Pb | Location | Style | Reference |
|-------------|---------------|--------------------------------------|--------------------------------------|--------------------------------------|-----------------------|------------------|------------------|
| QJK-16CP | Chalcopryrite | 38.1549 | 15.5531 | 18.2526 | Qianjin tunnel | Basalt hosted | This paper |
| QJK-16PR | Pyrrhotite | 38.3600 | 15.5897 | 18.3153 | Qianjin tunnel | Basalt hosted | This paper |
| QKJ-29CP | Chalcopryrite | 38.0446 | 15.5333 | 18.2135 | Qianjin tunnel | Basalt hosted | This paper |
| DGL-16PR | Pyrrhotite | 38.5680 | 15.6258 | 18.4434 | Donggualin tunnel | Skarn | This paper |
| DGL-15CP | Chalcopryrite | 38.7728 | 15.6662 | 18.5557 | Donggualin tunnel | Skarn | This paper |
| DGL-7PR | Pyrrhotite | 38.7171 | 15.6492 | 18.4473 | Donggualin tunnel | Skarn | This paper |
| DGL-2CP | Chalcopryrite | 38.8442 | 15.6656 | 18.5162 | Zhulin tunnel | Skarn | This paper |
| S79-04 | Galena | 38.721 | 15.622 | 18.410 | Shenxiashui | Skarn | Wu et al., 1983 |
| 80-L9 | Galena | 38.267 | 15.643 | 18.188 | Laochang 1-5# orebody | Skarn | Wu et al., 1983 |
| ZH1 | Galena | 38.740 | 15.630 | 18.410 | Laochang ore field | Carbonate hosted | Zhang, 2005 |
| ZH2 | Galena | 38.780 | 15.640 | 18.400 | Gaosong ore field | Carbonate hosted | Zhang, 2005 |
| ZH3 | Galena | 38.780 | 15.640 | 18.400 | Gaosong ore field | Carbonate hosted | Zhang, 2005 |
| ZH4 | Galena | 38.840 | 15.660 | 18.450 | Gaosong ore field | Carbonate hosted | Zhang, 2005 |
| Basalt | Whole rock | 38.7940 | 15.5620 | 18.4080 | Qilinshan | Wall rock | Li et al., 2006b |
| Granite1 | K-feldspar | 38.7230 | 15.6130 | 18.3590 | Longchahe | Granite | Yu et al., 1989 |
| Granite2 | K-feldspar | 38.7410 | 15.6400 | 18.4150 | Beipaotao | Granite | Yu et al., 1989 |
| Limestone-1 | Pyrite | 38.6300 | 15.6190 | 18.5510 | Gejiu Formation | Wall rock | Wang, 1983 |
| Limestone-2 | Pyrite | 38.5830 | 15.6440 | 19.0680 | Gejiu Formation | Wall rock | Wang, 1983 |

84.41 ± 0.92 Ma. The data, processed using the ISOPLOT/Ex program (Ludwig, 2004), yielded an isochron age of 84.2 ± 7.3 Ma, with MSWD = 2.40 (Fig. 8b).

The identical model ages and isochron ages for the two samples suggest that the analytical results are reliable.

6.2. Isotopes

6.2.1. Sulfur isotopes

Sulfur isotope data are presented in Table 6. 24 samples of this study and 3 samples from the literature covered all the mineralization units of the Kafang deposit. Large variations are exhibited by our samples, yielding δ³⁴S values in the range −3.2 to 11.1 per mil. All samples from skarn orebodies have negative δ³⁴S values (−3.2 to −0.9), and are in the range of the samples from granite (−3.7 to 0.1); whereas the samples from basalt-hosted stratiform Cu orebodies yield positive values (1.5 to 2.9), close to the range of the basalt (2.6 to 3.8). However, all the data of the four mentioned locations is distinguished from the Gejiu Formation sediments (Qin and Li, 2008).

6.2.2. Hydrogen and oxygen isotope data

The oxygen isotope ratios of ore-forming fluid in equilibrium with the quartz are calculated using the fractionation formulas

from Clayton and Mayeda (1963). The results show that the δ¹⁸O values fall within a range between 3.1 and 7.7‰ (the calculated temperature as listed in Table 2). The granite sample has a value of 7.7‰, the basalt-hosted ores are 7.2‰, skarn ores are 6.6‰ and the carbonate-hosted ores are 3.1‰. δD values vary between −73 and −98‰ with an average of −86.5‰. The values of δ¹⁸O are similar to those of magmatic fluids (+5.5 to +9.5 per mil) (Ohmoto and Goldhaber, 1997; Ohmoto and Rye, 1979) (Table 7). The slightly depleted in δ¹⁸O suggests that some meteoric water could have mixed with a magmatic fluid during the mineralization process.

6.2.3. Pb isotopic compositions of the ore deposits and the country rocks

New Pb isotope compositions of pyrrhotite and chalcopryrite and data from the literature from tin orebodies, granites, and wall rocks in the Gejiu district are listed in Table 3. Pb isotopic ratios of the samples from the Kafang orefield are similar to data from various rocks in the Gejiu district (Li et al., 2006b; Yu et al., 1988; Zhang et al., 2005). Our data show that the basalt-hosted stratiform ores have ²⁰⁶Pb/²⁰⁴Pb ratios from 18.214 to 18.315, with an average of 18.261 and ²⁰⁷Pb/²⁰⁴Pb from 15.533 to 15.590, with an average of 15.559. Chalcopryrite and pyrrhotite from skarn ores have ²⁰⁶Pb/²⁰⁴Pb ratios from 18.4434 to 18.556, with

Table 4
Zircon LA-ICP-MS dating results of the Xinshan granite.

| Spots | Th/U | Th (10 ^{−6}) | U (10 ^{−6}) | ²⁰⁷ Pb/ ²⁰⁶ Pb | ±1σ (±%) | ²⁰⁶ Pb/ ²³⁸ U | ±1σ (±%) | ²⁰⁷ Pb/ ²³⁵ U | ±1σ (±%) | ²⁰⁶ Pb/ ²³⁸ U | ±1σ (1σ) | ²⁰⁷ Pb/ ²³⁵ Pb | ±1σ (1σ) |
|--------|------|---------------------------|--------------------------|--------------------------------------|-------------|-------------------------------------|-------------|-------------------------------------|-------------|-------------------------------------|-------------|--------------------------------------|-------------|
| 022-1 | 1.02 | 332 | 326 | 0.0490 | 0.0006 | 0.0129 | 0.0001 | 0.0871 | 0.0012 | 82.67 | 0.7810 | 84.7723 | 1.1103 |
| 022-2 | 0.63 | 341 | 538 | 0.0477 | 0.0004 | 0.0130 | 0.0001 | 0.0856 | 0.0010 | 83.29 | 0.7153 | 83.3902 | 0.9142 |
| 022-3 | 1.11 | 389 | 351 | 0.0493 | 0.0024 | 0.0128 | 0.0002 | 0.0872 | 0.0045 | 81.94 | 1.0583 | 84.8562 | 4.1837 |
| 022-4 | 0.69 | 98 | 142 | 0.0472 | 0.0011 | 0.0129 | 0.0001 | 0.0840 | 0.0019 | 82.92 | 0.7785 | 81.8742 | 1.8245 |
| 022-5 | 0.74 | 228 | 307 | 0.0466 | 0.0005 | 0.0129 | 0.0001 | 0.0830 | 0.0012 | 82.81 | 0.8642 | 80.9878 | 1.1589 |
| 022-6 | 1.04 | 172 | 165 | 0.0490 | 0.0007 | 0.0130 | 0.0001 | 0.0878 | 0.0014 | 83.28 | 0.8177 | 85.4721 | 1.3048 |
| 022-7 | 1.02 | 327 | 320 | 0.0508 | 0.0007 | 0.0130 | 0.0001 | 0.0906 | 0.0012 | 83.16 | 0.8350 | 88.1033 | 1.1254 |
| 022-8 | 0.72 | 322 | 450 | 0.0484 | 0.0004 | 0.0129 | 0.0001 | 0.0865 | 0.0011 | 82.85 | 0.8472 | 84.2607 | 1.0715 |
| 022-9 | 1.14 | 352 | 309 | 0.0473 | 0.0005 | 0.0130 | 0.0001 | 0.0846 | 0.0011 | 83.04 | 0.7502 | 82.4278 | 1.0047 |
| 022-10 | 0.91 | 238 | 260 | 0.0470 | 0.0010 | 0.0129 | 0.0002 | 0.0836 | 0.0017 | 82.87 | 1.1801 | 81.5692 | 1.5927 |
| 022-11 | 0.74 | 106 | 143 | 0.0485 | 0.0010 | 0.0129 | 0.0001 | 0.0862 | 0.0017 | 82.70 | 0.7830 | 83.9557 | 1.6146 |
| 022-12 | 0.18 | 1615 | 8822 | 0.0630 | 0.0005 | 0.0130 | 0.0002 | 0.1132 | 0.0020 | 83.38 | 1.2253 | 108.9029 | 1.8043 |
| 022-13 | 0.15 | 1005 | 6559 | 0.0836 | 0.0009 | 0.0131 | 0.0002 | 0.1510 | 0.0033 | 83.66 | 1.2066 | 142.8182 | 2.8709 |
| 022-14 | 0.27 | 3287 | 12,102 | 0.0737 | 0.0008 | 0.0130 | 0.0001 | 0.1322 | 0.0016 | 83.38 | 0.9437 | 126.0699 | 1.4538 |
| 022-15 | 0.15 | 1011 | 6568 | 0.0770 | 0.0019 | 0.0130 | 0.0002 | 0.1403 | 0.0051 | 83.25 | 1.3600 | 133.3013 | 4.5065 |
| 022-16 | 0.30 | 807 | 2695 | 0.0493 | 0.0003 | 0.0131 | 0.0001 | 0.0887 | 0.0009 | 83.65 | 0.7783 | 86.3047 | 0.8054 |
| 022-17 | 0.17 | 1054 | 6031 | 0.0770 | 0.0016 | 0.0131 | 0.0002 | 0.1396 | 0.0039 | 83.76 | 1.0486 | 132.6967 | 3.4948 |
| 022-18 | 0.14 | 917 | 6555 | 0.0499 | 0.0003 | 0.0130 | 0.0001 | 0.0896 | 0.0009 | 83.38 | 0.7887 | 87.0849 | 0.8221 |

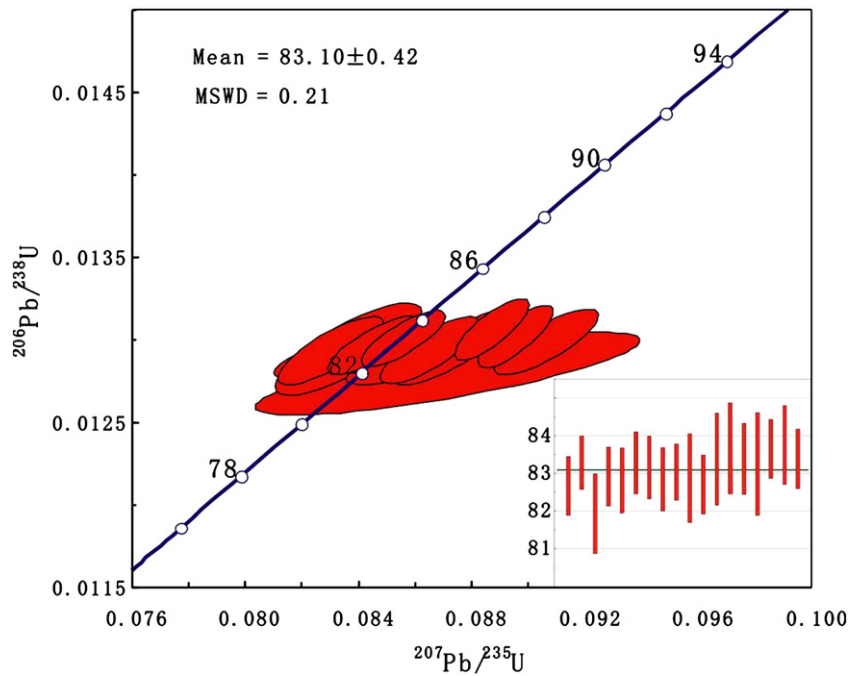


Fig. 7. U–Pb isochron of zircon from Xinshan granite.

an average of 18.500 and $^{207}\text{Pb}/^{204}\text{Pb}$ from 15.629 to 15.666, with an average of 15.646.

6.4. Fluid inclusion studies

6.4.1. Petrography and types

Most fluid inclusions are primary and pseudosecondary and are distributed in groups or isolated (Fig. 9), with size generally $8 \times 6 \mu\text{m}$, up to $14 \times 8 \mu\text{m}$. Secondary inclusions are presenting fractures cross-cutting host minerals. The majority of the inclusions are liquid-rich two-phase inclusion. Based on their compositions and physical properties, inclusions of this study can be classified into three types: (1) vapor-rich type (A type), where the volume of vapor is about 20% and generally 15% to 40%, with a few having larger bubbles and the vapor phase occupies ~50 vol.% (Fig. 9); (2) vapor phase-moderate type (B type), where the volume of vapor is about 10% and generally 5% to 15%; and (3) vapor phase-poor type (C type), with the volume of vapor is generally less than 5%. Co-existence of the three types of fluid inclusions in the Kafang ores indicates that the fluid inclusions captured heterogeneous fluids, i.e., boiling may have occurred during mineralization.

6.4.2. Microthermometry

Table 2 summarizes the microthermometric data. Salinities are calculated using the data of Bodnar (1985), and density is calculated from the empirical formula of Liu and Shen (1999).

For the A-type inclusions, 99 inclusions were analyzed from all the samples collected from the five mineralization environments (i.e., interior granite, granite margin, skarn, basalt-hosted and carbonate-hosted ores) (Table 2). The homogenization temperatures range from 279.3 to 452.0 °C, with an average of 336 °C, and the ice-melting temperatures were between –15.8 and –20.7 °C. The corresponding salinities of the inclusions were from 15.37 to 22.85 wt.% NaCl equiv., averaging 20.70 wt.% NaCl equiv., and all the densities range between 0.773 and 0.934.

The B-type inclusions, 88 inclusions were analyzed and the homogenization temperatures ranged from 161.6 to 342.4 °C, with an average of 243 °C, and the freezing temperature were –6.0 to –15.5 °C. The corresponding salinities of the inclusions were from 9.21 to 19.05 wt.% NaCl equiv., averaging 13.42 wt.% NaCl equiv., and most the densities are between 0.823 and 1.036.

52 inclusions were analyzed for the C-type inclusions, and the homogenization temperature ranged from 105.2 to 227.8 °C, with an average of 168 °C, and the freezing temperature were –1.1 to –12.9 °C.

Table 5
molybdenite Re–Os dating results of Kafang ore field.

| Sample | Weight/g | Re/ 10^{-6} | Os ng/g | Re187/ 10^{-6} | Os187/ 10^{-9} | Model age (Ma) |
|--|----------|-----------------|---------------------|------------------|------------------|------------------|
| <i>Sample from skarn mineralization</i> | | | | | | |
| C009-8 | 0.05046 | 23.6 ± 0.2 | 0.0145 ± 0.0150 | 14.9 ± 0.2 | 20.69 ± 0.18 | 83.54 ± 1.31 |
| C009-12 | 0.05055 | 29.8 ± 0.2 | 0.0274 ± 0.0149 | 18.7 ± 0.2 | 25.87 ± 0.15 | 82.95 ± 1.16 |
| C010-1 | 0.05046 | 39.1 ± 0.4 | 0.0204 ± 0.0049 | 24.6 ± 0.2 | 34.14 ± 0.20 | 83.35 ± 1.24 |
| C010-2 | 0.04999 | 25.09 ± 0.2 | 0.0203 ± 0.0086 | 15.7 ± 0.1 | 21.80 ± 0.12 | 83.25 ± 1.14 |
| C010-3 | 0.05159 | 36.66 ± 0.3 | 0.0401 ± 0.0144 | 23.0 ± 0.2 | 31.98 ± 0.21 | 83.49 ± 1.19 |
| <i>Sample from stratiform ore hosted by basalt</i> | | | | | | |
| CYB1008231 | 0.05140 | 9.271 ± 0.1 | 1.5680 ± 0.0320 | 5.827 ± 0.1 | 8.16 ± 0.1 | 83.96 ± 1.21 |
| CYB1008225 | 0.05066 | 13.16 ± 0.1 | 0.5523 ± 0.0126 | 8.274 ± 0.1 | 11.56 ± 0.1 | 83.82 ± 1.20 |
| CYB1008228 | 0.05028 | 7.717 ± 0.1 | 0.3336 ± 0.0077 | 4.850 ± 0.1 | 6.81 ± 0.1 | 84.25 ± 1.30 |
| CYB1008230 | 0.05194 | 10.70 ± 0.1 | 0.9783 ± 0.0194 | 6.723 ± 0.1 | 9.49 ± 0.1 | 84.68 ± 1.32 |
| CYB1008232 | 0.05058 | 10.73 ± 0.1 | 1.5160 ± 0.0150 | 6.744 ± 0.1 | 9.64 ± 0.1 | 85.74 ± 1.41 |

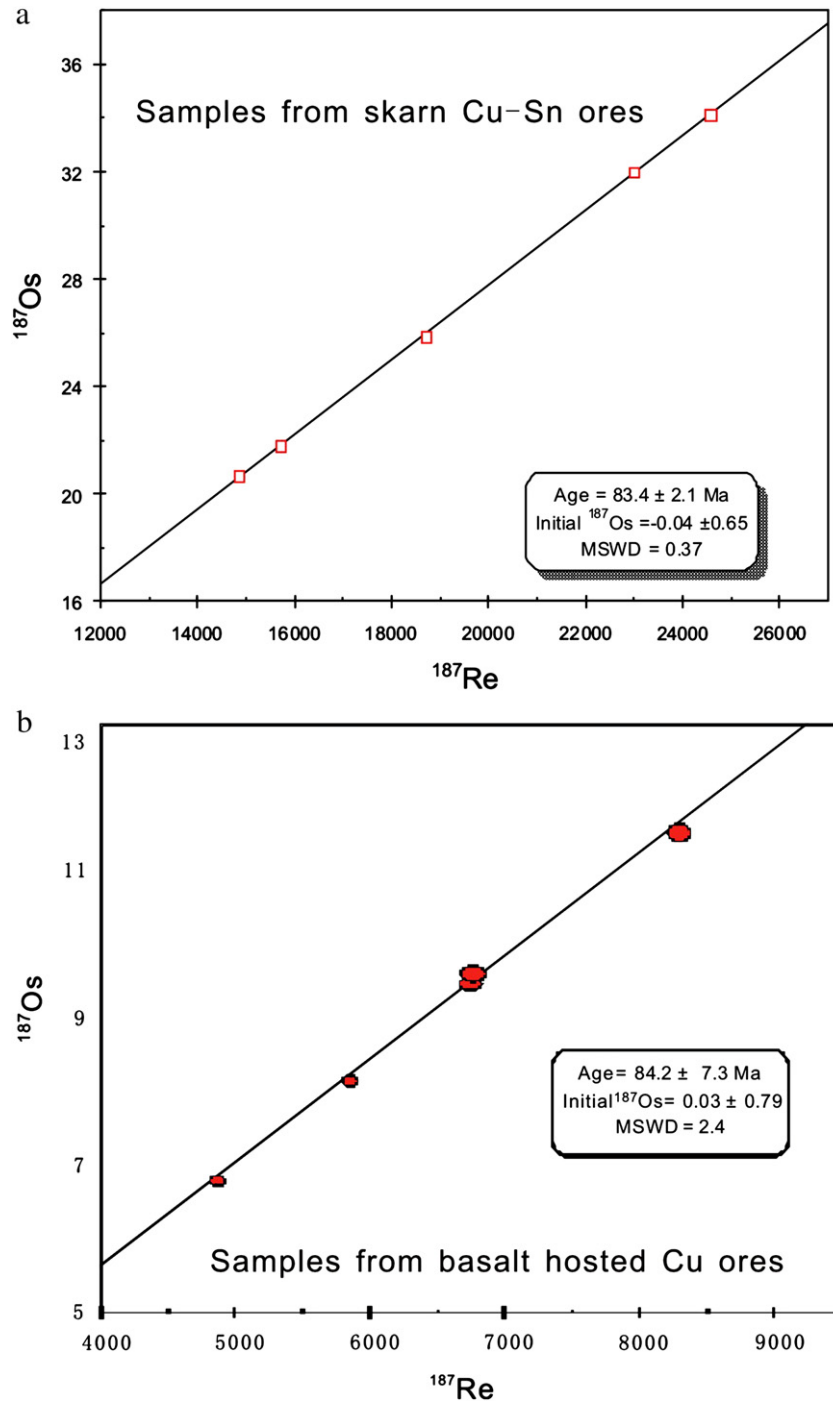


Fig. 8. Re–Os isochron of molybdenites from skarn and basalt hosted stratiform Cu ores.

The corresponding salinities of the inclusions were from 1.91 to 16.80 wt.% NaCl equiv., averaging 5.05 wt.% NaCl equiv., and the densities range from 0.860 to 1.055.

7. Discussion

7.1. Timing of magma emplacement and Cu–Sn mineralization

Numerous geochronological studies have been carried out on Xinshan granite and results vary widely, including 81 Ma by Rb–Sr (Wu et al., 1984), and 64–84 Ma by unknown methods (308 Geological Party, 1984; Dai, 1996). Qin and Li (2008) obtained several mica ^{40}Ar – ^{39}Ar

ages ranging from of 83.23 ± 2.07 Ma to 205.11 ± 4.38 Ma. An age range of 43.49 ± 0.87 Ma to 186.01 ± 3.72 Ma of cassiterite was also reported by Qin and Li (2008) by K–Ar methods. Previous age determinations for the granite and the ores vary widely and are not consistent. In this study, we obtained a zircon LA-ICP-MS U–Pb weighted mean age of 83.1 ± 0.4 Ma from the Xinshan granite and two Re–Os isochron ages for molybdenite samples of 83.4 ± 2.1 Ma and 84.2 ± 7.3 Ma from the skarn Sn–Cu ores and stratiform Cu ores interpreted to represent the age of the Xinshan granite, skarn Cu–Sn ores, and stratiform Cu ores hosted by basalt, respectively. These ages are consistent, and indicate that granite emplacement and the Cu–Sn mineralization were largely synchronous, in the Late Cretaceous.

Table 6
Composition of sulfur isotope in the Kafang copper deposit.

| Sample | Minerals | $\delta^{34}\text{S}_{\text{V-CDT}}(\text{‰})$ | Location | Style | Reference |
|------------|--------------|--|-------------------|---------------|------------------|
| QJK-16CP | Chalcopyrite | 1.5 | Qianjin tunnel | Basalt hosted | This study |
| QJK-16PR | Pyrrhotite | 2.8 | Qianjin tunnel | Basalt hosted | This study |
| QJK-10CP | Chalcopyrite | 1.5 | Qianjin tunnel | Basalt hosted | This study |
| QJK-43CP | Chalcopyrite | 2.9 | Qianjin tunnel | Basalt hosted | This study |
| QJK-29CP | Chalcopyrite | 2.6 | Qianjin tunnel | Basalt hosted | This study |
| QJK-3CP | Chalcopyrite | 2.3 | Qianjin tunnel | Basalt hosted | This study |
| JZL-2CP | Chalcopyrite | -2 | Zhulin tunnel | Skarn | This study |
| JZL-3PR | Pyrrhotite | -0.9 | Zhulin tunnel | Skarn | This study |
| JZL-4PR | Pyrrhotite | -2.1 | Zhulin tunnel | Skarn | This study |
| DGL-6PR | Pyrrhotite | -1.2 | Donggualin tunnel | Skarn | This study |
| DGL-7PR | Pyrrhotite | -2.4 | Donggualin tunnel | Skarn | This study |
| DGL-15CP | Chalcopyrite | -3.2 | Donggualin tunnel | Skarn | This study |
| DGL-15PR | Pyrrhotite | -2.2 | Donggualin tunnel | Skarn | This study |
| DGL-16CP | Chalcopyrite | -2.8 | Donggualin tunnel | Skarn | This study |
| CYB1008143 | Bulk powder | -0.7 | Malutang tunnel | Granite | This study |
| CYB1008193 | Bulk powder | 0.1 | Zhuyeshan tunnel | Granite | This study |
| CYB1008196 | Bulk powder | -2 | Zhuyeshan tunnel | Granite | This study |
| CYB1008210 | Bulk powder | -1.1 | Zhuyeshan tunnel | Granite | This study |
| CYB1008248 | Bulk powder | -3.7 | Malage 1690 | Granite | This study |
| ZKF08-11 | Bulk powder | 3.7 | Qianjin tunnel | Metabasalt | This study |
| ZKF08-12 | Bulk powder | 3.4 | Qianjin tunnel | Metabasalt | This study |
| ZKF08-14 | Bulk powder | 3.8 | Qianjin tunnel | Metabasalt | This study |
| ZKF08-26 | Bulk powder | 3.2 | Qianjin tunnel | Metabasalt | This study |
| CYB1008194 | Bulk powder | 2.6 | Zhuyeshan tunnel | Metabasalt | This study |
| TSY-1 | Bulk powder | 11.1 | Qilinshan | Carbonate | Qin and Li, 2008 |
| TSY-2 | Bulk powder | 11.02 | Qilinshan | Carbonate | Qin and Li, 2008 |
| TSY-3 | Bulk powder | 7.14 | Tangziwa 1800 | Carbonate | Qin and Li, 2008 |

7.2. Source and fluid evolution

7.2.1. Source of ore-forming materials

As described above, Cu mineralization is found in all the three types of orebodies while the Sn mineralization only developed in skarn orebodies and stratiform ores hosted by carbonate. Here, we attempt to constrain the key factors responsible for the formation of two types' stratiform ores and skarn-type ores using Pb and S isotope systematics.

Lead isotope compositions of basalt-hosted ores mainly plot between the orogenic belt evolution curve and the mantle evolution curve (Fig. 11), indicating a mixed origin between mantle and crust according to the "orogen" reservoir of Zartman and Doe (1981). Pb isotope compositions of the stratiform orebody are similar to those of basalt; however, they are different from the limestone of the Gejiu Formation and K-feldspar from the Xinshan granite. These features indicate that the ore-forming materials of the stratiform orebody mainly originated from the basalt. This is consistent with the S data of this study. Our results and previous results show that the $\delta^{34}\text{S}$ values are between 2.5‰ and 3‰ for basalt-hosted stratiform Cu ores. Thus, $\delta^{34}\text{S}$ values of the basalt-hosted stratiform Cu ores are close to those of mantle (0‰–3‰, Ohmoto and Goldhaber, 1997) and fall within the range of basalts (0‰–5‰, Ohmoto and Goldhaber, 1997); furthermore, they are also close to the range of the basalt in Gejiu area (2.6 to 3.8). Based on the S and Pb isotopic characteristics, we conclude that the source of the ore-forming materials in basalt-hosted stratiform orebodies is Triassic basalt.

Lead isotopes of skarn orebodies plot between the orogenic belt evolution curve and the upper crustal evolution curve (Fig. 11).

Lead isotope compositions of the skarn orebodies are similar to those of the Xinshan granite, indicating that ore-forming materials of skarn orebodies are mainly derived from the granite. Sulfur isotopic compositions of the skarn orebodies falls within a narrow range between -3.2‰ and -0.9‰ with an average of -1.7‰ and are similar with the data of the granite (Fig. 12). Sulfur isotopes in the Gejiu Formation carbonaterange from 7.14 to 11.1 (Qin and Li, 2008). This suggests that there is little contribution of sedimentary S for the skarn-type mineralization. Moreover, $\delta^{34}\text{S}$ values of skarn orebody in this study are consistently lower than those of the basalts (Fig. 12). Our data is therefore inconsistent with a sedimentary or basaltic S source. Considering both the Pb and S isotopes, we suggest that the source of sulfides in skarn orebody is the Cretaceous granite.

7.2.2. Fluid evolution

It is clear that from the granite outward, there is a progressive decrease trend in homogenization temperature and salinity for all the samples of the 5 mineralization environments i.e., interior granite, granite margin, skarn, basalt-hosted and carbonate-hosted ores. We suggest all the fluids of the 5 environments should belong to a same ore-forming fluid system. Moreover, as the similar microthermometric results of the granite and the 3 different mineralization environments, according to the coeval relationships of the magmatism and mineralization, we suggest that all the ore-forming fluids of the whole Kafang deposit derived from the same granitic magma, i.e., the Xinshan granite.

Hydrogen and oxygen isotopes are important monitors for the evolutionary history of ore-forming fluids. Zhao et al. (1990) and Zhao et al. (2003) pointed out that the δD (-90.3‰–-48.3‰,

Table 7
Hydrogen and oxygen isotopes composition of Kafang copper deposit.

| Sample | Mineral | Location | T (°C) | $\delta^{18}\text{O}_{\text{V-SMOW}}(\text{‰})$ | $\delta\text{D}_{\text{V-SMOW}}(\text{‰})$ | $\delta^{18}\text{O}_{\text{H}_2\text{O}}(\text{‰})$ |
|--------|---------|-------------------|--------|---|--|--|
| DGL-1 | Quartz | Donggualin tunnel | 194 | 15.20 | -92 | 3.1 |
| JZL-5 | Quartz | Zhulin tunnel | 317 | 12.92 | -73 | 6.6 |
| ZYK-1 | Quartz | Zhulin tunnel | 317 | 13.54 | -83 | 7.2 |
| ZYK-4 | Quartz | Zhulin tunnel | 320 | 13.88 | -98 | 7.7 |

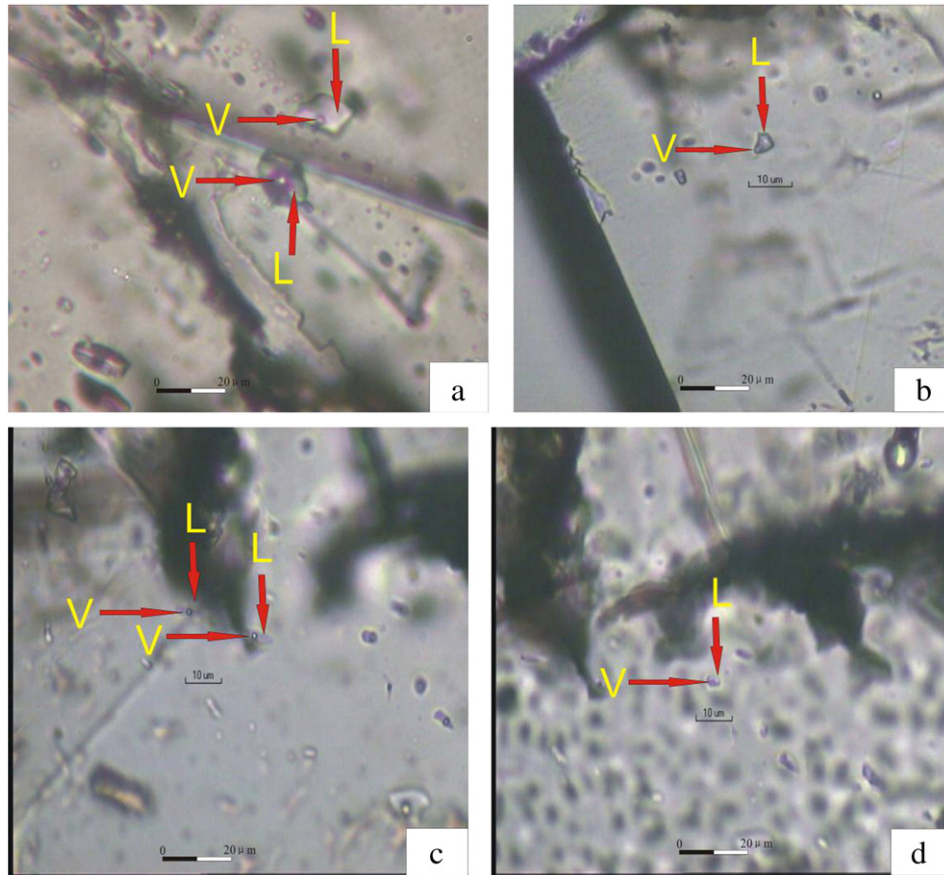


Fig. 9. Characteristics of fluid inclusions from Kafang copper deposit.

–67‰ in average) and $\delta^{18}\text{O}_{\text{H}_2\text{O}}$ (3.35‰–9.59‰, 5.9‰ in average) of granite-related skarn deposits are consistent with a predominantly magmatic source with a minor meteoric water contribution. In this study, the $\delta^{18}\text{O}_{\text{H}_2\text{O}}$ values of the quartz vary from 3.1 to 7.7‰ with an average of 6.15‰, while $\delta\text{D}_{\text{H}_2\text{O}}$ vary from –98‰ to –73‰ with an average of –86.5‰. $\delta^{18}\text{O}_{\text{H}_2\text{O}}$ values of sample JZL5 (from Jinzhulin adit) plot within the magmatic water box ($\delta\text{D}_{\text{H}_2\text{O}}$: –80‰––40‰, $\delta^{18}\text{O}_{\text{H}_2\text{O}}$: 5.5‰–9.0‰; Taylor, 1974), which indicates that these ore-forming fluids are dominantly magmatic water (Fig. 13). Two other samples (ZYK-1 and ZYK-2) have similar $\delta^{18}\text{O}_{\text{H}_2\text{O}}$ values as JZL5, but δD values are below the magmatic water box. Sample DGL-1 (from Donggualin adit) indicates significant mixing of meteoric water. The compositions of hydrogen–oxygen isotopes indicate that the ore forming fluid dominated by magmatic water in the early stage and it mixed with meteoric water in a later stage. This is supported by the large variations of fluid inclusion homogenization temperatures and salinities as discussed above (Fig. 10).

7.3. Mineralization process and ore genesis

Between ~83 and ~84 Ma, the Xinshan granitic magma intruded into the Triassic Gejiu Formation and associated mafic lavas, causing skarn and retrograde alteration in the wall rocks of the Kafang area. Temperature decrease decreases metal solubility in the ore-forming fluids (Barnes et al., 1967; Bourcier and Barnes, 1987; Crerar and Barnes, 1976; Giordano and Barnes, 1979; Romberger and Barnes, 1970). In the Kafang deposit, the homogenization temperatures of fluid inclusions range widely, which can be ultimately beneficial for the economic viability of the deposit. The wide temperature range, with corresponding salinities and densities, suggests multiple stages of evolution of the ore-forming fluid in Kafang deposit, which is also supported by the different H–O isotopes compositions of different

mineralization styles. Therefore, we suggest the mixing of granitic magma-derived fluid and meteoric water, along with decreasing temperature had a key role in the precipitation of the ore minerals.

Both S and Pb isotopes indicate that the Cu and Sn have distinct parental magmas: Cu was likely sourced from the basaltic magma, whereas Sn was likely sourced from the granite. Ore metals were transported by magma-derived hydrothermal fluids. This model is supported by the following observations: (1) both copper and tin are spatially centered around the Xinshan granite; (2) the alteration minerals are present throughout the whole orefield, including in the two stratiform types and the skarn ores; (3) in Kafang area, Cu is more widely distributed than Sn, as the former can be found in all the mineralization types, while the Sn ores only developed as skarn-type or carbonate–carbonate; (4) the Cu and Sn abundance in different units of this area (Table 8). The average Cu abundance of Xinshan granite is 15.6×10^{-6} , and Gejiu Formation is 20×10^{-6} , but the Cu abundance of basalt in Kafang orefield is 500×10^{-6} (Peng, 1992). The Cu abundance of basalt is 32 and 25 times higher than the granite and sedimentary rocks.

Much research has shown that high oxygen fugacity is beneficial for the enrichment of Cu in magmatic melts and the continuous release from ore-forming fluid (Sun et al., 2004; Wyborn and Sun, 1994). Conversely, the deposition environment of Sn in the granitic magma favors low oxygen fugacity, which is common for most tin granite world-wide, under a NNO system (Heinrich, 1990). Available published data show that the Xinshan granite has a low oxygen fugacity (Li, 1985), which means that granitic magma in Kafang Sn–Cu mine with low oxygen fugacity decreases the Cu solubility and thus decreases the potential for Cu mineralization, but is favorable for tin mineralization. Though controversies about the genesis of Kafang Cu–Sn mineralization have existed for many years (308 Geological Party, 1984; Jin, 1991; Mao et al., 2008a; Peng, 1985; Qin et al., 2006; Yang et al., 2008; Zhuang et

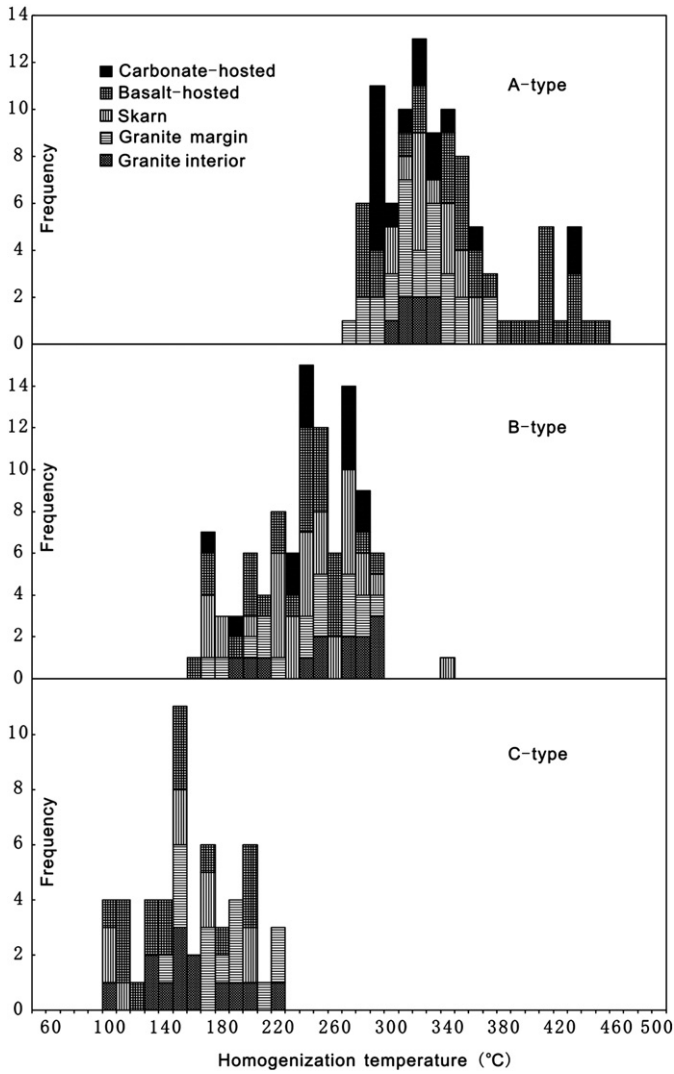


Fig. 10. Histogram of fluid inclusion homogenization temperatures of the Kafang copper deposit.

al., 1996), geological evidence and the new data of this study, led us to conclude that both granite and basalt played important role for the formation of the Kafang Cu–Sn deposit, where the granite acted as a source of fluids, S and some metals, but the Triassic basalt also contributed metals and S upon interaction with magmatic hydrothermal fluids.

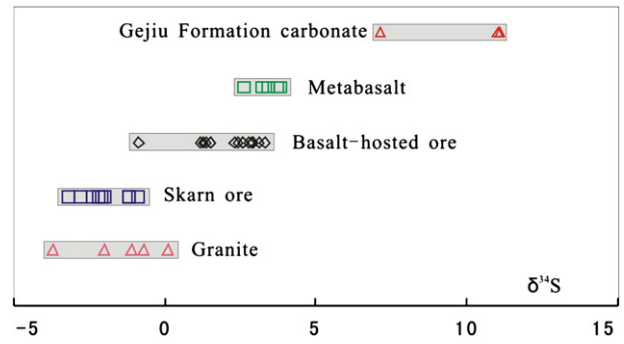


Fig. 12. $\delta^{34}\text{S}$ distribution of the different ore-related units of the Kafang copper deposit.

We propose the following genetic model for the Kafang deposit. A high temperature granitic magma-derived hydrothermal fluid interacted with cooler incoming meteoric water and formed the Sn ores and developed the related skarns and retrograde alteration along contact zones. The same hydrothermal fluid leached Cu from the basalt when it interacted with the basalt during its outward migration. As this fluid cooled and interacted with meteoric water, the stratiform Cu orebodies formed. Some of the magma-derived ore-forming fluid, transported Cu and Sn along the detachment structure of the Gejiu Formation (Mao et al., 2008a), and sulfide and cassiterite precipitated upon interaction with the carbonate layers, forming the carbonate-hosted stratiform Cu–Sn ores.

8. Conclusions

New LA-ICP-MS zircon U–Pb ages of the Xinshan granite (83.1 ± 0.4 Ma) and molybdenite Re–Os ages of the skarn ore (83.4 ± 2.1 Ma) and basalt-hosted ore (84.2 ± 7.3) in the Kafang orefield indicate a coeval relationship between magmatism and mineralization in Kafang deposit. Microthermometric results of fluid inclusions and H–O isotope data indicate that ore-stage minerals precipitated by the mixing of magma-derived fluid and meteoric water. According to the homogenization temperature, salinity and density data, it is inferred that fluid mixing along with fluid cooling played a key role in the formation of the Cu–Sn deposits in the Kafang area. A similar evolutionary trend of fluids suggests that the skarn, basalt-hosted and carbonate-hosted ores belong to a same ore-forming fluid system, which derived from the crystallizing Xinshan granite. S and Pb isotopes indicate that the ore metals came from different sources, i.e., Cu was likely sourced from the basalt, whereas Sn was likely sourced from the granite. Thus we conclude that the metallogeny of the Cu–Sn ores in Kafang area should be attributed to be the same intrusion-related hydrothermal system.

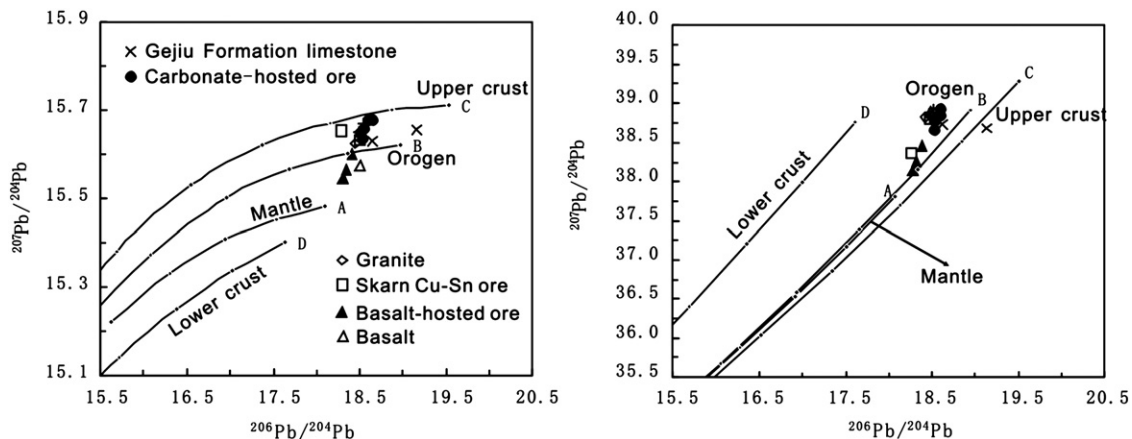


Fig. 11. Diagram of lead isotope composition of the Kafang copper deposit.

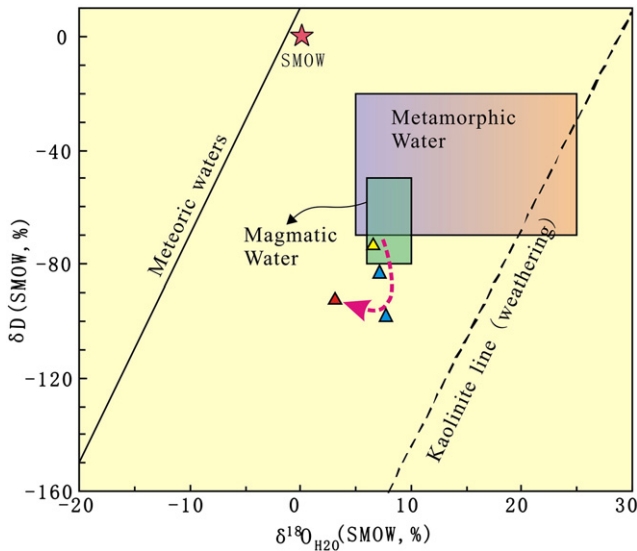


Fig. 13. $\delta D(\text{‰})-\delta^{18}O_{H_2O}(\text{‰})$ plot of Kafang copper deposit.

Table 8
Abundance of Cu in different rocks in Gejiu ore district ($\omega_B/10^{-6}$).

| Lithology | Cu abundance (ppm) | Reference |
|---------------------------|--------------------|----------------------------|
| Laochang-Kafang granite | 16 | Peng, 1992 |
| Kafang granite | 31 | Zhuang et al., 1996 |
| Laochang-Kafang granite | 57 | Li, 1998 |
| Xinshan granite | 25 | Zhang, 2005 |
| Gejiu Formation carbonate | 20 | Peng, 1992 |
| Gejiu Formation carbonate | 19 | |
| Gejiu Formation carbonate | 8 | Li, 1998 |
| Gejiu Formation carbonate | 16 | Liu et al., 2007 |
| Gejiu Formation carbonate | 6 | |
| Kafang meta-basalt | 101 | 308 Geological Party, 1984 |
| Kafang meta-basalt | 500 | Peng, 1992 |
| Kafang meta-basalt | 236 | Zhuang et al., 1996 |
| Kafang meta-basalt | 1120 | Zheng and Yang, 1997 |
| Kafang meta-basalt | 500 | Zhang et al., 2004 |
| Kafang meta-basalt | 4819 | Li et al., 2006a |
| Kafang meta-basalt | 135 | Liu et al., 2007 |

Acknowledgments

Prof. Franco Pirajno is thanked for valuable discussions during the field trip. Juan Zhang and Xiaolong Li from China University of Geosciences (Beijing) are thanked for their field and laboratory assistance. Anonymous reviewers are thanked for their critical but valuable comments, which greatly helped us finalize this manuscript. This study is supported by the National Science Foundation of China (40930419), Special Research Funding for the Public Benefits Sponsored by MLR (200911007-12), Research Program of Yunan Tin Group (2010-04A), the Geological Survey of China Geological Survey Project (1212011120994), and the Fundamental Research Funds for the Central Universities (2-9-2010-21).

References

308 Geological Party, 1984. Geology of Tin Deposits in Gejiu District. Metallurgical Industry Publishing House, Beijing. 256 pp. (in Chinese).
 Anderson, T., 2002. Correction of common lead in U–Pb analysis that do not report ^{204}Pb . Chem. Geol. 192, 59–79.
 Barnes, H.L., Romberger, S.B., Stempok, M., 1967. Ore solution chemistry, solubility of HgS in sulfide solutions. Econ. Geol. 62, 957–982.
 Bodnar, R.J., 1985. Pressure-volume-temperature-composition (PVTX) properties of the system H₂O–NaCl at elevated temperature and pressures. PhD dissertation, The Pennsylvania State University, 183 pp.
 Bourcier, W.L., Barnes, H.L., 1987. Ore solution chemistry VII, stabilities of chloride and bisulfide complexes of zinc to 350 degrees. Econ. Geol. 82, 1839–1863.

Cheng, Y.B., Mao, J.W., 2010. Age and geochemistry of granites in Gejiu area, Yunnan province, SW China: constraints on their petrogenesis and corresponding tectonic setting. Lithos 120, 258–276.
 Cheng, Y.B., Mao, J.W., 2012. Geochronology of the gabbro-mafic microgranular enclaves-granite association in Gejiu district, Yunnan province and their geodynamic significance. Acta Petrologica Sinica 86, 748–761 (in Chinese with English abstract).
 Cheng, Y.B., Mao, J.W., Xie, G.Q., 2008. Preliminary study of the petrogenesis of Laochang-Kafang granite in the Gejiu area, Yunnan province: constraints from geochemistry and zircon U–Pb dating. Acta Geol. Sin. 81, 1478–1493 (in Chinese with English abstract).
 Cheng, Y.B., Mao, J.W., Xie, G.Q., 2009. Zircon U–Pb dating of the granites in Gejiu supergenetic tin polymetallic ore-field and its significance. Miner. Deposits 28, 297–312 (in Chinese with English abstract).
 Clayton, R.N., Mayeda, T.K., 1963. The use of bromine pentafluoride in the extraction of oxygen from oxides and silicates for isotopic analysis. Geochim. Cosmochim. Acta 27, 43–52.
 Crerar, D.A., Barnes, H.L., 1976. Ore solution chemistry; V, solubilities of chalcopyrite and chalcocite assemblages in hydrothermal solution at 200 degrees to 350 degrees. Econ. Geol. 71, 772–794.
 Dai, F.S., 1996. Characteristics and evolution of rock series, lithogenesis, metallogenesis of crust-derived anatectin magma in Gejiu ore field. Geol. Yunnan 15, 330–344 (in Chinese with English abstract).
 Du, A.D., Wu, S.Q., Sun, D.Z., Wang, S.X., Qü, W.J., Stein, H.J., Morgan, J., Malinovsky, D., 2004. Preparation and certification of Re–Os dating reference materials: molybdenite HLP and JDC. Geostand. Geoanal. Res. 28, 41–52.
 Giordano, T.H., Barnes, H.L., 1979. Ore solution chemistry VI; PbS solubility in bisulfide solutions to 300 degrees. Econ. Geol. 74, 1637–1646.
 He, X.X., Zhu, X.K., Yang, C., Tang, S.H., 2005. High-precision analysis of Pb isotope ratios using MC-ICP-MS. Acta Geosci. Sin. 26, 19–22 (in Chinese).
 Heinrich, C.A., 1990. The chemistry of hydrothermal tin (tungsten) ore deposition. Econ. Geol. 85, 457–481.
 Hou, K.J., Li, Y.H., Tian, Y.Y., 2009. In situ U–Pb zircon dating using laser ablation-multi ion counting-ICP-MS. Miner. Deposits 28, 481–492 (in Chinese with English abstract).
 Jin, Z.D., 1991. Different views about the hydrothermal origin of the strataform orebodies in Gejiu district. Geol. Prospect. 1, 19–20 (in Chinese).
 Li, J.H., 1985. Study on the characteristic and petrogenesis about the granite in Gejiu area. Yunnan Geol. 4, 327–352 (in Chinese).
 Li, S.J., 1998. Discussions on the genesis of the Cu- & Sn-rich bodies in the Gejiu district, Yunnan Province. Geotectonica et Metallogenia 2, 148–155 (in Chinese with English abstract).
 Li, Y.S., Qin, D.X., Dang, Y.T., 2006a. Pb and S isotopes of the Gejiu tin deposits, Yunnan Province. Geology and Prospecting 24, 49–53 (in Chinese with English abstract).
 Li, Y.S., Qin, D.X., Dang, Y.T., Xue, C.D., 2006b. Lead and sulfur isotope in Gejiu tin deposit in Yunnan province. Geol. Prospect. 4, 49–53 (in Chinese with English abstract).
 Li, Y.S., Qin, D.X., Zou, T., Jia, F.J., Wan, C.Y., 2008. Geochemical features and tectonic setting of the Ladinian basalt in Gejiu, Yunnan Province. Journal of Jilin University. (Earth Science Edition) 4, 624–630 (in Chinese with English abstract).
 Li, Y.S., Qin, D.X., Cheng, X.Y., Guo, N.N., Luo, X., Xie, Y., Zou, T., 2009. Evidences of exhalative hydrothermal sedimentary mineralization of Indo-Chinese epoch of Gejiu tin-polymetallic deposits. Nonferrous Met. 61, 120–125 (in Chinese with English abstract).
 Liu, B., Shen, K., 1999. Thermal Dynamics of Fluid Inclusion. Geological Publishing House, Beijing. 290 pp.
 Liu, Y.P., Li, Z.X., Li, H.M., 2007. U–Pb geochronology of cassiterite and zircon from the Dulong Sn–Zn deposit: Evidence for Cretaceous large-scale granitic magmatism and mineralization events in southeastern Yunnan province, China. Acta Petrologica Sinica 23, 967–976 (in Chinese with English abstract).
 Ludwig, K.R., 2003. ISOPLOT 3.0: a geochronological toolkit for Microsoft Excel. Special Publication, 4. Berkeley Geochronology Center.
 Ludwig, K.R., 2004. Isoplot/Ex, version 3.0: a Geochronological Toolkit for Microsoft Excel. Berkeley Geochronology Center, Berkeley CA.
 Mao, J.W., Zhang, Z.C., Zhang, Z.H., Du, A.D., 1999. Re–Os isotopic dating of molybdenites in the Xiaoliugou W (Mo) deposit in the northern Qilian mountains and its geological significance. Geochim. Cosmochim. Acta 63, 1815–1818.
 Mao, J.W., Xie, G.Q., Li, X.F., Zhang, C.Q., Mei, Y.X., 2004. Mesozoic large scale mineralization and multiple lithospheric extension in south China. Earth Science Frontiers 11, 45–55.
 Mao, J.W., Wang, Y.T., Li, H.M., Pirajno, F., Zhang, C.Q., Wang, R.T., 2008a. The relationship of mantle-derived fluids to gold metallogenesis in the Jiaodong Peninsula: evidence from D–O–C–S isotope systematics. Ore Geol. Rev. 33, 361–381.
 Mao, J.W., Cheng, Y.B., Guo, C.L., 2008b. Gejiu tin polymetallic ore-field: deposit model and discussion. Acta Geol. Sin. 81, 1456–1468 (in Chinese with English abstract).
 Ohmoto, H., Goldhaber, M.B., 1997. Sulfur and carbon isotopes, In: Barnes, H.L. (Ed.), Geochemistry of Hydrothermal Ore Deposits, 3rd edition. John Wiley and Sons, New York, pp. 517–611.
 Ohmoto, H., Rye, R.O., 1979. Isotopes of sulfur and carbon. In: Barnes, H.L. (Ed.), Geochemistry of Hydrothermal Ore Deposits. Wiley-Interscience, New York, pp. 509–567.
 Peng, C.D., 1985. A discussion on the condition, types and model of Gejiu tin deposit. Yunnan Geology 4, 17–32 (in Chinese with English abstract).
 Peng, Z.X., 1992. Discussion on the deposit model of the Gejiu district. Yunnan Geology 11, 362–368 (in Chinese with English abstract).
 Qian, Z.K., Luo, T.Y., Huang, Z.L., Long, H.S., Yang, Y., 2009. Stratiform diopside: a new SEDEX origin rocks in Gejiu area. Acta Mineral. Sin. 29, 61–63 (in Chinese).
 Qin, D.X., Li, Y.S., 2008. Studies on the geology of the Gejiu Sn–Cu deposit. Science Press, Beijing, 1–180 (in Chinese with English abstract).

- Qin, D.X., Li, Y.S., Tan, S.C., Chen, A.B., Xue, C.D., Fan, Z.G., Dang, Y.T., Tong, X., Wu, J.D., Li, Y.X., Wang, H.Y., 2006. Metallogenic ages of Gejiu tin ore deposit in Yunnan province. *Chin. J. Geol.* 41, 122–132 (In Chinese with English abstract).
- Robinson, B.W., Kusakabe, M., 1975. Quantitative preparation of sulfur dioxide, for $^{34}\text{S}/^{32}\text{S}$ analyses, from sulfides by combustion with cuprous oxide. *Anal. Chem.* 47, 1179–1181.
- Romberger, S.B., Barnes, H.L., 1970. Ore solution chemistry: solubility of CuS in sulfide solutions. *Econ. Geol.* 65, 901–919.
- Selby, D., Creaser, R.A., 2004. Macroscale NTIMS and microscale LA-MC-ICP-MS Re–Os isotopic analysis of molybdenite: testing spatial restrictions for reliable Re–Os age determinations, and implications for the decoupling of Re and Os within molybdenite. *Geochim. Cosmochim. Acta* 68, 3897–3908.
- Shirey, S.B., Walker, R.J., 1995. Carius tube digestion for low-blank rhenium–osmium analysis. *Anal. Chem.* 67, 2136–2141.
- Simon, K., 2001. Does δD from fluid inclusion in quartz reflect the original hydrothermal fluids? *Chem. Geol.* 177, 483–495.
- Smoliar, M.I., Walker, R.J., Morgan, J.W., 1996. Re–Os ages of group IIA, IIIB, IVA, IVB iron meteorites. *Science* 271, 1099–1102.
- Stein, H.J., Scherstén, A., Hannah, J., Markey, R., 2003. Subgrain-scale decoupling of Re and ^{187}Os and assessment of laser ablation ICP-MS spot dating in molybdenite. *Geochim. Cosmochim. Acta* 67, 3673–3686.
- Sun, W.D., Arculus, R.J., Kamenetsky, V.S., 2004. Release of gold-bearing fluids in convergent margin magmas prompted by magnetite crystallization. *Nature* 431, 975–978.
- Taylor, H.P.J., 1974. The application of oxygen and hydrogen isotope studies to problems of hydrothermal alteration and ore deposition. *Econ. Geol.* 69, 843–883.
- Wang, Z.F., 1983. Discussion on some problems on mineralization of Gejiu tin deposit. *Acta Geologica Sinica* 57, 154–163 (in Chinese with English abstract).
- Wang, Q., Li, J.W., Jian, P., Zhao, Z.H., Xiong, X.L., Bao, Z.W., Xu, J.F., Li, C.F., Ma, J.L., 2005. Alkaline syenites in eastern Cathaysia (south China): link to Permian–Triassic transension. *Earth Planet. Sci. Lett.* 230, 339–354.
- Wu, Q.S., Xu, J.Z., Yang, Z., 1983. S and Pb isotopic characteristics of the tin granite in Gejiu ore district and their exploration significance. *Mineral Resources and Geology* 4, 293–302.
- Wu, Q.S., Xu, J.Z., Yang, Z., 1984. Study on Sr isotope character and prospecting criteria of tin-bearing granite of Gejiu area. *Geochemica* 293–302 (in Chinese).
- Wyborn, D., Sun, S.S., 1994. Sulphur-undersaturated magmatism: a key factor for generating magma-related copper–gold deposits. *AGSO Res. News.* 21, 7–9.
- Xu, Q.D., Xia, Q.L., Cheng, Q.M., 2009. Tectono-magmatic evolution related to metallogenic system in Gejiu, southeast Yunnan of China. *Earth Sci. J. China Univ. Geosci.* 34, 307–313 (in Chinese with English abstract).
- Yang, Z.X., Mao, J.W., Chen, M.H., Tong, X., Wu, J.D., 2008. Re–Os dating of molybdenite from the Kafang skarn copper (tin) deposit in the Gejiu tin polymetallic ore district and its geological significance. *Acta Petrol. Sin.* 24, 1937–1944 (in Chinese with English abstract).
- Yang, Z.X., Mao, J.W., Chen, M.H., 2009. ^{40}Ar – ^{39}Ar dating of muscovite from Laochang veinlet-like Sn deposit in Gejiu tin polymetallic ore district and its geological significance. *Miner. Deposits* 28, 336–344 (in Chinese with English abstract).
- Yang, Z.X., Mao, J.W., Chen, M.H., Cheng, Y.B., Zhao, H.J., Chang, Y., 2010. Geology, geochemistry and genesis of Kafang copper deposit in Gejiu, Yunnan Province. *Acta Petrol. Sin.* 26, 830–844 (in Chinese with English abstract).
- Yu, C.W., Tang, Y.J., Shi, P.F., Deng, B.L., 1988. The Dynamic System of Endogenic Ore Formation in Gejiu Tin-polymetallic Ore Region, Yunnan Province. China University of Geosciences Press, Wuhan. 251 pp. (in Chinese).
- Yu, C.W., Tang, Y.J., Shi, P.F., Deng, B.L., 1989. The dynamic system of endogenic ore formation in Gejiu tin-polymetallic ore region, Yunnan province. China University of Geosciences Press, Wuhan, 1–251 (in Chinese with English abstract).
- Zartman, R.E., Doe, B.R., 1981. Plumbotectonics—the model. *Tectonophysics* 75, 135–162.
- Zhang, H., 2005. Geochemistry and genesis of the supergiant Gejiu Sn polymetallic deposits. PhD Thesis. Institute of Geochemistry, Chinese Academy of Sciences 1–120 (in Chinese with English abstract).
- Zhang, H., Gao, Z.M., Ma, D.Y., Tao, Y., Liu, H., 2004. Distribution and genetic significance of Sn in oolitic pyrite and colloidal structure pyrite from Gejiu tin deposits. *Acta Mineralogica Sinica* 1, 70–75 (in Chinese with English abstract).
- Zhang, H., Gao, Z.M., Ma, D.Y., 2005. Lead and sulfur isotopic tracing for source of ore-forming material in the Gejiu tin polymetallic deposit. *Geol. Prospect.* 4, 17–20 (in Chinese with English abstract).
- Zhang, H., Tong, X., Wu, J.D., Luo, T.Y., Tao, Y., Zhu, D., 2007. Gejiu tin-polymetallic ore deposit: an example of landing of red sea-type submarine hydrothermal deposition. *Acta Mineralogica Sinica* 27, 335–341 (in Chinese with English abstract).
- Zhao, Y.M., Lin, W.W., Bi, C.S., 1990. Skarn Deposits in China. Geological Publishing House, Beijing. 354 pp. (in Chinese with English abstract).
- Zhao, Y.M., Dong, Y.G., Li, D.X., Bi, C.S., 2003. Geology, mineralogy, geochemistry, and zonation of the Bajiazhi dolostone-hosted Zn–Pb–Ag skarn deposit, Liaoning Province, China. *Ore Geol. Rev.* 23, 153–182.
- Zheng, Q.A., Yang, D.S., 1997. Evolutionary and deposit model of the Gejiu supergiant tin polymetallic deposits. *Exploration* 02, 67–96 (in Chinese with English abstract).
- Zhou, J.P., Xu, K.Q., Hua, R.M., Zhao, Y.Y., Zhu, J.C., 1998. Characteristics and genesis of exhalative sedimentary massive sulfide in Southeastern Yunnan province. *Acta Mineral. Sin.* 18, 158–168 (in Chinese with English abstract).
- Zhuang, Y.Q., Wang, R.Z., Yang, S.P., 1996. Tin-Copper Polymetallic deposit. Earthquake publishing house, Beijing, pp. 38–101 (in Chinese).

Chapter 7

Iron isotope fractionation during supergene weathering process and its application to constrain ore genesis in Gaosong deposit

Iron isotope fractionation during supergene weathering process and its application to constrain ore genesis in Gaosong deposit, Gejiu District, SW China

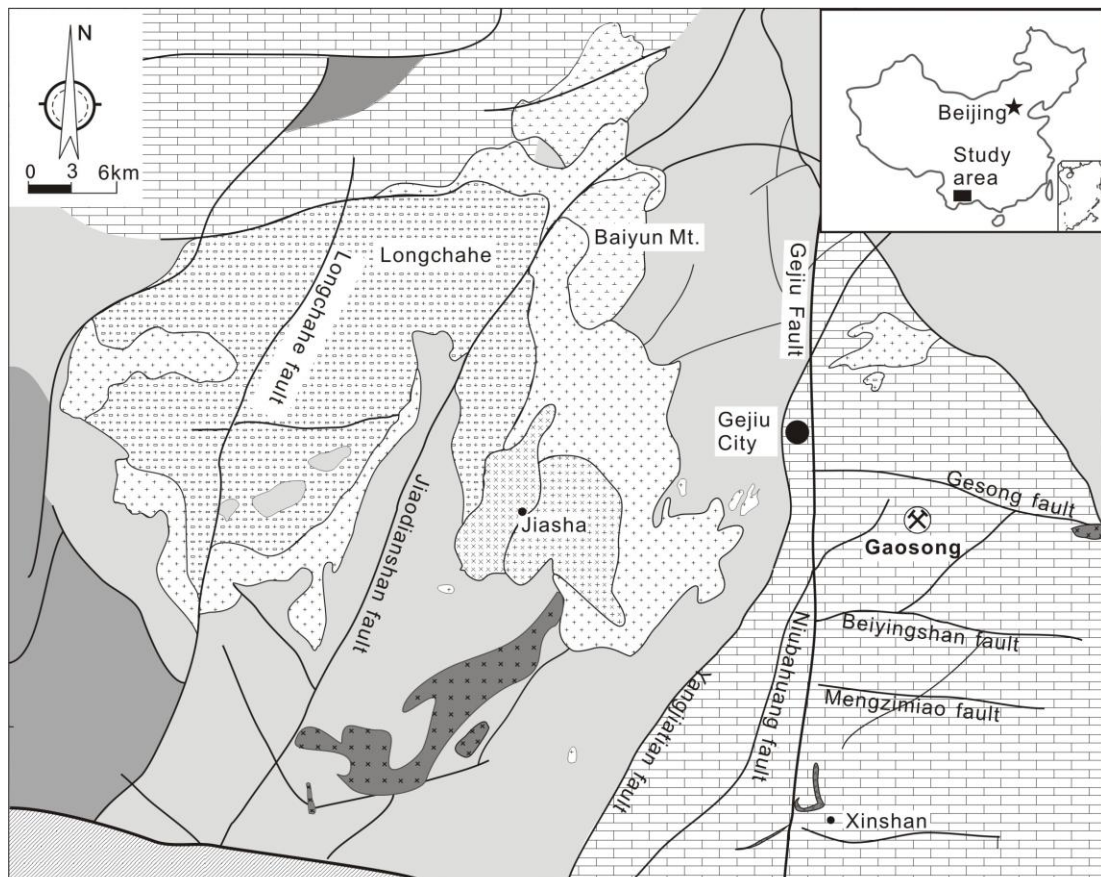
1 Introduction

As a direct mineralization element, Fe isotope has attracted much attention as a possible tool for monitoring mineralization processes ([Johnson et al., 2003](#); [Dauphas et al., 2004](#); [Whitehouse et al., 2007](#); [Li et al., 2008a, 2008b](#); [Zhu et al., 2008](#); [Sharma et al., 2001](#); [Beard et al., 2003](#); [Rouxel et al., 2004, 2008](#); [Markl et al., 2006](#); [Graham et al., 2004](#); [Wang et al., 2011](#)) and geochemical processes related to ore formation (e.g. [Anbar et al., 2005](#); [Johnson et al., 2002, 2005](#); [Wiesli et al., 2004](#); [Butler et al., 2005](#); [Fernandze et al., 2009](#)) in the past ten years. Some of these studies were focused on Fe isotopes fractionation during redox reactions (e.g. [Anbar et al., 2005](#); [Butler et al., 2005](#); [Johnson et al., 2002](#); [Welch et al., 2003](#); [Kavner et al., 2005](#); [Balci et al., 2006](#)) and re-working of primary Fe-minerals in hydrothermal-supergene iron ores ([Markl et al., 2006](#)), indicating that Fe isotopes can be fractionated in these processes and thus Fe isotopes may be used to identify the products and evolutionary of ore supergene weathering process. However, few studies have been taken so far to investigate iron isotopes variations during a continuous oxidation process in different oxidative degrees, which is crucial to trace Fe in supergene geochemical cycling process and constraint the genesis of secondary oxidized ores.

The Gejiu tin-polymetallic ore district is one of the largest and oldest mining districts in the world, which comprises five Sn-Cu-Pb-Zn polymetallic deposits, containing approximately 300 Mt of Sn resources at an average grade of 1% Sn, 300 Mt of Cu resources averaging 2% Cu and 400 Mt of Pb-Zn ores with an average grade of 7% Pb+Zn. Gaosong is one of the deposits in the world-class Gejiu ore district. Three types of

ores (i.e., primary sulfide ores, oxidized ores and gossan ores) are developed in this deposit. These ores have different oxidation degrees, representing a continuous oxidation process, and together with the gossan from this deposit, these samples provide an excellent opportunity to investigate the behavior of Fe isotopes during supergene weathering processes. In this paper we present new iron isotope data for the above three types of mineralization from the Gaosong deposit, with the following main purposes: (1) to understand the behavior of Fe isotopes during supergene weathering process, and (2) to constrain the genesis and metal source of the oxidized ores in Gaosong deposit.

2 Geological background



LEGEND

| | |
|--|-------------------------------------|
| Gabbro | Mineral deposit |
| Upper Triassic purple sandstone | Ailao Mt. metamorphic zone |
| Middle Triassic basaltic lava of the Falang Formation | Equigranular biotite granite |
| Middle Triassic sandstone, shale of the Falang Formation | Porphyritic biotite granite |
| Middle Triassic carbonate of the Gejiu Formation | Alkaline rocks |
| Lower Triassic shale of the Yongningzhen Formation | Granite bearing with mafic enclaves |

Figure 1 Sketch geological map of the Gejiu district, Yunnan Province, SW China (Modified from [308 Geological Party, 1984](#))

The world class Gejiu tin polymetallic ore district is located on the western margin of the South China Block, adjacent to the Yangtze Craton in the north and the Three Rivers Fold Belt in the west. Cambrian to Quaternary rock successions are well-preserved (mostly underground thus not shown in [Fig. 1](#)) in the Gejiu district, and most of the outcrops in the Gejiu area consist of Middle Triassic Gejiu Formation carbonate and Middle Triassic Falang Formation fine-grained clastic sedimentary rocks and carbonate with interlayered mafic lavas (1800 to 2800 m thick; [Qin and Li, 2008](#)). Numerous faults are present in the Gejiu region, including the NNE-trending Longchahe, Jiaodingshan and Yangjiatian faults, the NE-trending Baishachong fault and the N-trending Gejiu fault ([Fig. 1](#)). The Gejiu batholith is a prominent igneous body in this area, composed of Mesozoic gabbro, mafic microgranular enclaves (MMEs), porphyritic biotite granite, equigranular biotite granite, syenites and mafic dykes ([Fig. 1](#)).

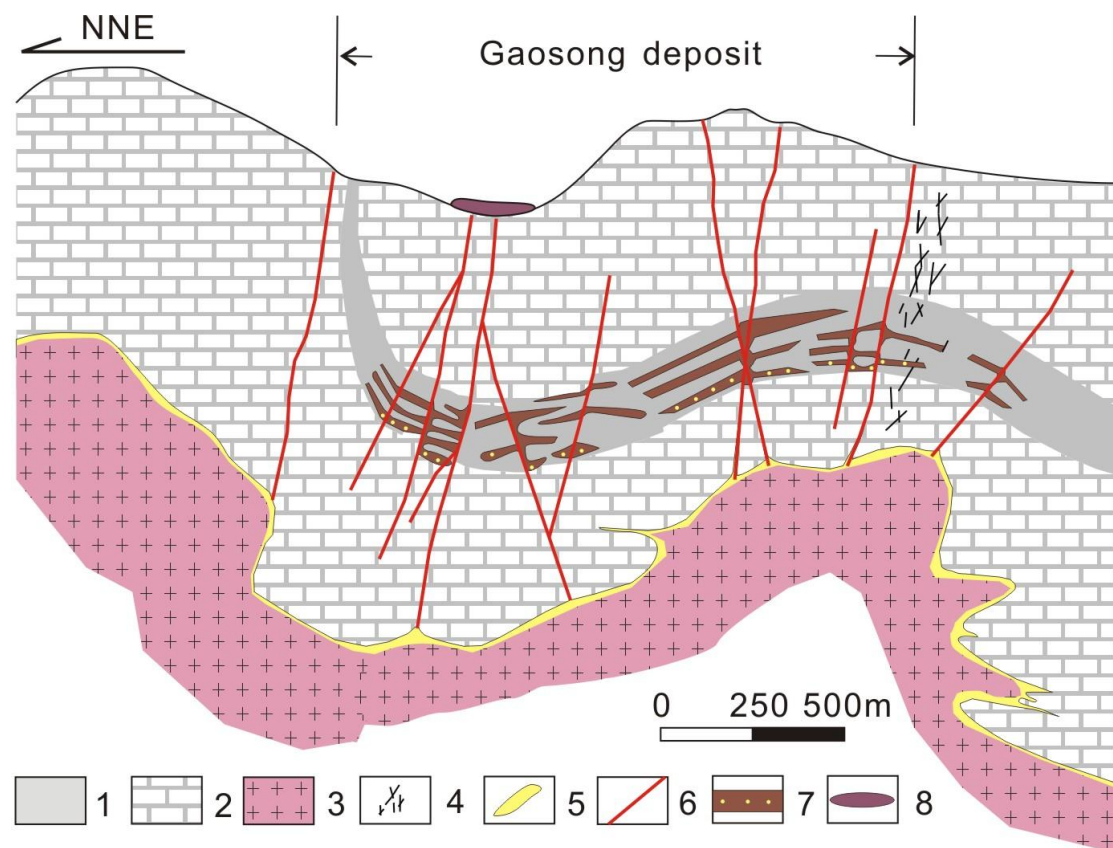


Figure 2 Representative cross section of the Gaosong deposit in Gejiu district.

1-Interlayers of limestone, dolomite and dolomitic limestone; 2-Carbonate of Gejiu Formation in mid-Triassic; 3-Cretaceous granite; 4-Vein type ores; 5-Sulfide ores; 6-Faults; 7-Stratabound oxidized ore with low oxidation degree ore; 8-Gossan. Tur-tourmaline, Cp-chalcopyrite, Po-pyrrhotite, Pyx-pyroxene, Lim-limonite, Fl-fluorite, Grt-garnet.

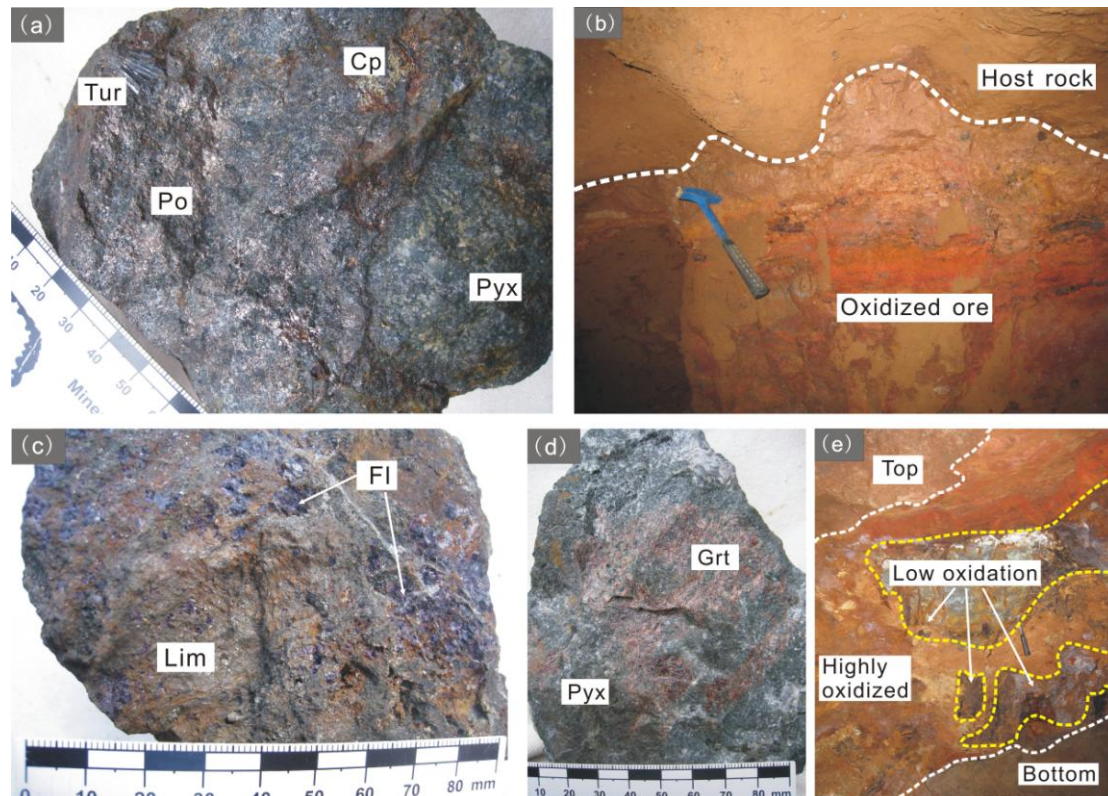


Figure 3 Typical hand specimen from the Gaosong deposit.

a-Sulfide ores with skarn; b-Contact of oxidized ore and wall rocks; c-Oxidized ore; d-Typical skarn; e-Oxidized ore and host low oxidation degree ore, both of which are hosted by Gejiu Formation carbonate. Tur-Tourmaline; Po-pyrrhotite; Cp-Chalcopyrite; Pyx-pyroxene; Fl-fluorite; Lim-limonite; Grt-garnet.

The Gaosong deposit is located in the middle-northern part of the mining district and occurs over approximately 40 km² (Fig. 1). The deposit is mostly underlain by the Mid-Triassic Gejiu Formation, which consists of three units: 1) the Bainidong Unit, consisting primarily of light gray to gray limestone, with minor banded and lenticular

calcareous dolomite; 2) the Malage Unit, consisting primarily of dark gray to gray limey dolomite, with minor dolomitic limestone; 3) the Kafang Unit, which is mainly composed of gray to light gray limestone and limey dolomite interlayers. The Kafang Unit is the main host of the Gaosong mineralisation. The 8-km long NE-trending Lutangba fault and its associated subsidiary faults are the major structures controlling the ore. They cut the Kafang Unit, acting as major conduits for ore-forming fluids. Greisen (quartz-muscovite) alteration, muscovite, sericite and skarn minerals have developed intensively on the margins of the granitic cupola and in the contact zone between granite and carbonate.

Skarn-sulfide ore occurs along the contact zones between granite and limestone and/or dolomite (Fig. 2). This type of ore hosted by skarn and characterized by disseminated textures, veinlet textures and massive textures. The primary skarn minerals are pyroxene, garnet and scapolite (Fig. 3). The ores are associated with retrograde skarn minerals (actinolite, tremolite and chlorite). The major ore minerals include arsenopyrite, pyrrhotite, chalcopyrite and marmatite (Fig. 3), with lesser amounts of cassiterite, pyrite, scheelite, native bismuth, molybdenite and magnetite. Another type of ore generally is weathering product and has complex orebody shapes, including stratabound, irregular banded, lenticular and veinlet. The orebodies occur in different layers that are controlled by detachment zones and fractures (Fig. 2) and typically consist of several ore layers at different levels, generally 3-5 layers, locally up to 8-9 layers. This type of orebody can be tens to hundreds of meters long and 100 - 200 m wide, consisting of limonite, hematite, goethite and clay minerals (Fig. 3), with minor amounts of cassiterite, marmatite, anglesite, pyrolusite and malachite. Gangue minerals include primarily scorodite, siderite, calcite, quartz, phlogopite, fluorite, tourmaline, chlorite, garnet, tremolite, pyroxene, with minor amounts of plagioclase, jarosite and kaolinite.

Gossan is occasionally developed along/around faults in the surface, and this represents the most oxidized end-member (Fig. 2). For the upper part of the oxidized ores, minerals including hematite, hydrohematite and minor limonite, hydrogoethite, plumbojarosite, minetisite, cassiterite, malachite and cerussite are present. By contrast, the lower parts of the oxidized ores mainly consist of limonite, colloform pyrite, melanterite, pyrrhotite, chalcopyrite, pyrite with minor cassiterite and phlogopite. The

lowest ores are the primary sulfide ores hosted by skarn and commonly developed between the contact zone of granite and carbonate. Vertical variations of mineral associations at different depths exhibit a continuous supergene alteration process (Fig. 2), as degrees of oxidation increases from the primary sulfide ores to the gossan, therein, the gossan always completely oxidized but the primary ores almost unaffected by later alteration.

3 Sampling and Analytical methods

3.1 Sampling

Samples of the three types of ores (23 rocks in total) were collected to study their iron isotope variations, with these chosen to encompass the range of mineral assemblages and inferred degree of oxidation at the Gaosong deposit (Fig. 4).

Eight fresh primary skarn-sulfide ore samples (i.e., c043, c048, c055, c064, c067, c071, c080, c085) were collected from three different adits of the Gaosong deposit to represent the most primary rocks. These ores were not affected by the secondary oxidization process.

Ten oxidized ore samples (i.e., c001, c003, c023, c024, c025, c027, c029, c233, c234, c237) were collected from two different adits of Gaosong deposit to represent the secondary primary rocks with the oxidation degree varying between primary and gossan ores. The distances between these sample locations and the underlying granite and their mineral compositions were distinguished (Table 1). The samples mainly consist of hematite, with minor malachite, azurite and cassiterite. some of these samples with relatively low oxidation degree contain pyrrhotite and/or pyrite, skarn minerals, galena and/or chalcopyrite.

Five gossan samples (i.e., c303, c304, c305, c307, c308) were collected from the surface to represent the most oxidized compositions. All of these samples were collected close to the Lutangba fault (Fig.2), which is considered to be the major ore-controlling fault in Gaosong deposit and cut the primary skarn-sulfide orebodies at the contact of granite and limestone / dolomite. As shown in Table 1, the distance between the sampling

locations and the fault is variable. The gossan samples mainly consist of clay minerals, limonite, and hematite, with minor malachite, calcite and cassiterite.

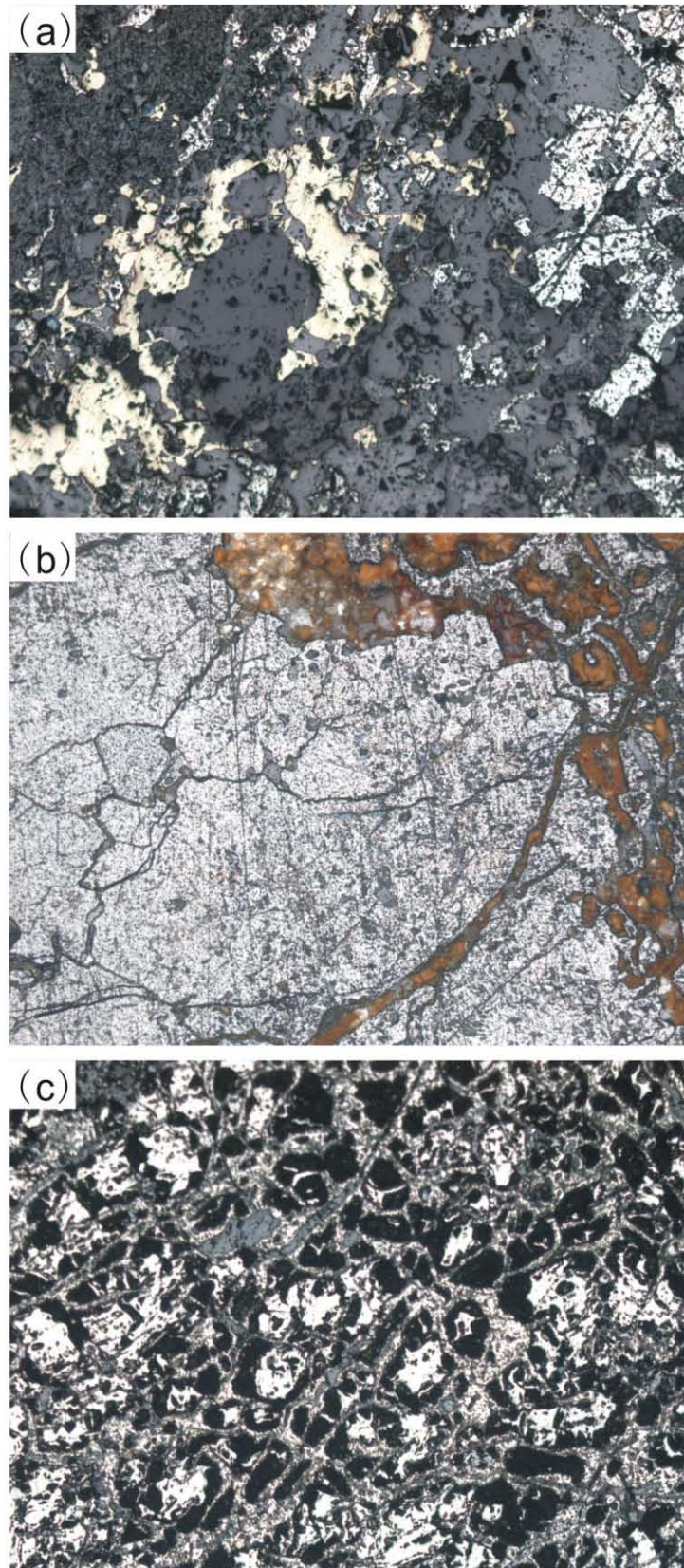


Figure 4 Typical microscope images from the Gaosong deposit showing different

oxidization degrees of the sample in this study. a-primary sulfide ore; b-light oxidized ore;
c-heavily oxidized ore.

3.2 Sample preparation

All 23 samples were carefully cleaned ultrasonically in purified Elga H₂O (18.2 MΩ) before crushing and milling. Approximately 10 mg of whole rock powder was digested in 4 ml of 6 M HCl, 5 M HNO₃ and concentrated HF on a hot-plate at 120°C and evaporated to dryness after complete dissolution. The residue was then added to 0.5 ml of concentrated HNO₃ and evaporated for three times to dryness to eliminate HF. The residue was dissolved in 0.5 ml of concentrated HCl to convert the cations to a chloride-form and evaporated to dryness after complete dissolution for three times. The final residue was dissolved in 1.5 ml 6 M HCl with 0.001% H₂O₂ to ensure all Fe was converted into Fe³⁺ before purification using anion exchange chromatography as described by [Zhu et al. \(2002\)](#).

3.3 Mass spectrometry

The purified samples were measured for Fe isotopes on a Nu Instruments multiple collector plasma source mass spectrometer at high-resolution mode using a standard-sample bracketing approach. Solutions of standard and samples were introduced into the mass spectrometer through a DSN-100 desolvating nebulizer at 5 ppm Fe in 0.1 M HNO₃ medium, and concentrations of samples and standard are matched to be within 10%. Runs of sample and standard were separated by washes using 2 M and 0.1 M HNO₃ for 3 and 2 min, respectively. Signals of ⁵⁴Fe, ⁵⁶Fe, ⁵⁷Fe were collected simultaneously together with ⁵³Cr, which was used to monitor the interference of ⁵⁴Cr on ⁵⁴Fe. In all cases ⁵³Cr signals were <10⁻⁴, and no ⁵⁴Cr correction was needed. Data were acquired in blocks of 10 ratios with 10-s integration times, and background measurements were taken prior to each data block. The Fe isotope results are expressed as deviations of a Fe isotope ratio of a sample from that of the reference material IRMM-14([Wang et al., 2011](#)):

$$\delta^{56}\text{Fe}_{\text{IRMM-014}} (\text{‰}) = \left[\frac{(^{56}\text{Fe}/^{54}\text{Fe})_{\text{sample}}}{(^{56}\text{Fe}/^{54}\text{Fe})_{\text{IRMM-014}}} - 1 \right] \times 1000$$

$$\delta^{57}\text{Fe}_{\text{IRMM-014}} (\text{‰}) = \left[\frac{(^{57}\text{Fe}/^{54}\text{Fe})_{\text{sample}}}{(^{57}\text{Fe}/^{54}\text{Fe})_{\text{IRMM-014}}} - 1 \right] \times 1000$$

Long-term repeatability of Fe isotope ratio measurements at high-resolution mode is

better than 0.05‰ amu⁻¹ at 95% confidence level. Details of the mass spectrometry have been described elsewhere (Zhu et al., 2008).

4 Results

Fe isotope compositions of bulk samples including eight samples of primary ores, ten samples of oxidized ores and five samples of gossans from Gaosong deposit in Gejiu district are reported in Table 1. When plotted on a three-isotope diagram, all iron-isotope data define a single mass-fractionation line with a slope of ~0.67 (Fig. 5). The correlation between $\delta^{56}\text{Fe}$ and $\delta^{57}\text{Fe}$ is $\delta^{56}\text{Fe} = (0.667 \pm 0.001) \delta^{57}\text{Fe}$, and $R^2 = 0.998$.

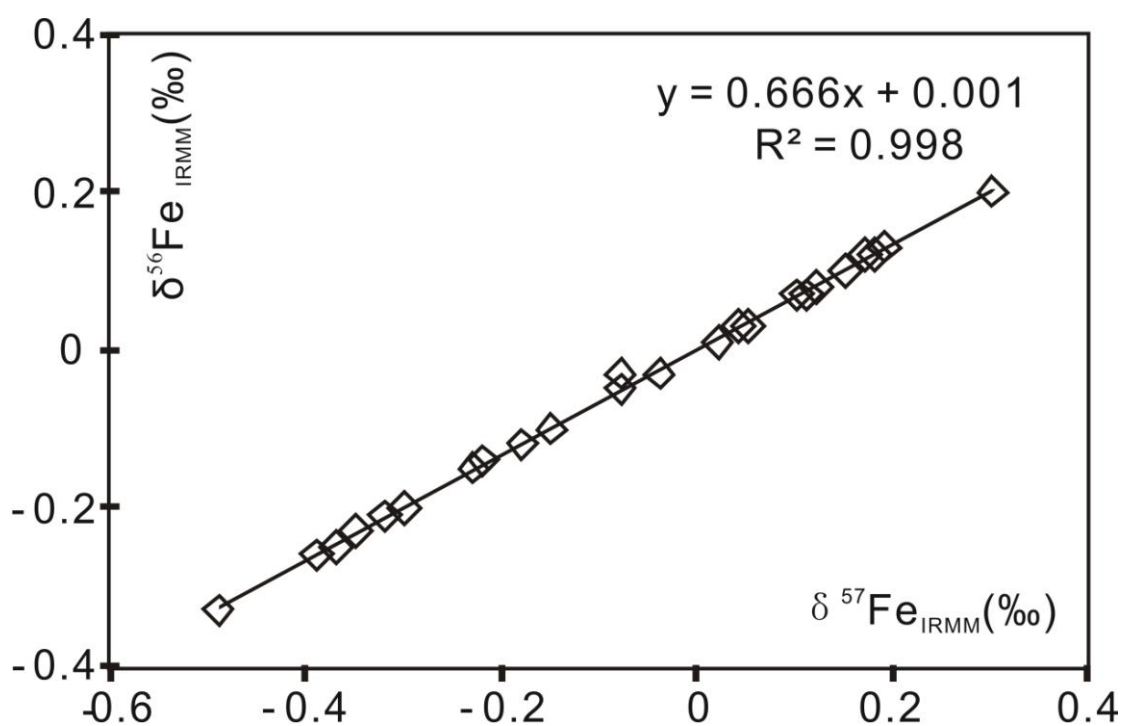


Figure 5 $\delta^{57}\text{Fe}$ versus $\delta^{56}\text{Fe}$ plot showing that all the Fe-isotope data of the samples in this study plot on a single mass-fractionation line.

4.1 Primary skarn-sulfide samples

The eight primary sulfide samples from Gaosong deposit have $\delta^{57}\text{Fe}$ values ranging from -0.49‰ to 0.15‰ with an average of -0.22‰ (Table 1). The $\delta^{57}\text{Fe}$ values of all samples are negative except for c071, whose $\delta^{57}\text{Fe}$ value is positive, perhaps because it contains a large amount of late-stage pyrite (Table 1), according to the paragenetic

sequence of the minerals in Gejiu ore district presented by [Cheng \(2012\)](#), which shows the skarn minerals, chalcopyrite and pyrrhotite formed earlier than all stages of pyrite. It has been suggested that late-formed sulfides always have heavier iron isotope compositions relative to early formed sulfides, because iron isotope fractionation occurs during fluid evolution ([Wang et al., 2011](#)).

4.2 Oxidized samples

Ten oxidized samples from Gaosong deposit yield $\delta^{57}\text{Fe}$ values ranging from -0.39‰ to 0.18‰ with average of -0.02‰ ([Table 1](#)). These samples are therefore, on average, slightly enriched in heavy iron isotopes relative to primary sulfide ores. As shown in [Table 1](#), three slightly oxidized samples (i.e., c001, c023, c237), mainly composed of pyrrhotite, pyrite and chalcopyrite with limonite and goethite, collected from the location relatively proximal to the granite have the lightest iron isotope compositions in all oxidized samples measured in this study ($\delta^{57}\text{Fe}$ ranging from -0.39 ‰ to -0.08‰, with an average of -0.23‰). Two samples (i.e., c233, c234) mainly composed of hematite collected from the location relatively distal to granite, which represent the most oxidized sample, have the heaviest iron isotope compositions of all oxidized samples measured in this study, with $\delta^{57}\text{Fe}$ values ranging from 0.10 ‰ to 0.18‰, and an average of 0.14‰. The Fe isotope compositions of moderately oxidized samples (i.e., c003, c024, c025, c027, c029) fall between those heavily oxidized samples and slightly oxidized samples, with a variation in $\delta^{57}\text{Fe}$ values from 0.02‰ to 0.11‰, and an average of 0.05‰.

4.3 Fe isotope compositions of gossan samples

Gossan samples from the Gaosong deposit have $\delta^{57}\text{Fe}$ values ranging from 0.11‰ to 0.30‰ with an average of 0.17‰ ([Table 1](#)). Fe isotope compositions of samples collected from different locations are variable. As shown in [Table 1](#), the $\delta^{57}\text{Fe}$ values of the three samples collected from relatively proximal to the Meiyuchong fault range from 0.12 ‰ to 0.30‰ with an average of 0.19‰, and $\delta^{57}\text{Fe}$ values of the other two samples collected from relatively distal to Meiyuchong fault range from 0.11 ‰ to 0.19 ‰ with an average of 0.15‰. There is no resolvable Fe isotope distinction between these two groups of gossan samples, despite different distances from sample locations to the fault.

5 Discussions

5.1 Fe isotope fractionation during supergene weathering process

It is an important issue that whether iron isotopes fractionate during supergene weathering process, as this kind of information is crucial in tracing supergene geochemical circulation using Fe isotopes, as well as in tracing mineralization processes and metal source of oxidized ores.

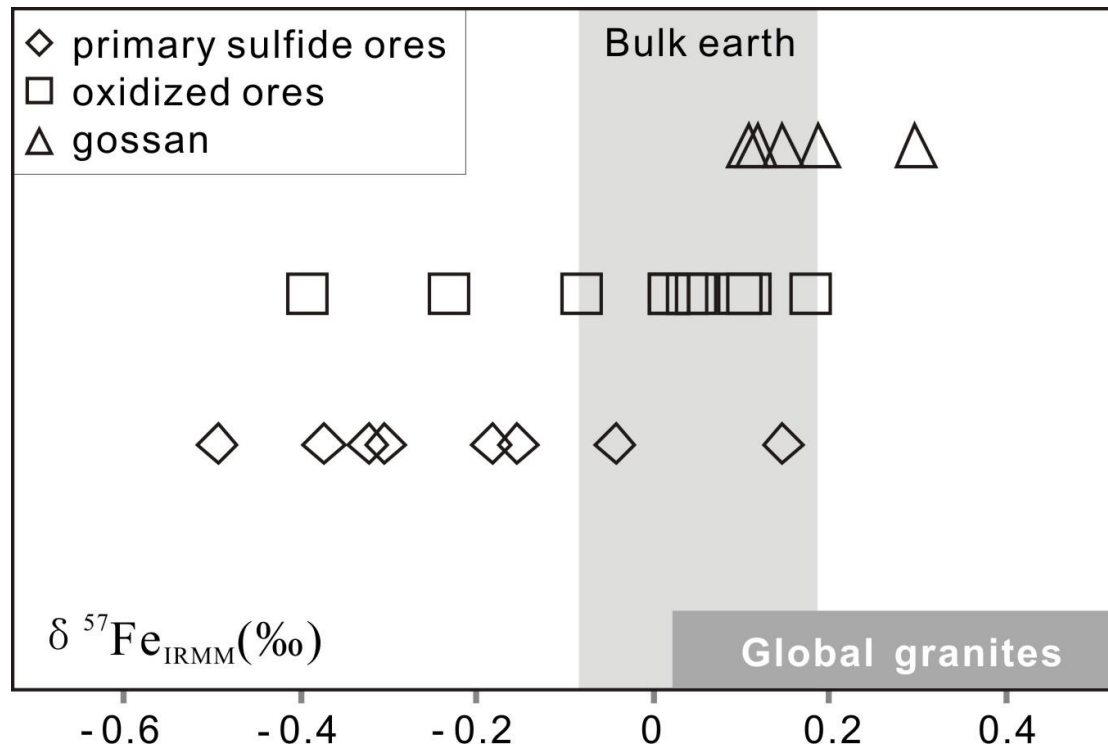


Figure 6 Fe isotopes of three different types of samples from the Gaosong deposit.

Primary sulfide ores, oxidized ores and gossan samples with different oxidation degree show a clear correlation between iron isotopes compositions and degree of oxidation (Fig. 6). The $\delta^{57}\text{Fe}$ values of primary sulfide ores, which represent the lowest degree of oxidation in Gaosong deposit, have the lightest iron isotope compositions in all measured samples in this study. Gossan samples are the most oxidized ones in this study, which have the heaviest iron isotope compositions. The $\delta^{57}\text{Fe}$ values of oxidized sulfide ores, of which oxidation degrees are higher than primary sulfide ores but lower than gossan samples, fall between those of primary sulfide ores and gossan ores. The above

variation patterns also exists in oxidized sulfide ores, as Fe isotope composition of these samples with different oxidization degree also exhibit a similar regularity (Fig. 7; Table 1). The heavily oxidized sample has the heaviest iron isotope compositions of all the oxidized samples while the slightly oxidized samples have the lightest iron isotope compositions. The Fe isotope compositions of moderately oxidized samples fall between those of heavily oxidized samples and slightly oxidized samples. In summary, iron isotope compositions of ores in this study become progressively heavier with the oxidation degree increase.

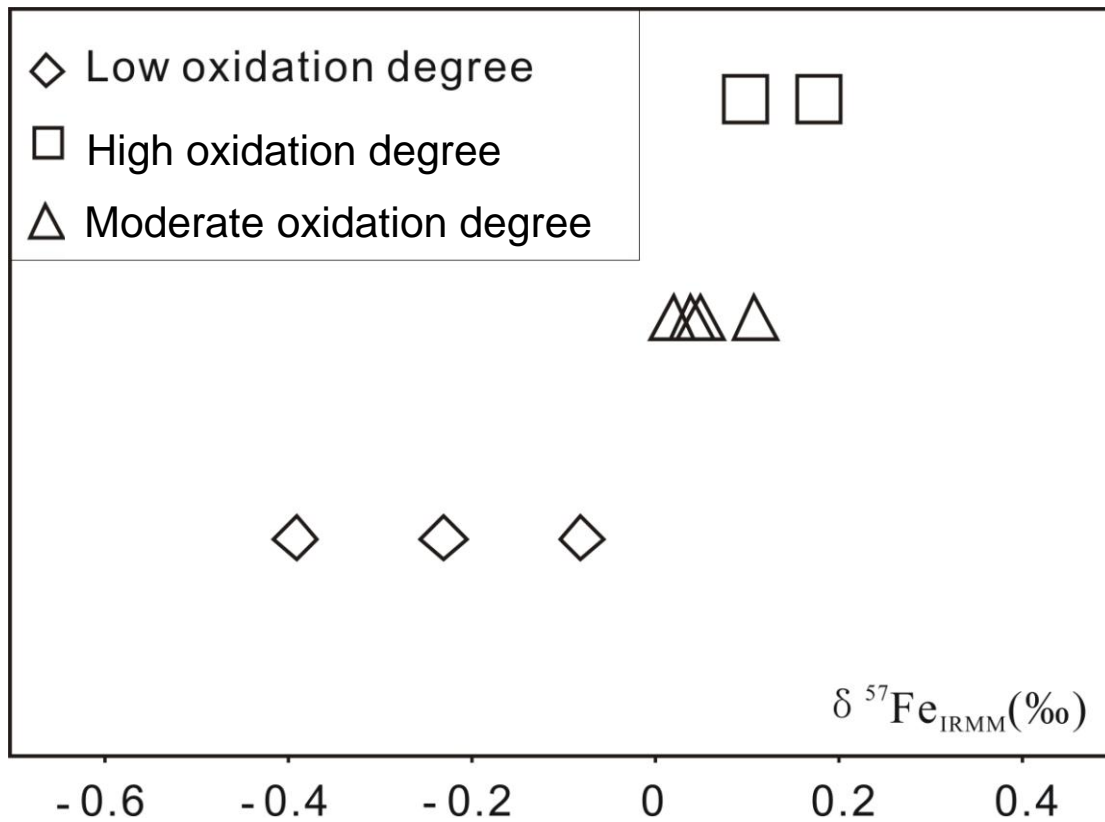


Figure 7 Fe isotopes of various oxidation degrees of the oxidized ores from Gaosong deposit.

This tendency of heavy iron isotopes getting enrichment as oxidation degree increase may be the result of two mechanisms: 1) interaction with fluids enriched in heavy iron isotopes during supergene alteration; 2) Fe-isotope fractionation during oxidation in the supergene environment.

For the Gaosong deposit, later fluids involved in the weathering process are

meteoric/ground water. However, previous iron isotope measurements of meteoric water and groundwater showed that the $\delta^{57}\text{Fe}$ values of these reservoirs are at or below zero (e.g. [Anbar et al., 2007](#); [Beard et al., 2003](#)). Moreover, it is a real challenge for meteoric water and groundwater to provide enough Fe to influence the iron isotope compositions of primary ores, because of the low Fe concentrations in these fluids (ppb level) ([Chilton, 1992](#)). Another question arises as to whether heavy Fe isotope compositions can be acquired from leaching wall-rock, which is enriched in heavy isotopes thus influenced the isotopic composition of rainwater/groundwater. Previous measurements have been made on marine carbonate showed that majority of carbonates have $\delta^{57}\text{Fe}$ values ranging from -1.5‰ to 0.50‰, and an average value of -0.34‰ ([Matthews et al., 2004](#); [Johnson et al., 2003](#); [Frost et al., 2007](#)). Although wall-rock in the Gejiu deposit was not investigated, these data, to some extent, can roughly represent the Fe isotopic distribution of carbonate. Moreover, it has been documented experimentally that fractionation of Fe isotopes occurs during oxidative weathering of sulfide-rich rock, and the $\delta^{57}\text{Fe}$ of the leachate is consistently lighter than the Fe isotopic composition of the bulk rocks under the pH \approx 5 condition ([Fernandze et al., 2009](#)). Not to mention, the content of Fe (TFe%) in wall-rock is down to 0.01 to 0.11% in the Gejiu district ([Gai, 2007](#)). Thus, the heavy end member of Fe isotope compositions of ores with high degree of oxidation cannot be influenced by incorporation of meteoric water and groundwater, showing that Fe isotope incorporation from meteoric water and ground water even if it has leached the wall-rock during supergene weathering process cannot be the principal cause of the heavy iron isotopes enrichment in ores with high oxidation degree.

Consequently, for the samples in this study, it is concluded that significant Fe isotope fractionation occurred during supergene weathering process; moreover, the oxidized ore is enriched in heavy Fe isotopes relative to the original rocks, and the higher degree of oxidation, the heavier iron isotope compositions. Moreover, there should be a complementary 'light' Fe reservoir in the area, which must have been carried from the oxidized rocks by the surface waters to be deposited somewhere else, although we did not find it yet.

This observation is supported by previous theoretical and experimental studies. In

these studies, Fe isotopes fractionate during redox process, and Fe (III) phases enrich heavier Fe isotopes than Fe (II) phases, while Fe (II) phases enrich heavier Fe isotopes than Fe (0) phases, showing a heavy iron isotope enrichment in high valence phases (e.g. [Anbar et al., 2005](#); [Butler et al., 2005](#); [Johnson et al., 2002](#); [Welch et al., 2003](#); [Kavner et al., 2005](#); [Balci et al., 2006](#)). As shown in [Table 1](#), the content of Fe (III) minerals increase from primary ores to oxidized ores, and then to gossan ores, as the oxidation degree becomes progressively higher. It is worth noting that as the Fe (III) minerals incorporate heavy Fe isotopes during the redox process, the Fe isotope compositions of the ores with high oxidation degree are heavier than that of the ores with low oxidation degree ([Figs. 6, 7](#)), which is consistent with the above observations and hypothesis.

In summary, the interpretation that Fe isotope fractionation takes place during in the supergene environment potentially makes Fe isotopes a valuable tool for tracing supergene geochemical circulation and metal source of the oxidized ores.

5.2 Link between Fe isotopic compositions and mineralogy

It is obviously showed that the large range of $\delta^{57}\text{Fe}$ values exists in the primary ores even on whole rock scale. It must be some mechanism affected the Fe isotopic compositions of them, as these samples are unaffected by supergene processes and all almost have the same degree of oxidation.

We consider it a result of differences in mineralogy. It has been documented in both natural and experimental cases that Fe (II) sulfide will preferentially incorporated light Fe isotopes relative to the fluid (e.g. [Butler et al., 2005](#), [Wang et al., 2011](#)). Therefore, the later formed Fe-bearing sulfides are enriched in heavy iron isotopes relative to earlier formed ones as a result of Rayleigh fractionation. For primary sulfide ores, as described in [Cheng et al. \(2011c\)](#), the paragenetic sequence is skarn minerals→pyrrhotite→chalcopyrite→pyrite→galena→sphalerite, thus in the Gejiu ore district, an enrichment of heavy iron isotopes can be expected in these samples with more late sulfides, while the samples which have more early-stage sulfides are expected to be enriched in light iron isotopes. As described in [Table 1](#), samples (i.e. [c043](#), [c048](#), [c064](#), [c080](#)) mainly composed of pyrrhotite and chalcopyrite are enriched in light iron isotopes relative to those samples (i.e. [c055](#), [c067](#), [c071](#), [c085](#)) mainly composed of pyrite.

The primary ores and oxidized ores are both significantly different in mineralogy, whereas almost no difference in mineral association amongst these gossan samples. This is why such large range of Fe isotopic variations occurred in primary sulfide ores and oxidized ores, but small range of Fe isotopic variations existed in gossan samples.

5.3 Fe source tracing by Fe isotopes

The source of metallic materials is a fundamental issue in mineralization studies. Various geochemical methods have been used to tackle this problem, including both stable (C, O, S) and radiogenic (Sr, Nd, Pb) isotopes. Although these methods have proved being useful, they cannot provide constraints directly on the ore-forming metals because most of them are not the metallic elements. Alternatively, as a metallogenic element, Fe isotopes provide a possibility to directly trace the metal source (Wang et al., 2011).

A key issue as to whether Fe isotopes can be used to trace the metal source is the geochemical behavior of Fe isotopes during the process of fluid exsolution from magma. In the study of Xinqiao Cu-S-Fe-Au skarn-type deposit, Wang et al. (2011) discovered that $\delta^{57}\text{Fe}$ values skarn and the earliest Fe-bearing metal mineral phase magnetite are lower than the quartz-monzodiorite stock, suggesting for the first time that Fe isotopes fractionate during high temperature fluid exsolution, whereby Fe isotope composition of the exsolved fluid is about ca.0.3 to ca.1.2 ‰ lower than the magma. For the primary sulfide ores of the Gaosong deposit in this study, geological characteristics, sulfur isotopes compositions and fluid inclusion studies demonstrate that the primary sulfide ore is typical of skarn-type deposits of hydrothermal origin (Cheng et al., 2012a; 2012b; 2012c), providing a sound fundamental premise to address this problem on whole-rock scale.

As shown in Table 1, eight measured whole rocks of primary sulfide ores show Fe isotope composition in $\delta^{57}\text{Fe}$ values ranging from -0.49‰ to 0.15‰, with an average of -0.22 ‰. Whereas, the $\delta^{57}\text{Fe}$ values range of granitic rocks from other parts of the world ranging from 0.01‰ to 0.54‰ with an average of 0.24‰ (e.g. Hemann et al., 2008; Beard et al., 2003; Dauphas et al., 2004; Wang et al., 2011; Wang and Zhu, 2012). Based on these published data, a preliminary judgment is that relative to granite, primary sulfide

ores of Gaosong deposit are enriched in light iron isotopes (Fig. 6).

There are two possibilities for the light Fe isotope composition of primary sulfide ores, it either could inherit from light isotopes enriched ore-forming fluid or from country-rock, both of which have light Fe isotope compositions. For the Gaosong deposit, however, Fe content of the country-rock (Triassic carbonate of Gejiu Formation) is as low as 0.01 to 0.11% (Gai, 2007) whereas the Fe content of granite is ranging from 0.94 to 1.60% (Cheng and Mao, 2011), suggesting that contribution of Fe from country-rock is insignificant. Thus, it is highly possible that the light isotopes enrichment in primary sulfide ores may precipitated from light Fe isotopes enriched hydrothermal fluid. This is consistent with the suggestion of Wang et al. (2011) that Fe isotope fractionate during fluid exsolution from magma and exsolve a fluid enriched in light isotopes relative to magma. Another point need to emphasize here is for the skarn ores in Gejiu district, geological reservoirs which possibly acted as their Fe source only include granite and/or carbonate, as the country-rock (carbonate) has been excluded above, we support the idea that the Fe in the skarn-type ore deposit is predominantly sourced from the ore-related igneous rocks.

6 Summary and conclusion

Fe isotope variations in Gaosong deposit have been investigated and several first-order observations and conclusions can be made.

The range of iron isotope values in ores with different oxidation degrees from Gaosong deposit is different. Primary sulfide ores, representing the lowest oxidation degree, are enriched in lightest isotopes, while $\delta^{57}\text{Fe}$ values of oxidized ores and gossan ores becoming heavier progressively as their oxidation degree increased. Spatially, upward away from igneous rocks to ground, $\delta^{57}\text{Fe}$ values of ores become heavier and heavier progressively. The most reasonable interpretation for this tendency is that Fe-isotope fractionate during supergene weathering process, leading to enrichment of heavy Fe isotopes in the oxidized products.

The range of $\delta^{57}\text{Fe}$ values of primary ores and oxidized ores are larger than that of

gossan samples. Combined with the mineral association, this Fe isotope features suggest that Fe isotope compositions are affected by mineralogy, and it is the primary mechanism of the large Fe isotopic variations in the primary ores.

The $\delta^{57}\text{Fe}$ values of primary sulfide ores are lower than the data for reported igneous rocks, suggesting Fe isotope fractionation occurs during fluid exsolution, and fluid enriched in light isotopes relative to the parental magma, thus Fe in the skarn-type ore deposit is inferred to be sourced from igneous rocks.

On the whole, the systematic variations of Fe isotope composition reported in this study show that Fe isotope studies have potential to constrain metal sources, ore genesis and evolutionary of hydrothermal deposit. Furthermore, the recognitions that significant Fe isotope fractionation occurs during supergene weathering process and fluid exsolution process laid an important foundation in using Fe isotopes as a tracer for supergene geochemical cycling and hydrothermal mineralization studies.

References

- 308 Geological Party. 1984. Geology of tin deposit in Gejiu area. Metallurgical Industry Publishing House, Beijing, pp 50–90 (In Chinese)
- Anbar AD and Rouxel O. 2007. Metal Stable Isotopes in Paleoceanography. *Annu. Rev. Earth Planet. Sci.* 35:717-746
- Anbar AD, Jarzecki AA and Spiro TG. 2005. Theoretical investigation of iron isotope fractionation between $\text{Fe}(\text{H}_2\text{O})_6^{3+}$ and $\text{Fe}(\text{H}_2\text{O})_6^{3+}$: Implications for iron stable isotope geochemistry. *Geochimica et Cosmochimica Acta* 69: 825-837
- Balci N, Bullen TD, Witte-Lien K, Shanks WC, Motelica M and Mandernack L W. 2006. Iron isotope fractionation during microbially stimulated Fe(II) oxidation and Fe(III) precipitation. *Geochim Cosmochim Acta*, 70: 622-639
- Beard BL, Johnson CM, Skulan JL, Nealson KH, Cox L and Sun H. 2003. Application of Fe isotopes to tracing the geochemical and biological cycling of Fe. *Chem. Geol.* 195: 87-117
- Butler BI, Archer C, Vance D, Lldroyd A and Rickard D. 2005. Fe isotope fractionation on

- FeS formation in ambient aqueous solution. *Earth Planet. Sci. Lett.* 236: 430-442
- Cheng YB., Mao JW. Chang ZS. 2012a. The origin of the world class tin-polymetallic deposits in the Gejiu district, SW China: constraints from metal zonation characteristics and ^{40}Ar - ^{39}Ar geochronology. *Ore Geology Reviews*, in submission.
- Cheng YB, Mao JW. 2012b. Petrogenesis of the Gejiu igneous complex in the western Cathaysia block, South China, and its geodynamic implications. *Lithos*, in submission.
- Cheng YB. 2012c. Spatial-temporal evolution of the magmatism and mineralization in the Gejiu supergiant Sn polymetallic district and insights into several key problems. PhD thesis, China University of Geosciences (Beijing) 340p, in Chinese with English abstract.
- Chilton J. 1992. Groundwater. In: Chapman D (ed) *Water Quality Assessments - A Guide to Use of Biota, Sediments and Water in Environmental Monitoring - Second Edition*. 651pp
- Dauphas N, van Zuilen M, Wadhwa M, Davis AM, Marty B and Janney PE. 2004. Clues from Fe isotope variations on the origin of Early Archean BIFs from Greenland. *Science* 306: 2077-2080
- Fernandez A and Borrok DM. 2009. Fractionation of Cu, Fe, and Zn isotopes during the oxidative weathering of sulfide-rich rocks. *Chemical Geology*, 264: 1-12.
- Frost CD, von Blanckenburg F, Schoenberg R, Frost BR and Swapp SM. 2007. Preservation of Fe isotope heterogeneities during diagenesis and metamorphism of banded iron-formation, *Contrib. Mineral. Petrol.* 153: 211-235
- Gai CK. 2007. The geochemistry of wallrock medium metallogenesis of Gejiu Sn field. *Yunnan Geology* 26: 277-283.
- Graham S, Pearson S, Jackson S and Griffin W. 2004. Tracing Cu and Fe from source to porphyry: in situ determination of Cu and Fe isotope ratios in sulfides from the Grasberg Cu-Au deposit. *Chem. Geol.* 207: 147-169
- Heimann A, Beard BL and Johnson CM. 2008. The role of volatile exsolution and sub-solidus fluid/rock interactions in producing high $^{56}\text{Fe}/^{54}\text{Fe}$ ratios in siliceous igneous rocks. *Geochimica et Cosmochimica Acta*, 72: 4379-4396

- Johnson CM, Beard BL, Beukes NJ, Klein C and O'Leary JM. 2003. Ancient geochemical cycling in the earth as inferred from Fe isotope studies of banded iron formations from the Transvaal Craton. *Contrib. Mineral. Petrol.* 144: 523-547
- Johnson CM, Skulan JL, Beard BL, Sun H, Neelson KH and Braterman PS. 2002. Isotopic fractionation between Fe(III) and Fe(II) in aqueous solutions. *Earth Planet Sci Lett* 195: 141-153
- Johnson CM, Roden EE, Welch SA and Beard BL. 2005. Experimental constraints on Fe isotope fractionation during magnetite and Fe carbonate formation coupled to dissimilatory hydrous ferric oxide reduction. *Geochimica et Cosmochimica Acta* 69, 963-993.
- Kavner A, Bonet F, Shahar A, Simon J and Young E. 2005. The isotopic effects of electron transfer: An explanation for Fe isotope fractionation in nature. *Geochimica et Cosmochimica Acta* 69, 2971-2979.
- Li ZH, Zhu XK and Tang SH. 2008a. Characters of Fe isotopes and rare earth elements of banded iron formations from Anshan-Benxi area: implications for Fe source. *Acta Petrologica et Mineralogica*, 27: 285-290 (in Chinese with English abstract)
- Li ZH, Zhu XK, Tang SH and Li YH. 2008b. Fe isotope fractionation between magnetite and pyrite during green schist-lower amphibolites facies metamorphism. *Acta Petrologica et Mineralogica*, 27: 291-297 (in Chinese with English abstract)
- Markl G, Blanckenburg F and Wagner T. 2006. Iron isotope fractionation during hydrothermal ore deposition and alteration. *Geochim. Cosmochim. Acta*, 70: 3011-3030
- Matthews A, Morgans-Bell HS, Emmanuel S, Jenkyns HC, Erel Y and Halicz L. 2004. Controls on iron-isotope fractionation in organic-rich sediments (Kimmeridge Clay, Upper Jurassic, Southern England). *Geochim. Cosmochim. Acta*, 68:3107-3123.
- Qin DX, Li YS. 2008. Studies on the geology of the Gejiu Sn-Cu deposit. Science Press, Beijing, pp 1–180
- Rouxel O, Fouquet Y and Ludden JN. 2004. Surface processes at the Lucky Strike hydrothermal field, Mid-Atlantic Ridge: evidence from sulfur, selenium, and iron isotopes. *Geochim. Cosmochim. Acta* 68: 2295-2311

- Rouxel O, Shanks WC, Bach W and Edwards K. 2008. Integrated Fe and S isotope study of seafloor hydrothermal vents at East Pacific Rise 9–10 N. *Chem. Geol.*, 252: 214–227
- Sharma M, Polizzotto M and Anbar AD. 2001. Iron isotopes in hot springs along the Juan de Fuca Ridge. *Earth. Planet. Sci. Lett.*, 194: 39-51
- Wang Y and Zhu XK. 2012. Fe isotope systematics and its implications in ore deposit geology. *Acta Petrologica Sinica*, in press.
- Wang Y, Zhu XK, Mao JW, Li ZH and Cheng YB. 2011. Iron isotope fractionation during skarn-type metallogeny: A case study of Xinqiao Cu-S-Fe-Au deposit in the Middle–Lower Yangtze valley. *Ore Geology Reviews*, 43: 194-202
- Welch SA, Beard BL, Johnson CM and Braterman PS. 2003. Kinetic and equilibrium Fe isotope fractionation between aqueous Fe(II) and Fe(III). *Geochimica. Cosmochimica. Acta.*, 67: 4231-4250
- Whitehouse MJ and Fedo CM. 2007. Microscale heterogeneity of Fe isotopes in >3.71 Ga banded formation from the Isua Greenstone Belt, southwest Greenland. *Geology*, 35: 719-722
- Wiesli RA, Beard BL and Johnson CM. 2004. Experimental determination of Fe isotope fractionation between aqueous Fe(II), siderite, and green rust in abiotic system. *Chem. Geol.*, 221: 343-362
- Zhu XK, Guo YL, Williams RJP, O’Nions RK, Matthews A, Belshaw NS, Canters GW, Waal EC, Weser U, Burgess BK and Salvato B. 2002. Mass fractionation processes of transition metal isotopes. *Earth Planet Sci Lett.*, 200:47-62
- Zhu XK, Li ZH, Tang SH and Li YH. 2008. Fe isotope characteristics of early Precambrian pyrite deposits and their geological significance: examples from Shandong and Hebei Provinces. *Acta Petrologica et Mineralogica*, 27: 429-434 (in Chinese with English abstract)



Chapter 8

Correlated cathodoluminescent textures, trace element chemistry and geochronology of cassiterite (SnO₂)



Correlated cathodoluminescent textures, trace element chemistry and geochronology of cassiterite (SnO₂): Provenance studies on Sn mineralization in a world class tin district

1 Introduction

Magmatic-hydrothermal ore deposits are major resources of the world's Sn resources. Tin mineralization is commonly associated with highly evolved and relatively reduced granite bodies (Lehamnn, 1987, 1990; Hedenqueist and Lowenstern, 1994), although mineralization is accepted to be primarily related to hydrothermal processes (Heinrich, 1990, 1995). Cassiterite, ideally SnO₂, is the most important Sn ore mineral. Studies have shown that cassiterite can have a wide range of chemical composition, colour, crystal morphologies, and shape and distribution of inclusions (Wang, 1985; Murciego et al., 1987; Murciego et al., 1997), depending on the conditions/environments of formation. Generally, cassiterite has very high surface relief under the microscope, and pleochroic haloes have been observed (Maldener et al., 2001). Cassiterite has a tetragonal lattice structure similar to that of rutile, belonging to the p42/mnm space group, in which a cation is in six fold coordination with oxygen. It has long been known that cassiterite can accommodate a wide range of trace elements (Fig. 1), and the most abundant elements including Fe, Ti, W, Ta, Nb, Mn and Sc. Nevertheless, the controls on the chemical and physical characteristics of cassiterite are poorly understood (Clark et al., 1976; Schneider et al., 1978; Moore and Howie, 1979; Florov et al., 1980; Izoret et al., 1985; Giuliani, 1987; Murciego, 1990).

One example is the substitution mechanisms of tin in the cassiterite lattice by trace elements, which have been the subject of several studies (Stevenson and Taylor, 1979; Giuliani, 1987; Möller et al., 1988; Neiva, 1996; Murciego et al., 1997; and references therein). It is suggested that substitutions such as $2(\text{Ta, Nb})^{5+} + (\text{Fe, Mn})^{2+} \leftrightarrow 3\text{Sn}^{4+}$ and

$W^{6+}+2Fe^{3+}\leftrightarrow 3Sn^{4+}$ are important mechanisms for Ta, Nb, W, Fe and Mn in corporation in cassiterite (Möller et al., 1988), and partial substitution of Sn^{4+} by Fe^{3+} with the introduction of OH^- in the cassiterite structure may occur in hydrothermal and epithermal deposits (Möller et al., 1988; Tindle and Breaks, 1998; Pieczka et al., 2007). It has been revealed that high temperature cassiterite (e.g., occurs in pegmatite) substitution is dominated by $3Sn^{4+}\leftrightarrow (Fe, Mn)^{2+}+2(Nb, Ta)^{5+}$; medium and low temperature cassiterite and the light zones are dominated by the mechanisms of $2Sn^{4+}\leftrightarrow Fe^{3+} + (Nb, Ta)^{5+}$ and $Sn^{4+}+O^{2-}\leftrightarrow Fe^{3+}+OH^-$ (Černý et al., 1985; Murciego et al., 1997). Furthermore, $2(Nb, Ta)^{5+}+(Fe, Mn)^{2+}\leftrightarrow 3(Sn, Ti)^{4+}$ is probably the main mechanism responsible for the darker pleochroic zones (high in Nb, Ta, Mn and Fe) in cassiterite (Neiva, 1996). However, as shown in Figure 1, although these elements are the most abundant ones in cassiterite, as they are of different valence to Sn, they cannot simple substitute into the lattice, thus more complicated coupled substitutions are needed to maintain charge balance.

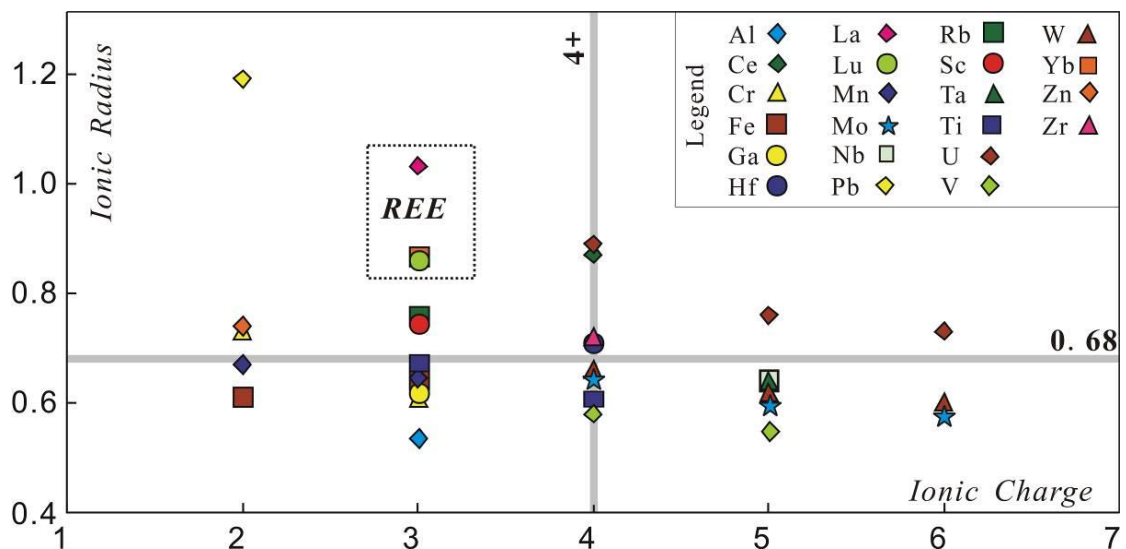


Figure 1 Ionic charge against ionic radius (Shannon, 1976) for elements investigated in this study.

Cathodoluminescence (CL) has been one of the most powerful analytical tools for revealing internal structure and zoning in minerals. Applications extend to analysis of the microstructure of rocks, structure and chemical composition of minerals (defects, zonal growth, internal textures, trace element contents and distribution), and aiding in understanding processes of mineral formation and alteration (e.g. Marshall, 1988; Pagel

et al., 2000; Götze et al., 2001; Rusk et al., 2002, 2006, 2008; Götze and Kempe, 2008). Laser ablation ICP-MS is a sensitive analytical method used for rapid multi-element determination at the trace and ultra-trace concentration level of solid sample materials. In recent years, the measurements of CL and LA-ICP-MS have been successfully combined to visualize micro-textures and their correlation with compositions in various minerals (e.g., quartz, zircon, apatite, monazite and plagioclase) (Rusk et al., 2002, 2008; Hammerli et al., 2013; Nelson et al., 2013). Such data are invaluable for unraveling complex geological histories recorded by mineral phases. However, few studies have applied these techniques to cassiterite, despite its cathodoluminescent properties (Farmer et al., 1991) and potential as a trace element host (Möller and Dulski, 1983; Möller et al., 1988; Plimer et al., 1991; Murciego et al., 1997; Serranti et al., 2002; Pieczka et al., 2007).

The Gejiu tin polymetallic ore district, known as the “tin capital” of China, represents the largest primary tin accumulation in the world with an endowment estimated at ~1000 million metric tonnes (Mt) of Sn-Cu-Pb-Zn ores (308 Geological Party, 1984; Zhuang et al., 1997). In this paper we examine cassiterite grains from six different ore styles from the Gejiu tin district using CL, LA-ICP-MS trace element analysis and laser ablation ICP-MS U-Pb dating. We report: (i) newly discovered micro-textures of cassiterite in cathodoluminescent images; (ii) concentration data for an extensive set of trace elements in cassiterite; (iii) possible correlation between micro-textures and trace elements in cassiterite; (iv) high precision LA-ICP-MS cassiterite U-Pb dating results. These results not only provide further insights into the ore genesis in the world-class Gejiu tin district, but also highlight the great potential of using cassiterite as a monitor of hydrothermal processes and for dating mineralization events.

2 Geological background

The Gejiu tin polymetallic ore district is one of the largest and oldest mining districts in the world. It has been mined since the Han dynasty (202 B.C. to 220 A.D.), intermittently for more than 2,000 years, and exploration in this district is still finding more ores to this day.

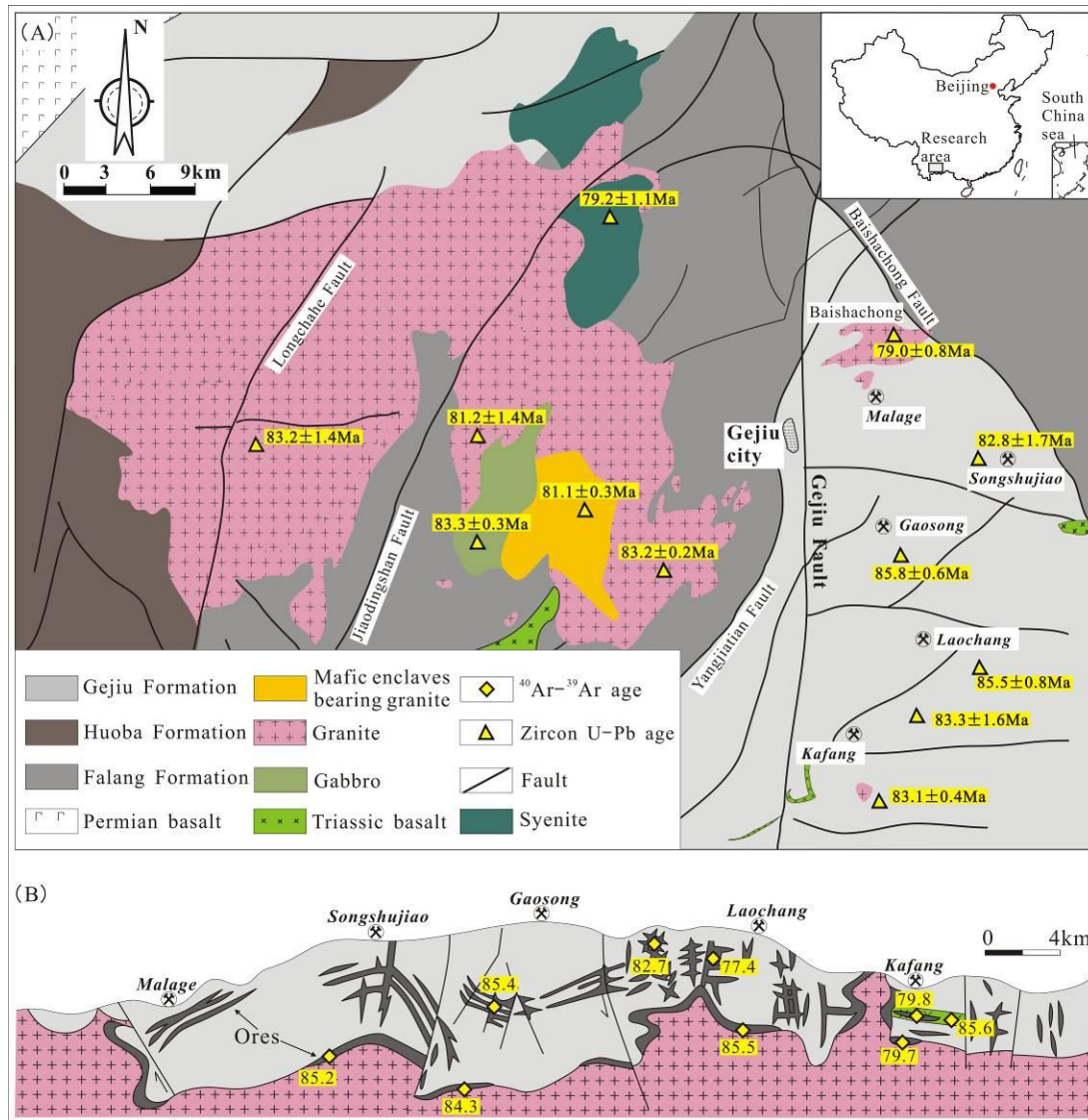


Figure 2 Geological map and of the Gejiu ore district and the cross section of the mining district (Modified from Mao et al., 2008)

The Gejiu District is located on the western margin of the South China Block, adjacent to the Yangtze Craton in the north and the Three Rivers Fold Belt in the west. It is ~1600 km² in area and most of the outcrops in the Gejiu area consist of Middle Triassic Gejiu Formation carbonate and Middle Triassic Falang Formation fine-grained clastic sediment and carbonate with interlayering mafic lavas (Fig. 2). Numerous faults are present in the district, including the NNE-trending Longchahe, Jiaodingshan and Yangjiatian faults, the NE-trending Baishachong fault and the N-trending Gejiu fault. The Gejiu batholith is composed of gabbro, mafic microgranular enclaves (MMEs), porphyritic biotite granite, equigranular biotite granite, syenites and mafic dykes (Fig. 2a) (Cheng and

Mao 2010, 2012). Mineralization in the Gejiu mining district, which comprises five Sn-Cu-Pb-Zn polymetallic deposits, from north to south namely Malage, Songshujiao, Gaosong, Laochang and Kafang, characterized by extensive hydrothermal alteration, multiple mineralization styles and clear metal zoning around granitic cupolas (Fig. 1a and 1b) (308 Geological Party, 1984; Peng, 1985; Zhao and Li, 1987; Luo, 1995; Zhuang et al., 1996; Mao et al., 2008; Cheng et al., 2012a). Recent studies have revealed that the Gejiu granite batholith formed between 85 Ma and 77 Ma (Fig. 2a) (Cheng and Mao, 2010), which is consistent with the Re-Os/⁴⁰Ar-³⁹Ar ages of various ores in this district (Fig. 2b) (Cheng et al., 2012a).

Tin mineralization in Gejiu area occurs as 6 ore styles, i.e., tin granite ores, greisen ores, skarn ores, carbonate-hosted vein-type ores, and oxidized and semi-oxidized stratiform ores (Fig. 2b). Cassiterite-bearing granite is not common in the ore district, and is only well developed in the interior of certain granite cupolas. Cassiterite in tin granite is always intergrown with fluorite. Greisen ores are also not common and mainly contain muscovite and quartz. Skarn-related ores are widely distributed in the whole ore district, and skarn type mineralization is economically the most important mineralization style. Vein-type ores have only been discovered in the Dadoushan area of Laochang deposit (Fig. 2a and 1b); ore veins contain skarn minerals and tourmaline. The oxidized stratiform style ores are products of the oxidation of primary sulfide ores, and mainly develops between carbonate layers distal to granite (Fig. 2a and 2b), which mainly contains hematite and limonite. Some incompletely oxidized ores in the oxidized stratiform orebodies contain hematite, limonite, pyrrhotite and minor pyrite (semi-oxidized ores), most of which are close to the surface and associated with small-scale faults (Fig. 2b).

3 Sampling strategy and analytical techniques

3.1 Sampling strategy

Cassiterite samples were collected from above six different mineralization styles, which represent six types of ore-forming environments in the Gejiu district. It is worth to note here that the spatial distances between sample locations and granitic pluton are

getting further from tin granite (Sample no. A0374-1) via greisen, skarn, semi-oxidized, oxidized to vein ore (Sample no. A0374-6), the purpose of which is to observe how cassiterite micro-texture, trace element composition and formation ages vary in different precipitation environments in one hydrothermal system. Brief background introduction about these samples has been outlined in Fig. 3 and Appendix 1.

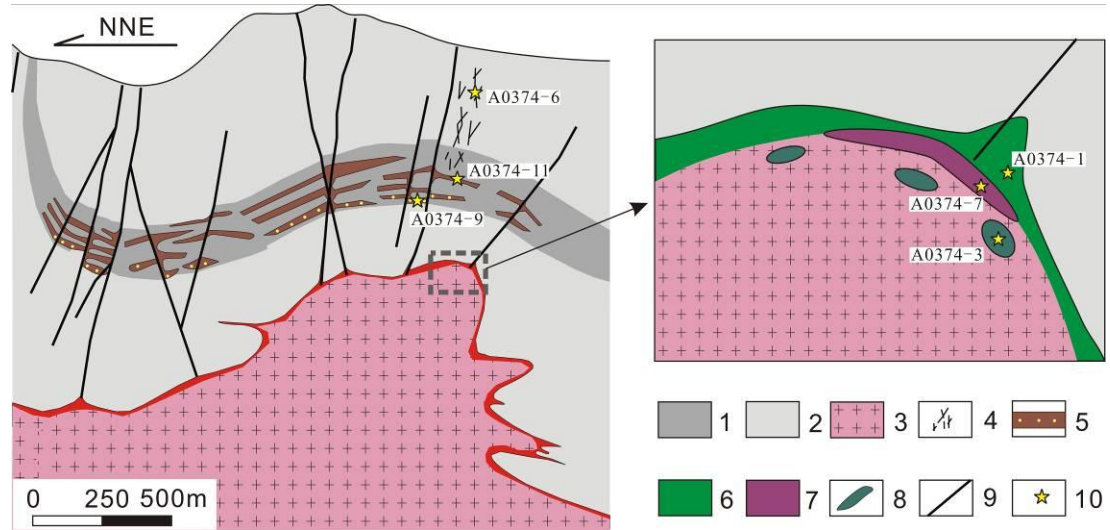


Figure 3 Representative cross section of the Gejiu ore district. 1-different carbonate interlayers; 2-pure carbonate; 3-granite; 4-vein ores; 5-stratiform oxidized ores with hosted semi-oxidized ores; 6-tin granite; 7-greisen ores; 8-skarn ores; 9-fault; 10-sample locations of this study

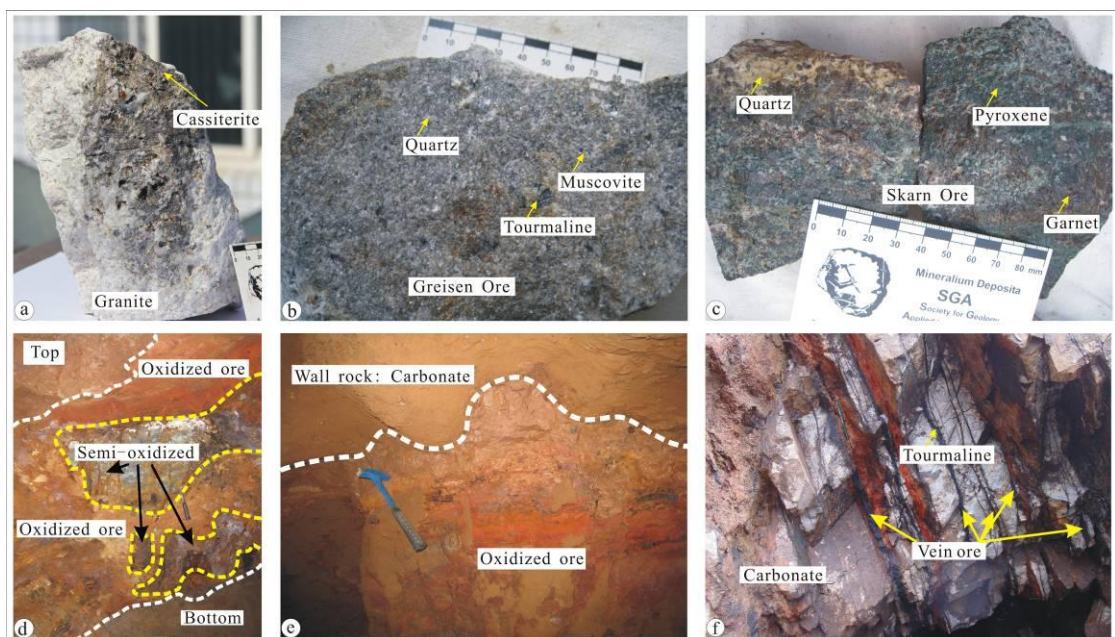


Figure 4 Six types of representative mineralization environments of the Gejiu ore district. a-tin granite; b-greisen ore; c-skarn ore; d-semioxidized ore; e-oxidized ore; f-vein ore.

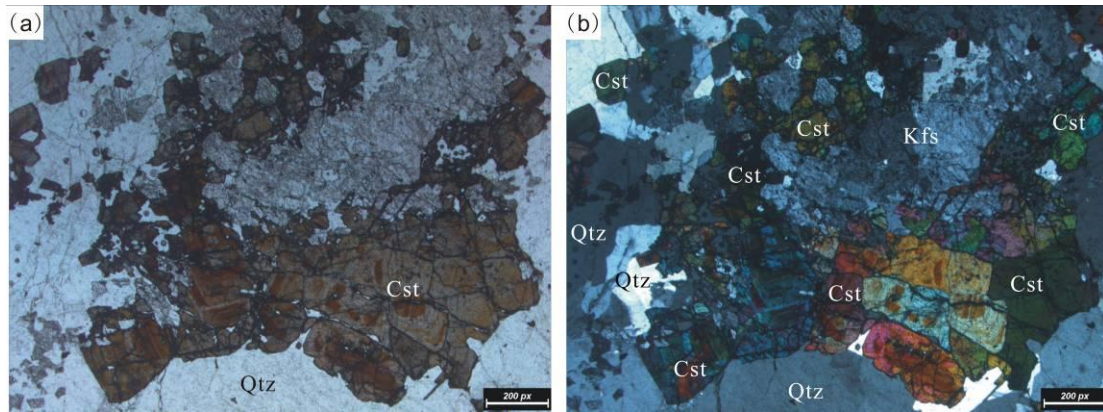


Figure 5 Microscope images under crossed polars (b) and plane polarized light (a) showing the intergrowth of K-feldspar, quartz and cassiterite from sample A0374-7.

Sample A0374-3 represent the cassiterite that occurs in tin granite, which is commonly located on the upper interior margin of ore-related granite cupolas (Fig. 3), representing the latest stage of highly evolved granite. Major minerals include K-feldspar and quartz, with various percentages of muscovite, fluorite, tourmaline and cassiterite (Figs. 4a and 5), mafic minerals, such as biotite and amphibole are rarely observed. Sample A0374-7 was collected from greisen ores, which is produced from the interaction of greisen-forming fluids with granite outside the contact of pluton (Fig. 3), mainly contains quartz and muscovite with minor tourmaline, fluorite and cassiterite (Fig. 4b). Sample A0374-1 was from skarn ores, which formed by the interaction of granitic-derived fluids with carbonate in the contact zone (Fig. 3), typically consist alteration minerals of garnet, pyroxene, tremolite, chlorite, epidote, tourmaline and calcite (Fig. 4c). Samples A0374-9 and A0374-11 were collected from the stratiform oxidized ores and semi-oxidized ores respectively (Fig. 3). Major minerals of oxidized ores include hematite, hydrohematite and minor limonite, hydrogoethite, plumbojarosite, minetisite, cassiterite, malachite and cerussite (Fig. 4e), while the semi-oxidized ore contains limonite, goethite, pyrite, arsenopyrite, galena, marmatite, chalcopyrite and cassiterite (Fig. 4d). Sample A0374-6 represents the cassiterite from vein ores, which is extensively developed in shallow

surface of the Dadoushan open pit (Fig. 3). The most common mineral is tourmaline, accompanied by skarn minerals (garnet, diopside, epidote, phlogopite) and beryl, and the main ore mineral is cassiterite, accompanied by minor chalcopyrite, pyrrhotite and pyrite, as well as scheelite (Fig. 4f).

3.2 Analytical methods

3.2.1 SEM-CL

Cassiterite SEM-CL images were obtained from polished ~4 mm thick resin mounts with a Jeol JSM5410LV instrument at the Advanced Analytical Centre in James Cook University, Australia. The Jeol JSM5410LV SEM with secondary electron imaging (SEI), backscatter electron imaging (BEI) and a Robinson cathodoluminescence detector (CL). Back-scattered electron (BSE) and CL images were taken immediately after each other under the same analytical conditions (acceleration voltage of 20 kV, untilted samples adjusted in height to the lower edge of the ellipsoidal CL mirror) using a Jeol Semafore digital image acquisition system. For the SEM-CL analyses, the samples were coated with a thin film of carbon to prevent charging during irradiation. This coating was removed for LA-ICP-MS analysis.

3.2.2 LA-ICP-MS

All analyses were done at Advanced Analytical Centre of James Cook University. A Coherent GeolasPro 193 nm ArF excimer laser ablation unit was connected to a Varian 820-MS Inductively Coupled Plasma Mass Spectrometer (ICP-MS) via a Tygon tubing, a 3-way mixing bulb was used between the ablation cell and the 820-MS for obtaining a smooth signal.

As there are no cassiterite standard available for U-Pb dating, GJ1 standard zircon was used to calibrate the instrument, the instrument was tuned such that element fractionation was reduced to a minimum, while keep the sensitivity obtained >5,000 cps/ppm ²³⁸U under the tuning condition of 5 Hz, 6 J/cm energy density at 44 μm laser beam sizes, and 0.8 l/min He carrier gas flow rate. Remaining fractionation and mass bias

was corrected by using standard bracketing techniques; every ten cassiterite sample measurements was bracketed by two measurements of GJ1 zircon (primary calibration standard) (Jackson et al., 2004), two Temora zircon and an additional closure measurement of GJ1 zircon (Black et al., 2003). For quantification of U and Th concentration in cassiterite samples, analysis of the NIST SRM 612 reference glass was conducted at the beginning, middle and end of every analytical session.

All data reduction was carried out by Glitter software (Van Achterbergh et al., 2001) first on-line in order to monitor progress of the dating work; final results were processed off-line after dating work finished. All time-resolved single isotope signals from standards and cassiterite samples were filtered for signal spikes or perturbations related to inclusions and fractures. Subsequently, the most stable and representative isotopic ratios were selected for further analysis taking into account possible mixing of different age domains and zoning. Drift in instrumental measurements was corrected within Glitter software following analysis of drift trends in the raw data using measured values for the GJ1 primary zircon standard. Secondary checks of Temora were used for verification of GJ1 following drift correction. Calculated isotopic ratios and mean raw CPS with background subtracted with respective 1σ errors were exported for further correction and data reduction.

Trace elements were analyzed by a Coherent 193 nm ArF Excimer laser ablation unit coupled to a Varian 820-MS Inductively Coupled Plasma Mass Spectrometer (ICP-MS), instrument set up and tuning is same as that for U-Pb dating. Laser beam size 60 μm , laser repetition rate 10 Hz, Energy density 6 J/cm^2 . NIST 612 glass standard was used as the calibration standard using the reference values of Spandler et al. (2011). Sn was used as the internal standard, assuming stoichiometric SnO_2 for quantification purpose, and data were processed off-line using the Glitter software.

4 Results

4.1 Micro-textures and crystal size variations

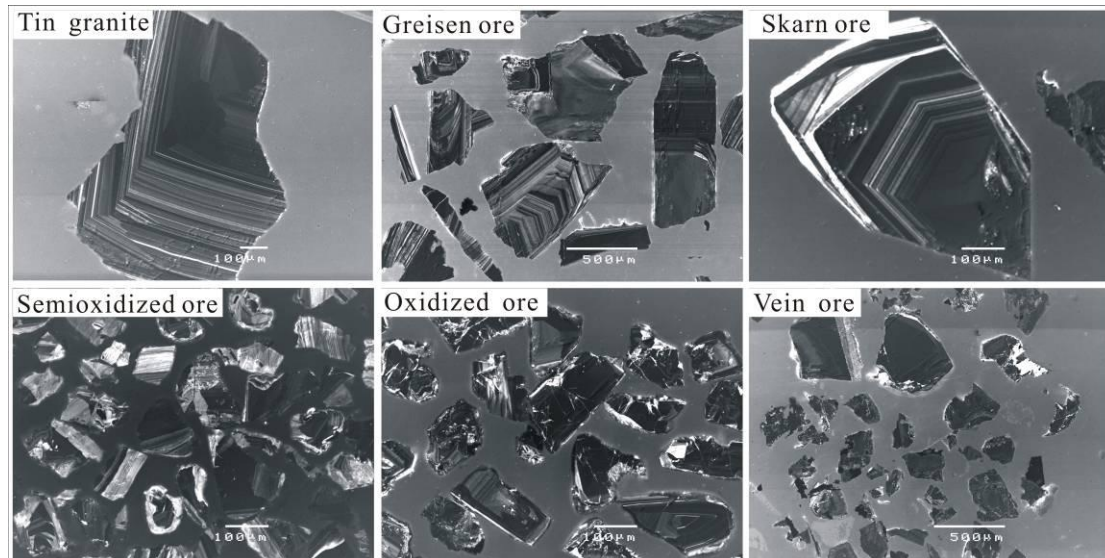


Figure 6 Selected cathodoluminescence (CL) images of the six types of cassiterite samples

The characteristics of cassiterite from different mineralization environments in Gejiu district with different micro-textural features have been revealed by SEM-CL in this study, which is characterized by well-defined growth zonings with variable luminescence intensities within different parts of grains (differential CL) (Fig. 6). Some cassiterite grains display indistinct, patchy, or mottled CL textures, whereas others have virtually homogeneous (non-differential) CL. Cassiterite crystals from all mineralization styles can be categorized into two groups based on their size, shape and CL texture differences. Firstly, cassiterites from tin granite, greisen and skarn ores share many similarities. They are generally large, about $400 \times 600 \mu\text{m}$ in size, and characterized by euhedral fine-scale oscillatory zoning (Fig. 6). In contrast, cassiterite from semi-oxidized ores, stratiform oxidized ores and veins are typically smaller (about $50 \times 200 \mu\text{m}$ in size), anhedral crystals with less regular zoning patterns. The micro-textures of the latter group are more complex than the former one (Fig. 6). For example, in the stratiform oxidized, semi-oxidized and vein samples, some cassiterite grains are completely bright while others are totally dark (weak or no CL), and some crystals display irregular variations between light and dark (strongly variable CL) (Fig. 6). As shown in Figure 3, the samples of the tin granite, greisen and skarn are close to the granite and the other 3 samples are

more distal. It appears that distance between samples and granites (the inferred source of hydrothermal fluids) may be one of the key factors controlling the cassiterite size and internal micro-texture variations, which may be used as an important tool for tin prospecting to be a fundamental exploration clue with potential economic significance.

4.2 Trace elements quantitative analysis by LA-ICP-MS

We analysed 25 elements simultaneously in 96 spots from the 6 cassiterite samples in this study as following: Al, Ca, Sc, Ti, V, Cr, Mn, Fe, Cu, Zn, Ga, Rb, Sr, Zr, Nb, Sb, La, Ce, Yb, Lu, Hf, Ta, W, Pb and U.

4.2.1 Cassiterite trace elements in different mineralization environments

The concentrations of most of the 25 analyzed elements are above limits of detections (LOD), but Ca in most of analysis spots were not detected in the Gejiu cassiterite samples because of their low contents. The most abundant trace elements in cassiterite from Gejiu district include Ti (3.25 to 5290 ppm), Fe (35 to 6560 ppm) and W (0.25 to 8460 ppm). The concentrations of Nb and Ta exhibit the largest variations amongst all the elements analyzed in this study, from ~0.01 ppm (spot 12 in greisen sample) to ~1800 ppm (spot 16 in vein sample) for Nb and from <LOD (spot 12 in greisen sample) to ~500 ppm (spot 3 in greisen sample) for Ta. Some other elements also vary over several orders of magnitude in concentration in a single sample (i.e., V, W and U). Al, Sc, V, Ga, Zr and Sb are commonly in lower concentrations ([Appendix 2](#)). As a whole, the spider patterns of the 6 samples are broadly similar, both in elements concentrations and positive/negative anomalies (not shown; [Appendix 2](#)). Except the large variation of Nb and Ta concentrations in all samples, some other mutual characteristics been observed. From tin granite, via greisen ore, skarn ore, semi-oxidized ore, oxidized ore to vein ore, the negative degrees of V, Cu, Zn, La and Ga are increasing, nevertheless, the Cr variations exhibit opposite tendency, as their positive anomalies are increasing in the above six samples.

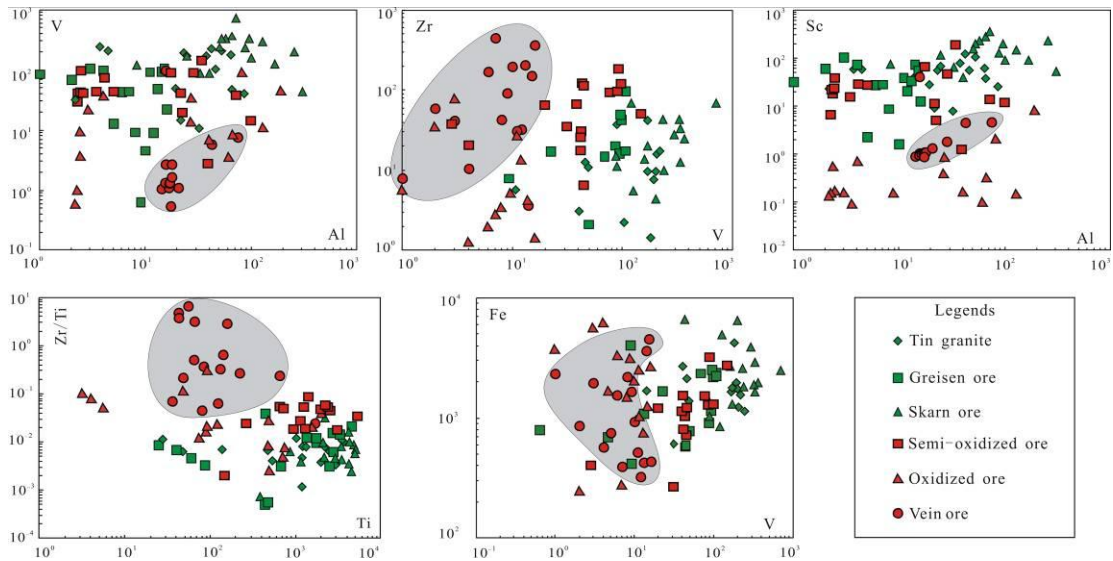


Figure 7 X-Y plots showing the variations of some trace elements hosted by cassiterite from Gejiu ore district. The shadowed areas mostly display the vein ore sample is distinguished from other samples.

However, geochemically, although the 6 samples share high similarities, some differences in some element concentrations or ratios exist. For example, all samples from the 6 mineralization types do not define a clear correlation relationship in most elements and/or ratios (Fig. 7, other plots are not shown), but cassiterite from skarn, greisen and tin granite samples generally contain more Ti and V than the vein, stratiform oxidized and semi-oxidized samples. Another prominent characteristic is present in almost in all the shown plots, the vein samples (sometimes also include the oxidized ore sample) always exhibit clear difference with tin granite, greisen ore and skarn ore samples (sometimes include semi-oxidized ore sample) (Fig. 7). No other correlations amongst trace elements are obviously exhibited. In general, the samples from tin granite, greisen and skarn ores contain higher Al, Ti and HREE contents, but lower Mn, Ce and Pb than the stratiform semi-oxidized, stratiform oxidized and vein samples (Appendix 2). Another distinct difference is between the total amounts of element concentration of tin granite and vein ore samples, some element highly enriched in tin granite sample, while the highest concentrations of some other elements occur in vein ore sample, which can be clearly observed in Appendix 2.

4.2.2 Trace element distribution in single cassiterite crystal

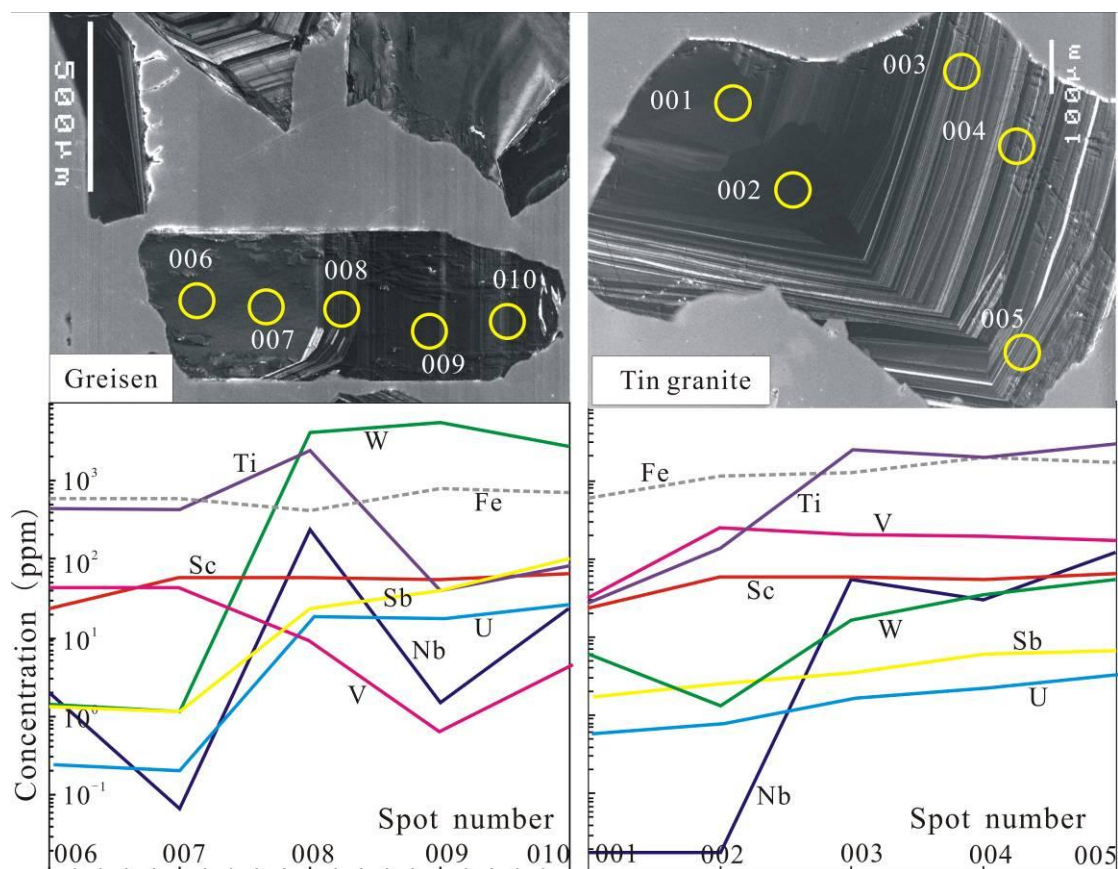


Figure 8 Trace elements distribution in single cassiterite crystal, examples from greisen and tin granite sample. The order of the analysis spots is from core to rim of the cassiterite crystal.

We measured the trace element profiles across several large cassiterite crystals from tin granite and greisen samples. Results are reported in [Appendix 2](#). In the tin granite cassiterite samples, the concentrations of Nb, U, Sb, W, Sc, V, Ti and Fe increase from core to rim of the crystal, as CL intensity increases. In the greisen, Sc, W, Sb and U show a roughly similar trend from core to rim, but the other elements do not follow this trend ([Fig. 8](#)). Another ambiguous observation is Ti is lower in darker areas relative to the bright zones in both grains. Other elements are not shown in the diagram for comparison as they neither exhibit a consistent increase/decrease tendency in certain one grain, nor display similar variations in both samples. Thus for the trace element distribution in a single cassiterite grain, the basic observation is that there is not a consistent trace element

concentration variation tendency from core to rim in a single cassiterite grain, and not an obvious uniform correlation between element concentrations and CL intensities revealed by laser ablation ICP-MS analysis in this study.

4.3 LA-ICP-MS U-Pb dating

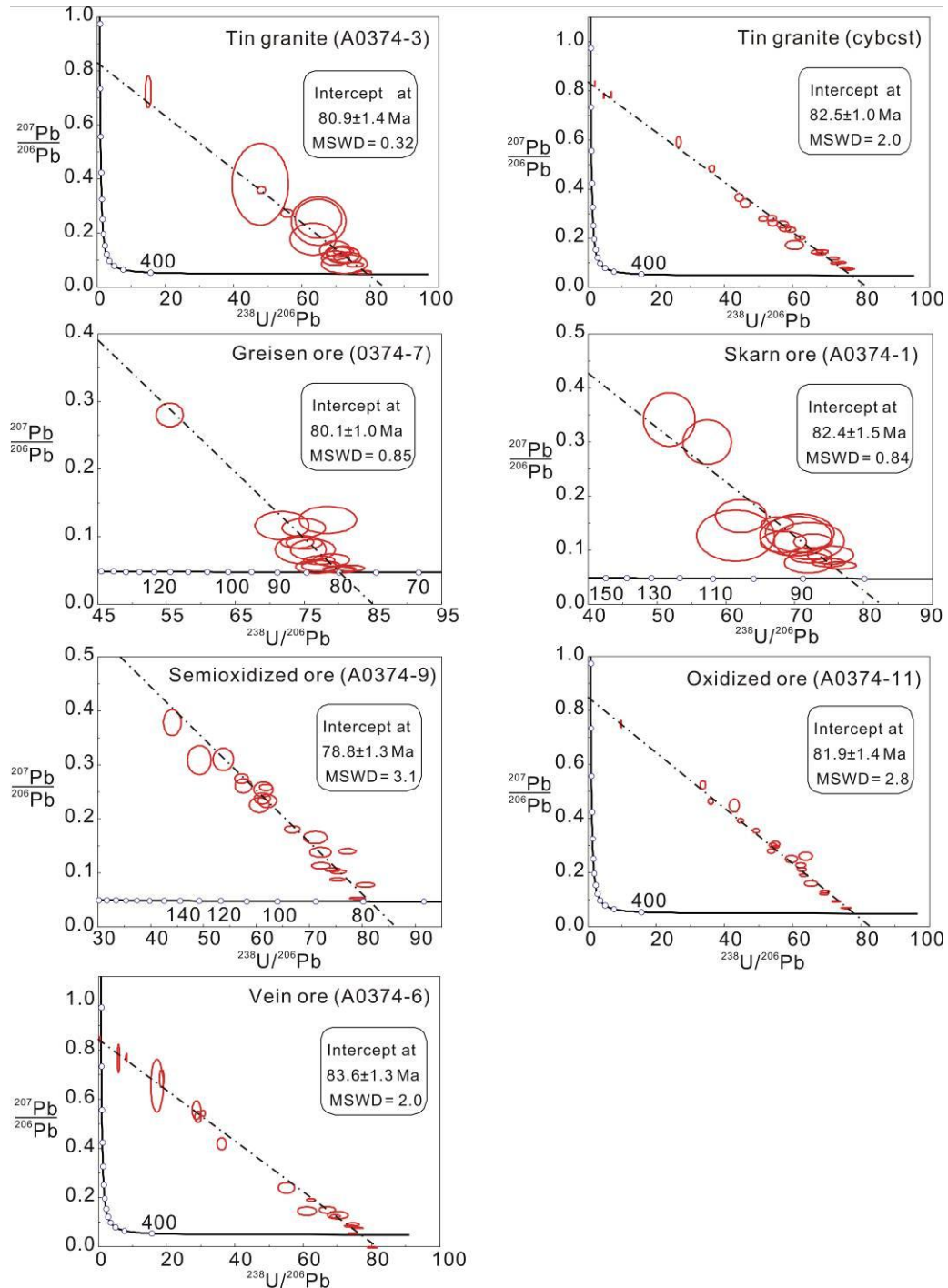


Figure 9 LA-ICP-MS cassiterite U-Pb age data for the seven samples from Gejiu ore district

Seven cassiterite samples (A0374-1, A0374-3, A0374-6, A0374-7, A0374-9, A0374-11, cybcst) were collected from the Gejiu tin district, which are the same ones used for SEM-CL imaging and laser ablation ICP-MS trace element analysis were picked up for LA-ICP-MS U-Pb dating. The age of each sample is given by the error-weighted mean of the common Pb-corrected $^{206}\text{Pb}/^{238}\text{U}$ ages of the selected grains at 95% confidence level. U-Pb data sets for all samples are given in [Appendix 3](#).

Seventeen analysis spots were performed by LA-ICP-MS on sample A0374-3 to examine the U-Pb age of cassiterite from tin granite ([Fig. 9](#)). These analyses have variable medium to high concentrations of U (57210–879407 ppm) and Th (7–482 ppm). They have indistinguishable $^{206}\text{Pb}/^{238}\text{U}$ ratios within analytical uncertainty, corresponding to a single age population with a weighted mean $^{206}\text{Pb}/^{238}\text{U}$ age of 80.9 ± 1.4 Ma (MSWD=0.32) ([Fig. 9](#)). In order to further confirm this data, we analyzed another cassiterite sample (cybcst) also collected from tin granite. LA-ICP-MS results from 24 grains yielded a weighted mean age of 82.5 ± 1.0 Ma (1σ) (MSWD = 2.0; [Fig. 9](#)). This age is consistent with the former data within errors and they are interpreted as the best estimate of the crystallization age of the cassiterite from tin granite.

Fifteen spots of cassiterite sample from greisen ore were analyzed. They show variable Th (0–821 ppm) and U (104625–1085296 ppm). Th/U ratios are between 0 and 0.0021. $^{206}\text{Pb}/^{238}\text{U}$ ages determined are indistinguishable within analytical errors, with a mean $^{206}\text{Pb}/^{238}\text{U}$ age of 80.1 ± 1.0 Ma ([Fig. 9](#)). This is interpreted as the age of sample A0374-7.

Fifteen analyses of cassiterite sample from skarn ore (A0374-1) yield a $^{206}\text{Pb}/^{238}\text{U}$ single age population of 84 to 123 Ma, with a weighted mean age of 82.4 ± 1.5 Ma, with MSWD=0.84 ([Fig. 9](#)). Their Th contents range from 7 to 482 ppm and U (57210–879407 ppm). Th/U ratios are between 0 and 0.0072.

Twenty spots of cassiterite sample from semioxidized ore were performed. They show variable Th (0–45811 ppm) and U (48147–927129 ppm). Th/U ratios are between 0 and 0.0561. $^{206}\text{Pb}/^{238}\text{U}$ ages determined are indistinguishable within analytical errors, with a mean $^{206}\text{Pb}/^{238}\text{U}$ age of 78.8 ± 1.3 Ma ([Fig. 9](#)). This is interpreted as the age of sample

A0374-9.

Twenty analyses of cassiterite from oxidized ore (A0374-11) give a weighted mean age of 81.9 ± 1.4 Ma, with MSWD=2.8 (Fig. 9). The Th content is from 0 to 8005 ppm and U (73156–865933 ppm). Th/U ratios are between 0 and 0.0534.

Twenty spots of cassiterite sample from vein ore were performed by LA-ICP-MS. They show variable Th (0–1339 ppm) and U (1056–990805 ppm). Th/U ratios are between 0 and 0.0107. $^{206}\text{Pb}/^{238}\text{U}$ ages determined are indistinguishable within analytical errors, with a mean $^{206}\text{Pb}/^{238}\text{U}$ age of 83.6 ± 1.3 Ma (Fig. 9). This is interpreted as the age of sample A0374-6.

5 Discussion

5.1 Relations between micro-textures and trace elements

It has been revealed that cassiterite is a mineral with a wide range of colour, from black to colourless through intermediate zones with yellow, orange, browns and red, and presents darker pleochroic zones and lighter translucent colorless zones under microscope, and these pleochroic zones have been considered to have correlation relationship with the EMP analyzed trace element (Clark et al., 1976; Taylor, 1979; Moore and Howie, 1979; Giuliani, 1987; Murciego et al., 1987; Neiva, 1996, 2008). The lighter zones are considered to be homogeneous and consist of nearly pure SnO_2 , whereas the darker pleochroic zones have higher contents of Nb, Ta, Ti and Fe (Hall and Ribbe, 1971; Neiva, 1996, 2008; Murciego et al., 1997; Costi et al., 2000). Nevertheless, other studies reported that almost no significant chemical distinction was found between different pleochroic zones within cassiterite, and also discovered no obvious chemical distinction in distinct paragenetic stages (Schneider et al., 1978; Moore and Howie, 1979; Neiva, 1996).

There are several factors which could potentially activate luminescence in minerals, including geochemical compositions (Farmer et al., 1991; Müller et al., 2000, 2002; Rusk et al., 2006, 2008), vacancy-induced non-stoichiometry (Bhalla and White, 1971), radiation damage (Mendelsohn et al., 1978) and dislocations (Grant and White, 1978). The various textures in cassiterite from Cornwall, England been interpreted by these two

factors: (i) variations in the composition of the ore forming fluid; (ii) variations in the tectono-hydrothermal conditions, i.e. pressure and/or temperature, governing cassiterite deposition (Farmer et al., 1991). It has been revealed that Ti and W impurities are the chief activators responsible for cathodoluminescence in hydrothermal cassiterite (Hall and Ribbe, 1971; Farmer et al., 1991), and Al and V were also suggested as CL activators in cassiterite (Rémond, 1973), whereas Fe is considered to quench luminescence and cause a lowering of spectra intensity in cassiterite (Hall and Ribbe, 1971; Rémond, 1973; Farmer et al., 1991).

The cassiterite in this study exhibits black, yellow, blue, red and green colors under microscope (Fig. 5). There are also clear pleochroic zones (Fig. 5) and CL zonings (Fig. 6) in the cassiterite samples from the Gejiu tin district. However, our high precise LA-ICP-MS trace element data shows there is not an evident correlation between the geochemistry and the CL textures. There are at least two possibilities to account for this: (i) the laser beam size used in this study is 44 μm , which is much larger than the width of the fine oscillatory zonings in most cassiterite grains, thus cannot tell the geochemical difference in each individual CL zonings; (ii) except the chemical compositional difference, some other factors, such as changing of fluid pressure, temperature, mixing of fluids, element diffusion rates and late-stage fluid alteration also the possible contributors for developing oscillatory zoning in cassiterite. The origin and significance of these CL micro-texture variations and their possible correlation with trace element need to be further studied.

5.2 Trace elements variation and substitution in cassiterite

Cassiterite trace elements geochemistry have been studied by EMPA for many years, and trace element Nb, Ta, Zr, Hf, Fe, Mn, Ti, Cu, Zn, As, Pb, Sb, W, Th, U and REE were reported as component of cassiterite by many studies (Möller and Dulski, 1983; Möller et al., 1988; Plimer et al., 1991; Murciego et al., 1997; Serranti et al., 2002; Pieczka et al., 2007). It is believed that Nb-Ta oxide minerals (rutile, columbite-tantalite and/or ixiolite) are the major mineral inclusions of cassiterite (Möller et al., 1988; Neiva, 1996), and Cu, Zn, As, Pb and Sb likely reflected the presence of subsurface inclusions of sulfides

(Serranti et al., 2002). In this study, according to crystallochemical similarities (charge, radius, coordination) compared with Sn^{4+} , as shown in Figure 1, the possible substituting cations mainly include the following ones: Ga^{3+} (0.62), V^{3+} (0.64), Cr^{3+} (0.615), Sc^{3+} (0.745), Sb^{3+} (0.74), W^{4+} (0.66), Zr^{4+} (0.72), Hf^{4+} (0.71), Ti^{4+} (0.605), W^{5+} (0.62), Nb^{5+} (0.64) and Ta^{5+} (0.64) (in brackets: effective ionic radii after Shannon, 1976).

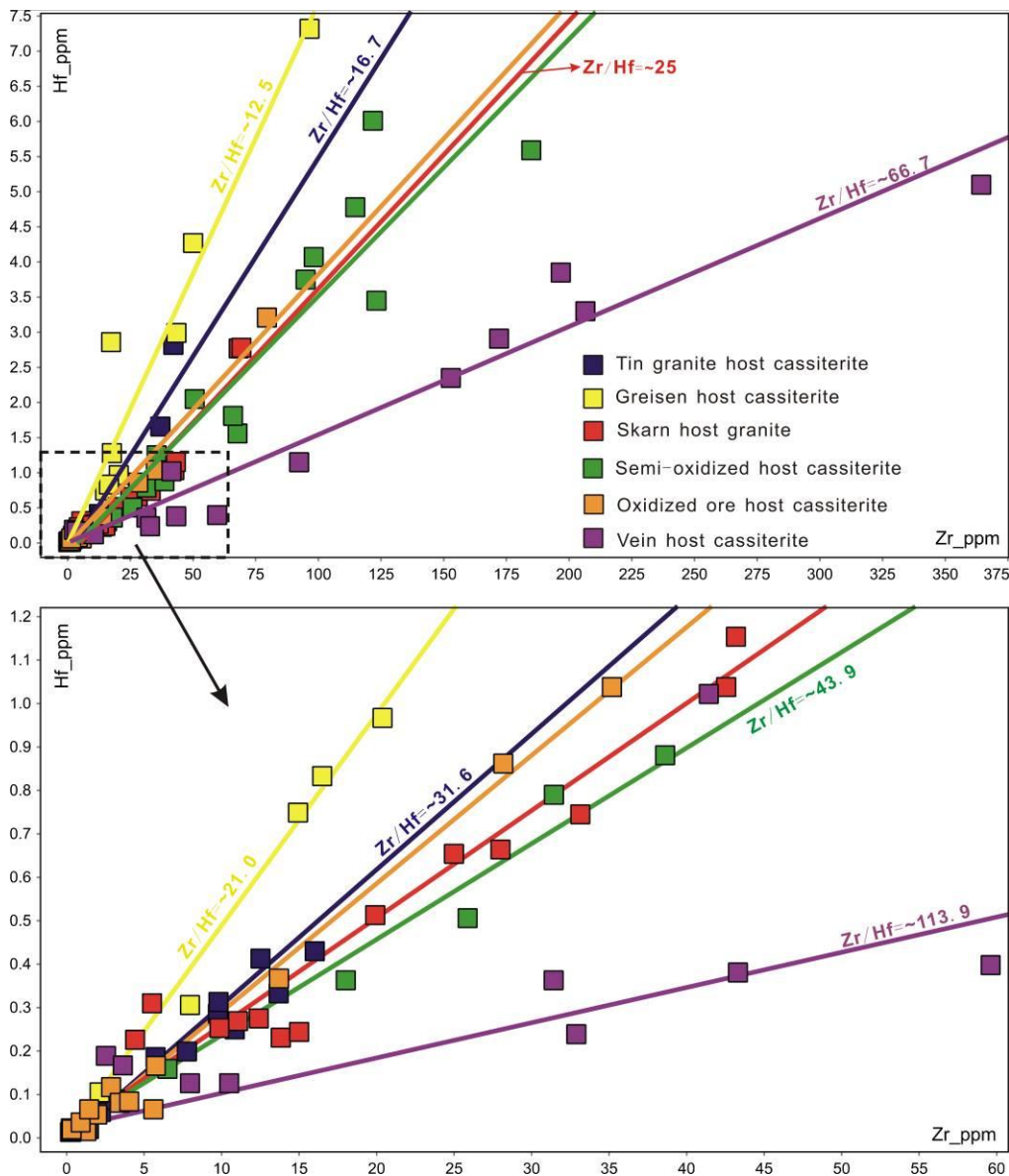


Figure 10 Systematic variations of Zr/Hf ratios of the samples in this study

For the 6 cassiterite samples from Gejiu tin district, although they exhibit high similarities, however, when take a closer observation, there are some differences in each sample compared to other 5 ones. For example, the greisen host cassiterite has the

highest Ta and Mn concentrations (spot 12); the skarn host cassiterite contains highest Sc, Cr and V content (spot 10); the oxidized ore cassiterite sample have the highest Cu, Pb, Zn concentrations (spot 4) and highest La, Ce and Sr concentrations (likely caused by cassiterite host inclusion contamination) (spot 5); and for the vein cassiterite sample, except the spot 16 have the highest Nb and Zr concentrations, most analyzed spots have relatively higher La, Ce, Sr contents and lower W and U contents ([Appendix 2](#), plots not shown) than the other 5 samples. It is worth to note that almost all above listed peak values of different elements always distribute in the same analysis spot, rather than scattered in different spots, a reasonable speculation for this is some mineral/fluid inclusions hosted in the cassiterite were ablated thus produced these anomalies, for example, the high Cu, Pb, and Zn in spot 4 in oxidized ore cassiterite sample is considered to represent sulfide mineral.

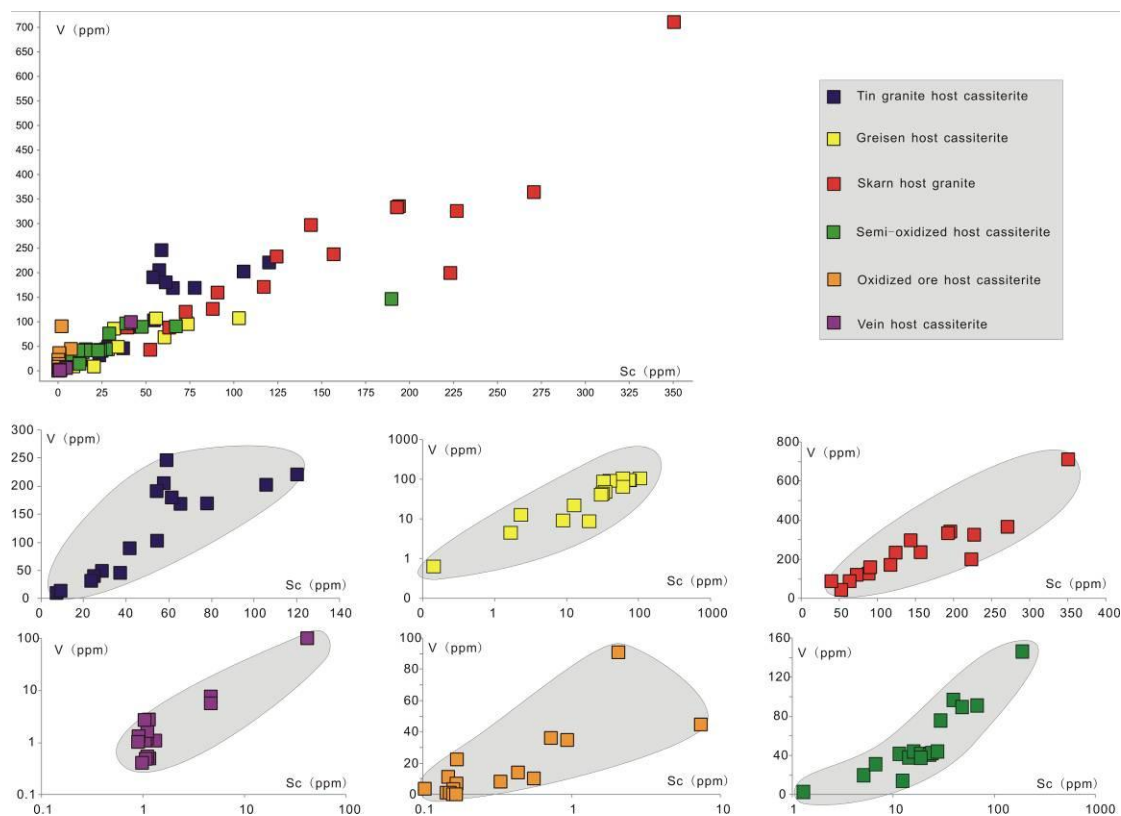


Figure 11 Positive correlations between Sc and V exhibit in all the six types of samples.

Zr and Hf are nearly identical geochemically, and therefore it maintains a relatively constant ratio in most geological systems (near chondritic Zr/Hf ratios: ~35-40) ([Ahrens](#)

and Erlank, 1969; Hoskin and Schaltegger, 2003; Claiborne et al., 2006). However, there are still a few cases show deviation of this ratio from chondritic values, but the reasons still in controversial, which been attributed either to metasomatism (e.g., Dupuy et al., 1992; Rudnick et al., 1993; Bau, 1996), to crystal fractionation involving accessory phases (e.g., Wolff, 1984; Linnen, 1998), to fluid fractionation (e.g., Dostal and Chatterjee, 2000), or to the preferential mobility of Zr by fluorine and boron in hydrothermal environments (e.g., Rubin et al., 1993; Jiang et al., 2005). Zr/Hf ratios of the 6 cassiterite from the Gejiu district exhibit gradual variation from greisens host cassiterite with Zr/Hf ratio about 12.5, to tin granite host cassiterite is ~16.7, to skarn/semi-oxidized/oxidized ore host cassiterite is ~25, to vein ore host cassiterite is ~66.7 (Fig. 10). According to geological observation, tourmaline is the most abundant mineral in vein ores, and fluorite also widely developed in this ore (Cheng et al., 2012b), of which enriched in boron and fluorine, respectively. It is suggested that fluorine may play a fundamental role in the mobility of Zr (Rubin et al., 1993; Jiang et al., 2005), and the mobility of Zr also has a close association with the enhanced activity of boron in a hydrothermal fluids (Jiang et al., 2005). Both element can render Zr more mobile in hydrothermal fluid, thus provide a Zr preference environment. This may interpret the high Zr/Hf ratio in vein host cassiterite than other samples. However, this is pretty speculative, more works needed in the future to make this clear.

The geochemical behavior of V and Sc in hydrothermal fluid is poorly understood currently, not to mention their geochemistry in cassiterite, and V in cassiterite seldom been reported previously. Only one related reported example is the Zheltorechenskoe U-Sc deposit in Ukraine, the ores from which deposit contain high V (Tarkhanov et al., 1991). In this study, an evident correlation between V and Sc been discovered in the cassiterite samples from Gejiu district, which exhibit a positive linear relationship both in individual sample or when plot all the 6 samples together (Fig. 11). Under geological conditions Sc only has one valence state (3+), while V has four possible valence states (2+, 3+, 4+ and 5+). The positive linear characteristics in cassiterite leads to speculation that the valence of V may occurs as 5+, then next substitution would be easily happen: $\text{Sc}^{3+} + \text{V}^{5+} = 2\text{Sn}^{4+}$, which can provide an interpretation for the correlation between V and Sc in this study. As mentioned above, many diadochic substitutions in cassiterite have

been recorded, and following Goldschmidt's (1937) rules which assume a simple ionic structure, elements with ionic radii within +12% of the Sn^{4+} radius (ionic radius: 0.68, Shannon, 1976) could substitute diadochically. Fe and W are the most abundant elements in Gejiu cassiterite samples, which must be the dominant roles influencing their charge balance state. Considering their high concentrations, if they are in charge balance, the ratio of total 3+ elements and 5+ elements would be near 1:1; otherwise some other materials were introduced into crystal lattice. This hypothesis been testified by the plots Figure 12, which shows most of the data scattered deviate from the 1:1 line, indicating Fe^{3+} and W^{5+} lose coupling relationship during elements substitution and crystal formation, and further suggesting one 1+ element, most probably H^+ , may be incorporated to keep their charge balance (Fig. 12).

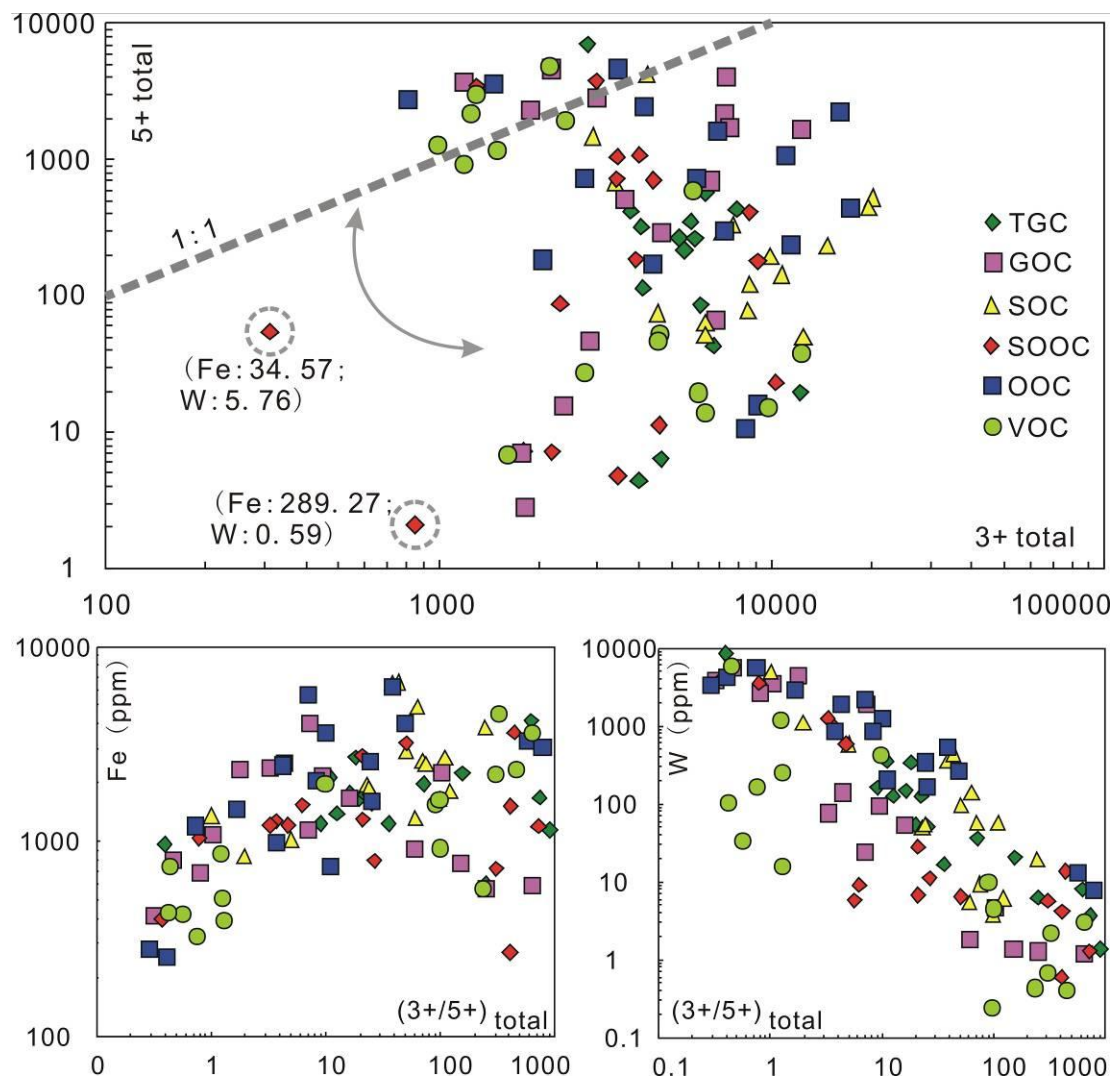


Figure 12 3+ and 5+ charge balance calculation diagrams of cassiterite from the Gejiu ore

district. The above plot showing the variations of total 3+ charge elements versus total 5+ charge elements, and in order to show the relationship more clear, all data in this plot been magnified 10000 times. The below two plots showing the concentrations of Fe and W versus the ratio of (total 3+ elements)/(total 5+ elements), respectively. Significance of these plots have been interpreted in the text. TGC-tin granite host cassiterite; GOC-greisen ore host cassiterite; SOC-skarn ore host cassiterite; SOOC-semioxidized ore host cassiterite; OOC-oxidized ore host cassiterite; VOC- vein ore host cassiterite.

5.3 Cassiterite U-Pb dating in Gejiu district and significance

Precise age determination of mineral deposits is vital for the proper understanding of the ore genesis. Cassiterite is one of the most stable minerals and commonly present in hydrothermal environments. Researchers have proved that cassiterite can be directly dated using the LA-ICPMS technique in addition to TIMS or ion microprobe (Liu et al., 2007; Yuan et al., 2008, 2011; Blevin and Norman, 2010; Bi et al., 2011). In this study, the LA-ICP-MS ^{206}Pb - ^{238}U ages from 78.8 ± 1.3 Ma to 83.6 ± 1.3 Ma for the 6 cassiterite samples from Gejiu district are in the expected range defined by other dating methods in this area, including the 13 ^{40}Ar - ^{39}Ar ages from 77.4 ± 0.6 Ma to 95.3 ± 0.7 Ma on hydrothermal mica (Cheng et al., 2012a), 2 Re-Os ages from 83.4 ± 2.1 Ma to 84.2 ± 7.3 Ma on molybdenite (Cheng et al., 2012c), and the 15 LA-ICP-MS/SHRIMP U-Pb ages from 77.4 ± 2.5 Ma to 85.8 ± 0.6 Ma on zircon from the igneous rocks in the Gejiu district (Cheng and Mao, 2010, 2012). The new ^{206}Pb - ^{238}U ages of individual cassiterite grains, which are consistent with above dating data by other methods from the Gejiu ore district, strongly suggest that the cassiterite U-Pb ages obtained in this study are reliable and demonstrate that LA-ICP-MS U-Pb dating of cassiterite has good potential for age determination of Sn deposits. These LA-ICP-MS cassiterite U-Pb ages are interpreted to represent the authentic age of tin mineralization in the Gejiu district; therefore, the absolute timing of tin mineralization in Gejiu ore district is 78–84 Ma.

Tin polymetallic ores in the Gejiu district have long been considered as typical hydrothermal origin and genetically related to Cretaceous granites (e.g., 308 Geological

Party, 1984; Peng, 1985; Zhao and Li, 1987; Luo, 1995; Zhuang et al., 1996; Mao et al., 2008; Cheng, 2012d). However, based on different dating results, include mica ^{40}Ar - ^{39}Ar ages ranging from 83.2 ± 2.1 to 205.1 ± 4.4 Ma (Qin et al., 2006) and cassiterite K-Ar ages from 43.5 ± 0.9 Ma to 186.0 ± 3.7 Ma (Li et al., 2009), it has been argued that Sn polymetallic ores in Gejiu district may be of syngenetic origin (Qin et al., 2006; Qin and Li, 2008; Li et al., 2006, 2009; Qian et al., 2011a, 2011b). Our new U-Pb ages for cassiterite are quite different from the above data but in excellent agreement with the Late Cretaceous ages, which clearly demonstrate that the hydrothermal alteration, sulfide and tin mineralization in the Gejiu district are coincident with the emplacement of the Gejiu granite. This establishes a temporal link between the granite and mineralization, which provides reliable evidence for an intrusion-related origin for tin-polymetallic mineralization. Available evidence obtained from geologic characteristics, fluid inclusions, isotopes and mineral chemistry also supports an intrusion-related origin for mineralization in the Gejiu tin district (Cheng, 2012d).

5.4 Insights into ore genesis and mineralization process in Gejiu tin district

It has been proved that cassiterite from different magmatic hydrothermal fluids with different sources would cause distinct chemical compositions (Neiva, 2008), however, cassiterite samples in different mineralization environments from the world class Gejiu tin district have similar elemental variation patterns (Appendix 2), indicating they possibly derived from the same hydrothermal fluid source. This idea is further supported by their highly consistent geochronological data (Figure 9; Table 3), as the coeval ages of ore-related granites (zircon U-Pb), hydrothermal alteration (mica ^{40}Ar - ^{39}Ar), mineralization (molybdenite Re-Os) (Cheng and Mao, 2010, 2012; Cheng et al., 2012a), and the new cassiterite U-Pb ages obtained in this study comprehensively demonstrate the close temporal connection amongst granitic magma, hydrothermal alteration and Sn mineralization. Above evidences support a granite-related hydrothermal origin for tin mineralization the Gejiu district.

In hydrothermal systems, both Ti and Sn are transported in the form of chlorine complexes and their precipitation in the form of TiO_2 and SnO_2 critically depends on the presence of oxygen (Patterson et al., 1981; Heinrich and Eadington, 1986; Taylor and Wall, 1993), coincidentally, the Ti content in cassiterite can be an indicator of fluid oxygen fugacity during SnO_2 crystallization (Seifert et al., 1997; Pieczka et al., 2007). For the cassiterite samples in this study, the Ti concentrations in tin granite, skarn and greisen ores are higher than the semi-oxidized ore, oxidized ore and vein ore samples, indicating the oxygen fugacity of cassiterite precipitated fluid is getting decreasing from proximal to distal to granite (Fig. 3). Moreover, it is suggested that Ti is more mobile under reducing conditions, and the presence of Ti may mean that reduced fluids deposited the mineral (Seifert et al., 1997; Serranti et al., 2002). According to this understanding, the higher Ti concentrations in the cassiterite of tin granite, greisen ore and skarn ore samples from Gejiu district (Fig. 7), which were collected in the vicinity of granite (Fig. 3), suggest that these Sn-transporting fluids were more reduced than the distal samples. It is also possible for the decreasing tendency of Ti concentration from skarn sample to vein sample that the meteoric water mixed with the granitic magma-derived hydrothermal fluid during mineralization process, which has been suggested by Cheng (2012d) based on fluid inclusion and H-O isotopes studies.

It has been pointed out that the existence of a continuous fluid evolutionary in space and time from early magmatic, spatially restricted, hydrothermal systems towards later, usually meteoric-dominated, mixed fluid during granite-related hydrothermal tin mineralization process (Tornos, 1997), and the changing of chemical composition of ore-forming fluid is presumed to be vital to cassiterite precipitation (Heinrich, 1990). Heinrich and Eadington (1986) showed that tin can be transported easily in acid and reduced fluids, and minor variations of the oxygen fugacity in the reduced fluid can influence the solubilities of Sn minerals (Tornos, 1997). These hypothesis may provide reasonable constraints on the above discussed geochemical variations in the Gejiu cassiterite samples, indicating the physical-chemical conditions may significantly changed in different mineralization environments, which is consistent with the critical cathodoluminescent micro-textures difference between the proximal cassiterites (tin

granite-, greisen- and skarn host) and the distal ones (semi-oxidized ore-, oxidized ore- and vein ore-host) from the world class Gejiu tin district, SW China.

6 Conclusions

Based upon a combination of CL textural, LA-ICP-MS trace element analysis and U-Pb dating results, several crucial implications for understanding the ore genesis and Sn mineralization in the world class Gejiu tin district has suggested:

(i) Cassiterites from tin granite, greisen and skarn ores are generally large, and characterized by euhedral oscillatory growth zones, while cassiterite from semi-oxidized ores, stratiform oxidized ores and veins are typically smaller, anhedral crystals with less regular zoning patterns. It appears that distance between samples and granites (the inferred source of hydrothermal fluids) may be one of the key factors controlling the cassiterite size and internal micro-texture variations, which may be used as an important tool for tin prospecting to be a fundamental exploration clue with potential economic significance.

(ii) Trace elements Al, Sc, Ti, V, Cr, Mn, Fe, Cu, Zn, Ga, Rb, Sr, Zr, Nb, Sb, La, Ce, Yb, Lu, Hf, Ta, W, Pb, U been detected in the cassiterite samples from Gejiu tin district, therein the most abundant elements are Fe, Ti and W, and the concentrations of Nb and Ta exhibit the biggest variations amongst all the elements. Zr/Hf ratios of the 6 samples exhibit gradual variation from greisens host cassiterite with Zr/Hf ration about 12.5, to tin granite host cassiterite is ~16.7, to skarn/semi-oxidized/oxidized ore host cassiterite is ~25, to vein ore host cassiterite is ~66.7, which been attributed as the various tourmaline and fluorite contents in different environments. An evident correlation between V and Sc been discovered, which may be caused by the substitution of $\text{Sc}^{3+} + \text{V}^{5+} = 2\text{Sn}^{4+}$. H^+ maybe introduced to keep charge balance.

(iii) Cassiterite U-Pb geochronology results obtained by LA-ICP-MS showing their ages lies in ~79 Ma to ~84 Ma. High consistent geochronology results support that the Gejiu tin deposits are hydrothermal origin and temporally, spatially, and genetically associated with the emplacement of the Gejiu granitic complex. Their geochemical and textural variations may reflect the temperature, oxygen fugacity and redox station of ore

forming fluids experienced significant changes during the tin mineralization process.

References

- 308 Geological Party (1984) *Geology of tin deposit in Gejiu area*. Metallurgical Industry Publishing House, Beijing.
- Ahrens L.H. and Erlank A.J. (1969) Hafnium. In *Handbook of geochemistry*, 2-5 sections B-O (ed. K.H. Wedepohl). Springer, Berlin.
- Bau M. (1996) Controls on the fractionation of isovalent trace elements in magmatic and aqueous systems: evidence from Y/Ho, Zr/Hf, and lanthanide tetrad effect. *Contrib. Mineral. Petrol.* 123, 323–333.
- Bhalla R. J. R. S. B. and White E. W. (1971) Intrinsic cathodoluminescence emission from willemite single crystals. *J. Lumin.* 4, 194-200.
- Bi X.W., Hu R.Z., Li H.M., Dong S.H., Chen Y.W. and Peng J.T. (2011) U-Pb cassiterite dating by LA-ICPMS and a precise mineralization age for the superlarge Furong tin deposit, Hunan Province, Southern China. *Goldschmidt Conference Abstracts*, 526.
- Black L.P., Kamo S.L., Allen C.M., Aleinikoff J. N., Davis D.W., Korsch R.J. and Foudoulis C. (2003) TEMORA 1: a new zircon standard for Phanerozoic U–Pb geochronology. *Chem. Geol.* 200, 155-170.
- Blevin P.L. and Norman M. (2010) Cassiterite-The Zircon of mineral systems? A scoping study, pp. 399–400. In *Geological Society of Australia, 2010 Australian Earth Sciences Convention (AESC) 2010, Earth systems: change, sustainability, vulnerability*. Abstract No 98 of the 20th Australian Geological Convention, National Convention Centre, Canberra, Australian Capital Territory. July 4-8.
- Černý P., Meintzer R.E. and Anderson A.J. (1985) Extreme fractionation in rare-element granitic pegmatites: selected examples of data and mechanisms. *Canadian Mineralogist* 23, 381–421.
- Cheng Y.B., Mao J.W. and Chang Z.S. (2012a) The origin of the world class tin-polymetallic deposits in the Gejiu district, SW China: constraints from metal zonation characteristics and ^{40}Ar - ^{39}Ar geochronology. *Ore Geology Review*, in revision.

- Cheng Y.B., Mao J.W. and Yang Z.X. (2012b) Geology and vein tin mineralization in the Dadoushan deposit, Gejiu district, SW China. *Mineralium Deposita*, doi: 10.1007/s00126-012-0409-4.
- Cheng Y.B., Mao J.W., Rusk B. and Yang Z.X. (2012c) Geology and genesis of Kafang Cu–Sn deposit, Gejiu district, SW China. *Ore Geol. Rev.*, doi:10.1016/j.oregeorev.2012.03.004.
- Cheng Y.B. (2012d) *Spatial-temporal evolution of the magmatism and mineralization in the Gejiu supergiant Sn polymetallic district and insights into several key problems*. PhD thesis, China University of Geosciences (Beijing) (in Chinese with English abstract).
- Cheng Y.B. and Mao J.W. (2010) Age and geochemistry of granites in Gejiu area, Yunnan province, SW China: constraints on their petrogenesis and corresponding tectonic setting: *Lithos* 120, 258–276.
- Cheng Y.B. and Mao J.W. (2012) Petrogenesis and geodynamic setting of the Gejiu igneous complex from the western Cathaysia block, South China. *Lithos*, in revision.
- Claiborne L.L., Miller C.F., Walker B.A., Wooden J.L., Mazdab F.K. and Bea F. (2006) Tracking magmatic processes through Zr/Hf ratios in rocks and Hf and Ti zoning in zircons: An example from the Spirit Mountain batholith, Nevada. *Mineralogical Magazine* 70, 517–543.
- Clark A.M., Fejer E.E., Donaldson J.D. and Silver J. (1976) The ^{119}Sn Mössbauer spectra, cell dimensions and minor element contents of some cassiterites. *Mineral. Mag.* 40, 895-8.
- Costi H.T., Horbe A.M.C., Borges R.M.K., Agnol R.D., Ross A. and Sighnolfi G. (2000) Mineral chemistry of cassiterite from Pitinga Province, Amazonian Craton, Brazil. *Revista Brasileira de Geociencias* 30, 775-782.
- Dostal J. and Chatterjee A. K. (2000) Contrasting behaviour of Nb/Ta and Zr/Hf ratios in a peraluminous granitic pluton (Nova Scotia, Canada). *Chem. Geol.* 163, 207–218.
- Dupuy C., Liotard J.M. and Dostal J. (1992) Zr/Hf fractionation in intraplate basaltic rocks: carbonate metasomatism in the mantle source. *Geochimica et Cosmochimica Acta* 56, 2411-2423.

- Farmer C.B., Searl A. and Halls C. (1991) Cathodoluminescence and growth of cassiterite in the composite lodes at South Crofty Mine, Cornwall, England. *Mineralogical Magazine* 55, 447-458.
- Florov B.L., Bichus B., Yakovlev Ya. V. and Kholmogorov A.I. (1980) Some typomorphic characteristics of cassiterites from Yakutia. *Zap. Vses. Min. Obshch.* 109, 174-86.
- Giuliani G. (1987) La cassiterite zonee du gisement de Sokhret Allal (Granite des Zaer, Maroc Central): composition chimique et phases fluides associees. *Mineral. Deposita* 22, 251-3.
- Goldschmidt V. M. (1937) The principles of distribution of chemical elements in minerals and rocks. *J. Chem. Soc.* 655-673.
- Götze J. and Kempe U. (2008) A comparison of optical microscope- and scanning electron microscope-based cathodoluminescence (CL) imaging and spectroscopy applied to geosciences. *Mineralogical Magazine* 72, 909-924.
- Götze J., Plotze M. and Habermann D. (2001) Origin, spectral characteristics and practical applications of the cathodoluminescence (CL) of quartz - a review. *Mineralogy and Petrology* 71, 225-250.
- Grant P. R. and White S. H. (1978) Cathodoluminescence and microstructure of quartz overgrowths. In *Scanning Electron Microscopy* (ed. Johari, O.), 789-94.
- Gulson B.L. and Jones M.T. (1992) Cassiterite: potential for direct dating of mineral deposits and a precise age for the Bushveld complex granites. *Geol.* 20, 355-358.
- Hall M.R. and Ribbe P.H. (1971) An electron microprobe study of luminescence centers in cassiterite. *American Mineralogist* 56, 31-45.
- Hedenquist J.W. and Lowenstern J.B. (1994) The role of magmas in the formation of hydrothermal ore deposits. *Nature* 370, 519 – 526.
- Heinrich C.A. and Eadington P.J. (1986) Thermodynamic predictions of the hydrothermal chemistry of arsenic, and their significance for the paragenetic sequence of some cassiterite-arsenopyrite -base metal sulfide deposits. *Economic Geology* 81, 511-529.
- Heinrich C.A. (1990) The chemistry of tin (-tungsten) ore deposition. *Econ. Geol.* 85, 529-550

- Heinrich C.A. (1995) Geochemical evolution and hydrothermal mineral deposition in Sn (– W - base metal) and other granite-related ore systems: Some conclusions from Australian examples. In *Magmas. Fluids and Ore Deposits* (ed. Thompson J.F.H.). Geol. Assoc. Canada Short Course Series, 23, 203-220.
- Hoskin P.W.O. and Schaltegger U. (2003) The composition of zircon and igneous and metamorphic petrogenesis. 27-62. In: *Zircon* (ed. Hancher J.M. and Hoskin P.W.O.). Reviews in Mineralogy and Geochemistry, 53, Mineralogical Society of America, Virginia and the Geochemical Society, Washington, D.C.
- Izoret L., Marnier G. and Dusausoy Y. (1985) Caracterisation cristalochimique de la cassiterite des gisements d'etain et de tungsteÁne de Galice, Espagne. *Canad. Mineral.* 23, 221-31.
- Jackson S.E., Pearson N.J., Griffin W.L. and Belousova E.A. (2004) The application of laser ablation-inductively coupled plasma-mass spectrometry to in situ U–Pb zircon geochronology. *Chem. Geol.* 211, 47–69
- Jiang S.Y., Wang R.C., Xu X.S. and Zhao K.D. (2005) Mobility of high field strength elements (HFSE) in magmatic-, metamorphic-, and submarine-hydrothermal systems. *Physics and Chemistry of the Earth* 30, 1020–1029.
- Lehmann B. (1987) Tin granites, geochemical heritage, magmatic differentiation. *Geologische Rundschau* 76, 177-185.
- Lehmann B. (1990) Metallogeny of tin. Springer, Berlin.
- Li Y.S., Qin D. X., Dang Y.T. and Xue C.D. (2006) Lead and sulfur isotope in Gejiu tin deposit in Yunnan province. *Geology and Prospecting* 4, 49-53 (In Chinese with English abstract).
- Li Y.S., Qin D.X., Cheng X.Y., Guo N.N., Luo X., Xie Y. and Zou T. (2009) Evidences of exhalative hydrothermal sedimentary mineralization of Indo-China epoch of Gejiu tin-polymetallic deposits. *Nonferrous Metal* 61, 120-125 (In Chinese with English abstract).
- Linnen R. L. (1998) The solubility of Nb–Ta–Zr–Hf–W in granitic melt with Li and Li+F: constraints for mineralization in rare metal granite and pegmatite. *Econ. Geol.* 93, 1013–1025.

- Liu Y.P., Li Z.X., Li H.M., Guo L.G., Xu W., Ye L., Li C.Y. and Pi D.H. (2007) U–Pb geochronology of cassiterite and zircon from the Dulong Sn–Zn deposit: evidence for Cretaceous large-scale granitic magmatism and mineralization events in southeastern Yunnan Province, China. *Acta Petrologica Sinica* 23, 967–976 (in Chinese with English abstract).
- Luo J.L. (1995) The model of Sn, W, Zn, Pb, Ag deposits in southeast Yunnan Province. *Yunnan Geology* 14, 319-332 (in Chinese).
- Maldener, J., Rauch, F., Gavranic, M., and Beran, A. (2001) OH absorption coefficients of rutile and cassiterite deduced from nuclear reaction analysis and FTIR spectroscopy. *Mineralogy and Petrology* 71, 21-29.
- Mao J.W., Cheng, Y.B, Guo, C.L, Yang, Z.X. and Zhao, H.J. (2008) Gejiu tin polymetallic ore-field: deposit model and discussion. *Acta Geologica Sinica* 81, 1456-1468 (in Chinese with English abstract).
- Marshall D. J. (1988) *Cathodoluminescence of Geological Materials*. Unwin Hyman, Boston.
- Mendelssohn M. J., Milledge H. J., Vance E. R., Nave E. and Woods P. A. (1978) Internal radioactive haloes in diamonds. In *Industrial Diamond Review*, 31-6, London.
- Möller P. and Dulski P. (1983) Fractionation of Zr and Hf in cassiterite. *Chem. Geol.* 40, 1-12.
- Möller P., Dulski P., Szacki W., Malow G. and Riedel E. (1988) Substitution of tin in cassiterite by tantalum, niobium, tungsten, iron and manganese. *Geoch. Cosmoch. Acta* 52, 1497-1503.
- Moore F. and Howie R.A. (1979) Geochemistry of some Cornubian cassiterites. *Mineral. Deposita* 14, 103-7
- Müller A., Kronz A. and Breiter K. 2002. Trace elements and growth patterns in quartz: a fingerprint of the evolution of the subvolcanic Podlesi´ Granite System (Krune´ hory Mts., Czech Republic). *Bulletin Czech Geological Survey* 77, 135-145.
- Müller A., Seltmann R., and Behr H.J. (2000) Application of cathodoluminescence to magmatic quartz in a tin granite: A case study from the Schellerhau granite complex, eastern Erzgebirge, Germany. *Mineralium Deposita* 35, 169–189.

- Murciego A., Sanchez A.G., Dusauso Y, Pozas J.M.M. and Ruck R. (1997) Geochemistry and EPR of cassiterites from the Iberian Hercynian Massif. *Mineralogical Magazine* 61, 357-365.
- Murciego A. (1990) *Estudio mineralogico y cristalocquómico de la casiterita. Relacion con sugenesis*. PhD. Thesis, Univ. Salamanca. 610 pp.
- Murciego A., Garcõa Sanchez A. and Martõn Pozas J.M. (1987) Microinclusiones de casiteritas de distintos tipos de yacimientos del Centro-Oeste de Espana. *Cuad. Lab. Xeol. Laxe* 12, 273-88.
- Neiva A.M.R. (2008) Geochemistry of cassiterite and wolframite from tin and tungsten quartz veins in Portugal. *Ore Geology Reviews* 33, 221–238.
- Neiva A.M.R. (1996) Geochemistry of cassiterite and its inclusions and exsolutions products from tin and tungsten deposits in Portugal. *Can. Mineralogist* 34, 745-768.
- Pagel M., Barbin, V., Blanc, P. and Ohmenstetter, D. (2000) *Cathodoluminescence in geosciences*. Springer, New York.
- Patterson D.J., Ohmoto H. and Solomon M. (1981) Geologic setting and genesis of cassiterite- sulphide mineralization at Renison Bell, western Tasmania. *Economic Geology* 76, 393–438.
- Peng C.D. (1985) A discussion on the condition,types and model of Gejiu tin deposit. *Yunnan Geology* 4, 17 – 32 (in Chinese).
- Pieczka A., Goebowska B. and Parafiniuk J. (2007) Geochemistry and origin of the cassiterite from Redziny, Lower Silesia, Poland. *Mineralogia Polonica* 38, 219-229.
- Plimer I.R., Lu J., Kleeman J.D. (1991) Trace and rare earth elements in cassiterite - sources of components for the tin deposits of the Mole Granite, Australia. *Mineralium Deposita* 26, 267-274.
- Qian Z.K., Luo T.Y., Huang Z.L., Tong X., Yang B.F., Yang W.B. and Lu R.Y. (2011b) Geology, geochemistry and genesis of Xinshan stratabound diopside rocks in Gejiu, Yunnan. *Acta Mineralogica Sinica* 31, 338-352.
- Qian Z.K., Wu J.D., Kang D.M., Lu R.Y., Yang B.F., Hu Y., Luo T.Y. and Huang, Z.L. (2011a) Geological characteristics of cassiterite-hematite-calcite vein-type orebody and its geological significance. *Acta Mineralogica Sinica* 31, 328-337.

- Qin D.X. and Li, Y.S. (2008) *Studies on the geology of the Gejiu Sn-Cu deposit*. Science Press, Beijing.
- Qin D.X., Li Y.S. and Tan S.C. (2006) Metallogenic ages of Gejiu tin deposit in Yunnan Province. *Chinese Journal of Geology* 41, 122-132 (in Chinese with English abstract).
- Remond G. (1973) Exemples d'identification et de localisation des 616ments en traces dans les minéraux luminescents (cassitdrites), l'aide de l'analyseur ionique. *Bull. Soc. franf. Mindral. Crist.* 96, 183-98.
- Rubin J.N., Henry C.D. and Price J.G. (1993) The mobility of zirconium and other immobile elements during hydrothermal alteration. *Chem. Geol.* 110, 29–47.
- Rudnick R.L., McDonough W.F. and Chappell, B.W. (1993) Carbonatite metasomatism in the northern Tanzanian mantle: petrographic and geochemical characteristics. *Earth Planet. Sci. Lett.* 114, 463–475.
- Rusk B. and Reed M. (2002) Scanning electron microscope-cathodoluminescence of quartz reveals complex growth histories in veins from the Butte porphyry copper deposit, Montana. *Geology* 30, 727–730.
- Rusk B., Lowers H. and Reed M. (2008) Trace elements in hydrothermal quartz: relationships to cathodoluminescent textures and insights into hydrothermal processes. *Geology* 36, 547–550.
- Rusk B., Reed M., Dilles J. and Kent A. (2006) Intensity of quartz cathodoluminescence and trace element content of quartz from the porphyry-copper deposit in Butte, Montana. *American Mineralogist* 91, 1300–1312.
- Schneider H.J., Dulski P., Luck J., Moeller, P. and Villalpando, A. (1978) Correlation of trace element distribution in cassiterites and geotectonic position of their deposits in Bolivia. *Mineral. Deposita* 13, 119-22.
- Seifert T., Schwarz-Schampera U., Herzig P.M., Hutchinson R.W., Hennigh Q. and Wagner R. (1997) Trace element characteristics of cassiterite in granite-related tin and tin-bearing VMS deposits. In *Society of Economic Geologist Field Conference 1997* (ed. F.J.A.S. Barriga,), Lisbon, Portugal, 113.
- Serranti S., Ferrini V., Masi U. and Cabri L.J. (2002) Trace-element distribution in cassiterite and sulfides from Rubane and massive ores of the Corvo deposit, Portugal.

- The Canadian Mineralogist* 40, 815-835.
- Shannon R. D. (1976) Revised effective ionic radii and systematic studies of interatomic distances in halides and chalcogenides. *Acta Cryst.* A32, 751-767
- Spandler C., Pettke T. and Rubatto D. (2011) Internal and External Fluid Sources for Eclogite-facies Veins in the Monviso Meta-ophiolite, Western Alps: Implications for Fluid Flow in Subduction Zones. *J. Petrology* 52, 1207-1236
- Stevenson B.G. and Taylor R.G. (1973) Trace element contents of some cassiterites from Eastern Australia. *Proc. R. Soc. Queensland* 84, 43-54.
- Tarkhanov A.V., Kudlaev A.R., Petrin A.V. and Kozyr'kov V.D. (1991) The Zheltorechinskoe vanadium–scandium deposit. *Geologiya Rudnykh Mestorozhdenii* 33, 50–56.
- Taylor J.R. and Wall V.J. (1993) Cassiterite solubility, tin speciation and transport in a magmatic aqueous phase. *Economic Geology* 88: 437–460.
- Taylor R.G. (1979) *Geology of tin deposits*. Amsterdam and New York.
- Tindle A.G. and Breaks F.W. (1998) Oxide minerals of the separation rapids rare-element granitic pegmatite group, Northwestern Ontario. *Canadian Mineralogist* 36, 609–635.
- Tornos F. (1997) A numerical approach for the formation of chlorite and sulphide-bearing greisen: a study based on the Navalcubilla system (Spanish Central System). *Mineralogical Magazine* 61, 639-654.
- Van Achterbergh E., Ryan C., Jackson S.E. and Griffin, W.L. (2001) Appendix 3 data reduction software for LA-ICP-MS. In *Laser-Ablation-ICPMS in the Earth Sciences*. *Mineralogical Association of Canada, Short Course* (ed. Sylvester, P.), 239-243.
- Wang R. (1985) Etude mineralogique des inclusions dans les cassiterites de quelques gisements d'etain. *Memoire D.E.A. UPS*, Toulouse.
- Wolff J.A. (1984) Variation in Nb-Ta during differentiation of phonolitic magma, Tenerife, Canary Islands. *Geochim. Cosmochim. Acta* 48, 1345–1348.
- Yuan S.D., Peng J.T., Hu R.Z., Li H.M., Shen N.P. and Zhang, D.L. (2008) A precise U–Pb age on cassiterite from the Xianghualing tin–polymetallic deposit (Hunan, South China). *Miner. Deposita* 43, 375–382.
- Zhao Y.M. and Li D.X. (1987) Metasomatism in granite contact in Gejiu tin deposits,

Yunnan Province. *Journal of Chinese Academy of Geological Sciences* 16, 237-252.
Zhuang Y.Q., Wang R.Z. and Yang S.P. (1996) *Tin-copper polymetallic deposits in Gejiu district*. Earthquake Publishing House, Beijing (in Chinese).

Chapter 9

Conclusion

Conclusion

The aim of this chapter is to summarize the links between the magmatism and mineralization in Gejiu ore district, and to present a consistent geological evolution history in the Gejiu ore district during Late Cretaceous (Fig. 9.1).

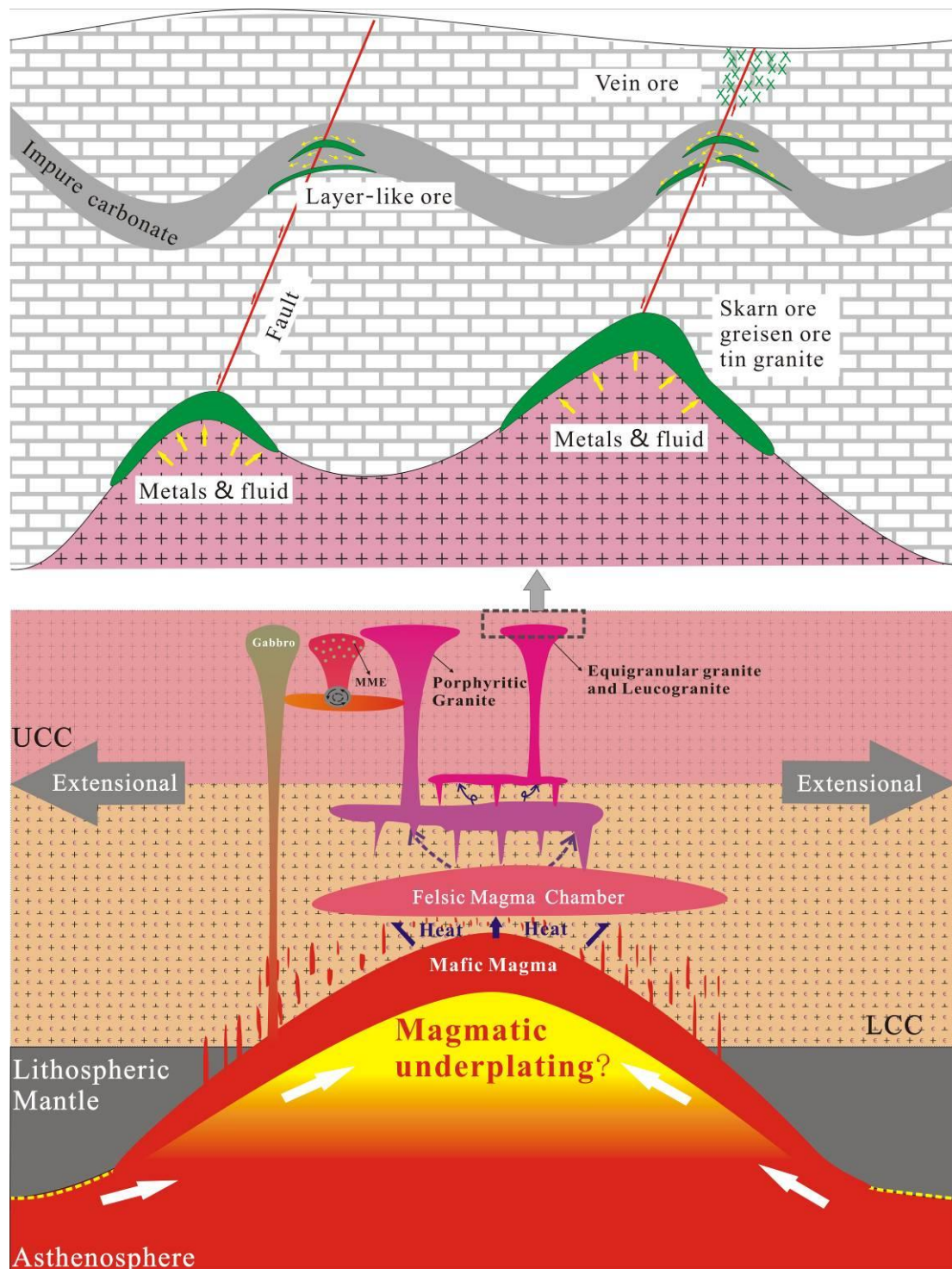


Figure 9.1 Simplified illustration showing the magma generation and formation processes in the Gejiu district, as well as major controlling factors of the mineralization in this area, all of which are the mainly studied aspects of this thesis

Combined zircon dating results, geochemical and Sr–Nd–Hf isotopic data suggest that the ~80 Ma Gejiu granitic magmas experienced a high degree of fractional crystallization after they had formed by partial melting of Mesoproterozoic crust, with minor input from mantle-derived magmas. Moreover, intrusive rocks of the Gejiu District underwent magma mixing via a range of different mechanisms. It is also suggested that bulk physical mixing of magmas may be efficient at relatively high temperature in the lower crust, while at upper crustal levels, mixing/mingling of mafic and granitic magmas can commonly lead to enclave formation and hybridization via element inter-diffusion (Fig. 9.1). This hypothesis is consistent with the regional evidence of lithospheric extension in the western Cathaysia block during the Late Cretaceous. These ideas are also consistent with the studies of Lehmann (1990), which suggested that many tin-related granites resembled I-type or anorogenic (intraplate) A-type granites, which been attributed to mantle-crust interaction at the time of generation of tin granite melts. Variable degrees of involvement of mantle material and a high degree of fractional crystallization are the general features of the granitic rocks associated with tin mineralization.

Almost all the orebodies in the Gejiu ore district are spatially associated with granites. The new ages presented in this study suggest that the deposits and the granites formed contemporaneously at ~80 Ma, hence, the genetic connection of Gejiu granites and the mineralization is well supported, which is also consistent with the ore element zonation patterns in this district. The degree of crystal fractionation is the key factor to evaluating the ore potential of the granite. In the Gejiu district, this study revealed that the degree of fractional crystallization increases from the Longchahe porphyritic granite, via the Laochang porphyritic granite, Masong porphyritic granite, Laochang equigranular granite, to Xinshan equigranular granite. The Longchahe granite is the least fractionated, and has have the lowest potential for association with ore.. In contrast, the Xinshan granite is highly fractionated, and is

associated with significant volumes of mineralized rock. Fractional crystallization progress leads to Sn enrichment in the highly fractionated volatile residual liquid that accumulates in granite cupolas (Lehmann, 1990). In these cupolas the volatiles streaming out from the magma chamber causes extensive granite auto-metasomatism and both endo- and exocontact alteration. Cassiterite accumulates in the greisen, skarn, as well as preferential zones or faults occur as veins and stockworks (Fig. 9.1).

These understandings are not only helpful to interpret why there are so many ore deposits formed in the Gejiu ore district, but also can provide a series of crucial clues and guidelines for discovering deposits in the future. Firstly, the ores are closely related with highly evolved granite, so examine the fractionation degree of granite is the first principle of prospect evaluation. Secondly, the lithology of host sedimentary rocks is another crucial controlling factor, as at Gejiu interlayers of impure carbonate are preferential sites of ore mineral precipitation. Thirdly, the location and geometry of large-scale structures are important for channelling hydrothermal fluids that lead to ore formation in Gejiu district, thus special concern should be paid to faults and fault intersections. Finally, the predictable ore metal zonation patterns described here can be used as vectors to ores, once general geological relationships are established and one ore metal association has been recognized.